Spring 2021

The Role of Microvascular Signaling in the Neurogenic Niche

Rita Matta
Yale University Graduate School of Arts and Sciences, rita.matta@uconn.edu

Abstract

The Role of Microvascular Signaling in the Neurogenic Niche

Rita Matta

2021

Stroke is among the leading causes of death and disability worldwide, partly due to the lack of effective therapies to facilitate the recovery of damaged brain tissue. Stem cell therapies used to treat neurological diseases are promising, owing to their innate ability to enhance endogenous repair mechanisms and promote functional recovery. However, the maintenance of stem cells in a quiescent state throughout delivery remains a significant challenge. This challenge only exacerbates the difficulty of therapeutic strategies attributed to the low survival rate of engrafted cells within the inflamed, cytotoxic brain. Tissue engineering provides the opportunity to develop cell delivery strategies that maintain cell quiescence and reduce inflammation during and post-delivery, thereby promoting cell survival, migration, and success following engraftment.

The subventricular zone (SVZ), located lateral to the lateral ventricle, is the largest region in the adult brain where proliferating neural stem cells (NSC) reside. For NSC to differentiate in response to injury into the functionally specific cell types that comprise healthy brain tissue, they must first migrate rostrally into the olfactory bulb (OB). This process is dependent upon signaling from microvascular endothelial cells (EC) and pericytes (PC) within the SVZ, ultimately directing NSC along the rostral migratory stream (RMS) to the OB. Diffusible secreted signals from EC can increase survival, proliferation, and differentiation of SVZ NSC *in vitro* as well as *in vivo*.

Here, we investigate the role of vascular cells in NSC functionality, particularly, NSC migration and survival. Our results demonstrate that, with the microvascular structure, EC, and not PC, promote NSC migration and cluster formation, both by cell-cell contact and soluble factor secretion. Using a 3D scaffold that mimics the biomechanics, biochemistry, and biostructure of specific regions of the brain, we can visualize the migration of NSC clusters throughout the pores

of this functionalized scaffold towards EC. Due to N-cadherin's established role in NSC polarization and cytoskeletal rearrangement, we demonstrate that EC secreted MMP2 leads to NSC clustering, increased N-cadherin expression, and enhanced NSC migration. When the NSC cluster leader cell was ablated using a microfluidic system, the cluster no longer can migrate, even when in the presence of EC soluble factors, confirming that NSC clustering is a prerequisite for migration.

The novelty of the compositional, architectural, and mechanical mimicking scaffold has allowed us to probe biofunction and inform us about important signals to incorporate into a delivery structure. Due to the positive impact EC have on NSC, we use polymeric microbeads for their co-encapsulation to be delivered into the brain. We demonstrate that NSC encapsulated with EC have increased NSC survival and maintained quiescence, prior to and post injection to a non-injury model, as compared to NSC encapsulated alone. Once injected into the brain, NSC encapsulated with EC present reduced immune cell activation and enhanced cell survival as compared to freely injected cells. Furthermore, NSC encapsulated with EC delivered to two rat stroke models demonstrate enhanced cell infiltration and migration into the stroke damaged tissue with the use of extracellular matrix (ECM) as a suspension vehicle. Our work provides convincing evidence that engineered mimics of the neurovascular niche may serve as a neuroprotective delivery vehicle, reducing inflammation upon transplantation, ultimately improving the state of current delivery systems.

As we aim to enhance the construction of our bioengineered niche, we observe the impact of vascular cells on NSC survival during injury-like conditions, specifically when deprived of glucose. We demonstrate that EC, but not PC, promote NSC cell proliferation and reduce cytotoxicity during glucose deprivation by direct cell-cell contact and soluble factor secretion. This effect is diminished when NSC VEGFR3, abundantly expressed by NSC in the SVZ, is blocked. In addition, we demonstrate that NSC and EC co-cultures have elevated levels of VEGF-C, not seen for NSC alone. To further assess NSC survival *in vivo*, we delivered microbeads to a mouse stroke-injured brain, where NSC encapsulated with EC have high VEGF-C expression around the

injection site compared to microbeads with NSC encapsulated alone. Our results demonstrate a novel role for VEGF-C/VEGFR3 in promoting NSC survival during injury which can significantly enhance current therapies. In summary, our work can aid the creation of a novel cell delivery therapeutic for stroke, promoting NSC migration and survival upon transplantation. Together our findings highlight the potential for neural-vascular coupling to promote functional and long-term recovery in the stroke injured brain.

The Role of Microvascular Signaling in the Neurogenic Niche

A Dissertation

Presented to the Faculty of the Graduate School

of

Yale University

in Candidacy for the Degree of

Doctor of Philosophy

by

Rita Matta

Dissertation Director: Anjelica L. Gonzalez, Ph.D.

June 2021

Table of Contents

List of Figures

Figure 5. 7. Microsphere-based cell delivery to a tissue cavity caused by stroke. A. ECM hydrogel-based implantation of green fluorescent protein (GFP)-tagged neural stem cells (NSCs) and endothelial cells (ECs) encapsulated in microspheres. B. There is widespread distribution of microspheres throughout the cavity, but there is also evidence that a cortical tissue defects (#) was not filled due white matter separating it from the main striatal cavity. Some loss of microspheres in the main cavity are evident due to tissue processing (*). NSCs migrated to the area of cortical tissue damage and more extensively throughout the cavity as well as into surrounding damaged tissue. ECs mainly remained within the main cavity where microspheres were implanted. C. At the base of the lesion microspheres were well compacted and presented a mixture of sizes. Some cells were evident in the microsphere, but a large number of cells populated the ECM hydrogel in between the microspheres. D. In the core of the cavity, microspheres were also well compacted and distributed, but no very large microspheres were evident. ECs were very evident in this region compared to NSCs. E. Only NSCs were invading into the surrounding tissue. F. Migration of NSCs along white matter tracts and invasion into damaged cortical tissue was also observed. G. Invasion of NSCs into the damaged striatum was widespread. H. A few microspheres were present in damaged cortical tissue, which was along the implantation pathway, but no microspheres were present in adjacent tissue. Nevertheless, extensive invasion and migration of NSCs in the damaged cortical tissue was evident. I. it is unclear in the corpus callosum if NSCs from the few microspheres in the cortex migrated along these white matter fibers or if NSCs from the main striatal tissue cavity invaded the corpus callosum to migrate to damaged cortical tissue. J. Some migration of implanted NSCs was evident towards the subventricular zone, which is the inverse migration pattern observed by endogenous NSCs. K. NSCs at the base of the tissue cavity also migrate ventrally along the trajectory of the MCA. 144

Figure 5. 8. Co-implantation of neural stem cells and endothelial cells in microspheres produces an improved survival of cells in the stroke cavity. A. The injected volume of microspheres with NSCs and ECs (n=2) was approximately twice the volume of microsphere with

List of Tables

Acknowledgments

I would like to thank my advisor Dr. Anjelica Gonzalez and my committee members: Drs. Karen Hirschi, Lauren Sansing, and W. Mark Saltzman, who have provided me with significant experimental advice and support throughout the completion of this work. I am grateful for such an incredible committee with a variety of expertise that have helped shape my research direction. Dr. Gonzalez not only has she made groundbreaking impact in the sciences, but she has made Yale and beyond a better place. I am inspired by her every day and beyond lucky to have learned so much from her. I would also like to thank the Gonzalez lab members who I have had the absolute pleasure of working with during my time at Yale. Particularly, I would like to thank Drs. Holly Lauridsen and Amanda Pellowe for their mentorship and training over the years. I would like to acknowledge Dr. Catherine Kim, Laura Morales, and Michelle Wu who were so wonderful to work with for many years, bringing a positive attitude and the kindest, most supportive atmosphere to our workplace. I would like to thank many students and visiting interns from Yale College and beyond who I had the opportunity to work with and mentor, particularly, Chloé Pezzana, Jannet Rivera, Araceli Lopez, Tracy Chung, and Carly Israel. I am extremely grateful for having such an upbeat, and incredibly intelligent lab family over these five years that made Malone feel like home. In addition, Alex and Jackson brought light, energy, and laughter during their Malone visits, and I will forever refer to "microbeads" as "micro-robots" because of them. Lastly, the administrative staff in the BME department and SEAS have been instrumental at facilitating all things, and I truly could not have done this without them.

Within my time at Yale, I have had the delight to work with multiple collaborating groups who have provided me with resources, support, and significant contributions. This includes Drs. Michael Murrell, Lauren Sansing, Jean-Leon Thomas, Karen Hirschi, and Michael Modo, whose students, staff, and post-docs have made contributed to sophisticated microfluidics and *in vivo* work

in my dissertation. I would like to acknowledge my undergraduate research advisor Dr. Sangamesh Kumbar for his phone calls, emails and visits, and conversations that constantly encouraged me throughout my trajectory. In addition, I acknowledge my Medtronic team and mentors, Angela Throm, Rebecca Cain, Jane Mayotte, Marisha Godek and Jonathan Thomas. These incredible mentors brought me the most love, light, and support I could ask for during this journey, and I will always cherish the meals, walks, and catch-up sessions we have had here around New Haven.

Most importantly, I would like to thank my family and friends who made the continuation of this journey possible. My mother spoke on the phone with me at all hours of the day and night while I finished experiments or walked home from the lab. My sister, Marie, endured the editing of grant applications and manuscript drafts, and through it all, she continued to support me through my most difficult moments. My grandmother was my favorite phone call every day, and my extended family's encouraging texts and calls always motivated me to reach for the stars. I am profoundly grateful for my friends who have become my extended family here at Yale, including the lovely ladies of Yale GradSWE, fellow Graduate Affiliates, and staff at Branford College, fellow GSAS students, spin class friends, and my amazing roommate, Momo. These friendships at Yale have kept me grounded, sane, and entertained over these past five years, and it would have been catastrophic without these incredible people. Lastly, I would like to acknowledge my friends and faculty from both the University of Connecticut, especially Dr. Nicole Piscopo and Alyssa Fasciano for their support, motivation, and friendship, as well as those from Sacred Heart Academy who have helped fuel my scientific passion. This would not have been done without Sr. Mary Jane Paolella, who I miss every day, Mrs. Gniadek, and Dr. Sengupta.

Chapter 1: Introduction & Outline

Portions of this chapter were printed with permission from Matta and Gonzalez, 2018 [1]

1.1 Stroke Impact and Background

Stroke is among the most prominent public health issues in the world, ranking among the top five leading causes of death and disability and impacting 1 in 6 people worldwide [2]. In the U.S alone, someone suffers a stroke every 40 seconds [3]. Both the incidence and prevalence of stroke have been correlated to an aging population as well as socioeconomic burden [4], causing trends in incidence and severity of stroke outcomes to vary significantly between states and countries. The only current therapy for ischemic stroke being administration of recombinant tissue plasminogen activator (rtPA). While the treatment of rtPA therapy can be beneficial, it is currently constrained to just 2-5% of stroke patients, as rtPA is only effective if administered 4.5 hours following symptom onset [5]. For patients who are unable to meet the criteria for rtPA therapy, intracranial hemorrhage often causes permanent neurological functional deficits [5]. A need for therapies that can be administered beyond a short therapeutic window remains, in addition to those that have the potential to restore the damaged tissue cavity that is formed by hypoxic conditions following stroke.

Responsible for approximately 85% of strokes [4], ischemia occurs when there is a blockade of a cerebral artery by a foreign clot or mass. This prevents sufficient blood flow through macrovessels and the invested microvasculature, thereby limiting oxygen exchange into the surrounding tissue. Reduction of blood supply under 15-20% of baseline levels contributes to tissue necrosis and irreversible damage [6]. Vascular occlusion disrupts the cells and proteins that maintain the tightly regulated barrier at the vascular-tissue interface, known as the blood brain barrier (BBB). The BBB contains endothelial cells (EC), pericytes (PC), a basement membrane, and astrocytic feet. Damage to one or all these components causes increased permeability and subsequent edema and neuroinflammation. Furthermore, soluble factors including tumor necrosis

factor alpha (TNF-α), thrombin, hemoglobin and iron sulfate can be released into the local area through diffusion of soluble blood and blood plasma constituents, which may cause cytotoxic effects to the milieu [7]. The volume of necrotic lesion core resulting from cellular and tissue damage is directly correlated to the extent of motor impairment experienced by the patient. The final infarct size, or area of dead tissue due to hypoxia, varies from patient to patient, contributing to the heterogeneity and complexity of this disorder [8].

In an effort to achieve neurological function after stroke, neurogenesis creates new neurons (neuroblasts) in two germinal regions in the adult mammalian brain: the subventricular zone (SVZ) of the lateral ventricles and the subgranular zone (SGZ) in the hippocampus [9]. Under normal conditions, the adult brain inhibits new axonal sprouting. Recent studies have demonstrated that existing neurons may sprout new connections after the occurrence of ischemic stroke [10]. The SVZ is highly vascularized and neural stem cells (NSC) are in close contact with the rich vascular system, as evidenced by close interactions between type-B astrocytic cells, ependymal cells, EC, and PC. Direct contact between each of these cells and NSC promote NSC self-renewal and neurogenesis in the SVZ [11].

In addition to neurogenesis, the process of angiogenesis, or development of new blood vessels, is necessary to achieve functional neurological recovery following stroke [5]. The peri-infarct area is hypoxic, triggering angiogenesis through up-regulation of EC-secreted vascular endothelial growth factor (VEGF) within 6-24 hours following occlusion. Angiogenesis is followed by a coordinated up-regulation of the VEGF-receptor after 48 hours [12]. Due to this signaling cascade, EC proliferation and sprouting contribute to early and necessary microvessel formation, as the number of new vessels formed in the ischemic penumbra is associated with longer survival for ischemic stroke patients [13]. Many factors beyond VEGF, such as fibroblast growth factor (FGF) and brain-derived neurotrophic factor (BDNF) regulate angiogenesis. These function to promote vasodilation and increase circulation and tissue oxygenation as initial steps for repair following ischemic damage [5].

Angiogenesis and neurogenesis are coupled processes critical for functional and structural recovery of the brain infarct region following stroke. Neural stem cells (NSC), cells with the capacity to differentiate into cells of all glial and neuronal lineages, can populate central nervous system (CNS) regions. NSC are natively resident in the SVZ niche and secrete growth factors and chemokines that promote proliferation and expansion of the NSC pool. Regenerative capacity is maintained by switching from asymmetric division, a process allowing stem cells to self-renew, to symmetric division, a process enabling cells to expand in number after injury. Following NSC proliferation, neuroblasts (cells differentiated from NSC that are committed to neuronal fate) migrate to the ischemic region and boundary of the infarct region. This migration is characterized by cellular interactions between immature neuroblasts and blood vessels, suggesting that angiogenesis and neurogenesis are time-dependent and codependent upon one another [5].

1.2 Goal of Tissue Engineering Strategies

In order to improve behavioral recovery following stroke, the goal of regenerative medicine is to successfully transplant stem or progenitor cells that can differentiate into neurons and integrate with the host microenvironment, improving both neurological and behavioral outcomes. Ideally, the act of transplantation and cell survival would enhance the endogenous repair processes, including axonal sprouting, neurogenesis, brain plasticity, and motor remapping. Integrated neural progenitor cells have the potential to replace and rebuild impacted circuitry and reduce lesion size, in conjunction with the fine-coordinated events of angiogenesis and neurogenesis. This repair includes recruitment of vascular cells for increased neovascularization and vascular stabilization [14, 15].

Neural stem cells enact cell proliferation and recruitment through the production and secretion of growth factors that are correlated with recovery following ischemia. Some growth factors such as VEGF have a short-term impact, having demonstrated an increase in vascularity of infarcted tissue following stroke [16] and presenting upregulation in rat middle cerebral artery occlusion (MCAO) models after 3 hours [17]. Both insulin-growth factor-1 (IGF-1) and BDNF

have also demonstrated promising results as acute therapies, beginning administration after 30 and 15 min post MCAO, respectively, and primarily attributed to reduction in infarct volume [16]. Growth factor presentation in various forms is integral to promoting repair and functional recovery following stroke.

Tissue engineering constructs for the goal of neural regeneration and repair of the stroke region require that cell survival and activity be sustained and, often, enhanced for appropriate integration of exogenous transplanted cells into the host tissue. The successful use of biomaterials that recreate the SVZ native niche should support cell survival, proliferation, growth factor production, and protein secretion as necessary for appropriate cellular delivery and engraftment into the damaged area. Combining tissue engineering and cell transplantation advances can directly influence the differentiation and survival of neural progenitor and stem cells *in vitro* and *in vivo*.

Both homophilic and vasophilic migration play a critical role throughout the RMS in response to injury. Homophilic migration is characterized by chains of migrating neuroblasts that use each other's somas to cluster and form a chain migration and are regulated by chemoattraction. Chemoattractants include netrin, neuregulin, ephrin, and brain-derived neurotrophic factor (BDNF). NSC also use blood vessels to guide vasophilic locomotion, although the exact mechanisms that guide neuroblast migration along vessels without direct contact to EC are not fully understood. Studies demonstrate the importance of factors such as BDNF released by EC, providing chemoattraction for neurons to the RMS [18]. A neuroinflammatory response is induced following brain injury, seen by release of chemokines and growth factors including CXCL12, angiopoietin-1, monocyte chemoattractant protein-1 (MCP-1), VEGF, and BDNF. CXCL12, the best characterized molecule for directing NSC migration, can signal to NSC through ligation of the CXCR4 receptor. EC secretion of CXCL12 as well as angiopoietin-1 secretion from remodeling blood vessels after lesion initiate NSC migration [18]. These increase neurogenesis and migration to inflamed tissue, although the release of chemokines and growth factors by PC has yet to be elucidated.

While we have come to understand many of the cellular and structural interactions that occur during stroke recovery, we remain unable to harness this knowledge to enhance therapeutic recovery. To date, there remains no effective treatment to foster recovery following ischemic stroke, though cell therapy has emerged as a promising approach to encourage functional replacement of the damaged neurons. As a therapeutic approach, transplanted NSC have the potential to differentiate into numerous phenotypes required for neurogenesis in response to biological cues and may integrate with the host environment to recover the effects of neurodegeneration. By incorporating factors that enhance both neurogenesis and angiogenesis through cell therapy, a neuro-restorative therapy can be created to promote re-growth in the neurogenic niche. This approach demonstrates the potential to repair the injured brain, though many limitations must be overcome. These include promoting cell survival, controlling cell differentiation, and ensuring proper engraftment of exogenous cells within a fragile microenvironment.

1.3 Objective

Here, we aim to contribute understanding to how vascular cells in the neural niche impact neural cells, and how we can utilize these cell types together to create an effective tissue engineered strategy. We investigate the role of EC and PC in promoting NSC viability under glucose deprivation, hypothesizing vascular cytokines may reduce NSC cytotoxicity and promote cell proliferation. In addition, we observe EC and PC impact on promoting NSC clustering and directing NSC migration using sophisticated 3D models, specifically elucidating the role of N-cadherin in this effect. The investigation of these molecular mechanisms at homeostasis and upon injury, specifically on NSC enhanced viability and pro-migratory state, dictate our constructed engineered niches for sustained NSC delivery to the stroke injured brain. The goal of these findings is to use cell-encapsulated microbeads as a minimally invasive delivery therapeutic for ischemic stroke.

1.4. Specific Aim

Aim 1: Investigate the role of vascular cells in promoting NSC clustering and directing NSC migration. Determine the mechanism by which NSC clustering is enhanced in the presence of vascular cells. Elucidate if EC or PC activate EGFR through MMP2 secretion, and thereby promote N-cadherin cleavage. Conduct 3D migration experiments using a porated, mechanically and biochemically mimetic PEG hydrogel to visualize NSC migration with EC+/-PC.

Aim 2: Construct engineered microbeads that enable sustained delivery of cells and optimize their delivery into the damaged CNS. Assemble niche to enable NSC survival and quiescence in the presence of vascular cells, in particular EC or PC with NSC, enhancing constructs with inclusion of biomimetic peptide sequences. Optimize and characterize degradation, visualization, processing, and delivery technique of microbeads with encapsulated cells into 1) a mouse wild-type model and 2) two rat stroke models. Observe how injected cells enhance and promote functional recovery and neural circuitry.

Aim 3: Determine the mechanism by which vascular cell secreted factors sustain NSC viability during stroke-like conditions. Characterize NSC proliferation and cytotoxicity during glucose deprivation with EC+/- PC. Probe the role of VEGF-C in promoting NSC survival and the dependence Deliver blank microbeads and NSC and NSC+EC encapsulated microbeads into a mouse stroke model and observe VEGF-C expression in the stroke tissue.

Chapter 2: Background & Motivation

Portions of this chapter were printed with permission from Matta and Gonzalez, 2018 [1]

2.1 Subventricular Zone and Biology

2.1.1 Cytoarchitecture

The subventricular zone (SVZ) is one of the two niches in the adult brain where neurons can regenerate [9]. This highly organized microenvironment begins to form during embryonic development with the generation of excitatory neurons. New excitatory neurons are generated in the ventricular zone that faces the lateral ventricle; an area adjacent to the SVZ. Upon migration towards the brain surface during the developmental period, neurons that are born earlier are in deeper layers while neurons born later remain superficial [19]. The SVZ is highly vascularized and neural stem cells (NSC) are in close contact with the rich vascular system, as evidenced by close interactions between NSC, ependymal cells, and endothelial cells (EC). Direct contact between each of these cells and NSC promote NSC self-renewal and neurogenesis in the SVZ, as seen in Figure 2.1. [11].

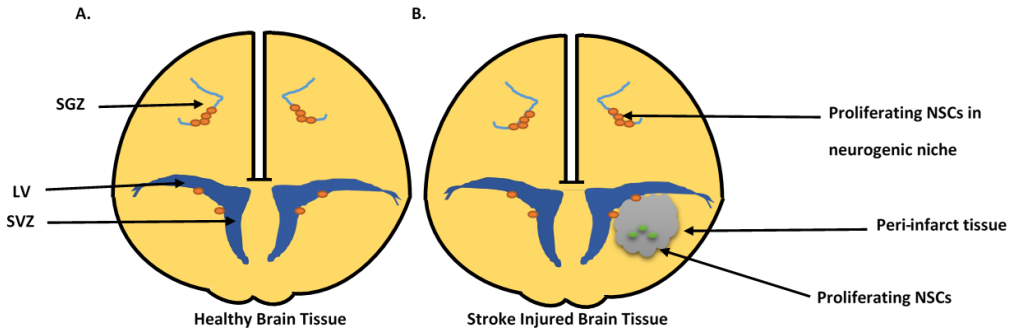

Figure 2. 1: Schematic of the SVZ in and stroke injured brain. A) Healthy brain tissue with proliferating NSC in the two germinal zones of the brain. B) Peri-infarct tissue contains proliferating NSC that become activated following injury.

The microvasculature of the SVZ contains a more expansive vascular network than other areas of the brain. While the microvasculature of the SVZ maintains vascular integrity to support

the blood brain barrier (BBB), there are regions of the SVZ blood vessels where contact with astrocytic endfeet and microvasculature support cells, particularly pericytes (PC), is absent. The intermittent absence of astrocytic and PC contact with the vessel allows for transit amplifying NSC to directly contact the endothelium, enabling rapid signaling and molecular exchange between the two cells [20]. The unique SVZ microvasculature suggests that a modified BBB in this niche exists [21].

Extrinsic factors that directly influence cells of the SVZ originate from blood vessels [22], the ependymal layer [23], and cerebrospinal fluid (CSF). In particular, the CSF is a major supplier of both proteins and small molecules responsible for signaling this niche [24]. The choroid plexus determines the composition of CSF in order to directly delivery these proteins and molecules to the SVZ and impact the behavior of neural progenitor cells [22, 23]. Secreted CSF is important in maintaining normal brain function as well as response to neuropathological conditions, where changes in CSF to the SVZ may alter the brain parenchyma metabolism.

The interactions between both EC and PC with NSC, as well as with each other, are critical for maintaining vessel integrity and niche cell maintenance, as seen in Figure 2.2. The connection between type-B cells and EC is characterized by short, thick processes extended from the body of NSC in the ventricular zone. These processes allow cells to anchor to the basement membrane and migrate rapidly along the vessel length, enabling interactions critical for both NSC self-renewal and cell differentiation [25]. Clustering progenitor cells in close contact with cerebral EC are supported in their proliferation and response to ischemia, though the process by which EC mediate this support has yet to be elucidated [26]. Like EC, PC also intricately interact with type-B cells, where NSC both project and ensheath PC of the SVZ capillaries [27]. While abundant in large numbers within the SVZ, PC distribution along the length of brain microvessels varies, which is not surprising since the vascular endothelial tissue is extremely heterogeneous. Type-B cells control capillary tone in the SVZ due to the contractile nature of PC [21]. As a result, the interactions between vascular cells and NSC are critical to the SVZ functioning as a neurogenic network.

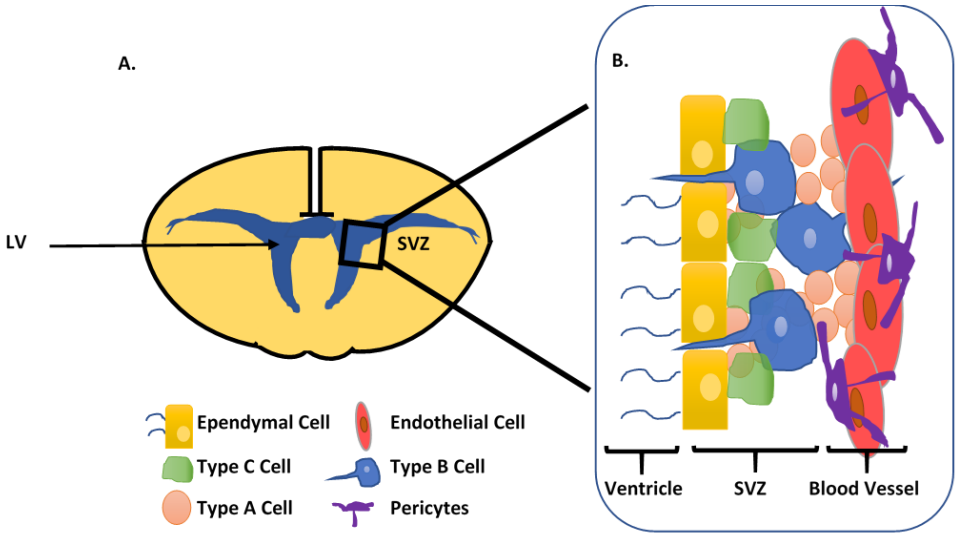

Figure 2. 2: Subventricular zone cytoarchitecture. A) Subventricular zone (SVZ) located on lateral wall of lateral ventricle (LV). B) Resident cells lining ventricles, in the SVZ, and blood vessels.

2.2 Cell Types

Numerous cell types reside and interact in the SVZ. Here, we discuss some of the main cell types, their secreted factors and cellular markers, and their impact on surrounding cell types in the SVZ, outlined in Table 1.

Cell Type	*Markers*	*Secreted Factors*	*Impact*
Endothelial Cells	Tight junction markers (ZO-1, ZO-2, and claudin-5)	PDGFβ	Influence pericytes function
			NSC self-renewal
		PEDF	
	NCAM		NSC proliferation
		Betacellulin	
	Laminin		NSC proliferation
		NT3	NSC quiescence
Ependymal Cells	BMP	PEDF	May promote NSC self-renewal
	β-catenin		
	N-cadherin		Potential role in NSC maintenance
	Vimentin		
	α-tubulin	Noggin	
Pericytes	αSMA	TGF-β	Induce, up-regulate BBB function
		IGF-2	Impact neurogenesis to be explored
Microglia	Iba-1	TNF- α	Monitor brain microenvironment
		IL-1	Phagocytosis of foreign substance
		Cytokines: pro and anti-inflammatory	Inhibit or induce deleterious effects

Table 1. 1: Resident cell types of the subventricular zone niche, including endothelial cells, ependymal cells, pericytes, and microglia, with their respective cellular markers, secreted factors, and impact to other cells present in the niche.

2.2.1 Neural Stem Cells

The goal of stem cell-based therapy is to replace dying and dead cells in the brain to restore damaged neural circuitry. There is a broad pool of stem cells with the potential to be used as therapeutic agents with the goal of *de novo* neuron and glial cell generation in following stroke-induced neurodegeneration [28].

In the adult brain, NSC can be subdivided into 3 types: 1) type-B quiescent stem cells, 2) type-C cells, which are transit-amplifying progenitors derived from activated type-B cells, and 3) type-A neuroblasts, which are formed from amplifying type-C cells that ultimately migrate to the olfactory bulb (OB) where they differentiate into interneurons [29]. Type-B cells, commonly

referred to as SVZ astrocytes, are in close proximity to the vasculature and interact with EC directly. Type-B cells are characterized both by their distinct morphology of long projections with specialized endfeet, as well as their expression of glial-fibrillary acidic protein (GFAP) [30]. Because the interactions between quiescent type-B NSC and EC are key to the stability and remodeling of the SVZ, their relationship remains a highly active area of investigation [9, 29].

NSC are able to generate neural tissue that possesses some capacity for self-renewal, as well as the ability to undergo asymmetric cell division to produce cells other than themselves, including neurons or glial cells [31]. They can give rise to neurons, astrocytes, and oligodendrocytes *in vitro* and *in vivo*, and have been positively correlated with replacement or repair to damaged brain tissue in animal models of stroke. NSC in the adult brain are consistently present in the SVZ and the hippocampus [32]. NSC isolation for use *in vitro* requires excision of these regions of the brain and agitation of the tissue to dissociate cells [31]. *In vitro*, cellular fate has been determined through staining with antibodies specific for neuron-specific class III B-tubulin (TUJ1), a marker specific for identification of NSC derived neurons. GFAP has been used for identification of astrocytes, and galactosylceramide (GalC) is a marker used to identify oligodendrocytes. *In vitro* and *in vivo* observation of NSC differentiation suggests that cell fate to a specific lineage can be induced by withdrawing mitogens or by exposing cells to factors, such as FGF-2, to permit neurogenesis [30, 31].

NSC are located within close proximity to the abundant vasculature of the SVZ. More than 50% of NSC nuclei within the murine SVZ are located within 20 micrometers of blood vessels. Additionally, NSC proliferation occurs close to blood vessels, suggesting that neurogenesis is dependent upon direct and indirect interaction with the vasculature. Endothelial signaling, specifically ephrin-B/EphB, regulates NSC proliferation and niche cell plasticity, while Notch signaling regulates NSC maintenance [33, 34]. These signaling pathways facilitate EC inhibition of NSC differentiation and limit NSC proliferation. EC of the SVZ vasculature are functionally important for the NSC lineage by regulating these cell processes [22].

2.2.2 Endothelial Cells

EC comprise the lumen of the brain microvasculature and are critical for regulating tissue homeostasis and facilitating information transfer between neurons and glial cells. During ischemic stroke, microvascular EC are damaged by oxygen and nutrient deprivation, which results in degradation of tight junctions that produces an increase in BBB permeability. Following stroke, disturbance of the EC framework and local cytokine levels poses danger to the milieu due to EC' role in maintaining the BBB integrity when responding to injury [20].

As previously discussed, angiogenesis and neurogenesis are interdependent processes that intrinsically rely upon each other. In the BBB, the vascular framework is formed through tight junctions, which are responsible for regulating vascular permeability and stabilizing the vessel wall. As the BBB is notably impermeable to large, polar molecules, true biomimetic i*n vitro* models must maintain endothelial specific markers that facilitate vascular integrity and restrict permeability. Experimental use of the immortalized mouse brain EC line, bEnd3 is common because these cells retain the expression of mRNA and proteins that are required for the formation of tight junction proteins. These include zonal occludins-1 and -2 (ZO-1 and ZO-2), and claudin-5 [35, 36]. Utilizing brain EC through benchtop work allows researchers to re-create complex 3D environments and contribute to our understanding on how they contribute to vascular remodeling and BBB breakdown. In addition to controlling differentiation and promoting quiescence, EC are critical for healing the neuronal niche following ischemic damage. Specifically, EC promote NSC survival through Notch signaling regulated growth factor secretion. Growth factors, including vascular endothelial growth factor (VEGF), can stimulate neurogenesis, demonstrating that the NSC lie directly adjacent to the vasculature in an inter-dependent manner, ultimately promoting NSC homeostasis and survival [22].

2.2.3 Pericytes

PC are microvascular mural cells that are instrumental to vasculogenesis, the process of new blood vessel formation during embryonic development, and vascular stability. PC enact their

roles in neurovasculature development and integrity maintenance through direct contact with microvascular EC and exchange of soluble factors between the two cells, where the highest density of PC (EC:PC ratio 1:1) is in neural tissues [37] [38]. PC are capable of expressing proteoglycans, specifically chondroitin sulfate proteoglycan 4, and other extracellular matrix proteins. They are known to support the structure of the microvasculature and provide signals necessary for the differentiation of plastic cells within the SVZ [37]. There is no universal marker to identify PC, rather they are typically recognized by their co-expression of multiple markers and absence of EC, fibroblast, leukocyte, and smooth muscle cell specific markers. Positive identifying markers for PC include chondroitin-sulfate proteoglycan neuron-glial antigen 2 NG2, platelet-derived growth factor-beta (PDGFβ) receptor, and CD13 – a type II membrane metalloprotease (MMP) that is specific for brain pericytes [39]. PC markers may be downregulated during various stages of development and location within organs, suggesting a heterogeneity among PC. PC heterogeneity is correlated with specialized function required for vascular homeostasis in specific microenvironments [20, 39].

PC respond to EC secreted PDGFβ, where PDGFβ receptor is functionally involved in PC recruitment during angiogenesis [39, 40]. PC promote neurovasculature maturation and are influenced by transforming growth factor-beta (TGF-β) to regulate cell proliferation, differentiation, and survival. Secretion of TGF-β by EC is elevated following ischemic stroke, indicating that the injured brain may induce mural cell expansion in order to promote neovascularization and repair [41]. Primary rat brain PC in co-culture with mouse brain capillary EC have exhibited both induction and up-regulation of microvascular integrity. This was demonstrated by a decrease in permeability to sodium fluorescein, where the enhancement of integrity was inhibited when TGF-β activity was neutralized via antibody binding. This suggests that brain PC contribute to BBB maintenance through TGF-β production [42].

Although PC are present in the SVZ niche, their role is poorly understood. The contractile nature of PC is known to regulate blood flow in *ex vivo* cerebellar brain slices and retina

preparations, however the mechanisms driving regulation of capillary tone and blood flow in the SVZ remain unknown [39]. Recent work in mouse models suggests that type-B NSC send projections that ensheath PC on SVZ capillaries may indirectly regulating capillary blood by activating purinergic receptors on PC. Despite their ambiguous role, PC are known regulators of oxygen and glucose, directly impacting niche cell proliferation and metabolic changes within the environment [27]. Continued studies investigating the signaling mechanisms involved in PC regulated blood flow are critical for a better understanding of the neuronal niche.

2.2.4 Microglia

Microglia are resident immune cells known to maintain brain homeostasis. These cells monitor the microenvironment by responding to injury through the secretion of cytokines and phagocytosing cellular debris at the site [43, 44]. Within minutes following stroke, the brain tissue surrounding the core contains activated microglia that accumulate within the lesioned cavity [45]. Microglia are detected using Iba-1 and Mac-2, markers for cells of myeloid origin and activated/proliferating resident microglia, respectively. Flow cytometry provides the ability to distinguish between residential and infiltrating microglia and myeloid cells, defined by low and high expression of cell surface marker CD45, respectively. However, the stability of this marker during pathological state is in question [46].

Microglial activation is triggered by ischemic stroke, where endogenous neuronal-glial interactions are disrupted, leading to upregulation of proinflammatory cytokines. CD200, a transmembrane glycoprotein expressed on neurons, and its receptor expressed on myeloid cells, modulate microglial activation under homeostasis, promoting quiescence until the occurrence of injury. Following stroke, CD200 gene transcription in the ischemic hemisphere is decreased [45], facilitating alternative activation of microglia. In addition, following injury the quiescence of microglia is also disrupted through a decrease in neurons secreting the cytokine fractalkine (CX3CL1). ATP release from dying neurons, as well as monocyte chemotactic protein-1 (MCP-1)

secretion from surrounding brain cells, induce chemotaxis and migration of microglia to the ischemic area [45].

Following tissue damage, changes in microglia migration patterns, cell surface protein expressions, and functions are observed. Motility of microglia towards injury site is seen within minutes. Microglial polarization promotes the development of two phenotypes: M1 or M2. M1 is a classical proinflammatory activation phenotype, increasing pro-inflammatory mediators including TNF-α, IL-6, IL-1, nitric oxide, and proteolytic enzymes including MMP-3 and MMP-9. M2, an alternative activation, releases anti-inflammatory mediators including IGF-1, TGF-B, IL-10, IL-4 and IL-13 [45]The fine-tuned balance of M1 and M2 are offset by stroke. Identifying microglia of each subpopulation can contribute understanding of functional changes post stroke [45].

The proinflammatory mediators associated with the M1 phenotype can be detrimental to injured brain tissue. MMPs breakdown the extracellular matrix (ECM) and BBB post stroke. This adverse effect is diminished using an MMP knock out mouse model, demonstrating less neuronal injury post ischemia. In addition, TNF-α is rapidly up-regulated in the brain following injury within 1 hour after induction of ischemia [47] and inhibition of this pleiotropic cytokine has been displayed in studies to be neuroprotective [48]. Microglia thereby play a detrimental role in the acute phase by exacerbating the inflammatory phase.

Recent evidence suggests that activated microglia may actually provide benefits to the SVZ following stroke by orchestrating brain tissue repair. Following cerebral ischemia in transgenic mice, a resident proliferating microglia population presents an endogenous pool of neurotrophic molecules, including IGF-1, where activated microglial proliferation peaks 48-72 hours post injury [46]. At 72 hours post-ischemic injury, resident microglia undergo proliferative expansion and neutrophil infiltration is diminished, suggesting that microglia are resolving the acute inflammatory phase of repair and promoting reparative environmental remodeling [49]. Stimulating microglial

proliferation can thereby be explored as a therapeutic tool in order to assess the neuroprotective properties of these resident immune cells.

2.3 Role of the Extracellular Matrix

The ECM compromises 20% of the brain tissue volume and presents structural and functional proteins that are necessary for cellular function [50]. Brain-specific ECM varies in density and composition, as well as association with specific neuron types within different areas of the brain. Areas with mature synaptic activity show densely packed areas, known as perineuronal nets, directly impacting neuronal activity in this tight network [51]. The ECM comprises the basement membranes that support epithelia and vascular EC. The BBB contains an endothelium basement membrane in addition to a parenchymal basement membrane. Under normal conditions, these two basement membranes are closely in contact. The parenchymal basement membrane is formed by astrocytes and creates a barrier for leukocyte migration into the brain parenchyma. The anatomical location between EC and astrocytes regulates barrier function, provides physical support and anchoring for cells, and contains ligands that regulate cell processes and signaling through integrin and ECM receptor interactions.

There is a bidirectional relationship between cells and ECM proteins, where ECM proteins, once secreted, interact with cells to both induce and maintain the regulatory properties of this barrier system [52]. These proteins include collagen, fibronectin, laminin, tenascin, and proteoglycans, interacting closely with EC, astrocytes, PC, and microglial, which secrete these proteins post stroke. Many tissue engineering strategies aim to expose cells to an environment within a scaffold that possesses biological ECM-derived molecules to drive cellular function [53].

The general structure of the ECM includes a variety of macromolecules including proteoglycans and fibrous proteins, each of which are expressed to different degrees in tissues throughout the body. For example, more than 20 distinct collagens have been identified which are expressed differentially in specific tissues based on mechanical requirements of the area. Laminins demonstrate multiple isoforms, synthesized by a variety of cells in a tissue specific manner,

expressing explicit α, β, and γ chains. The effect of laminin on adjacent cells is exerted through integrins that recognize laminins, heightening the role of laminin mediating cell-ECM interactions. Laminin 2, specifically, promotes neurite outgrowth from neural cells, where laminin 5 and 10 are seem predominantly in the vascular basement membrane to mediate adhesion of platelets, leukocytes, and EC. The tenascin family, a group of glycoproteins with strikingly diverse expression patterns, possess complex domain structures, implying the molecule can interact with multiple ECM proteins. Tenascins are not expressed in normal adult tissues, however, under pathological conditions, including injury induced neovascularization, tenascin-c is expressed. Proteoglycans, heavily glycosylated proteins consisting of a core protein with covalently attached glycosaminoglycan chains, are grouped into several families, characterized by their composition. For example, decorin, a key member of a leucine-rich repeat proteoglycan family, is involved in signal transduction via EGF receptor. It is involved in modulation and differentiation of epithelial and endothelial cells, and also interacts with TGF-β. The heparin sulphate proteoglycans have high affinity bonding to a range of cytokines and growth factors, including FGF and VEGF, implying a key role in pathological processes including the modulation of cell migration, proliferation, and differentiation. MMPs, the main ECM enzymes with proteolytic degradation potential, are responsible for the constant ECM remodeling, facilitating the synthesis and deposition of new ECM proteins and thereby plays an essential role in tissue repair and cell metastasis. At homeostasis, the adult brain has very little MMP expression and activity, though is the microenvironment is rapidly altered when activated by cytokines and growth factors that trigger tissue remodeling [54]. Overall, this intrinsically complex ECM system is essential for normal development as well as response to disease and injury, consequently there is an intricate interplay between resident cells and this matrix.

2.3.1 ECM-Stem Cell Interactions

ECM components supply a microenvironment that promotes the maintenance of stem cell homeostasis, dictated by signals derived by both ECM-cell interactions and soluble factors.

Integrins, a family of heterodimeric transmembrane receptors connecting extracellular environments to intracellular cytoskeletons, are key receptors that facilitate cellular processes including migration and differentiation. Integrins and cell presented matrix receptors mediate a number of interactions by activating downstream signaling. As an example, integrins directly activate downstream signaling through focal adhesion kinase (FAK) and phosphoinositide 3-kinase (PI3K), thereby regulating self-renewal and proliferation of cells including hematopoietic stem and progenitor cells. Epithelial cells in the brain express high levels of α6 and/or β1 integrins, which heterodimerize in order to generate a laminin receptor [55]. In particular, α6β1 integrin facilitates cell binding to laminin and is required for NSC adhesion to SVZ blood vessels, where adult SVZ progenitor cells express α6β1 receptor. Blocking this receptor inhibits adhesion to EC, negatively impacting SVZ progenitor cell proliferation *in vivo*, and highlights the importance of these integrin mediated interactions [22]. In addition, integrins can bind directly to laminin, collagen, and fibronectin, and to cell-surface adhesion molecules including intercellular adhesion molecule-1 (ICAM-1) and vascular cell adhesion molecule-1 (VCAM-1), both present in the stem cell niche.

In addition to integrins, cadherin molecules mediate both cell-cell adhesions and interactions with cytoskeleton-associated proteins. Scaffold proteins β-catenin and α-catenin can interact with intracellular domains of cadherins, thereby connecting cadherins to the cytoskeletal network and forming stable adherens junctions by clustering cadherin molecules. E-cadherin, expressed by ependymal cells in the SVZ, forms adherens junctions between ependymal cells and NSC. When eliminating E-cadherin *in vitro*, NSC self-renewal is reduced as seen *in vivo* by disrupting E-cadherin through mutations in areas where NSC specifically reside [56]. NSC use both cadherin and integrin to interact with the niche and exploiting the necessity of these adhesion molecules can aid transplantation approaches [57].

The ECM can regulate stem cell activity by non-canonical growth factor presentation. It both avidly binds growth factors, regulating their local availability, and functions as a reservoir, making growth factors unavailable and insoluble. By capturing FGF-2 from the milieu, the ECM

of the NSC niche in the SVZ promotes growth factor activity in the niche and regulates the neurogenic niche. Thereby, the ECM is extremely dynamic in its response to regulating stem cell maintenance and activity by providing and controlling access to growth factors in the milieu [58].

Due to the important role of ECM proteins in cell survival and function, many ECM moieties have been incorporated into engineered scaffolds as a strategy for creating microenvironments that promote neuronal regeneration [59]. Within biomimetic polymer scaffolds, presentation of laminin, collagen, or fibronectin to MSC in culture demonstrates that laminin, in contrast to fibronectin or collagen, is a strong promoter of neuronal differentiation. Laminin also positively impacts neurite length and the formation of a growth cone, the structure that drives axon extension, through integrin-dependent signaling. Laminin-211 can both increase and decrease neurite extension due to the affinity of integrin binding, demonstrating its ability to drive precise and complex integrin mediated pathways [53, 60]. While the entirety of the laminin protein has been used in investigation matrix derived cell function, isolated laminin derived peptides are responsible for specific cell function. Laminin derived peptides, including and Tyr–Ile–Gly–Ser–Arg (YIGSR) and Ile-Lys-Val-Ala-Val (IKVAV) sequences, are responsible for outgrowth of dorsal root ganglion neurons, and are widely utilized in a variety of polymeric based scaffolds [53]. The use of a scaffold to guide cell survival and differentiation *in vivo* includes incorporation of ECM components or derived peptides. As one example, the inclusion of fibronectin derived Arg-Gly-Asp (RGD) to poly-(ethylene glycol) (PEG) hydrogel systems illustrates improved human MSCs cell survival *in vitro*. [61]. Human plasma fibronectin and human plasma fibrinogen demonstrate enhanced survival of cells and increased cell metabolic activity *in vitro* when encapsulating human MSCs in fibronectin or fibrinogen containing hydrogel capsules, most likely due to integrin clustering and activation of extracellular signaling cascades such as the mitogen activated protein kinase cascade [62]. Thereby, the use of ECM proteins can enhance therapeutic cell survival *in vivo* by triggering native cell pathways.

2.3.2 ECM Following Stroke

Following stroke, basement membranes of the BBB are degraded. New ECM proteins are deposited, either by secretion of ECM proteins, or leakage of plasma proteins into the CNS. Degradation of basement membranes after stroke demonstrates notable changes at later time points after injury, for instance, 12-18 hours after MCAO in a rat model, although changes in cell presented matrix receptors occur within a few hours. Degradation occurs through proteolysis, mainly by MMPs and plasmin, where these are up-regulated and activated following pathological conditions such as stroke [52]. MMP-9, synthesized by both macrophages as well as EC, is present within and at the periphery of infarct within 24 hours, thereby creating a significant disturbance to BBB integrity following stroke. These degradation pathways are correlated with increased BBB disruption, as well as secondary inflammation and edema and the promotion of vascular permeability [63].

As an inherent method of tissue repair following stroke, ECM proteins are deposited or penetrate the CNS to recover the structure of the microenvironment. In particular, osteopontin (OPN), a secreted glycosylated phosphoprotein, binds receptors that act on several cell types, and is expressed in neurons, macrophages, and astrocytes. Following stroke, OPN is upregulated around the infarct zone, and appears to be beneficial after ischemic insult. In rat pups, OPN injections are correlated with reduction in infarct volume and improvement in functional recovery following ischemia [52]. Fibrinogen, a major plasma protein involved in blood coagulation, cannot normally penetrate the CNS parenchyma due to the BBB. In stroke, however, fibrinogen can occlude blood vessels and leak in the brain, forming deposits and potentially increasing inflammation. In order to remove fibrin to re-establish blood flow, enzymatic degradation by plasmin as well as MMP-2/9 activity is mechanistically helpful. [52]. Considering the alteration of the ECM composition in response to BBB disruption and the direct impact on neurologic disease are functionally important when considering ECM functions in physiology and disease pathology.

2.4 Cell-based Therapies

Cell therapies have demonstrated some ability to induce spontaneous recovery following stroke and can promote endogenous neurogenesis [64]. Current methods of cell therapy include exogenous, autologous, and allogenic cell delivery into experimental stroke models, each presenting their own set of advantages and drawbacks. Exogenous cell therapy, in which cells are derived from a source external to the stroke, has demonstrated impact on cell migration, survival, and differentiation which subsequently promote functional recovery in animal models. However, these transplanted cells may induce an immunogenic response. An alternative to exogenous cell therapy is the use of autologous cells, which avoids the risk of rejection. This therapy presents its own challenges, though, as limited access to these cells often requires *in vitro* expansion, which may delay treatment. Allogenic cell therapy, or transplanting stem cells from a genetically similar donor, is potentially the most successful method of cell transplantation. The use of allogenic cells presents advantages of reduced immunogenicity, in addition to being readily available. Of note, ongoing research is still required in order to improve patient selection regarding eligibility for allogenic based therapy [64]. Stereotaxic implantation, a minimally invasive surgical method relying on exact 3D coordinate anatomical systems, is challenging due to time constraints, where lesion size varies greatly over time and from patient to patient. Intravenous (IV) delivery, a non-invasive delivery route, can overcome this set back, though there is a lack of a direct pathway of cells to the ischemic area. Although intra-arterial (IA) delivery can deliver cells to the peri-infarct area directly, occlusion of the target artery that persists can create a blockade for a route of delivery while also compromising survival of delivered cells [64]. Interestingly, there is a lack of evidence that IA delivery is superior to IV when delivering bone derived mesenchymal stem cells to a mouse stroke model. With no difference in functional or structural outcomes detected [65], the ideal route of administration to optimize the effect of cell therapy, in particular that of stem cells, remains a matter of debate.

Stem cells can be used in stroke therapies to dynamically respond to a stroke damaged tissue, in which stem cells have phenotypic properties that allow direct interaction with the host environment. Engrafted stem cells, unlike terminally differentiated cells, can respond dynamically to temporal and spatial changes of the environment that follow ischemic injury [64, 66, 67]. Delivery of stem cells to a brain-injury site has effectively reduced lesion size and host cell death. Additionally, successfully delivered stem cells have the potential to replace lost circuitry by forming new synaptic contacts. Even the use of stem cell xenografts in animal models has been shown to decrease infarct area, promote expression of the neuronal proteins such as synaptic proteins, and restore synaptic activity. In fact, stem cells can also strengthen existing synapses [14, 68], promoting enhanced signaling among uninjured neurons. Further, an induction of host brain plasticity has been observed following exogenous cell engraftment. In this context, increased levels of factors, including fibroblast growth factor (FGF) and brain derived neurotrophic factor (BDNF), that induce angiogenesis resulted in successful integration of transplanted cells with the host circuitry, as well as increased neovascularization and recruitment of endogenous progenitors [14, 28].

The use of cell therapy requires collaboration between neurologists and engineers to create new and effective delivery methods. Cellular behavior manipulation and induction are explored to enhance cell state prior to and after delivery [69]. The approaches utilized for cell transplantation, including the control of differentiation and proliferation, are necessary to provide insight for *ex vivo* models that address relevant biological questions regarding SVZ cell interactions. Fundamental considerations include the cell type, cell number, and delivery vehicle and route.

2.5 Limitations to Successful Cell Therapy

The major restriction to successful transplantation of neural cells into the stroke damaged area has been the survival of exogenous cells, which ranges from 1-32% [70]. Cell survival is compromised by delivery mechanisms that increase distorting force during syringe needle flow such as pressure drop, shearing and stretching forces [71]. Viscosity and composition of delivery

fluid contribute to cell distribution in solution and shear forces applied to cells during delivery. Additionally, sedimentation in carrier fluid becomes a limiting factor in successful cell delivery, causing the first partial injection volume to contain more cells than those delivered later. In order to achieve precise cell suspensions and cells with minimal damage, cellular delivery methods are the focus of innovation and optimization in stroke recovery therapeutics [71, 72].

The BBB and CSF barrier pose limitations to delivering therapeutics to the brain. Established delivery methods can be invasive, causing further damage to the ischemic area. Although systemic, intravenous delivery methods can be non-invasive, they often lead to an accumulation of cells in clearing organs, including kidney and spleen, rather than the brain. Targeted intracerebral cell injection can be applied directly to the peri-infarct region, however the multiple injections required to deliver adequate numbers of cells can cause further damage to the already injured tissue [44]. With minimal damage to an already fragile environment, invasive approaches are unfavorable due to the threat of further disruption of tissue and the BBB. Recent advances take these limitations in current therapeutic strategies into account, focusing on development of minimally invasive and non-damaging injections or delivery routes.

Biomimetic strategies face obstacles when considering clinical translation due to the fact the optimal cell type for transplantation therapy has not been determined. The use of stem cells is impacted by ethical issues, where fetal and embryonic derived cells can create controversy. Generating an abundance of cells that maintain and recapitulate stemness is a challenge that limits the use of other cell types. Just as it has been seen with direct implantation and delivery of stem cells, many restrictions impact the success of these new therapies. First, the stroke injured brain may compartmentalize areas of damaged tissue, creating a physical barrier to therapeutic deliveries. Stroke injured brains also contain varying degrees of necrotic, avascular tissue, limiting access to systemic delivery of materials and cells through the vasculature. The variation in injury observed from person to person in each stroke occurrence causes significant difficulty in normalization of therapeutic methods. Due to the high variability of tissue damage and resultant function between

patients, there is a lack of a standardized way to quantify both the severity and recovery of the disease. To form an effective therapy, these ambiguities must be addressed to formulate a common language that can measure functional outcomes in stroke trials

2.6 Biomaterial-based Biomimicry

We have detailed the importance of native and remodeled microenvironments in the SVZ and their role in driving cell function. The resident cell types have been described in addition to the ways these cells interact and impact one another. Both direct and indirect interactions with ECM molecules impact cell behavior, providing biomimetic scaffolds the opportunity to regulate cell behavior by modifying scaffolds to provide cues that cells in the host environment would have [53]. Together, knowledge of SVZ cells, exogenous cells, and the ECM molecules that control cell fate and maintain the SVZ niche, tissue engineers can create biomaterials to produce a bio-replicative system that may improve experimental and therapeutic approaches.

Ideally, direct implantation of a biomaterial into the stroke damaged area would promote cell adhesion and survival, cellular cues for healthy tissue development, and induce the recovery of the damaged ischemic core. Here, we discuss critical scaffold attributes required to facilitate post-stroke healing in the brain, and two classes of biomaterials that have been demonstrated advantageous for brain repair: synthetic and natural materials.

2.6.1 Considerations for Development of an Ideal Scaffold

The goal of a biomimetic scaffold is to facilitate neural tissue regeneration and functional recovery following stroke. A scaffold must promote survival and proliferation of transplanted cells within the damage site, engage healthy interaction with endogenous cells, and promote the recovery of damaged neural circuitry. The mechanical and physical properties of a biomaterial impact the administration of the scaffold, the target injection site, and endogenous/exogenous cell response. Solid scaffolds must present a compressive modulus allowing for cell survival rather than promoting tissue stress and damage upon implantation. A decrease in NSC proliferation in 3D

alginate scaffolds is correlated with an increase in the material modulus, where the greatest differentiation expression was attributed to the softest hydrogels. These soft hydrogels possess an elastic modulus comparable to brain tissue (100-1000 Pa) [73]. In addition to mechanical constraints, the initiation of the cellular and molecular cascade following transplantation must be considered. A biocompatible material is one that can coexist with living tissues without eliciting a local and systemic immune response in host tissue. Biocompatible materials do not promote a foreign body response, do not produce cytotoxic effects to the milieu, and limit the inflammatory and immune reaction in the brain [4]. Byproducts from biomaterial degradation can be bioactive, influencing the surrounding environment and affecting both host and transplanted cells, thereby producing detrimental effects. Photopolymerization processes, which are crosslinking reactions that occur with light exposure, are often used for hydrogel production, however these reactions can lead to the formation of free radicals that compromise cell survival. Polymers that can polymerize at physiological conditions, dependent on temperature or pH, avoid these potential toxic effects [44]. Consideration of how biomaterials will interact with host tissue is critical to contribute to functional recovery of both the infarct area and surrounding tissues.

Scaffold degradation over time to create or restore neural circuitry in stroke-damaged tissue. Degradation allows for integration of transplanted cells into the cavity. There is a fine balance between supporting cells during transplantation and controlling the rate of degradation. Injectable biomaterials, including hydrogels, are attractive candidates for stroke injury lesion cavities, which vary in size and morphology between patients. Hydrogels that structurally fill the cavity space and induce repopulation of cell depleted tissue space can be advantageous, if the mechanical properties are controlled in a manner that avoids further damage to the lesion cavity caused by increased intracerebral pressure with large volume of hydrogel injection. In fact, Modo et. al. observed that microglia and astrocytes were able to infiltrate an ECM hydrogel where cell infiltration allows for a repopulation of host cells and ECM remodeling [74]. While bulk hydrogel implantation into infarcted and lesion cavities has demonstrated some benefit, implantation of

microencapsulated biological moieties has also demonstrated promise around stroke recovery and repair. Microencapsulation techniques in which cells are encapsulated in approximately 95 microsphere diameter polymeric hydrogel spheres can be used to control the microenvironment an implanted cell is initially exposed to, thereby maintaining proper function of the cell type. In particular, is the maintenance of cell function is applicable to the SVZ niche where the cytoarchitecture organization is important to maintaining cellular and biochemical cues [75]. Growth factor incorporation into biomaterials can contribute to creating biomimetic microenvironments. As one example, growth factors, including IGF-1, that are encapsulated into gelatin microspheres, promoted increased endogenous neurogenesis in the SVZ of adult mice. Hepatocyte growth factor containing microspheres also increased neuroblast migration from the SVZ to the stroke-injured tissue in the same model [76]. FGF-2 in heparin-chitosan scaffolds demonstrates sustained survival and growth of NSC, where these multifunctional, biocompatible microspheres are optimized for NSC grafting [77]. The use of stem cells and growth factors in conjunction with biocompatible and degradable scaffolds shows high potential to create a microenvironment that promotes functional recovery following injury. The use of 2D polymer scaffolds has been advantageous as a means of exploring conditions for optimal cell growth and survival, for probing cell-surface interactions, and for trialing manipulations of the microenvironment that are impactful to cell response. In fact, such models that have been used to deconstruct the SVZ niche include the presentation of FGF covalently attached to a network of polyamide nanofibers. The scaffold maintained biological efficacy of FGF-2, strongly activating FGF receptors [78]. In addition, EGF tethered to poly(methyl methacrylate)-graft-poly(ethylene oxide) promotes MSC spreading and survival around the biomaterial [79]. These advantageous promote the use of 2D polymeric substrates as bioreplicative constructs is a method of optimizing conditions for cell culture prior to advancement to 3D replicates of the SVZ niche. In a 2D model, cell-cell adhesions are confined to a horizontal plane, while a 3D model allows for adhesions on all

sides. A 3D environment constrains cells to an artificial niche, enabling dynamic variation or continuous remodeling, which are not capable in a 2D monolayer model.

Elastic, polymeric scaffolds make an ideal candidate for neurosurgical techniques to deliver scaffolds to the SVZ. While the goal is to fill the stroke cavity with a pliable and tunable scaffold which resembles mechanical properties of the native environment that will temporarily replace lost tissue, the material must also promote the infiltration of new and healthy cells. Rat-derived NSC vary their cellular fate depending on the hydrogel stiffness, stressing the importance of biomaterial mechanical properties on differentiation potential [80]. Stiffness and diffusion capacity must be carefully assessed prior to scaffold delivery to avoid detrimental effects to surrounding tissues in addition to differentiation to undesired cellular fates.

2.6.2 Synthetic Polymeric Materials

Synthetic biomaterials enable direct control of key properties, including degradation rate, material stiffness, and protein incorporation. Cell incorporation in combination with these materials calls for careful observation of cell-scaffold interactions, consequently allowing for control of cell processes such as differentiation, morphological formation and extension to ultimately enhance connectivity in the ischemia area [44].

2.6.2.1 Poly-(ethylene glycol)

PEG is a biologically inert, non-toxic polymeric material, presenting excellent biocompatibility and resistance of protein adsorption. The mechanical properties of PEG depend on its molecular weight, as increasing the chain length of PEG increases stiffness and viscosity [81]. PEG can be chemically modified by tethering peptides or proteins through cross-linking reactions. Due to its inert nature, the incorporation of biologically active peptides cell-adhesive peptides, such as RGD and YIGSR, promotes cell attachment to the material [82]. PEGylation, the process of attaching PEG polymer chains to molecules and macrostructures, changes the chemical and physical properties of the material [83], making PEG a highly used polymer in a broad spectrum

of tissue engineering applications. PEG-based microspheres modified by adhesive sequence RGD and metalloproteinase sensitive sequence have been utilized to encapsulate murine neural stem cells and brain endothelial cells, demonstrating 60-80% cell viability, cell spreading, and migration through the scaffold [75].

To observe PEG as a candidate for neural repair and recovery, degradation characteristics as well as delivery of both cells and growth factors are under investigation. As one example, varying mass profiles of PEG were examined. The astrocyte response varied with degradation rate, where slowly degrading/non-degrading gels display a prolonged astrocytic response. Astrocytes extended their processes into the hydrogel, where microglia infiltrated the hydrogel and facilitated the enzymatic process. Hydrogels decreased acute microglial response during the week following implantation, suggesting PEG based materials are beneficial for CNS delivery for both drugs and cells [84]. In addition, PEG-based hydrogels with increased lactic acid content and encapsulated neural cells, including postmitotic neurons and multipotent precursor cells, demonstrate an increase in cell proliferation and survival, establishing an advantage of rendering PEG materials as degradable in order to be relevant to neural cells delivered to the stroke injured brain [85]. Delivery of EGF using modified PEG hydrogels demonstrates a significant increase in tissue penetration as well as endogenous NSC and progenitor cells in the SVZ when delivered to the ventricles of the brain. PEG modification in this way decreased EGF degradation by proteases, allowing for a greater protein accumulation in surrounding tissues, penetrating deeply into the tissues, seen in both the healthy and stroke injured mice brain [86]. Thereby, these studies provide support for the use of PEG as a highly adaptable and tunable scaffold to be utilized for delivery of both cells and growth factors in stroke repair applications.

2.7 Mimicking Stroke *In Vitro*

The primary cause of neurological damage post stroke is neuronal damaged caused by ischemic conditions and reperfusion injury. Ischemia can limit the supply of oxygen and glucose to the brain and has detrimental effects on cell survival. Typically, mimicking stroke-like conditions

in vitro utilizes an oxygen glucose deprivation (OGD) environment. Through these conditions, NSC respond to stress signals similar to how they would in the cytotoxic, damaged brain *in vivo*. OGD is induced by removal of oxygen and glucose or via chemical or enzymatic inhibition of metabolism. For removal of oxygen, the normal O_2/CO_2 medium is replaced with N_2/CO_2 equilibrated medium, and cells are maintained in a hypoxic chamber, and for removal of glucose, glucose free medium is used. The exposure to OGD may vary, and experiments may allow for a re-oxygenation period to stimulate the reperfusion stage in transient ischemia *in vivo.*

It has been demonstrated that diffusible secreted signals from EC can increase survival, proliferation, differentiation, and migration of SVZ NSC both *in vitro* using an OGD model and *in vivo* during ischemia [87-89]. Such factors include BDNF and VEGF upregulated in response to injury [12, 90] In addition, NSC have been shown to proliferate and differentiate during hypoxic conditions [90-92]. While it is known soluble factor secretion of EC play a role in promoting NSC survival during OGD, the mechanism as to how EC may play a role during solely glucose deprivation has been poorly investigated. In fact, there evidence that glucose deprivation is the detrimental factor during OGD, as neurons and neural progenitor cells have shown a reduction in cell viability without glucose in the presence of oxygen [92, 93].

2.8 NSC Migration in Response to Injury

In addition to a need for therapeutics to address endogenous cell viability, platforms by must support, and if not, enhance, native cell migration. During injury, NSC from the SVZ, the largest area pool of proliferating NSC in the adult brain, become activated. For NSC to differentiate into the functionally specific cell types that comprise healthy brain tissue, they must first migrate rostrally into the OB. This process is dependent upon signaling from microvascular EC and PC within the SVZ, ultimately directing NSC along the rostral migratory stream (RMS) to the OB. This pathway is dictated by homophilic and vasophilic migration, where chains of migrating NSC, known as neuroblasts, use each other's somas to cluster and for a chain migration. NSC use blood vessels to guide vasophilic locomotion, although the exact mechanisms that guide neuroblast

migration along vessels without direct contact to EC are not fully understood. Neuroinflammation following injury induces upregulation of chemokines and growth factors including CXCL12, monocyte chemoattractant protein-1 (MCP-1), VEGF, and BDNF. EC secretion of CXCL12 as well as angiopoietin-1 secretion from remodeling blood vessels after lesion initiate NSC migration [18]. Although many EC secreted factors have been characterized, the release of chemokines and growth factors by PC during this migration has yet to be elucidated.

In addition, it is unknown as to how vascular signaling cues promote NSC to cluster into their migratory phenotype. A study by Klingener *et al.* conducted proteomic analysis to distinguish SVZ proteins present during injury. These proteins played roles in progenitor cell proliferation, adhesion, and migration, such as N-cadherin. N-cadherin is upregulated in response to injury, where injury simulates increased levels of heparin-binding epidermal growth factor (HB-EGF). This activates EGF receptor (EGFR), that leads to disintegrin and metalloproteinase domain-containing protein 10 (ADAM10) activation [94]. ADAM10 is responsible for the shedding of N-cadherin, and this cleavage allows for exposure of the homophilic binding site on NSC. N-cadherin cleavage, therefore, allows for neural progenitor cytoskeletal rearrangement and polarization, and *ex vivo* data from this group suggests N-cadherin-mediated cell polarization is a prerequisite for directional migration. There is a need for further investigation as to how vascular cells play a role in the cleavage of N-cadherin. Understanding how vascular cells can direct NSC migration and promote their clustering can improve current therapeutics by encouraging NSC transition into this pro-migratory state.

2.9 Motivation for Work

There is a great need for a therapeutic against neurological diseases, particularly stroke. Although stem cell therapies in theory have a plethora of benefits, their delivery to an injured environment is a significant challenge. To overcome the limitations of our current delivery systems, researchers can use the intricate coupling of neurogenesis and angiogenesis to complement implantation of NSC. Specifically, EC and PC are known to impact the BBB prior to and post

injury, and their proximity and interactions via cell-cell contact and soluble secretion are under investigation. The insight gained from probing the mechanisms by which EC and PC can support NSC functionality can revolutionize the status of delivery vehicles to promote functional recovery following ischemia.

Chapter 3: Endothelial cell secreted metalloproteinase-2 enhances neural stem cell N-cadherin expression, clustering, and migration

Portions of this chapter were printed with permission from Matta *et al.* 2021[95]

3.1 Abstract

Neuroblasts have a clustered phenotype critical for their unidirectional migration, which in part is dependent on signaling from microvascular endothelial cells (EC) and pericytes (PC). Diffusible signals secreted by vascular cells have been demonstrated to increase survival, proliferation, and differentiation of subventricular zone resident neural stem cells (NSC); however, the signals that promote the necessary initiating step of NSC clustering are undefined. To investigate the role of vascular cells in promoting NSC clustering and directing migration, we created a 3-D hydrogel that mimics the biomechanics, biochemistry, and architectural complexity of brain tissue. We demonstrate that EC, and not PC, have a crucial role in NSC clustering and migration, further verified through microfluidic chamber systems and traction force microscopy. Ablation of the extended NSC aggregate arm halts aggregate movement, suggesting that clustering is a prerequisite for migration. When cultured with EC, NSC clustering occurs and NSC coincidentally increase their expression of N-cadherin, as compared to NSC cultured alone. NSC presented N-cadherin expression was increased following exposure to EC secreted metalloproteinase-2 (MMP2). We demonstrate that inhibition of MMP2 prevented NSC N-cadherin surface expression and subsequent NSC clustering, even when NSC were in direct contact with EC. Furthermore, with exogenous activation of EGFR, which serves as a downstream activator of N-cadherin cleavage, NSC form clusters. Our results suggest that EC secretion of MMP2 promotes NSC clustering through N-cadherin expression. The insight gained about the mechanisms by which EC promote NSC migration may enhance NSC therapeutic response to sites of injury.

3.2 Introduction

In the subventricular zone (SVZ), there are three types of neural stem cells (NSC) that are responsible for tissue homeostasis and response to injury - type A, B, and C. In healthy conditions,

type B cells are quiescent NSC that intricately contact the ependymal cells that line the lateral ventricle. These cells are also directly in contact with endothelial cells (EC) and pericytes (PC) that compose the vasculature [22]. The contacts between NSC and resident cells enable NSC to receive soluble signals and environmental cues from both the lateral ventricle, the circulating blood, and the microvasculature itself. During the acute phases of brain injury, activated type B cells give rise to proliferating type C cells, ultimately generating type A cells, known as migratory neuroblasts [96, 97]. As injury persists, neuroblasts migrate towards the olfactory bulb (OB) as a cluster. NSC aggregates travel via a clustered chain-like migration, through a network of interconnecting paths that converge to give rise to the rostral migratory stream (RMS) [22, 98, 99]. Migrating NSC are ensheathed by glial fibrillary acidic protein positive astrocytes [100] which enclose neural cells that are positive for doublecortin, a microtubule-associated protein required for migration [101]. Once NSC have migrated to the OB, they differentiate into interneurons, which allows them to directly repair the injured and indirectly signal for additional cell contribution to tissue remodeling and repair. In total, the ability of NSC to migrate through the RMS pathway, differentiate at the OB, and promote repair to damaged tissue highlights their importance in endogenous repair mechanisms.

Neural and vascular interactions are highly coupled and dependent upon each other. Specific to the brain, NSC intricately interact with EC and PC in the neural niche, likely due to the uniquely high density of EC:PC (1:1) in the brain's microvasculature [22, 102]. The abundance of EC and PC in this region suggests that soluble and insoluble signal exchange between vascular cells and NSC are necessary for function in both healthy and pathological states. In fact, in the healthy neural niche, EC promote NSC self-renewal, inhibit NSC differentiation [103], and maintain NSC quiescence via direct cell contact [104]. Recently, we demonstrated that co-delivery of encapsulated NSC and EC to the non-injured mouse brain maintained NSC quiescence both prior to and post-delivery [105]. By harnessing the ability of EC to enhance NSC functionality, investigators have developed methods to improve stem cell delivery strategies, further

strengthening the hypothesis that vascular cells may regulate important NSC function as an effective therapeutic approach to neural injury and disease recovery.

While we understand that EC have a specific role in the regulation of NSC proliferation, activation, and differentiation, to date, several gaps remain in our understanding of vascular regulation of NSC migration. Broadly, vasophilic guidance is known to direct NSC migration through the RMS. The vasculature is arranged parallel to the NSC migration route, allowing neuroblasts to directly follow vascular EC and PC, using microvessels to guide vasophilic migration. This directional migration is regulated by chemoattractants secreted by vascular cells, including vascular endothelial growth factor (VEGF) which activates VEGF receptor 2 [106, 107] and stromal cell-derived factor-1 (SDF-1) which in turn activates C-X-C motif chemokine receptor 4 [108, 109]. Neuroblast clustering occurs though NSC-NSC homotypic and heterotypic gap and adherin junction binding [98, 99]. These junctions allow NSC to guide one another, as links in a chain, during migration through each region of the RMS. In fact, pharmacological decoupling of NSC adherens junction binding can halt NSC migration in the SVZ and RMS, as demonstrated by migration experiments in explanted tissue [99]. The requirements for vascular engagement and NSC-NSC signaling have been demonstrated to be required for efficient and functional neuroblast migration from the SVZ. However, many of the mechanisms that initiate the distinct steps that promote chain-like directional migration require further investigation, including, the mechanisms that drive the initiating and necessary step of NSC clustering.

Proteomic analysis of SVZ tissue has identified multiple proteins upregulated during injury, many of which play roles in progenitor cell proliferation, adhesion, and migration. Of these, N-cadherin, a transmembrane adhesion molecule which mediates calcium-dependent cell-cell adhesion, is upregulated in progenitor cells following injury. Coincidentally, injury leads to increased levels of heparin-binding epidermal growth factor (HB-EGF) which subsequently activates the epidermal growth factor receptor (EGFR) [94]. This results in disintegrin and metalloproteinase domain-containing protein 10 (ADAM10) activation and shedding of

membrane-presented N-cadherin. N-cadherin is cleaved from the cell membrane, releasing the extracellular domain, which contains homophilic binding sites [110], thereby enhancing NSC-NSC adhesion. *Ex vivo* data suggests that N-cadherin-mediated cell polarization is a prerequisite for directional migration. This cell polarization facilitates enhanced migration out of the SVZ, signifying a role for the EGFR, ADAM10, and N-cadherin signaling pathway in the neural reparative processes [94]. Secondary mechanisms of EGFR activation have been identified, including activation of EGFR through the binding of matrix metalloproteinase-2 (MMP2) [111]. Because EC secrete high levels of MMP2 [105], it is likely that EC play a direct role in regulation of N-cadherin mediated cytoskeletal remodeling that facilitates NSC clustering**.** Specifically, here, we test the hypothesis that EC secretion of MMP2 activates EGFR, leading to N-cadherin cleavage by ADAM10, NSC polarization that facilitates cluster formation, and NSC migration.

Much of the work described above and those of typical *in vitro* NSC migration assays use commercially available transwell inserts; however, the stiffness of polycarbonate transwells (~2.5 GPa) [112] does not mimic the viscoelastic mechanics of brain tissue (~1,000 Pa) [113]. Mechanotransducive signaling is key to cell migration, and therefore, limits the ability to translate the findings from transwell experiments into a corollary of the *in vivo* migratory processes. Beyond mechanical properties, transwells contain pores of specified size with regular pore distribution, which differs from the naturally fibrillar and porated cytoarchitecture of brain tissue. Finally, transwells often have coatings with soluble extracellular matrix (ECM) proteins, providing a 2D presentation of proteins that are, *in vivo*, presented in a matrix ligated 3D structure. To overcome the limitations of biomechanics, biochemistry, and microenvironment architecture encountered with the commercial transwell system, we have created a porous, fibrillar, and tunable poly-ethylene glycol (PEG)-based scaffold with an elastic modulus similar to that of brain tissue. Using this engineered biomimetic scaffold, we can observe NSC migration under conditions that more closely replicate those of the human RMS.

Using our 3D biomimetic scaffold, we have conducted migration experiments with NSC monoculture or NSC in the presence of vascular EC, PC, or EC and PC. Our results demonstrate that NSC-EC cell contact and EC secreted factors promote NSC clustering and direct NSC migration. This is in stark contrast to PC, which we demonstrate have negligible direct effect on NSC clustering and migration. Clustering is an inherently mechanical behavior, in that cells must coordinate cell-cell adhesion, cell-ECM adhesion and internal force generation. The latter involves the generation of surface traction, cytoskeletal-based forces transmitted through focal adhesions that underlie forward motion. By imaging cluster motion on compliant substrates, we show that motion is initiated through the extension and adhesion of a leader arm that generates traction stresses and guides forward motion. Upon laser ablation of this arm, traction stresses are attenuated, and motion is reduced, highlighting the importance of NSC clustering prior to migration. We further validated these results using microchannel experiment chambers to observe NSC clustering and migration with and without EC secreted factor accessibility. Our findings suggest that NSC only cluster when provided access to EC secreted factors. EC secrete significantly higher levels of MMP2 compared to NSC, which allow for increased NSC clustering and N-cadherin expression, completely diminished through inhibition of MMP2. In contrast, exogenous EGFR activation in the absence of MMP2 activation, NSC do cluster, supporting our hypothesis that EC secreted MMP2 can lead to N-cadherin cleavage and NSC clustering. By furthering our understanding by which vascular cells promote NSC migration, we can enhance the state of current therapeutic approaches for NSC delivery in injury models.

3.3 Materials and Methods

3.3.1 Cell maintenance

Established adherent neural cell lines (ANS4; kindly provided by S. Pollard) cultured in serum-free basal medium were supplemented with N2, B27, laminin, and 10 ng/mL EGF and FGF-2. GFP transfected ANS4s (NSC-GFP) were used to recognize ANS4 in co-cultures [114]. The

immortalized mouse brain endothelial cell line (bEND.3, ATCC) was cultured according to manufacturer's protocol, using DMEM, 10% fetal bovine serum and 1x Penicillin/Streptomycin. We assessed the purity of bEND.3 through flow cytometry to verify EC are $CD31^{+}$/VE-$Cadherin^{+}$ and VE-$Cadherin^{+}$/$CD45^{-}$ (Supplemental Figure A1.1). Fibroblast growth factor-2 (FGF-2), present in NSC media, has been demonstrated to stimulate EC function to increase proMMP2 and stimulate MMP activation [115], thereby we are utilizing activated EC when cultured in NSC media to mimic injury. The mouse brain vascular pericytes cell line (MBVP, ScienCell) were cultured according to manufacturer's protocol using Pericyte Medium (PM, Cat. #1231). For ANS4, bEND.3 (EC), and MBVP (PC), culture medium required changes three times weekly and maintenance at 37°C in 5% CO2 atmosphere. PC temporarily dyed with PKH26 red fluorescent cell linker kit (Sigma) according to manufacturer's protocol distinguished cells in co- and tri-culture experiments.

3.3.2 Scratch assay

NSC-GFP, EC, and PC were cultured in 12 well plates at a density of 100,000 cells/ml and maintained in NSC media. Co-cultures of NSC+EC and NSC+PC, and EC+PC had a 1:1 cell ratio maintained in NSC media. Tri-cultures of NSC+EC+PC had a 1:1:1 cell ratio maintained in NSC media, with PKH26 dyed PC. Following 24 hours, a scratch using a 10-microliter pipette tip and a ruler was created down the middle of every well that allowed for imaging at 0, 24, and 48-hour time points (3 images/well). To quantify percent closure using ImageJ, we calculated ((initial distance - final distance)/ initial distance) x 100. In addition, we quantified the number of NSC clusters formed and cluster area produced using ImageJ.

3.3.3 Polyacrylamide gel preparation

Traction force microscopy (TFM) experiments were carried out on polyacrylamide (PA) gels that were polymerized onto 25mm diameter coverslips. Briefly, the coverslips were treated with a combination of aminopropylsilane (Sigma Aldrich) and glutaraldehyde (Electron Microscopy Sciences) to make the surface reactive to the acrylamide. The ratios of polyacrylamide to bis-

acrylamide for the gels used were 7.5%:0.03% and 7.5%:0.1% to yield gels with an elastic modulus (E) of E=0.7 kPa and 2.8 kPa, respectively. A concentration of 0.05% w/v ammonium persulfate (Fisher BioReagents) and 20nM beads (Molecular Probes) were embedded in the gel mixture prior to polymerization. 15 µl of the gel solution was added to the coverslip and covered with another coverslip, which was made hydrophobic through treatment with Rain-X®. The gels were polymerized on the coverslips for 30 minutes at room temperature, then reacted with the standard 1mg/ml Sulfo-SANPAH (Thermo Fisher Scientific). The surface of the gels was then coated with fibronectin (F002, Sigma-Aldrich) at a 1mg/ml concentration. The reaction proceeded for 12 hours overnight incubated in the dark, and the coverslips were rinsed and stored in 1X PBS.

3.3.4 Aggregate preparation

NSC aggregates were prepared from confluent cell cultures using a suspension-spinning method. Aggregates ranging from 40 to 200 µm in diameter are obtained from 5 ml of cell suspension in CO_2-equilibrated culture medium at a concentration of 4×10^5 cells per mL in 25 ml Erlenmeyer flasks, which were placed on a gyratory orbital shaker at 75 rpm at 37°C for 5-10 hours. The flasks were pretreated with 2% dimethylchlorosilane in chloroform to prevent adhesion of cells to the glass surface.

3.3.5 Traction force microscopy

TFM was used to measure the forces exerted by cells on the substrate. Time-lapse confocal imaging of small NSC aggregates were performed for 12 hours on 0.7kPa and 2.8 kPa PA gels. “Force-loaded” images (with cells) of the beads embedded in the polyacrylamide gels were obtained using a 20X objective (Leica Microsystems). The “null-force” image was obtained at the end of each experiment by adding detachment enzymes to the cells for 1 hour. Images were aligned to correct drift (StackReg for ImageJ) and compared to the reference image using PIV software (http://www.oceanwave.jp/softwares/mpiv/) in MATLAB. The traction forces were used to

calculate the energies of deformation (strain energies) in the substrate using the spatial distribution of forces F and displacements x, using custom-written code by Ulrich Schwarz [116].

3.3.6 Laser ablation

Laser ablation was performed using a 435 nm laser (Andor Technology). A 20X objective (Leica Microsystems) was used for ablation and the laser power was held at 90%. The leader cell of the extended arm from aggregate was ablated at the leading edge at a single point. Images were acquired before and after ablation for 1 second intervals for 16 minutes with a confocal microscope (ANDOR, Oxford Technologies, Belfast, Northern Ireland).

3.3.7 Conditioned media studies

In a 12 well plate, NSC were cultured at a density of 100,000 cells/ml, and in a separate plate, EC, PC, and EC+PC at a 1:1 ratio were cultured in NSC media. After 48 hours, we washed the NSC monolayer with PBS 3x and then treated the NSC monolayer with conditioned media (CM) from the EC, PC, and EC+PC plate. We imaged wells after 24 hours and quantified the number of NSC clusters formed and cluster area using ImageJ.

3.3.8 Phalloidin staining

NSC fixed with 4% paraformaldehyde (PFA) were stained for F-Actin using Rhodamine Phalloidin (ThermoFisher, 1:200), then mounted with Dapi (Vector Laboratories). Samples were imaged using fluorescent microscopy (Leica).

3.3.9 Microchannel fabrication and experiments

The device was designed in LayoutEditor to generate spatially confining channels. Molds were fabricated using standard SU8 lithography techniques where the photoresist was exposed to patterned UV from the designed mask, etched and finally cleaned. To generate both channels and media outlets, we used the mask aligner (SUSS MJB4 Mask Aligner) and a standard spin coater for a two-step fabrication process. Then, the mask was cleaned with ethanol and air dried and a PDMS mixture (Dow Corning 184 Sylgard®) with a ratio of 10:1 was poured into the mold and

baked at 80°C for 2 hours. The PDMS devices were removed and cut into appropriate sizes and punched with holes for inlets by 5 mm or 8 mm biopsy punch (Miltex). The channels created had a width of 3 μm, height of 5 μm, and length of 200 μm. Channels are coated with laminin (10μg/ml) for 2 hours at room temperature and cells were seeded 12 hours prior to imaging.

3.3.10 Particle image velocimetry

Particle image velocimetry (PIV) was applied in MATLAB (MathWorks®) to NSC-GFP images, (mPIV, https://www.mn.uio.no/math/english/people/aca/jks/matpiv/) yielding displacement and velocity vector fields.

3.3.11 Alignment calculation

The local degree of alignment was calculated between adjacent windows within 3×3 kernels. The local nematic order is calculated for the central window in each kernel using the modified order parameter equation, where θ is the difference in F-Actin orientation between the central window and the 8 surrounding windows. This process is repeated for all possible 3×3 kernels over an image, yielding a nematic director field with defined director magnitude and orientation for each window over an image. We show the director fields in red, and $\hat{n}$ is the unit direction of the vectors. Perfect alignment between adjacent regions within an F-actin network results in an order parameter equal to one.

3.3.12 Synthesis of zinc oxide microparticles

Zinc oxide (ZnO) microparticles formed based on established methods [117, 118] required a 1M NaOH solution added to a 0.04M $Zn(NO_3)^{2}$*$6H_20$ solution while stirring in a preheated (60°C) mineral oil bath. Following 4 hours of the solution mixing at 100°C, the solution was filtered using a Büchner funnel with an 11 μm pore size and dried overnight to produce ZnO microparticles. Microparticles were then collected and imaged using Scanning Electron Microscopy (SEM, Hitachi SU-70) at 10 kV to ensure formation of ZnO particles with a star-like morphology.

3.3.13 Creation of porated, functionalized PEG-DA hydrogels

The synthesis of 10 kDa poly-ethylene glycol diacrylate (PEG-DA) was done using previously established methods [82]. In brief, PEG was reacted with acryloyl chloride and trimethylamine overnight in dichloromethane. Potassium carbonate induced a phase separation, where we then collected and dried the organic phase with magnesium sulfate. Diethyl ether precipitated PEG-DA that was dialyzed and lyophilized prior to use. PEG was conjugated to fibronectin and laminin using previously described methods [119]. In brief, fibronectin (fibronectin purified protein, Sigma) was conjugated to acryloyl–PEG–N-hydroxysuccinimide (PEG-NHS, MW 3500 Da) in a 1:250 molar ratio in sodium bicarbonate. Laminin (laminin basement membrane, Sigma) was first dialyzed in PBS overnight, followed by dialysis in sodium bicarbonate buffer, and then conjugated to PEG-NHS in a 1:250 molar ratio. The final products were dialyzed and lyophilized prior to use.

Porated, fibrillar PEG-DA hydrogels were developed by modifying previous methods [120]. A 10% (w/v) addition of ZnO microparticles was dissolved in PBS, vortexed, and briefly pulsed to collect undissolved aggregates. A serial dilution of ZnO was created (1x, 3x, and 5x) and dissolved in PBS to form a variety of templated hydrogels. The solution containing 10 mg/ml 10kDa PEG-DA, PEG-fibronectin (1% w/v), PEG-laminin (1% w/v), and photoinitiator (1% v/v) was then casted solution on sterile 25 mm glass coverslips in a biological hood evaporated and dried in the dark overnight. Coverslips were then crosslinked under UV light (365 nm) for 10 minutes and rinsed with 1 M HCl until the gels released from the coverslips, followed by multiple rinses in PBS to remove any residual acid. Hydrogels were allowed to swell in the incubator overnight.

To characterize the morphology of the hydrogel, PFA fixation, an ethanol dehydration series, and HDMS produced dried hydrogels for SEM. Gels were sputter coated with iridium at a thickness of 2 nm and imaged using SEM at 10 kV. Quantification of pore size and frequency distribution for the 1x, 3x, and 5x concentration was done using ImageJ.

3.3.14 Rheology

Mechanical properties of porated and non-porated PEG-DA gels were characterized using a rheometer (Anton Paar MCR 302) after the hydrogels swelled overnight. The hydrogels were placed between two 25-mm parallel plates and a strain sweep at 10 Hz with a strain ramp of 10 points/decade was conducted.

3.3.15 3D migration assay

A monolayer of EC, PC, or EC+PC cultured at 100,000 cells/ml in a 12 well plate one day prior was maintained in NSC media. The next day, the hydrogel was held above the well using a similar design as a traditional transwell; a custom-made laser cut acrylic holder placed at the periphery of the bottom of the well, followed by two circular disks holding the hydrogel in between, supported the elevated hydrogel (Supplemental Figure A1.2). NSC-GFP were added atop the hydrogel at a seeding density of 10,000 cells per 0.4 cm^2 disk area and imaged at 4 and 24 hours via fluorescent microscopy, allowing for observation of NSC cluster formation and migration in the presence of no monolayer, EC, PC, and EC+PC monolayer. Images were taken through all z-planes and at the well bottom permitting for quantification of the number of NSC clusters and their area which have migrated to the well bottom.

3.3.16 N-cadherin imaging and flow cytometry

NSC and NSC+EC cultured on laminin coated coverslips cultured at 100,000 cells/ml in a 12 well plate. Following 24 hours, samples were fixed using PFA, blocked and permeabilized for one hour at room temperature, and stained against N-Cadherin (Novus Bio, 1:1000) at 4°C overnight. The following day, secondary antibodies were added for 2 hours at room temperature. Samples were then mounted with Dapi (Vector Laboratories) and imaged using fluorescent microscopy.

For N-cadherin quantification using flow cytometry, NSC, NSC from NSC+EC, and EC, were fixed in PFA, blocked and permeabilized for one hour at room temperature, and stained against N-cadherin as mentioned above. Accutase detaches NSC from NSC+EC co-culture without detaching

EC. Following secondary antibody incubation for 2 hours at room temperature, flow cytometry using an Attune Flow Cytometer was conducted and data was analyzed using FlowJo.

3.3.17 MMP2 ELISA and inhibition

Cell supernatants were collected from NSC, NSC+EC, and EC cultured in a 12 well plate at a density of 100,000 cells/ml in NSC media after 24 hours. An MMP2 ELISA was conducted following the manufacturer's protocol (RayBiotech) and read at 450 nm immediately following substrate reagent incubation. To inhibit secretion of MMP2, cells were treated with Batimastat (BB-94, Sigma), a widely used and specific MMP inhibitor [121, 122]. A 10 nM BB-94 concentration treated cells cultured at a density of 100,000 cells/ml in NSC media for 24 hours. Supernatant was collected 24 hours after treatment with BB-94. Fixation and staining for cultured cells on coated coverslips using immunofluorescence or flow cytometry against N-Cadherin allowed for visualization and quantification of N-Cadherin expression, as mentioned above.

3.3.18 EGFR activation

EGFR activator (NSC 228155, MedChemExpress) binds to the extracellular EGFR region and enhances tyrosine phosphorylation of EGFR [123]. A 100 μM concentration of EGFR activator was added to a monolayer of NSC in a 12 well plate, compared to an NSC media control. Brightfield imaging and N-cadherin flow cytometry analysis as mentioned above were conducted 24 hours following incubation.

3.3.19 Statistics

GraphPad Prism utilized for all statistical analysis used either a one-way or two-way ANOVAs with levels of significance denoted as * against control. All conditions have a sample size of three or more samples. Results graphed signify the average ± standard error of the mean, unless explicitly stated.

3.4 Results

3.4.1 EC promote NSC migration and clustering

We assessed NSC migration with a standard scratch assay conducted on a confluent monolayer of NSC, EC, PC, or co-culture combinations of these cell types. NSC migration assessed over 48 hours (Figure 3.1a) allowed us to quantify the percent closure of the ~200 μm scratch **(**Figure 3.1b). The culture of NSC with a GFP tag and PC dyed with PKH26 in co-and tri-cultures allowed for each cell type to be distinguished. Our results demonstrate that NSC alone are not highly migratory, but did proliferate rapidly over 48 hours; however, they did not fully close the scratch area (25.05% ± 3.95 closure). EC, on the other hand, proliferated rapidly and completely covered the scratch area (100% closure, $P<0.0001$) within 24 hours. PC proliferated slowly and there was no statistical difference in percent closure compared to NSC (28.36% ± 5.50, $P=.9307$). A co-culture of EC+PC resulted in complete closure (100%, $P<0.0001$) with apparent immature tubule vessel formation [124].

Following monoculture studies, we observed the effect of EC and/or PC cell contact on NSC migration by culturing NSC with EC, PC, or EC+PC in a 1:1 ratio. In the presence of EC, NSC began to cluster, and interestingly, the clusters (GFP^+ NSC) began migrating towards the scratched area (46.67% ± 3.80 closure, $P<0.0001$), significantly more than NSC alone (25.05% ± 3.95 closure). There is no significant difference in percent closure for NSC in the presence of PC, as compared to NSC cultured alone at 48 hours. Consistently, in a tri-culture of NSC+EC+PC, the scratch was completely closed. We quantified NSC cluster area **(**Figure 3.1c) and the number of clusters formed **(**Figure 3.1d) and we see no clusters of NSC formed in monocultures of NSC. However, in the presence of EC, there were 4.39 ± 0.72 and 8.11 ± 0.86 NSC clusters formed per imaged area at 24 and 48 hours, respectively. This suggests that not only do EC enhance NSC migration, but EC also promote the clustering of NSC. In contrast, there was no significant difference in percent closure, nor the number of clusters formed for NSC+PC compared to NSC alone at 48 hours. Consistently, in a tri-culture of NSC+EC+PC, we saw complete scratch closure

and 1.56 ± 0.41 and 8.78 ± 1.78 NSC clusters formed at 24 and 48 hours, respectively. This demonstrates that EC, and not PC, are necessary for promoting NSC clustering as a precursor to NSC migration.

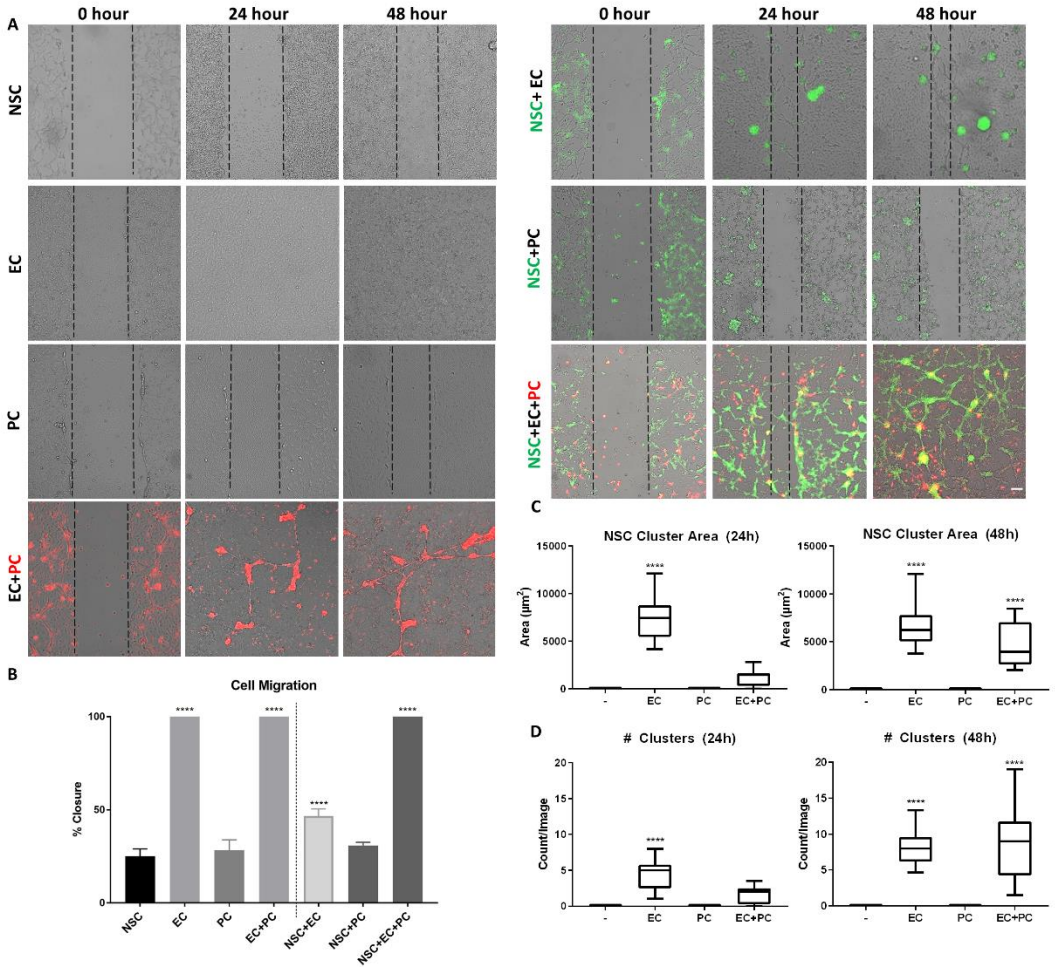

Figure 3. 1. NSC migration and cluster formation tracked in co-cultures of EC and PC. A) Mono, co, and tri-cultures of NSC, EC, and PC at 0, 24, and 48 hours post scratch. Scale bar (100 µm) representative of all images. B) Quantified percent closure at 48 hours. C) NSC cluster area at 24 and 48 hours. D) Number of NSC clusters formed at 24 and 48 hours.

3.4.2 NSC aggregates require leader cell arm to guide migration of clusters

It has been well demonstrated that individual NSC cytoskeletal rearrangement and cell polarization is a pre-requisite for NSC migration. However, NSC clusters migration are guided by extended cell arms. Figure 3.2a-b shows that these extended arms are initiated randomly and are

solely responsible for the generation of traction forces during migration. These cell arms are initiated and extended by the leader cell who bears most of the traction force load. The strain energy density of migrating clusters on 0.7kPa and 2.8kPa stiffness substrates shows no significant difference, indicating that for small variation in substrate stiffness, the cluster migration was not affected (Figure 3.2c). When NSC are in the presence of EC, separated by a distance of 1000 µm in microfluidic chambers (Figure 3.2d). NSC are drawn towards EC, and we have calculated the aggregate maximum displacement in the direction of EC, further suggesting that EC play a role in guiding NSC migration (Figure 3.2e). To further clarify the role of leader cell in arm initiation and extension and cluster migration, we ablated the leader cells with a laser (Figure 3.2f). Following ablation, the arm quickly retreats towards the cluster, where the time of retraction was captured by imaging (frame rate: 1sec). This shows that leader cell with strong traction forces can only initiate an extended arm, however, without any leader cell, there is no arm formation nor cluster migration towards EC (Figure 3.2f). Lastly, clusters also seek connection with nearby clutters through leader cell guided extending arms. We demonstrate that ablation of cell-cell contacts (connecting cell cord) between aggregates prevents NSC aggregate migration towards EC **(**Figure 3.2g) suggesting that the lead arm is essential for movement.

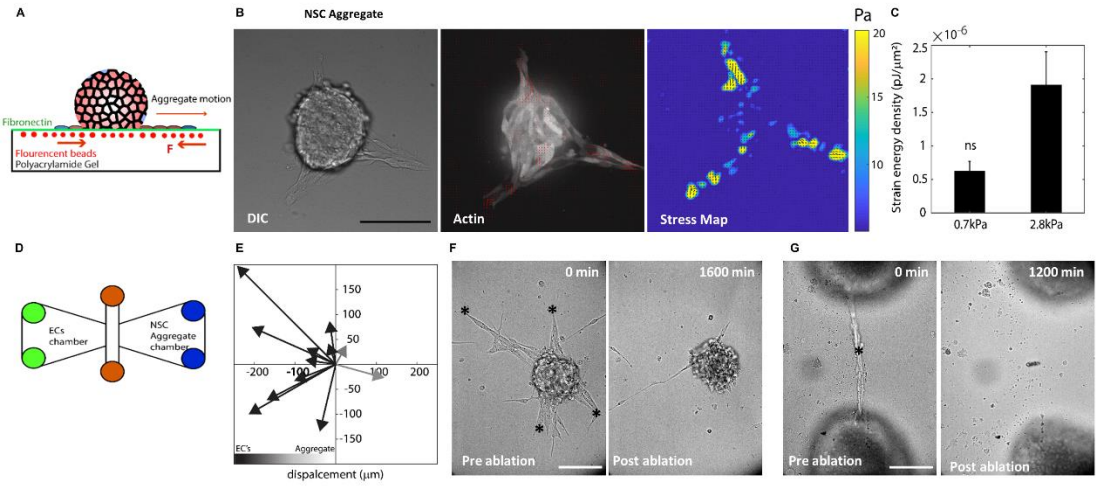

Figure 3. 2. NSC aggregate spreads by extending long cell arms and applying forces on the substrate. A) Experimental setup of aggregate on PA gel to measure forces exerted. B) DIC images

of NSC aggregate with extended cell arms in random directions, where the leader cell guides the migration by guiding migration, as seen through the F-Actin staining and stress map. C) Aggregates on soft (0.7 kPa) and hard (2.8 kPa) substrates have the same energy strain. D) Experimental set up of EC and NSC separated in chambers. E) Aggregate maximum displacement in the direction of EC. F) Ablation of leader cell of aggregate, where * is the ablation location. G) Ablation of cell-cell contacts between two aggregates, where * is the ablation location. Scale bar (100 μm) representative of all images.

3.4.3 EC promote NSC clustering but not speed

To quantify speed distribution of individual migrating cells within co-culture, we used particle image velocimetry (PIV) on NSC-GFP in three different culture conditions: NSC, NSC+EC co-culture, and EC, measuring cell velocity vector fields (Supplemental Figure A2.3). NSC in an NSC+EC co-culture have no significant difference in speed compared to NSC cultured alone (Supplemental Figure A2.2), suggesting that EC promote NSC clustering, but do not enhance their migratory speed.

3.4.4 EC conditioned media promotes formation of NSC clusters

Direct NSC-EC interaction was determined to induce NSC cluster formation, though, whether NSC cluster formation requires cell contact with EC or soluble factors secreted by vascular cells remains unknown. To determine the extent to which EC secreted signals can mediate NSC clustering, we treated NSC with conditioned media (CM) from EC, PC, and EC+PC, using NSC media as a negative control (Figure 3.3a). Following 24 hours, we observed and quantified the number of clusters formed (Figure 3.3b) and their cluster size (area) (Figure 3.3c). EC CM led to the formation of significantly more NSC clusters compared to control (7.52 ± 0.79 NSC clusters per area, cluster area of 169.6 ± 4.78 μm^2, P <.0001. In contrast to NSC grown in NSC media, NSC did not cluster when grown in PC-conditioned media (P >0.999). However, upon NSC treatment with EC+PC CM, NSC formed significantly more clusters compared to control (4.82 ± 0.75 clusters per area, average area of 57.24 ± 2.11 μm^2, P <0.0001). Therefore, EC+PC CM facilitated the formation of about half as many clusters that formed when NSC were cultured with only EC CM, suggesting that EC, and not PC, secreted factors are responsible for NSC clustering. We also stained

against F-Actin to observe the NSC cytoskeleton, and we see that NSC cultured in NSC media and PC CM demonstrate a linear morphology of the filament. This is in stark contrast to EC CM and EC+PC CM (Figure 3.3d), wherein the presence of EC CM, the intensity of the phalloidin stain around NSC clusters is no longer linear. We have quantified the F-Actin alignment (Figure 3.3e) where our results demonstrate a significant reduction in alignment for F-Actin in the presence of EC CM and EC+PC CM. There is no difference between our control and PC CM, suggesting that cytoskeletal rearrangement in EC+PC CM is primarily due to EC. This further demonstrates that EC CM leads to NSC aggregate formation and changes in NSC cytoskeletal reorganization.

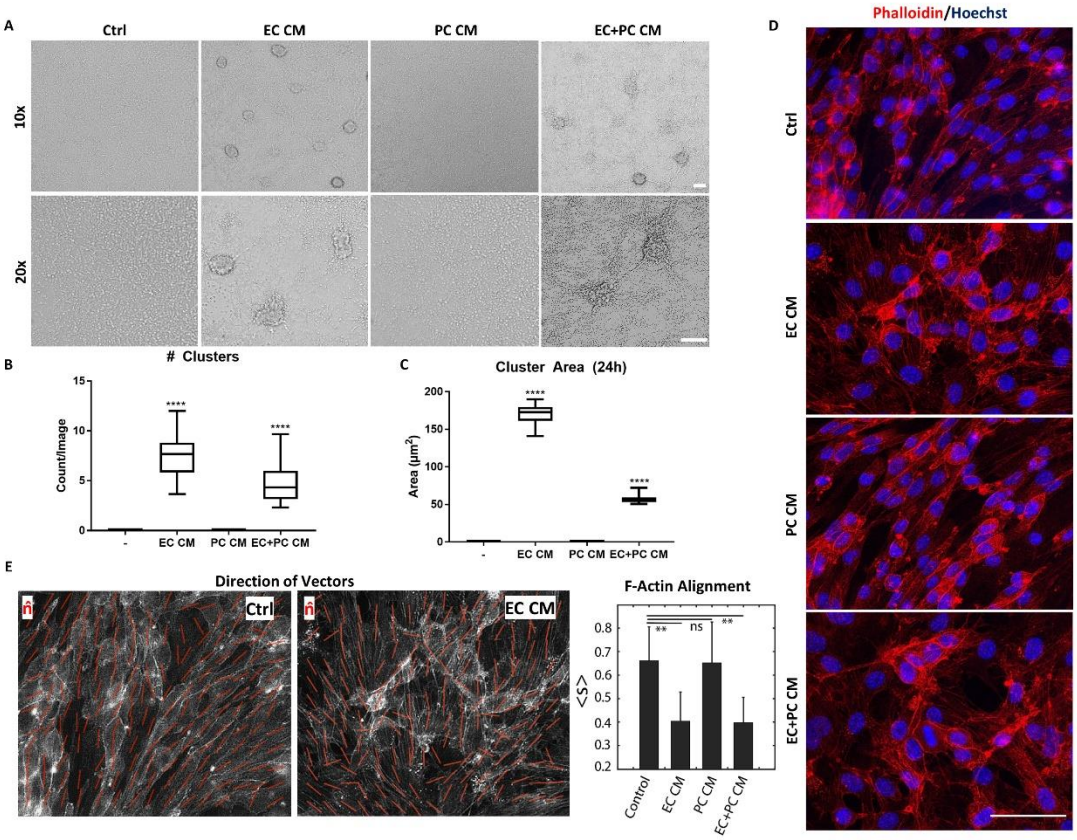

Figure 3. 3. EC conditioned media promotes NSC clustering. A) 10x and 20x brightfield images of NSC with conditioned media (CM) treatment. Scale bar (100 μm) representative of all images. B) Number of NSC clusters and C) cluster area and formed at 24 hours. D) NSC polarization visualized through Phalloidin (red) and Hoechst (blue) staining, E) quantifying F-Actin alignment. Scale bar (50 μm) representative of all images.

To confirm the extent to which soluble factors can drive cluster formation and leader cell-induced migration, we created a microchannel device in which NSC and EC were separated by microchannels (5 µm wide and 200 µm long) (Figure 3.4a). When no EC secreted factors are present, NSC are retained as a monolayer (Figure 3.4b)**.** However, the presence of factors secreted from the EC led to NSC aggregation, as seen in Figure 3.4c. Due to the diffusive manner by which the cells are exposed to EC secreted factors, the cluster formation is slowed (12 hours to 24 hours) as compared to cells in direct contact within co-culture conditions (4 hours to 8 hours). Nonetheless, NSC actively migrate toward the EC chambers and form clusters in the EC chambers. This suggests that over time, EC secreted factors alone do lead to NSC clustering, even without direct NSC-EC contact.

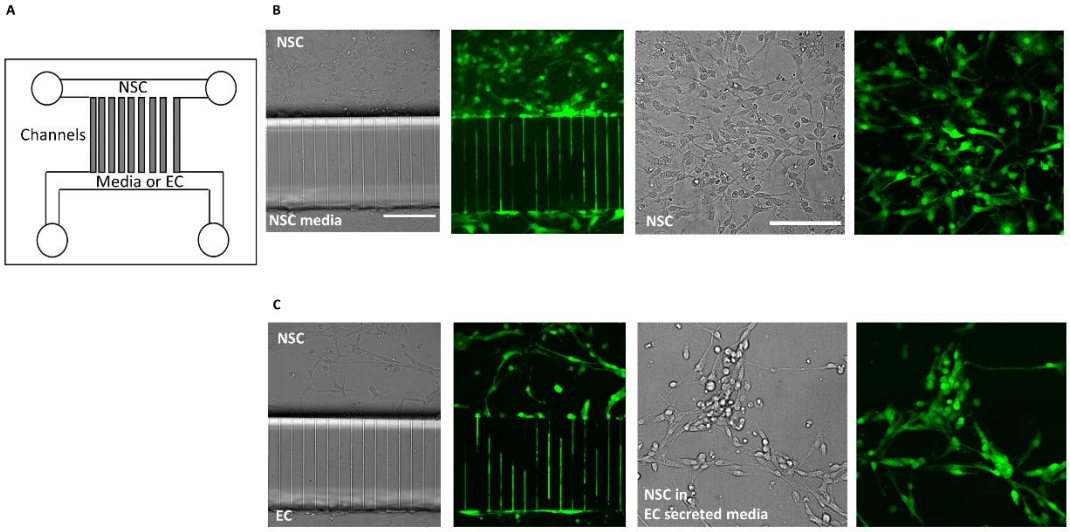

Figure 3. 4. EC secreted factors through microchannels promote NSC clustering. A) Set up of microchannel device where NSC alone and NSC separated from EC. EC were cultured in the chambers, which are separated by microchannels. B) NSC-GFP culture in one chamber with NSC media in the other chamber observed after 12 hours. C) NSC and EC cultured in different chambers, separated by microchannels, observed after 12 hours. Scale bar (100 µm) representative of all images.

3.4.5 EC enhance NSC clustered migration across 3D hydrogel brain biomimetic

NSC respond to substrate stiffness by altering their differentiation state and rate of proliferation [123]. In order to determine whether substrate stiffness would also influence NSC

migration in the presence of vascular cells, we created a porated biomimetic hydrogel. To do this, chemical synthesis of zinc oxide (ZnO) salts with a star-like morphology created a templated system (Figure 3.5a) Hydrogel porosity analyzed using SEM images allowed us to visualize the porous network of the templated hydrogel compared to brain tissue (Figure 3.5b-c), and pores were found throughout the entirety of the scaffold (Supplemental Figure A1.3). ZnO salts added to the PEG pre-gel solution at concentrations of 1X, 3X, and 5X led to an increase in pore size distribution with an increase in concentration of ZnO salts, ranging from 3.82 to 11.14 μm, 2.05 to 13.10 μm, and 4.07 to 19.39 μm, respectively. In addition, using rheology we obtained mechanical data for the PEG hydrogels with or without ZnO templating particles at 1X, 3X, and 5X concentrations. A non-templated 10 kDa PEG hydrogel has an elastic modulus of 23,376 ± 954.3 Pa. However, brain tissue, one of the softest tissues in the body, has a modulus ranging from 500 Pa to 1000 Pa [125, 126]. We were able to more closely mimic brain elasticity by templating the PEG hydrogels through the removal of ZnO salts at concentrations of 1X, 3X, and 5X, which resulted in an elastic modulus of 2,607 ± 122.3, 1,303 ± 93.14, and 586.5 ± 11.8 Pa respectively (Figure 3.5e-f). For subsequent studies, a concentration of 3X salts allowed us to expose cells to a range of stiffnesses similar to that of brain tissue. In addition, we functionalized our scaffold through the addition of PEG-fibronectin and PEG-laminin, two of the most abundant ECM proteins found in the brain [22] (Supplemental Figure A1.4). Through addition of these proteins, cultured NSC can adhere to the soft, functionalized scaffold, unlike NSC on stiffer, inert PEG hydrogel without pores; this is demonstrated with F-actin staining (Figure 3.5g). By mimicking mechanics, architecture, and conjugated proteins, we have more closely replicated brain tissue, as compared to standard transwells.

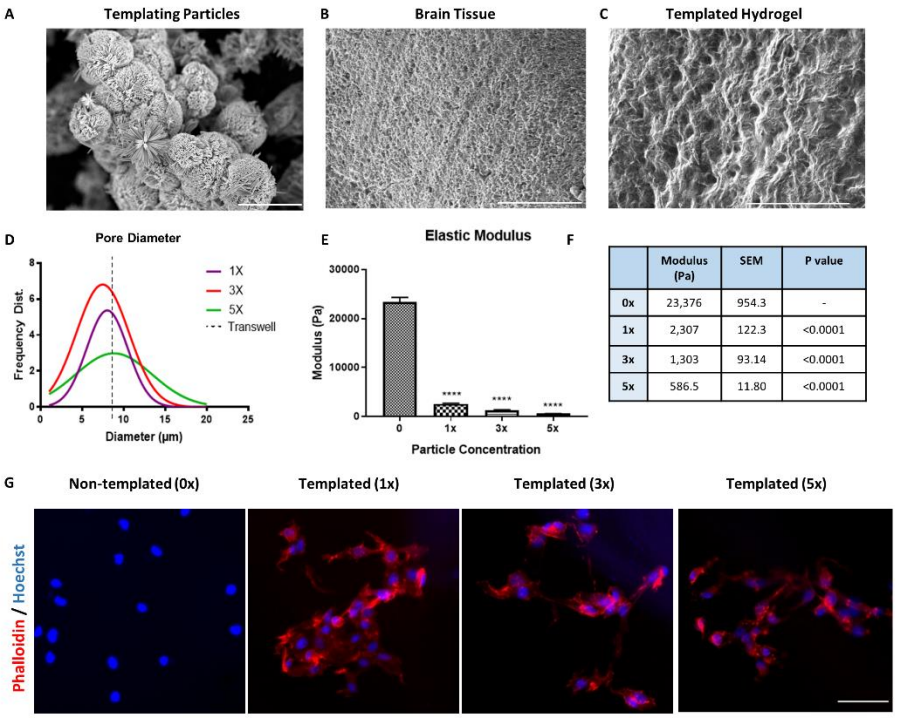

	Modulus (Pa)	SEM	P value
0x	23,376	954.3	-
1x	2,307	122.3	<0.0001
3x	1,303	93.14	<0.0001
5x	586.5	11.80	<0.0001

Figure 3. 5. Creation of a mimetic hydrogel for elastic brain tissue. A) Synthesis of zinc oxide salts with star-like morphology; scale bar (10 μm). B) SEM image of brain tissue and C) templated hydrogel; scale bar (100 μm). D) Pore diameter frequency distribution quantification. E) Elastic moduli of templated hydrogels tabled in F. G) Phalloidin (red) and Hoechst (blue) fluorescent images for NSC on non-templated or templated hydrogels. Scale bar (100 μm) representative of all images.

Migration experiments conducted with our biomimetic hydrogel were done with experimental design that is similar to that of standard transwell migration assays. In this case, we elevate the hydrogel above a cell well and submerge the hydrogel in media. To support the hydrogel, a custom fabricated holder was placed at the well periphery and used to elevate the hydrogel that was stabilized between two circular acrylic rings (Supplemental Figure A1.2). Atop the hydrogel, NSC-GFP were added with or without an EC or PC monolayer at the well bottom. This system allowed us to observe NSC migration towards the cell monolayer after 4 and 24 hours of incubation (Figure 3.6a). When NSC were added atop the hydrogel with no monolayer at the well bottom, there was little cell migration observed throughout the thickness of the hydrogel at 4

hours (images 1-4). Additionally, there were no clusters of NSC observed at the well bottom at 24 hours (left, top corner). Similarly, when a PC monolayer was cultured on the well bottom (right, top corner), very few NSC clusters were observed at 4 or 24 hours (1.78 ± 0.24 per area, with an average area of 558.6 ± 98.17 μm^2) (Figure 3.6c-d). In contrast, the presence of an EC monolayer at the well bottom (left, bottom corner) induced a pronounced migration of clustered NSC throughout the gel pores at 4 hours and a significant number of clusters at the well bottom by 24 hours (17.65 ± 2.62 per area, with an average area of 1438 ± 135.3 μm^2) (Figure 3.6c-d). These results suggest that EC secreted factors are sufficient to induce NSC clustering and to induce NSC clustered migration towards the EC monolayer. We detected NSC clusters migrating throughout the pores of the hydrogel in the direction of the EC monolayer as seen in Figure 3.6b. In the presence of an EC+PC monolayer (right, bottom corner) NSC formed a significant number of clusters (7.75 ± 1.21, with an average area of 822.1 ± 116.2^2) (Figure 3.6c-d), which also migrated to the well bottom by 24 hours, although not as quickly as EC alone. These results demonstrate that EC and not PC are vascular contributors to NSC clustering and migration.

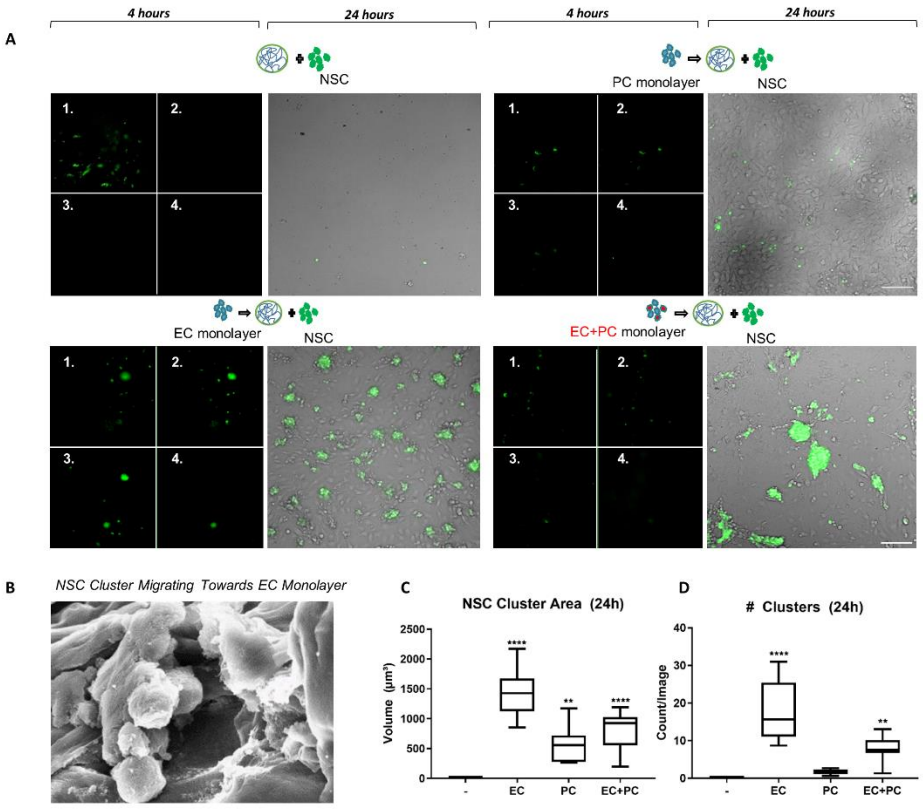

Figure 3. 6. EC Promote NSC Migration and Clustering in 3D. A) Panel of fluorescent NSC images from top to bottom (1-4) of hydrogel at 4 hours and bottom of well at 24 hours, with no monolayer at well bottom (top, left), PC monolayer (top, right), EC monolayer (bottom, left) and EC+PC monolayer (bottom, right). Scale bar (100 µm) representative of all images. B) SEM image of NSC migrating through hydrogel pore. Scale bar (10 µm). C) NSC cluster area and D) number of NSC clusters formed at 24 hours.

3.4.6 EC secreted MMP2 promotes NSC clustering and increases N-cadherin expression

FGF-2, present in NSC media, is known to stimulate EC function to increase proMMP-2 and stimulate MMP activation [115]. It is well established that MMP2 activates EGFR, which leads to downstream N-cadherin cleavage. Previously, we have demonstrated EC have high MMP activity [105]. In order to quantify MMP2 levels, we conducted an MMP2 ELISA to compare NSC, NSC+EC, and EC secreted levels of MMP2 (Figure 3.7a). NSC+EC had a significantly higher MMP2 secretion than NSC alone (P=0.0049). In addition, EC secrete more MMP2 than do NSC (P<0.0001). Following MMP2 quantification, we then assessed N-cadherin expression via immunofluorescent staining of NSC and NSC+EC (Figure 3.7b). N-cadherin is intensely stained

on the perimeter of the NSC clusters that were formed in co-culture with EC. Minimal staining of N-Cadherin was observed on NSC that were cultured alone. Flow cytometry was used to quantify N-cadherin expressed by NSC alone, NSC from the NSC + EC co-culture, and EC alone. NSC in co-culture with EC have significantly higher N-cadherin expression as compared to NSC that were cultured alone (*P=0.0299*), suggesting that EC secreted MMP2 may enhance N-cadherin expression on NSC (Figure 3.7c).

To verify that MMP2 plays a role in this pathway, we treated cells with MMP2 inhibitor, Batimastat (BB-94) (Figure 3.7d), noting a significant reduction in secretion compared to control (*P <0.0001).* We immunostained for N-cadherin with immunofluorescence for NSC and NSC+EC (Figure 3.7e), where we visualize the difference in N-cadherin intensity between NSC+EC with and without BB-94. Inhibition of MMP2 prevents NSC clustering while in culture with EC. NSC from NSC+EC have no significant difference in N-cadherin expression compared to NSC alone (Figure 3.7f), stressing the importance of EC secreted MMP2 for NSC clustering and N-cadherin expression.

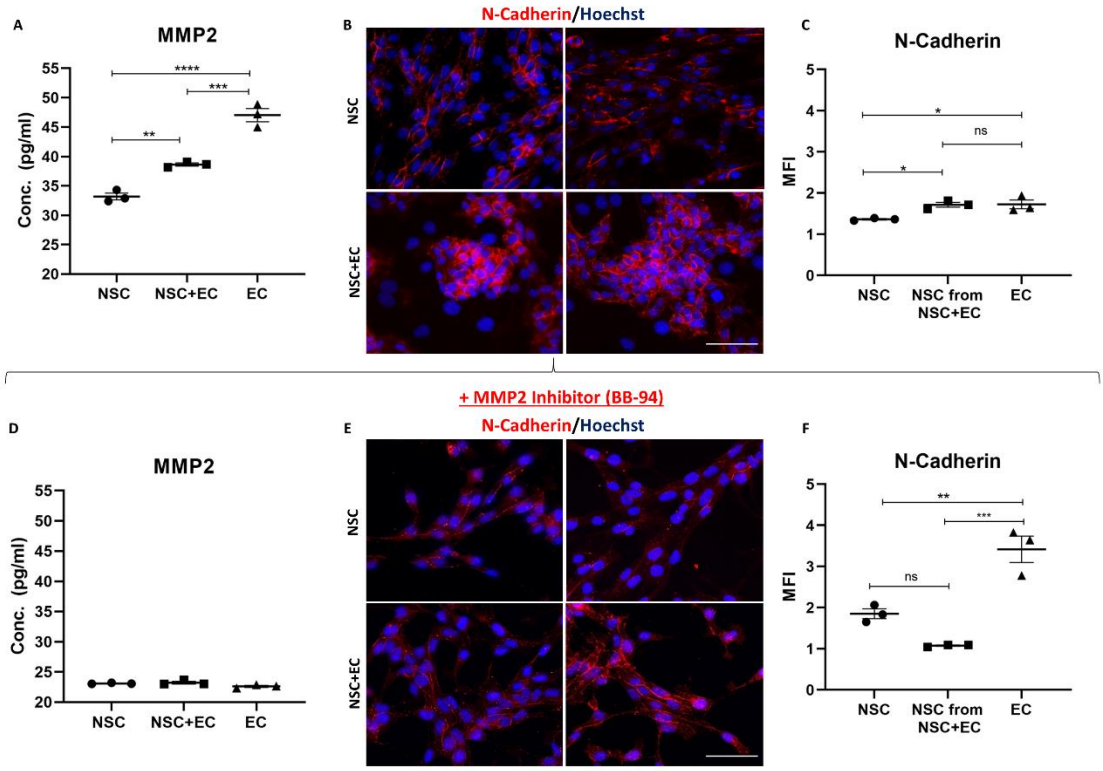

Figure 3. 7. EC secreted MMP2 promotes NSC clustering and increases NSC N-cadherin expression. A) MMP2 ELISA for NSC, NSC+EC, and EC cell supernatants 24 hours after culture. B) Immunofluorescent images against N-cadherin (red) and Hoechst (blue) for NSC alone and NSC+EC co-culture (bottom). C) N-cadherin quantification using flow cytometry for NSC, NSC from NSC+EC co-culture, and EC. D) MMP2 Elisa for NSC, NSC+EC, and EC cell supernatants following 24 hours with BB-94 (MMP2 inhibitor). E) Immunofluorescent images against N-cadherin (red) and Hoechst (blue) for NSC alone and NSC+EC co-culture (bottom) following 24 hours of BB-94 treatment. F) N-cadherin quantification using flow cytometry for NSC, NSC from NSC+EC co-culture, and EC following 24 hours of BB-94 treatment. Scale bar (50 μm) representative of all images.

3.4.7 EGFR activation enhances NSC clustering and N-cadherin expression

EGFR-dependent N-cadherin signaling is necessary for neural progenitors in the SVZ to respond to injury cues and to promote repair. To assess whether EGFR is necessary for NSC clustering, without MMP2 activation, we activated a monolayer of NSC with an exogenous EGFR activator. Following 24 hours of activation, NSC clustered, similarly to the clustering seen during direct NSC-EC contact or NSC treatment with EC CM, and in contrast with the NSC control, which did not cluster (Figure 3.8a). N-cadherin expression on NSC was significantly higher with EGFR

activation compared to NSC inactivated control (*P*=0.0004), as seen in Figure 3.8b. This result indicates that EGFR signaling may stimulate N-cadherin cleavage and activation, allowing NSC to undergo cytoskeletal rearrangement.

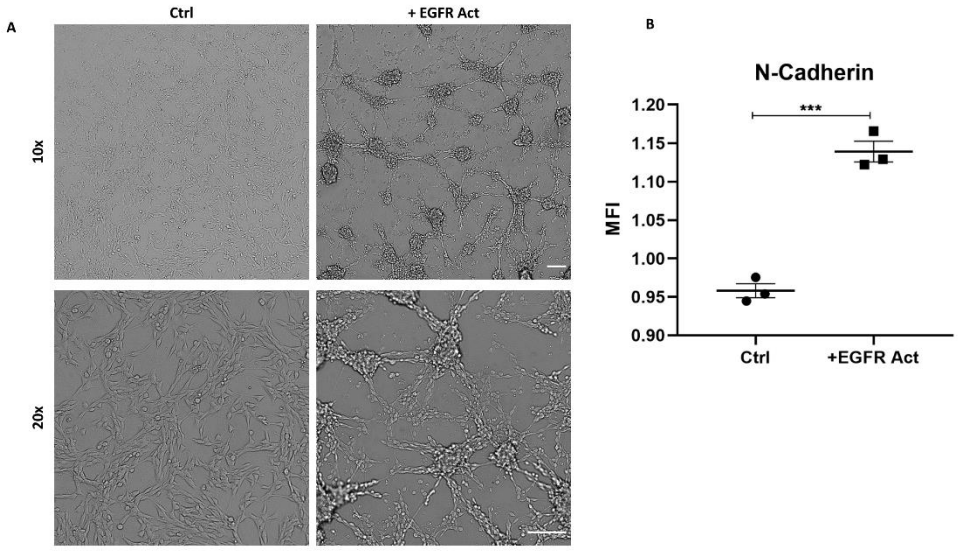

Figure 3. 8. EGFR activation enhances NSC clustering and N-cadherin expression. A) NSC treated with NSC media (control) and EGFR activator for 24 hours, imaged at 10x and 20x (bottom). B) N-cadherin expression quantified with flow cytometry for control and EGFR activated NSC. Scale bar (100 μm) representative of all images.

3.5 Discussion

There is currently no effective long-term solution to repair tissue and promote motor recovery following stroke. In order to advance therapeutic approaches to neurological disorders and diseases, researchers are actively investigating the SVZ neurogenic niche as a source of proliferating NSC that interact directly with neural vasculature [22]. In fact, it is through direct interaction with the vascular bed and ventricle that SVZ-resident NSC are activated to migrate the long distance along the RMS to the OB, where they then differentiate into neurons and induce endogenous repair mechanisms. Although many chemoattractants and chemorepellents are known to regulate migration of NSC to the olfactory bulb, the exact mechanism by which NSC cluster and migrate along the RMS remains unknown.

In the current study, we investigate the role of microvascular EC and/or PC in promoting NSC clustering, and thereby migration, via cell-cell contact and/or soluble factor secretion. Using a 2D scratch assay we demonstrate that NSC form clusters when in direct contact with EC and when treated with EC conditioned media. To further validate that the pronounced NSC migration in the presence of EC is not due to cell proliferation, we measured NSC speed in mono- and co-cultures. Interestingly, we see that NSC alone versus NSC in the presence of EC have no significant difference in cell speed, as seen by the vector velocity fields calculated. Although several vascular chemoattractants have been determined to promote directional NSC migration, such as VEGF [106] and SDF-1 [108] our results suggest that EC do not enhance the rate of NSC migration, but rather facilitate the initial clustering step of chain migration.

In addition, using microchannels, we observed the stark difference in NSC morphology when EC secreted factors are available through the microchannels, where NSC begin to form aggregates. Interestingly, NSC clustering does not occur in the presence of PC, which is to our knowledge, the first time PC and EC have been shown to have different impacts on NSC. Notably, the EC-induced NSC clustering was increased as an effect of NSC co-culture with EC+PC, suggesting that PC heighten the effect EC on NSC aggregatory behavior. Clustering requires NSC polarization and F-actin cytoskeletal reorganization. In fact, an increase in F-actin disorder results in actomyosin contractility or a change in rigidity of the cell cortex. Within the microchannels, NSC stretch their lengths and becoming extremely elongated, and alterations in these properties may be advantageous towards the clustering of NSC. This would be critical in the establishment of a leader cell, in that the cell must stretch and deform over large distances and generate large traction stresses to guide forward motion. Thus, EC-mediated changes in cell mechanical properties may be essential for the initial step in cluster formation.

To date, numerous platforms have been utilized to mimic NSC migration in the brain. Biologic biomaterials consisting of ECM proteins can create complex, mimetic matrices that can promote NSC migration. For example, Crapo *et al.* demonstrated that central nervous system-

derived ECMs can promote differentiation of NSC into neurons, suggesting ECM scaffolds can facilitate postinjury healing[127]. Also, i*n vitro* models of the NSC-vascular niche that incorporate brain vasculature and the ECM microenvironment allowed NSC to reduce neuronal generation while promoting NSC differentiation [128]. In addition, Ghuman *et al.* have characterized and delivered a porcine bladder-derived ECM into a rat stroke cavity, inducing cell invasion and promoting structural remodeling of the lost tissue [129]. These studies provide support that the presence of ECM proteins can directly impact NSC function. The mechanics of biologic scaffolds have also directly impacted NSC differentiation [130, 131], stressing the importance of native brain mechanics for neural cell maintenance and differentiation. However, although ECM materials have shown effective for delivery to the stroke-inured brain, as well as their influence on NSC differentiation, a scaffold which is porous and fibrillar is necessary to allow for the observation of cell migration. Typically, *in vivo* migration can be observed for NSC in the RMS by labeling neural progenitors with dyes, allowing for time-lapse imaging. For *in vitro* migration, a standard polycarbonate transwell is often used which allows for the culture of mono-or bi-layers on respective sides of the membrane. Although the transwells can be coated by factors, such as collagen, fibronectin, and laminin, this 2-D coating is not representative of the fibrillar protein microenvironment NSC access *in vivo*. In addition to the limitations in the biocomposition of transwells, they also are extremely stiff compared to soft brain tissue, where mechanical properties can directly impact NSC migration and differentiation. Furthermore, these membranes do not allow for time-lapse imaging. To overcome these limitations and to mimic migration more closely in 3-D, we have created a brain-mimetic hydrogel that encompasses the brain stiffness, biocomposition, and porous nature. By leaching of chemically synthesized ZnO salts, we obtain a distribution of pore sizes throughout a 3-D structure to better mimic tissue, especially when compared to the porosity of a standard transwell insert, which has a pore size of 8 μm with no pore size variability. Using a hydrogel in place of a traditional transwell, we visualize in real-time NSC migrating in clusters when an EC monolayer is present at the well bottom. The migration of clustered NSC

toward the EC monolayer was not as enhanced with an EC+PC monolayer, further suggesting that EC promote NSC clustering and migration, while PC do not. Although we do not see PC play a direct role in this phenotypic switch, PC may play an indirect role *in vivo* which requires future investigation.

The role of MMP activity is under investigation for its role in enhancing brain cell response to tissue injury. It is known that MMP substrates include cell adhesion molecules that must be cleaved to influence cellular function [132]. MMP production by EC, triggered by angiogenic growth factors, is a critical component during angiogenesis during normal and pathological conditions that allows for cells to migrate appropriately [115]. Under injury-like stimuli, MMPs mediate ECM degradation and dissociation, and EC secreted MMPs are critical for promoting the invasiveness of gliomas. Studies have demonstrated that cell invasion and migration is enhanced by MMP9 secretion by EC, suggesting a direct relationship between MMP levels and cell migratory rate [133]. In fact, the observation of molecular mechanisms regulating cellular communication of sensory neurons with EC has further demonstrated that MMP2 and MMP9 protein concentration and enzymatic activity are upregulated when ECs are co-cultured with sensory neurons [134]. This heightens the interconnectivity of angiogenesis and neurogenesis; neural and vascular cultures together play a role in inducing ECM remodeling in response to injury, which allows for cell migration. Recently, we have demonstrated that EC exhibit high MMP activity, and it is well established that the angiogenic factor FGF can stimulate EC MMP production [115]. MMP2 by activated EC has caused an enhanced migration of neuroblasts, diminished using a MMP inhibitor [135]. EGFR signaling has proven to be vital for progenitor cells to migrate during pathological conditions, where EGFR in the SVZ can be activated by HB-EGF [94] allowing for N-cadherin cleavage and activation. N-cadherin cleavage was found to be a prerequisite to migration [94], and because EGFR can be activated by MMP2 as well, we investigated if EC secreted MMP2 plays a role in NSC clustering and migration. It is evident that enhanced NSC clustering and increased N-cadherin expression occurs when in the presence of EC, and both these effects were diminished

with the use of an MMP2 inhibitor, suggesting the role of EC in promoting this behavior. Interestingly, there is an increase in both NSC clustering and N-cadherin expression using an endogenous EGFR activator, validating the role of MMP2 in activating EGFR to promote N-cadherin cleavage.

In summary, we demonstrate for the first time that EC-secreted MMP2 promotes NSC presented N-cadherin expression, thereby allowing NSC cytoskeletal polarization, cell clustering, and migration. Although stem cell therapies in theory have a plethora of benefits, their delivery to an injured environment is a significant challenge. In order to overcome the limitations of current delivery systems, researchers can use the intricate coupling of neurogenesis and angiogenesis to complement implantation of NSC. The identification of signaling pathways that can promote the migratory phenotype of NSC can significantly enhance our current NSC delivery systems to include pro-migratory stimuli, thereby designing efficient cell strategies for brain repair.

Chapter 4: Minimally Invasive Delivery of Microbeads with Encapsulated, Viable and Quiescent Neural Stem Cells to the Adult Subventricular Zone

Portions of this chapter were printed with permission from Matta, Lee, *et al.* 2019 [1]

4.1 Abstract

Stem cell therapies demonstrate promising results as treatment for neurological disease and injury, owing to their innate ability to enhance endogenous neural tissue repair and promote functional recovery. However, delivery of undifferentiated and viable neuronal stem cells requires an engineered delivery system that promotes integration of transplanted cells into the inflamed and cytotoxic region of damaged tissue. Within the brain, endothelial cells (EC) of the subventricular zone play a critical role in neural stem cell (NSC) maintenance, quiescence, and survival. Therefore, here, we describe the use of polyethylene glycol microbeads for the coincident delivery of EC and NSC as a means of enhancing appropriate NSC quiescence and survival during transplantation into the mouse brain. We demonstrate that EC and NSC co-encapsulation maintained NSC quiescence, enhanced NSC viability, and facilitated NSC extravasation in vitro, as compared to NSC encapsulated alone. In addition, co-encapsulated cells delivered to an *in vivo* non-injury model reduced inflammatory response compared to freely injected NSC. These results suggest the strong potential of a biomimetic engineered niche for NSC delivery into the brain following neurological injury.

4.2 Introduction

The subventricular zone (SVZ) is one of the two germinal regions in the adult mouse brain where neurogenesis occurs. The SVZ is prominent on the lateral wall of lateral ventricles (LVs), and is characterized by a highly organized and vascularized microenvironment [22, 136]. Neural stem cells (NSC) interact with endothelial cells (EC) and vascular pericytes (PC) that line the wall of infiltrating blood vessels and deliver blood borne and secreted factors [137, 138]. NSC interactions with the vasculature and LVs are responsible for maintaining brain homeostasis and facilitating appropriate response to injury, particularly in the context of neurogenesis following

stroke. It is well-established that the interactions between NSC and EC regulate NSC proliferation and quiescence through ephrin-B/EphB signaling [34] and Notch signaling [33], respectively. Under normal homeostatic condition, EC prohibit NSC differentiation and promote a quiescent state [4]. However, following neurovascular injury, such as stroke, EC junctions and extracellular matrix (ECM) are disturbed by oxygen and glucose deprivation resulting from the loss of cerebral blood flow. Consequently, damaged EC are unable to regulate typical NSC function, resulting in enhanced NSC proliferation and neuronal differentiation [139]. Despite the activation of NSC, endogenous repair mechanisms are insufficient to foster recovery and functional replacement of damaged neurons.

Stem cell therapies are currently considered a viable opportunity for replacement of lost neural populations and restoration of neural circuitry following injury. However, current therapies require improved engraftment strategies for better cell survival, which in turn can help expedite and enhance the generation of new cells in the cytotoxic area following cerebral ischemia [140, 141]. To address these limitations, tissue engineering advances provide a promising platform to facilitate the recovery of damaged tissue [1]. Recently, hydrogel scaffolds were designed to enhance stem cell delivery, taking into consideration the biocompatibility, biodegradation, and mechanical stresses associated with integration of cells to a hydrogel [142-145]. As demonstrated by these efforts, effective tissue engineered approaches to improve behavioral and functional recovery must promote exogenous cell survival and transplantation, while promoting endogenous repair mechanisms.

Here, we have created a polyethylene glycol (PEG)-based scaffold for NSC and EC encapsulation and delivery into the mouse SVZ for cell engraftment into host tissue. PEG, known for its bioinert nature, can be chemically modified by immobilizing biologically active peptide sequences from the ECM to promote cell interactions *ex vivo*, thereby supporting cell adhesion among other cell functions [82, 119, 146]. The tunable nature of polymeric platforms facilitates the engagement of multiple cell types. Two of the most abundant ECM proteins in neural tissue are

fibronectin and laminin [141], where the fibronectin derived peptide arginine–glycine–aspartic acid-serine (RGDS) and laminin derived peptide tyrosine-isoleucine-glycine-serine-arginine (YIGSR) have each demonstrated the ability to support cell adhesion of EC and NSC, respectively [82, 147]. In this study, we have conjugated these adhesive peptides to PEG at high efficiency to promote dual-cell adhesion. To facilitate degradation of PEG *in vivo*, we have also conjugated the degradable sequence glycine-glycine-leucine-glycine-proline-alanine-glycine-glycine-lysine (GGLGPAGGK; LGPA) which is susceptible to degradation by cell-secreted collagenases [147, 148], allowing for the extravasation of encapsulated cells and promoting exogenous cell integration within host tissue.

In the present study, we have created and optimized the generation of cell-encapsulated PEG microbeads with PEG-YIGSR and PEG-RGDS to support both mono- and co-culture systems of NSC and EC. Importantly, we demonstrate that EC enhance NSC survival and maintain NSC quiescence within our co-culture system, *in vitro*. Furthermore, EC accelerate the degradation of PEG microbeads through proteolytic MMP activity, facilitating the escape of NSC from the microbeads. Consistent with our *in vitro* results, we found that co-encapsulated NSC and EC delivered to the murine SVZ in the microbeads retained NSC quiescence and accelerated microbead degradation. Moreover, cells encapsulated within microbeads diminished immune cell infiltration and increased the number of endogenous SVZ neural stem and progenitor cells, following their delivery *in vivo,* as compared to freely injected cells. Our work provides strong evidence that engineered PEG-based mimics of the neurovascular niche may serve as a valuable delivery device for cell therapies in response to neurological disease.

4.3 Results

4.3.1 Addition of 0.25% Pluronic is Optimal for Microbead Diameter Constraint and Encapsulated Cells

Using an oil emulsion technique, we produced microbeads with a mean diameter of 100-150 μm while maximizing the number of encapsulated cells. Using polymer and photochemicals in an oil emulsion, we obtained a microbead diameter of 264.1 ± 20.81 μm with 181.4 ± 12.1 cells encapsulated per bead. To achieve microbeads of our target size with encapsulated cells, we incorporated Pluronic, a PEG-based and cell compatible surfactant, at various concentrations: 0.1, 0.25, and 0.5% (v/v) (Figure 4.1a), yielding a mean diameter of 191.5 ± 8.70 μm, 150 ± 25.38 μm, and 100.9 ± 3.23 μm, respectively (Figure 4.1b). With increased concentration of Pluronic, the mean bead diameter decreases significantly (Figure 4.1c). Using a comparable starting cell concentration, 0.1, 0.25, and 0.5% (v/v) concentrations of Pluronic facilitated the encapsulation of 126.8 ± 6.79, 111.7 ± 8.76, and 39.5 ± 2.17 cells, respectively (Figure 4.1d-e). A 0.25% Pluronic addition was chosen for *in vitro* and *in vivo* experimentation in subsequent studies, yielding microbeads with a mean diameter of ~150 μm, containing ~112 cells encapsulated per bead, thereby

meeting our size constraint for adequate oxygen delivery to the core of the microbead.

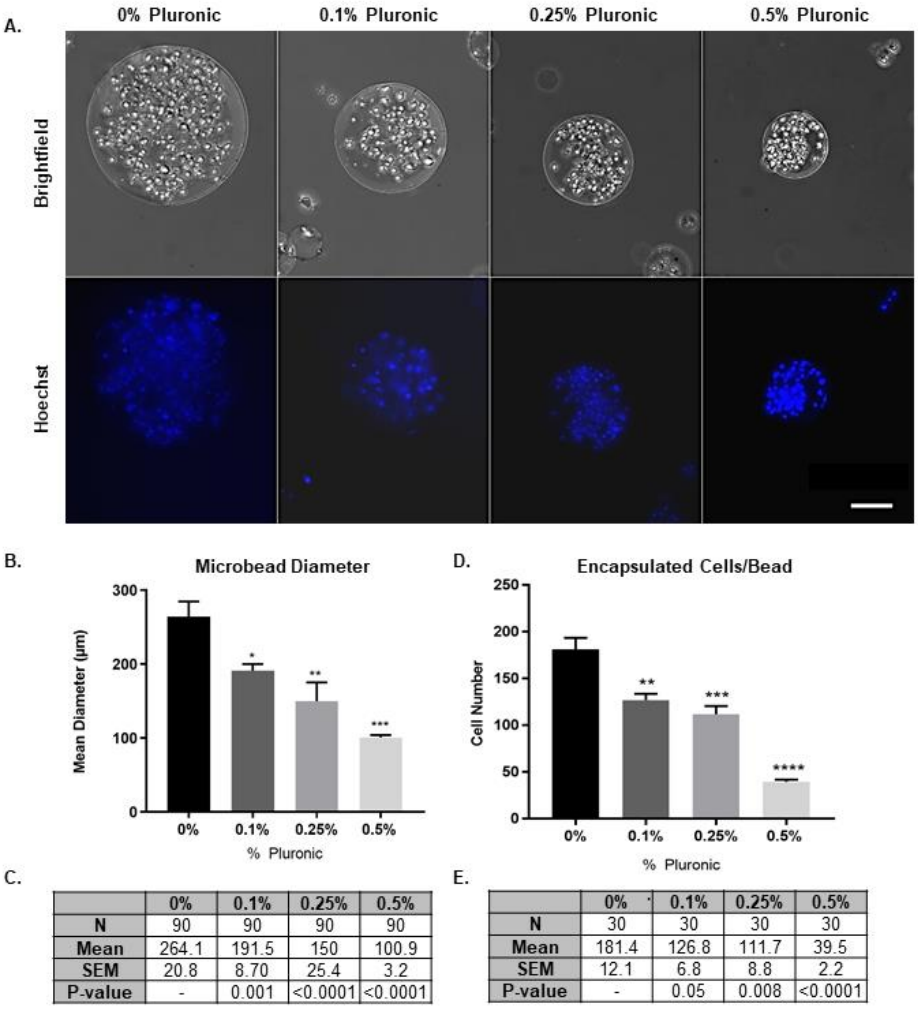

C.

	0%	0.1%	0.25%	0.5%
N	90	90	90	90
Mean	264.1	191.5	150	100.9
SEM	20.8	8.70	25.4	3.2
P-value	-	0.001	<0.0001	<0.0001

E.

	0%	0.1%	0.25%	0.5%
N	30	30	30	30
Mean	181.4	126.8	111.7	39.5
SEM	12.1	6.8	8.8	2.2
P-value	-	0.05	0.008	<0.0001

Figure 4. 1. **Creation and Optimization of Cell-Encapsulated Microbeads.** A) Brightfield images of NSC encapsulated in microbeads (top row) and nuclei stained with Hoechst (bottom row), demonstrating influence of Pluronic concentrations from 0 to 0.5% additions. B) Microbead mean diameter for varying Pluronic concentration (n=3). Values tabled in C. D) Cells encapsulated per bead for varying Pluronic concentrations (n=3). Values tabled in E. Error bars represent SEM. Scale bar (50 µm) representative of all images. * $p \leq 0.05$, ** $p \leq 0.01$, $p \leq 0.001$, and **** $p \leq 0.0001$ compared to 0% Pluronic determined by 1way ANOVA with multiple comparisons.

4.3.2 Co-encapsulation of EC and NSC Promotes NSC Quiescence and Enhances NSC Viability

Delivery of NSC in an undifferentiated, quiescent state is critical for NSC to respond properly to injury. EC induce NSC quiescence through Notch signaling as an effect of cell-to-cell

contact [29]. To determine the optimal ratio of NSC:EC for co-encapsulation, a seeding curve was conducted for 4 different ratios: 100:0, 75:25, 50:50, and 25:75, distinguishing NSC from EC in live culture by using GFP transfected NSC (Figure 4.2a). Mean fluorescence intensity (MFI) of $Ki67^+$ NSC was determined through flow cytometry (Figure 4.2b). NSC:EC ratios of 100:0 and 75:25 produce a MFI of 368.7 ± 55.97 and 312 ± 78.5, respectively. However, a 50:50 seeding ratio significantly reduces MFI to 105.4 ± 5.0. In this way, $Ki67^+$ NSC are reduced approximately 3-fold. Although a seeding ratio of 25:75 results in the greatest reduction of proliferating NSC, there is not a significant difference in MFI between the 50:50 and 25:75 seeding densities. In addition, a seeding density of 25:75 would diminish the effective goal of delivering an abundance of NSC, as a 25:75 ratio construct would be majority EC. From this point on, studies were conducted at a 50:50 encapsulation ratio of NSC: EC.

Once our encapsulation density was optimized, we evaluated NSC proliferation via immunostaining for NSC marker Sox2 and proliferative marker Ki67 (Figure 4.2c). For mono- and co- encapsulated microbeads, we quantify proliferating NSC as $Sox2^+Ki67^+$ cells, normalized to the total number of $Sox2^+$ cells (Figure 4.2e). One day following encapsulation, we observed a $Sox2^+Ki67^+$/ $Sox2^+$ ratio of 70.41 ± 3.57 and 62.07 ± 1.19 proliferating NSC in the mono-and co-culture system, respectively. Importantly, by day 3, we observed a reduction of $Ki67^+$ NSC in the co-culture to 40.23 ± 2.19 compared to NSC alone, with a proliferating population of 68.76 ± 2.52. This significant reduction of proliferating NSC in the co-culture is maintained by day 7, where the mono-and co-culture present 70.72 ± 3.49 and 31.53 ± 4.65, respectively, suggesting that NSC maintain a non-proliferative, quiescent state in the presence of EC.

Another major limitation to successful stem cell delivery is survival of transplanted cells in the cytotoxic and inflamed brain tissue [44]. To probe NSC viability in mono- and co-encapsulated microbeads, we stained for apoptotic marker cleaved caspase-3 (Figure 4.2d) quantifying $Sox2^+Caspase\text{-}3^+$ cells normalized to $Sox2^+$ cells to assess NSC viability (Figure 4.2f). One day following encapsulation, the ratio of cell viability in mono and co-cultures was 70.73 ±

4.18 and 73.50 ± 0.81, respectively. However, by day 3, NSC encapsulated alone had a significant decrease in viability to 58.51 ± 3.01 compared to the co-culture viability of 72.92 ± 2.48. Similarly, at day 7, NSC alone presented a significant decrease in viability to 53.62 ± 3.25 compared to the co-culture viability of 81.27 ± 3.75, suggesting EC play a role in promoting NSC viability.

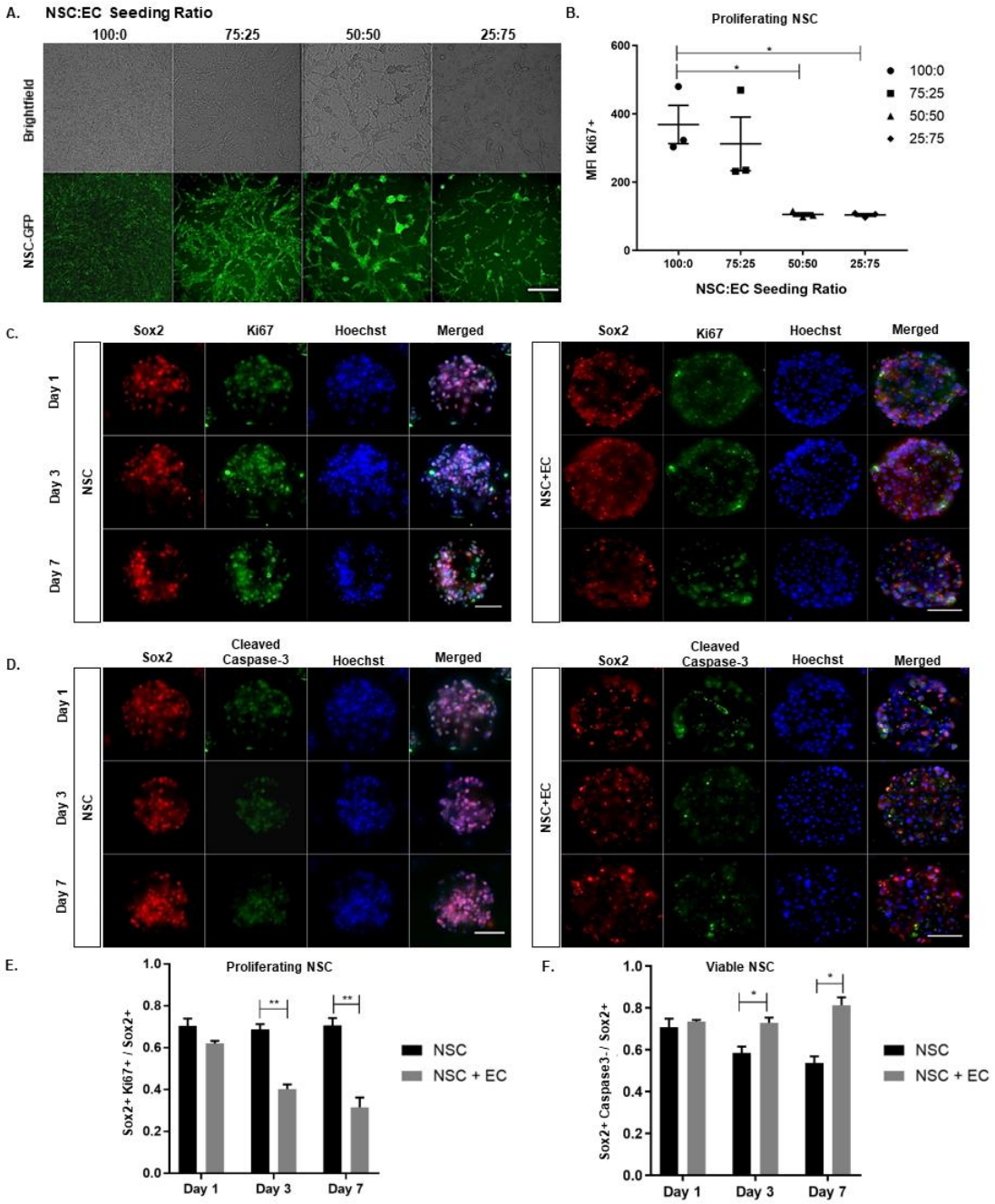

Figure 4. 2. Co-encapsulation of EC and NSC Promotes NSC Quiescence and Enhances NSC Viability. A) NSC:EC seeding density depicting brightfield (top row) and GFP-tagged NSC

(bottom row) at 4 different ratios B) Quantification for cell mean fluorescence intensity for $Ki67^+$ NSC 4 different ratios of NSC:EC determined through flow cytometry (n=3). C) Fluorescent images of NSC mono- and co-culture (left and right panel, respectively), stained for Sox2, Ki67, Hoechst, and merged. Imaged at 1, 3, and 7 days (top, middle, bottom panel, respectively) with quantified Sox2+Ki67+cells in E (n=3). D) Fluorescent images of NSC mono- and co-culture stained for cleaved caspase-3 with quantified Sox2+Caspase3- cells in F (n=3). Error bars represent SEM. Scale bar (50 μm) representative of all images. *p≤0.05, *** p≤0.001, ****p≤0.0001 determined by an unpaired t test.

4.3.3 EC MMP Activity Facilitates Degradation of Microbeads

Cell extravasation from the scaffold and integration into the host tissue is necessary post-delivery. The incorporation of the collagenase-sensitive peptide LGPA renders microbeads specifically susceptible to degradation by cell-secreted MMPs. The LGPA peptide has a cleavage site between leucine and glycine, demonstrating specificity only to collagenase degradation [149, 150]. To assess the effect of cultured media (CM) on degradable microbeads, CM of either NSC, NSC and EC, or EC were added to degradable microbeads (Fig. 3a). Changes in microbead morphology and integrity with NSC CM resembled microbeads in PBS, demonstrating no change in shape of the beads, however that of EC CM demonstrated a bead hallowing effect and surface erosion within 24 hours. NSC and EC CM began to promote microbead morphological changes within 48 hours. (Figure 4.3a). This suggests CM with EC-secreted MMPs accelerated microbead degradation and that the use of a co-encapsulated cell construct would be beneficial for cells to escape the beads at a faster rate than NSC encapsulated alone.

To further assess MMP activity, *in situ* zymography was performed using a fluorescein salt conjugated to gelatin, where gelatin serves as a target for collagenases. MMP-2 and -9 degradation [151]. Quantification of cell enzymatic activity was determined through the mean fluorescence intensity normalized to cell number, subtracting background. The gelatin substrate containing

quenched fluorogenic molecule demonstrated a robust and significant proteolytic activity of EC (22.93 ± 1.18) compared to NSC (0.92 ± 0.10) (Figure 4.3b-c).

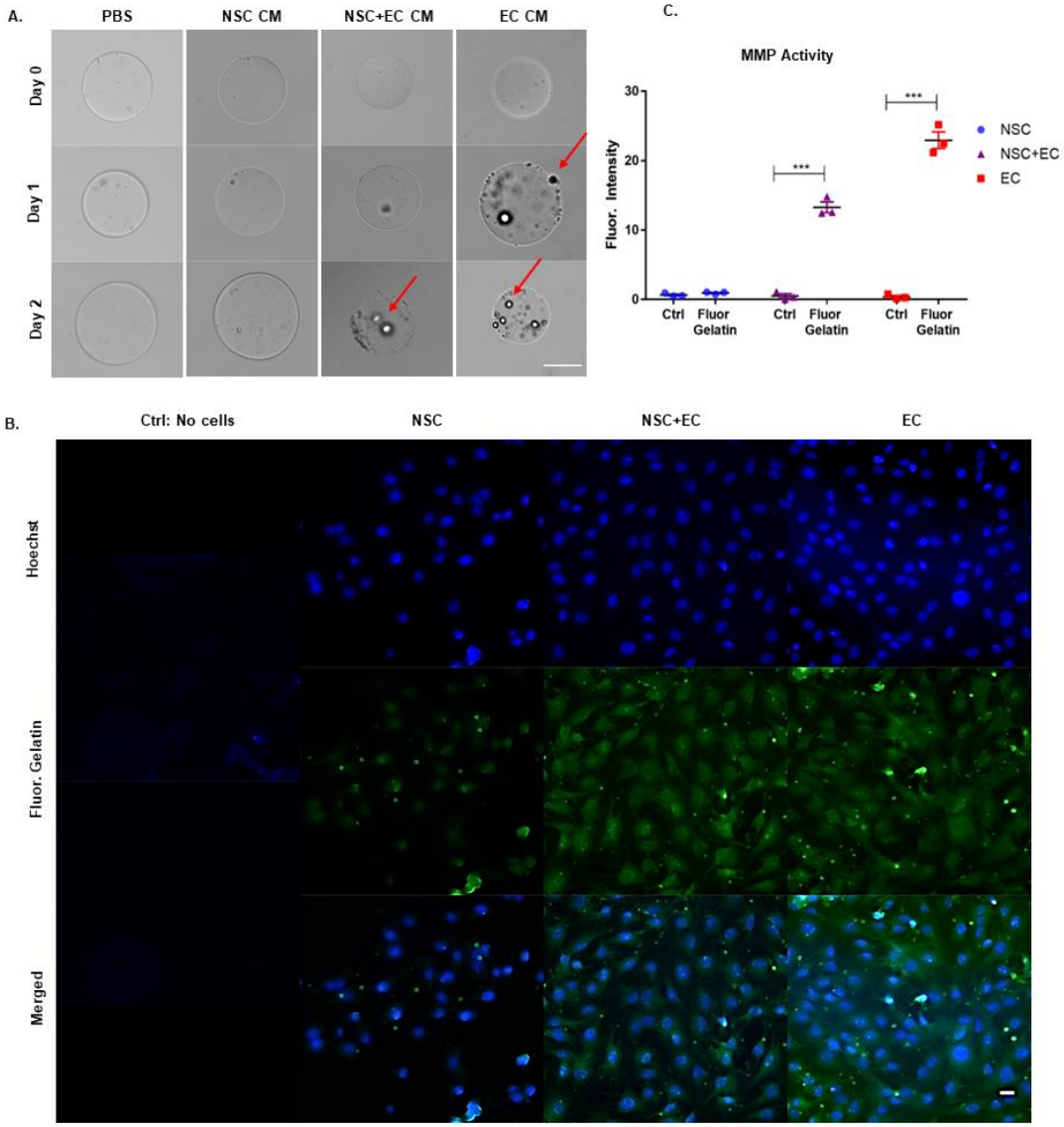

Figure 4. 3. EC MMP Activity Facilitates Degradation of Microbeads. A) Degradable microbeads in PBS, collagenase, NSC culture media (CM), NSC+EC CM, and EC CM, at 0, 1, and 2 days. Arrows point to areas of microbead surface corruption. B) In situ zymography with no cells (control), NSC, NSC and EC and EC monolayers. Cells stained with Hoechst (top row) are incorporated into an agarose gel with fluorescein gelatin to detect cell secreted MMPs (middle row), quantified in C) using ImageJ (n=3). Error bars represent SEM. Scale bar (50 µm) representative of all images. **p≤0.01 determined by an unpaired t test.

Interestingly, NSC with EC demonstrated proteolytic activity in a linear fashion compared to the two cell types alone (13.26 ± 0.77), suggesting EC are the major contributor to MMP activity in the co-culture condition. These data suggest that EC are necessary to facilitate NSC extravasation from the engineered microbead and into the host tissue.

4.3.4 EC Accelerate Quiescent NSC Extravasation from Microbead *in Vivo*

The transplantation strategy of microbeads is depicted in Figure 4.4a with injection parameters outlined in Figure 4.4b. A needle stab injury was used to cause direct injury to the cortex, corpus callosum and striatum. This intracerebral injection induced an alignment of $Iba1^+$ microglial cells and $GFAP^+$ astrocytes along the needle tract (Supplementary Figure A2.2). For delivery of the NSC, encapsulated mono-, co-cultures, or freely injected cells were prepared on the day of implantation. A total of ~$1x10^4$ cells encapsulated in microbeads were stereotaxically transplanted into the striatum (coordinates: 0.75mm anterior and 1.5mm lateral to the bregma, and 2.5mm ventral) of adult male mice (8-10 weeks old). To observe the response of microglia and tissue macrophages to grafted encapsulated cells, no immunosuppressive drug treatment was administered to mice prior to injection. Importantly, when we analyzed the brain slices at day 2, we found that the microbeads encapsulated with co-cultures were completely degraded, allowing for NSC to migrate into the surrounding tissue (Figure 4.4c). Notably, the microbeads loaded with monoculture remained intact, supporting the observation that EC expedite microbead degradation (Figure 4.3). Additionally, consistent with our *in vitro* results (see Figure 4.2), delivered NSC remained quiescent ($GFP^+/Sox2^+/Ki67^-$) when encapsulated with EC, whereas those encapsulated alone were increasingly dividing/proliferating ($GFP^+/Sox2^+/Ki67^+$; Figure 4.4d).

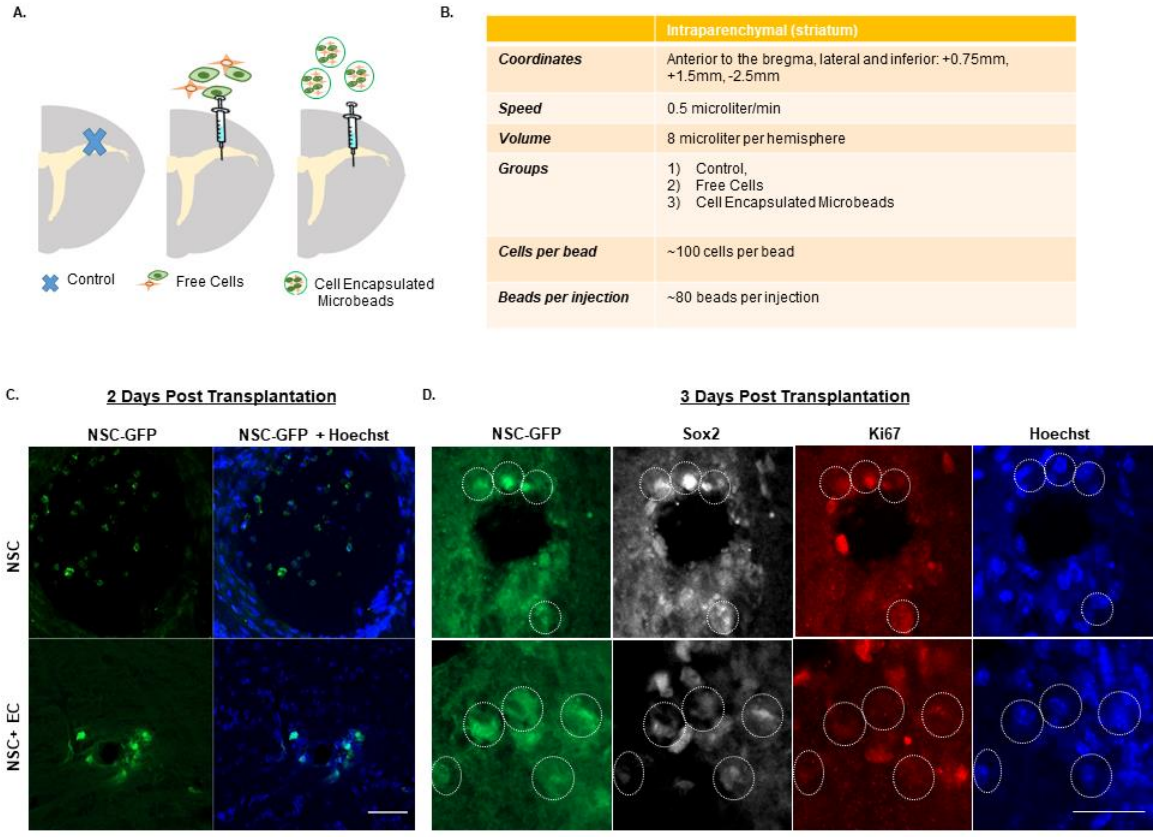

Figure 4. 4. EC Accelerate Quiescent NSC Extravasation from Microbead. A) Schematic overview depicting the transplantation target site (striatum) in the adult mouse brain for control, free cells, and cell encapsulated microbeads with transplantation parameters outlined in B. C) Confocal images of GFP-tagged NSC and Hoechst mono- and co-cultures encapsulated in microbeads to observe cell extravasation at 2 days post transplantation and D) expression of GFP-tagged NSC, Sox2, Ki67, and Hoechst to observe cell proliferation at 3 days post transplantation. Scale bar (25 μm) representative of all images.

4.3.5 Transplanted NSC in Microbeads Increase Endogenous NSC Proliferation and Differentiation in SVZ

Microbeads were delivered into the striatum, at a distance which is 250 μm $\pm$ 150 μm from the SVZ, at most, 50-100 μm to the lateral ventricle wall. At one week after implantation, encapsulated GFP-tagged NSC remained within the local vicinity of microbeads. Due to their limited migration, we do not see mixing of engrafted GFP-tagged NSC populations with endogenous SVZ located NSC (Figure 4.5a) To determine whether exogenous NSC can affect the endogenous NSC activity in the SVZ, brain tissue sections were prepared at 3- and 7-days post-

transplantation (dpt), and subjected to staining against Sox2, Ki67, and neuroblast marker, doublecortin (DCX). Quantitative analysis demonstrated that, at 3 dpt, the number of proliferating endogenous neural stem and progenitor cells ($Ki67^{+}Sox2^{+}$) were found to increase by 71.01 ± 6.66% and 60.57 ± 24% in mono- and co-encapsulation groups, respectively, compared to the control group (Figure 4.5b). At 7 dpt, a similar increase (67.48 ± 20.1%) in the number of endogenous $Sox2^{+}/Ki67^{+}$ cells was observed for the co-culture group compared to the control group. On the other hand, a significantly higher increase (~113.8 ± 28.18%) in this cell population was observed in monoculture group compared to the control group. The percentage of endogenous DCX^{+} cells along the SVZ wall, although essentially unchanged at 3 dpt, was significantly increased (~3-fold) at 7 dpt in the mono-culture group (Figure 4.5c). However, this cell population remained unchanged in co-culture group from 3 to 7 dpt. These results indicate that the exogenous NSC released from transplanted microbeads promote endogenous neural stem and progenitor cell proliferation and differentiation in the SVZ. On the contrary, exogenously delivered EC had a subtle but potent effect on endogenous neural stem and progenitor cell activity to inhibit their differentiation into newborn neurons.

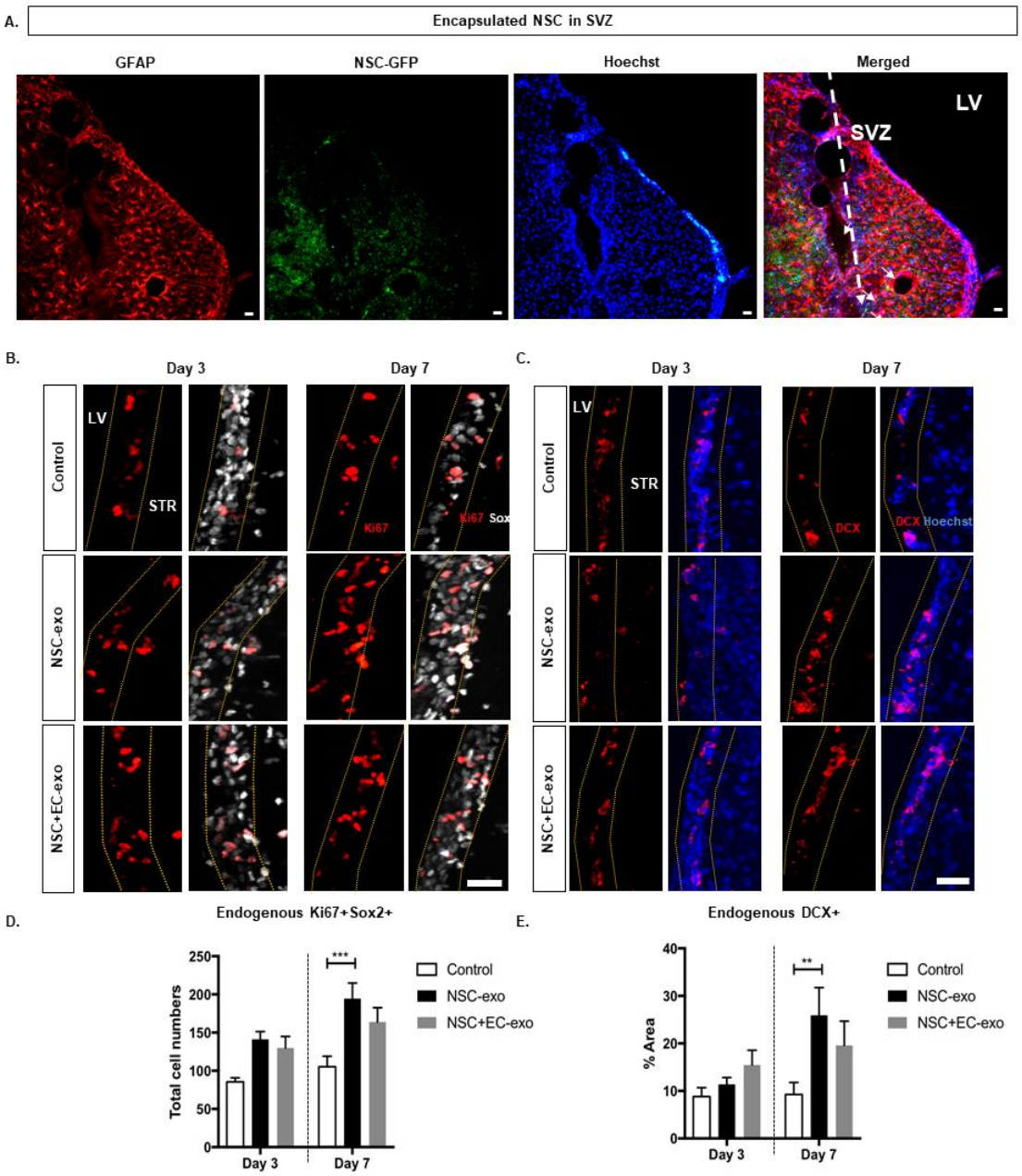

Figure 4. 5. Encapsulated Cells Increase Endogenous Cell Proliferation. A) Confocal image of injected microbeads position into the striatum relatively to the lateral ventricle (LV). Few GFP-tagged NSC were observed migrating towards SVZ two weeks after injection, however at day 3, no GFP-tagged NSC were founded in the subventricular zone (SVZ). B) Confocal images staining for Ki67 and Sox2 stained tissue sections of control (upper panel), encapsulated NSC (middle panel) and encapsulated NSC and EC (lower panel) groups, quantifying co-localization of proliferating NSC ($Ki67^+/Sox2^+$) in SVZ tabled in D. C) Confocal images staining for DCX and Hoechst to visualize endogenous NSC maturation in SVZ, quantifying endogenous DCX^+ cells tabled in E. Error bars represent SEM. Three different SVZ regions were selected from each brain tissue for the analyses (n=3-5). $^{**}p<0.01$ determined by one-way ANOVA with multiple comparisons. Scale bar (25 µm) representative of all images.

4.3.6 Co-encapsulation of EC and NSC Ameliorates Leukocyte Infiltration, Microglial Activation and Cell Death at the Site of Injection

The local immune response to transplanted exogenous NSC and its modulation are critical in enabling successful exogenous cell engraftment. Previous studies have indicated promising characteristics of PEG-based microbeads for producing minimal inflammation when transplanted into brain tissue [152]. To evaluate the local inflammatory response to the implanted microbeads, the extent of leukocyte (CD45) recruitment and microglia ($Iba1^{+}/CD45^{-}$) response were compared between encapsulated co-culture and control (freely injected co-culture) groups (Supplementary Fig. 2). As shown in Figure 4.6, free co-cultures induced a greater leukocyte infiltration around the injection site compared to the encapsulated co-cultures 2 days after transplantation (Figure 4.6a-b). Iba1+ microglia were found in proximity of the injection site in both groups (Figure 4.6a) Interestingly, while most, if not all, NSC (GFP^{+}) were colocalized to $Iba1^{+}$ cells with retracted processes in the control group, they were not colocalized with $Iba1^{+}$ cells in the encapsulated co-culture group. We next examined whether microbead encapsulation protects exogenous NSC from apoptotic cell death by immunohistochemistry for cleaved caspase-3 in both groups. For NSC+EC freely injected cells, viability was about 33.37% ± 16.74, whereas there was significantly higher viability observed in encapsulated co-culture group at 2 days following transplantation (75.92% ± 6.81) (Figure 4.6b).

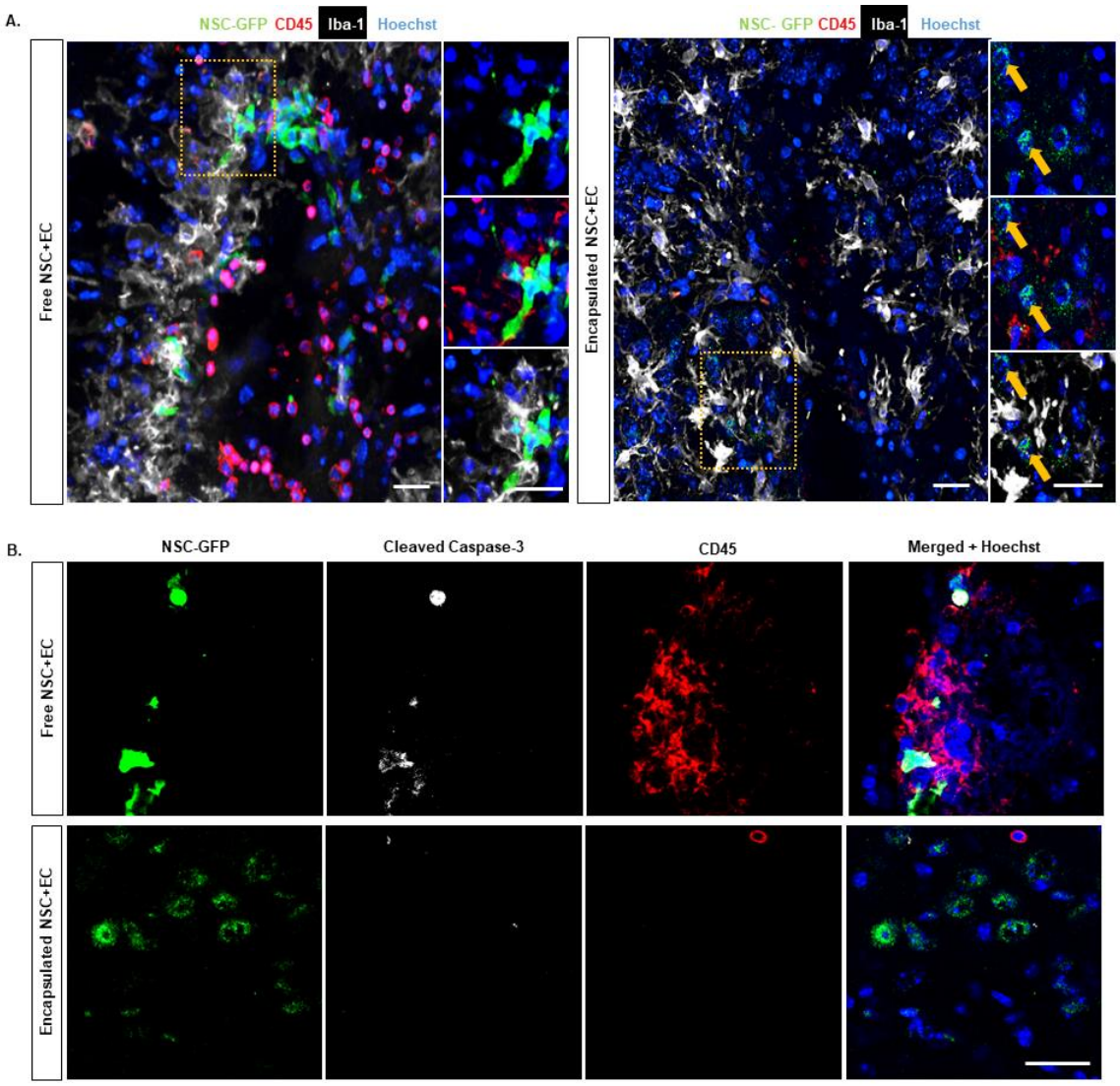

Figure 4. 6. Encapsulated Cells Exhibit Less Immune Response Compared to Free Cells. A) Immunofluorescence representative images of free (left panel) and encapsulated (right panel) GFP-tagged NSC with EC at 2 days showing expression of GFP-tagged NSC, CD45, Iba-1, and Hoechst. B) Confocal microscopy showing colocalization of anti-GFP, cleaved caspase-3, CD45 and Hoechst in free (top panel) and encapsulated (lower panel) co-culture transplantation groups. Scale bar (25 µm) representative of all images.

4.4 Discussion

A major limitation to cell based neurorestorative therapies is the engraftment of undifferentiated, viable cells to host tissue. In particular, NSC [153] and bone marrow stromal cells [154, 155] delivered directly to stroke injury models have shown a fraction of engrafted cells undergoing differentiation into mature neurons post injection, however the *in vivo* survival rate is

extremely low [141]. The use of other stem cell types, such as induced pluripotent stem cells, is limited by a lack of control over *in vivo* differentiation [156]. Another setback of stem cell injection is the extremely cytotoxic microenvironment of the post brain trauma. This injured tissue can lead to cell engulfment by infiltrating leukocytes or activated microglia. Hence, a tissue engineered scaffold that can deliver viable cells to the host tissue while maintaining a quiescent cell state presents a potential therapeutic advantage to recover the effects of neurodegeneration. The scaffold can also serve to protect encapsulated cells from immune cells that are recruited during early phases of cell transplantation, preventing exogenous cell apoptosis by ensheathing cells temporarily.

PEG, known for its tunable properties, can be used to serve as a biomimetic scaffold by which native ECM ligands for cell adhesion and spreading can be presented to cells. Here, we have utilized PEG as a scaffold for microencapsulation, mimicking the positive influence of EC on NSC in the SVZ niche. We have functionalized our scaffold, incorporating laminin-derived YIGSR and fibronectin-derived RGDS peptides to mimic two of the most abundant ECM proteins of the SVZ. By doing so, we consider the biochemical properties seen *in vivo* to support dual-cell encapsulation. Two critical considerations when optimizing our protocol included 1) maintaining the integrity of microbeads taken up through a syringe needle for *in vivo* delivery and 2) protecting cells from diffusion-limited oxygen and glucose access upon encapsulation. Optimization of our oil emulsion through addition of 0.25% Pluronic, a cell-compatible and PEG-based surfactant, has allowed us to produce microbeads with a mean diameter of 100-150 microns, facilitating uptake through a syringe needle and allowing for diffusion to cells at the core of the scaffold. Importantly, the size of these microbeads is below the threshold of 200 μm, where hydrogels at this size may threaten the diffusion of nutrients and oxygen to the core of the scaffold. Through conjugation of MMP degradable LGPA peptide to the PEG domain, we allow cell extravasation from the microbead post-injection through a syringe needle, allowing for integration of viable, quiescent NSC in the presence of EC into the murine SVZ.

The vasculature of the SVZ is a critical component of the NSC niche where direct cell-cell contact between EC and NSC enforce quiescence and promote stem cell identity. Quiescence and stem cell identity are maintained, at least in part, through EC presented ephrinB2 and Jagged1 signaling, respectively, which maintain NSC in a pro-differentiation state [29]. Recently, EC amyloid precursor protein has also demonstrated to support the maintenance of NSC quiescence [157]. In turn, NSC promote EC formation of capillary tube formation, suggesting a continued collaborative effort between NSC and EC in the SVZ niche [158, 159]. Our experimental NSC:EC seeding density curve, suggested that NSC and EC encapsulation at an equal ratio (50:50) would support maintenance of NSC quiescence and survival during the transplantation process. Our results demonstrate that NSC have increased viability and maintained non-proliferative state in the presence of EC prior to and post transplantation. Finally, we demonstrate the neuroprotective effect of our PEG scaffold, protecting cells from the activated immune cells post injection, and ultimately promoting exogenous cell viability.

NSC offer a promising therapeutic benefit in restructuring and repairing cytotoxic brain tissue by replacing cells that were lost following cerebral ischemia. Although NSC are one potential source of cell for transplantation into the injured brain, there are a range of complications of delivering NSC, including the control of NSC survival, proliferation, and differentiation post-delivery [139]. To address these limitations, an increasing number of studies have investigated the potential of co-transplantation therapy to enhance NSC viability in disease models such as stroke. For instance, it was previously reported that when NSC were co-transplanted with astrocytes in a rat model of stroke, there was a higher ratio of transplanted NSC survival and proliferation, and neuronal differentiation, compared with transplanting NSC alone [160]. However, as mentioned previously, it is crucial to maintain NSC quiescence upon delivery as activated exogenous NSC may disrupt endogenous repair mechanisms. Interestingly, our *in vivo* results observing the effect of exogenous NSC on endogenous SVZ-NSC activity are in line with previous studies demonstrating that transplanted NSC from various sources, including humans [161] and rats [162]

have the potential to induce endogenous NSC to proliferate and differentiate. Furthermore, our co-culture transplantation of NSC and EC showed that exogenous EC not only promote quiescence of exogenous NSC but also have an impact on endogenous NSC to some degree. Additional studies have reported the successful co-transplantation of freely injected EC and neural stem/progenitor cells to stroke-induced mice cortex, demonstrating survival and proliferation of neural stem/progenitor cells, in addition to accelerated neuronal differentiation [139]. Through the reduction of the localized inflammatory response observed of our encapsulated delivered niches, we predict that, in a pathological state, co-encapsulated cells will have increased viability as compared to freely injected cells.

In the present study, we focused on the role of EC in promoting NSC survival and quiescence, ignoring to date the potential impact of other cells native to the SVZ, including ependymal cells, pericytes, and microglia. Using our tunable PEG system, we can continue to optimize the microbead environment to include additional adhesive and degradative ligands to accommodate additional cell types and facilitate additional cell-cell and cell-ECM interactions. In doing so, we will create an SVZ *ex vivo* biomimetic niche for optimized delivery of healthy and viable reparative cells. Our *in vivo* data indicate promising results in a non-injury murine model, and future work will transition the use of encapsulated neural stem and endothelial cells to a stroke injury model. We can then observe the integration of cells in the inflamed, large cavity, as we continue to optimize our microbead formulation to protect cells post transplantation with the goal of promoting functional and long-term recovery.

4.5 Experimental Procedures

All experiments were performed in accordance with relevant guidelines and regulations.

4.5.1 Cell Maintenance

The features of this cell line have been characterized to establish growth of NSC as pure culture in defined serum-free conditions. In brief, established adherent neural cell lines (ANS4;

kindly provided by S. Pollard) were cultured in serum-free basal medium supplemented with N2 and B27 1 mg/mL laminin, and 10 ng/mL EGF and FGF-2 growth factors. For tracking *in vivo*, GFP transfected ANS4s were utilized [114]. The commercially available immortalized mouse brain endothelial cell line (bEND.3, ATCC) was cultured according to manufacturer's protocol. In brief, cells were cultivated in DMEM with 4 mM L-glutamine, 4500 mg/L glucose, 1 mM sodium pyruvate, and 1500 mg/L sodium bicarbonate, 10% fetal bovine serum and 1x Penicillin/Streptomycin. For both NSC and bEND.3 cells, culture medium was changed three times weekly at a seeding density of 2-2.5x10^5 cells/T25 flask and 4x10^6 cells/T75 flask, respectively. Cells were maintained at 37°C in 5% CO2 atmosphere and passages 27-33 were used for all studies.

4.5.2 PEGDA Synthesis

Poly (ethylene glycol) diacrylate (PEGDA) was prepared as previously described [82, 119]. Briefly, dry 10,000 Da PEG (0.1 mmol/ml) was combined with acryloyl chloride (0.4 mmol/mL) and trimethylamine (0.2 mmol/mL) in anhydrous dichloromethane, to react in argon overnight. The solution reacts with potassium carbonate to allow for phases to separate. Lastly, the lowest organic phase is dried with magnesium sulfate and precipitated with diethyl ether, filtered, and dried overnight.

4.5.3 Bioactive and Degradable Polymer Synthesis

The peptide sequences utilized for cell adhesion and degradation properties were RGDS, YIGSR, and LGPA. The LGPA was synthesized with >85% purity and characterized by free HPLC and mass spectroscopy. Bioactive peptides were conjugated to PEG as previously described [82, 119]. RGDS and YIGSR were conjugated to PEG monoacrylate by reacting the peptides respectively with acryloyl-PEG-N-hydroxysuccinimide Ester (PEG-NHS, 3500 Da) in 50 mM sodium bicarbonate (pH 8.5) at a 1:1 (peptide: PEG) molar ratio for 2 hours at room temperature. PEGylated products were then dialyzed for 24 hours using SnakeSkin™ Dialysis Tubing, frozen, and lyophilized. NMR was conducted to observe the disappearance of the proton peak of NHS at

2.9 mM. The collagenase degradable LGPA sequence was conjugated to PEG as previously described [163], reacting the peptide in sodium bicarbonate at a 1:2 (peptide:PEG) molar ratio for 24 hours at room temperature. PEG-LGPA-PEG was then dialyzed, frozen, and lyophilized.

4.5.4 Microbead Synthesis

Microbeads are formulated based on an oil emulsion technique previously described [75, 164] which have been optimized to create non-degradable, fluorescent microbeads in addition to degradable or non-degradable microbeads with encapsulated NSC+/-EC. Our methods have been aimed to increase packing density into a 24G Hamilton syringe without damaging the integrity of the microbeads, as well as maximize the number of NSC and EC encapsulated. To meet this criterion, we incorporated Pluronic, a PEG-based and cell compatible surfactant, at various concentrations: 0.1, 0.25, and 0.5% (v/v), determining the optimal addition to be 0.25% used in subsequent *in vitro* and *in vivo* studies.

4.5.4.1 Cell-Encapsulated Microbeads

An aqueous pre-gel solution was prepared with the additions of 0.1 g/mL 10 kDa PEGDA, 1.5% (v/v) triethanolamine in 1X Dulbecco's Phosphate Buffered Saline (PBS), 3.4 µl/mL 1-Vinyl-2-pyrrolidinone, 10 µM Eosin Y, and 0.25% (v/v) Pluronic. Photoinitiator (300 µg 2, 2Dimethoxy-2-phenyl-acetophenone/ mL NVP) was added at a concentration of 3 µL /mL of mineral oil in a glass tube.

Due to PEG being an inert polymer, we incorporated fibronectin-derived peptide RGDS and laminin-derived peptide YIGSR to render the polymer bioadhesive. Concentration of adhesive peptides were determined following a titration curve (2-6 mM) by seeding cells on coverslips coated with polymer in PBS to ensure the concentration was sufficient for cell attachment (not shown). The concentration of photochemicals and the methodology remains consistent as described above. For monocultures of NSC, 4 mM PEG-YIGSR was added, where for co-cultures 2 mM PEG-YIGSR and PEG-RGDS were added. To encapsulate cells, NSC and EC were lifted using

Accutase or 0.25% Trypsin/EDTA, respectively, and resuspended in pre-gel at a final concentration of 75 x 10^6 cells/ml. For co-culture encapsulation, a 50:50 ratio of NSC:EC was used and cultured in NSC media. Photoinitiator (300 μg 2, 2Dimethoxy-2-phenyl-acetophenone/ mL NVP) was added at a concentration of 3 μL /mL of mineral oil in a glass tube. To the mineral oil and photoinitiator phase, 25 μl pre-gel and cell solution was added, and the phases were vortexed for 13 seconds. The oil emulsion phase was then exposed to white light from a fiber optic illuminator (Cole Parmer High Intensity Illuminator, 67% intensity) for 3 minutes. Microbead were separated from the oil phase by adding 1 ml of NSC media and centrifuging for 5 minutes at 1200 RPM, decanting between three washes. Microbeads were transferred to a multiwell plate for culture in NSC media.

4.5.4.2 Verification of Microbead Synthesis Parameters Prior to Cell Encapsulation

A titration assay was done for all photochemicals mentioned above, adding the pre-gel solution to a monolayer of NSC and EC (not shown here). Final concentrations chosen were non-toxic, where cells maintained their morphology in this aqueous solution. Monolayers of cells were exposed to white light as to mimic the photo-crosslinking process, and similarly, cells maintained their morphology. Similar mechanical agitation was done in pre-gel solution in the absence of white light (emulsifying in mineral oil, vortexing, and centrifuging/decanting the mineral oil several times). Once cells were collected from the separated phases and seeded in media, they were healthy. This suggests the chemical and mechanical aspects of our protocol are non-toxic and non-damaging to cell integrity.

4.5.4.3 Degradable, Cell-Encapsulated Microbeads

For *in vivo* studies with encapsulated cells, 0.1 g/mL 10 kDa PEGDA was replaced with 0.1 g/mL PEG-LGPA-PEG to allow cells to extravagate from the microbeads and integrate with host tissue. Degradation assessment was conducted using 2 mg/ml collagenase, artificial cerebrospinal fluid (CSF), and media (control) to observe complete degradation within 24 hours in collagenase buffer (Supplementary Figure A2.1).

4.5.5 Characterization of Cell Response in Mono and Co-culture

4.5.5.1 NSC:EC Seeding Ratio

GFP transfected NSC and EC were seeded in 12 well culture plates at a final seeding density of 0.1 x 10^6 cells. To determine the optimal NSC:EC seeding ratio, a seeding density curve was conducted at 100:0, 75:25, 50:50, and 25:75 cells. After one day, wells were imaged, distinguishing NSC from EC via GFP tag expression. NSC were lifted using Accutase, which does not lift EC, ensuring EC remained in the well post NSC collection. NSC were then fixed in 4% PFA for 10 minutes, blocked and permeabilized with 5% normal donkey serum and 2% Triton X-100 in PBS for 1 hour at room temperature**,** and stained overnight against Ki67. Following secondary antibody incubation, cells were assessed through flow cytometry (n=3) and quantification was conducted using FlowJo.

4.5.5.2 Immunocytochemistry

Cell survival and cell quiescence after 1, 3 and 7 days of culture was assessed via quantification of cell apoptotic marker cleaved caspase-3 and proliferative marker Ki67 positive immunofluorescent staining, respectively. Specifically, microbeads with encapsulated NSC+/-EC were fixed in 4% PFA for 10 minutes, rinsed, and blocked and permeabilized with 5% normal donkey serum and 2% Triton X-100 in PBS for 1 hour at room temperature. Following rinses in PBS, samples were stained for Sox2, Ki67 and cleaved caspase-3 at 4°C overnight. Respective secondary antibodies and Hoechst were added for 2 hours at room temperature at a dilution of 1:1000. Immunofluorescent images were taken using a confocal and fluorescent microscope. ImageJ was used to quantify $Sox2^+Caspase\text{-}3^+$ cells or $Sox2^+Ki67^+$ cells to determine the survival and proliferation of NSC, respectively.

4.5.5.3 Cell Secreted Metalloproteinases

To assess metalloproteinases mediated degradation of microbeads, cultured media (CM) was collected from NSC, NSC and EC, and EC confluent monolayers following 24 hours.

Degradable microbeads were resuspended in PBS and CM, and incubated for 48 hours, imaging samples using brightfield microscopy every 24 hours to visualize degradation of samples.

To quantify cell-secreted metalloproteinases, *in situ* zymography was performed as previously described (Bowden et al., 2001; Chhabra et al., 2012). First, 2 mg/ml gelatin was dissolved in a buffer containing 61 mM NaCl and 50mM $Na_2B_4O_7$ (pH 9.3) and incubated at 37°C for 1 hour. Then, 2 mg/ml fluorescein sodium salt was added, reacting for 2 hours under constant rotation in darkness. The mixture was dialyzed at room temperature for two days, then stored at 4°C. NSC, EC, or NSC and EC were seeded on 12mm laminin coated coverslips (10 µg/ml) at a density of 6,000 cells/slip. One day later, samples were fixed with 4% PFA and washed with PBS 3 times. A 0.5% agarose solution in fresh digestion buffer (50 mM Tris-Cl (pH = 7.4), 150 mM NaCl, 5 mM $CaCl_2$) was allowed to cool to 45–50°C, and gelatin (control) or fluorescent gelatin were added at a 1:1 ratio. Hoechst was added (1:1000) for nuclei visualization. Solution was added in a thin layer to a pre-heated glass slide, placing the fixed cells with the cell side facing down into the solution. Following gel solidification, samples were incubated in digestion buffer at 37°C then observed under fluorescent microscope. Mean intensity fluorescence (MIF) and cell count were quantified using ImageJ, subtracting background fluorescence, and normalizing MIF to cell number.

4.5.6 Animals

C57Bl6 mice (Jackson Laboratories) were maintained in the Animal Research Center at Yale University on a 12-hour light/dark cycle with free access to water and food. All mice experiments were performed under a protocol approved by Institutional Animal Care Use Committee of Yale University.

4.5.7 Intra-parenchymal Stereotaxic Injections

All grafts were carried out within a 3 hour-time window of sample preparation. After anesthetizing mice with ketamine (80 mg/kg; i.p.) and xylazine (10 mg/kg; i.p.), blank beads (n=8), free NSC and EC (n=6), encapsulated NSC alone (n=8) or encapsulated NSC and EC (n=8) were

injected into the striatum at the following stereotaxic coordinates relative to bregma: +0.75 mm anterior, +1.5 mm lateral and 2.5 mm deep, as described previously [165]. Blank microbeads, encapsulated monoculture, free or encapsulated co-cultures were bilaterally injected using a 10µl Hamilton microsyringe (24-gauge), in volume of 8µl (100 beads per injection: 10,000 cells total/hemisphere) at a rate of 0.5µl/min. The syringe was remained in place for a period of 5 min before being withdrawn slowly to prevent potential reflux of the cells/beads. The craniotomy was sealed with bone wax, and the scalp was closed with tissue adhesive. Mice were allowed to recover on a heating pad before being returned back into their home cage. Animals were euthanized after 2, 3, 7 and 14 dpt for histological analyses.

4.5.8 Tissue processing and Immunohistochemistry

Mice were perfused with 0.01M PBS, followed by 4% PFA by cardiac puncture. Brains were removed and post-fixed overnight in 4% PFA at 4°C prior to cryoprotection in sucrose at 4°C for up to 48 h. Brains were cryosectioned coronally at 50 µm thickness. Sections were incubated with blocking solution (PBS containing 1% bovine serum albumin, 10% normal donkey serum and 0.1%Triton X-100) for 1 hour at room temperature then incubated overnight with primary antibodies diluted in blocking solution. The following antibodies were utilized in this study: cleaved caspase-3, CD45, doublecortin (DCX), Hoechst, Iba-1, Ki67, and Sox2. Appropriate secondary antibodies were used at a dilution of 1:500 and sections were coverslipped using Dako Fluorescence Mounting Medium. Samples were observed under a fluorescent microscope, spinning disk confocal, SP5 confocal and ophthalmology confocal microscope. Quantification of NPSC proliferation ($Sox2^{+}Ki67^{+}$) was performed manually, whereas for the NPSC quiescence and differentiation were analyzed automatically (% of area covered by respective cells) using ImageJ.

4.5.9 Statistics

All statistical analyses were performed using GraphPad Prism 7 software. Unless indicated otherwise, a sample size of 3 was conducted for *in vitro* studies and a sample size of 3-8 for *in vivo*

studies. Significance was determined with either a one-way ANOVA with multiple comparisons, or by an unpaired t-test as appropriate. Data are expressed as mean ± SEM and the differences were considered significant at P values of <0.05.

Chapter 5: ECM hydrogel improves the delivery of PEG microsphere-encapsulated neural stem cells and endothelial cells into tissue cavities caused by stroke.

Portions of this chapter were printed with permission from Ghuman, Matta, Tompkins, *et al.* 2020 [166]

5.1 Abstract

Intracerebral implantation of neural stem cells (NSCs) to treat stroke remains an inefficient process with <5% of injected cells being retained. To improve the retention and distribution of NSCs after a stroke, we investigated the utility of NSCs' encapsulation in polyethylene glycol (PEG) microspheres. We first characterized the impact of the physical properties of different syringes and needles, as well as ejection speed, upon delivery of microspheres to the stroke injured rat brain. A 20G needle size at a 10 µL/min flow rate achieved the most efficient microsphere ejection. Secondly, we optimized the delivery vehicles for in vivo implantation of PEG microspheres. The suspension of microspheres in extracellular matrix (ECM) hydrogel showed superior retention and distribution in a cortical stroke caused by photothrombosis, as well as in a striatal and cortical cavity ensuing middle cerebral artery occlusion (MCAo). Thirdly, NSCs or NSCs+endothelial cells (ECs) encapsulated into biodegradable microspheres were implanted into a large stroke cavity. Cells in microspheres exhibited a high viability, survived freezing and transport. Implantation of 110 cells/microsphere suspended in ECM hydrogel produced a highly efficient delivery that resulted in the widespread distribution of NSCs in the tissue cavity and damaged peri-infarct tissues. Co-delivery of ECs enhanced the in vivo survival and distribution of ~1.1 million NSCs. The delivery of NSCs and ECs can be dramatically improved using microsphere encapsulation combined with suspension in ECM hydrogel. These biomaterial innovations are essential to advance clinical efforts that aim to improve the treatment of stroke using intracerebral cell therapy.

5.2 Introduction

The transplantation of neural stem cells (NSCs) for chronic stroke is rapidly emerging from a pre-clinical proof-of-concept approach [167-169] to a clinical treatment modality [170, 171]. However, less than 5% of implanted cells remain within their injection site in the damaged peri-infarct tissue [168]. An improvement in retention and survival of intracerebral transplantation can be achieved by optimization of delivery parameters [172-174], as well as incorporating thermo-responsive biomaterials to reduce shear stress during the injection process [71] and prevent efflux of cells from the brain [105, 175]. A magnetic resonance imaging (MRI)-guided injection into brain tissue is required [168], as implantation of cells in a vehicle suspension into a tissue cavity lacks structural support for cells to be retained and survive in the liquid cyst environment [176, 177].

Provision of a structural support to NSCs through attachment to poly-lactic glycolic acid (PLGA) microparticles, nevertheless, affords direct delivery to the lesion cavity and dramatically increased the number of cells delivered to the stroke-damaged brain [176-178]. A major advantage of this approach is that microparticles can also be engineered to secrete growth factors, such as vascular endothelial growth factor A (VEGF-A), which improves the survival of NSCs and can promote neovascularization [178]. A major disadvantage of solid particles is that their degradation erodes the structural support for NSCs in the cavity and they do not readily provide a physical substrate for migration into the damaged peri-infarct tissue [177, 178]. The use of extracellular matrix (ECM)-derived hydrogel affords a consistent suspension of NSCs throughout the injectate and provides an efficient means to deliver and retain large quantities of cells inside a stroke cavity [179]. Short-term survival of NSCs can be achieved through the small quantities of growth factors in the ECM hydrogel, but the medium to long-term thriving of these cells, expected to serve as a source for repopulating the peri-infarct tissue, requires vascular support [180, 181].

Co-transplantation of NSCs with endothelial cells (ECs) into peri-infarct tissue improves NSC survival [139, 182] and potentiates growth factor release from both types of cells [183]. The effect of NSCs on host ECs and vasculature is also emerging as a pivotal mechanism involved in meditating the therapeutic effects of NSCs [168, 184, 185]. The crosstalk and close proximity of NSCs and ECs in the neural stem cell niche is further evidence of how intimately the fate of both cell types is intertwined [186-188]. ECs can influence NSCs to maintain their stem cell state, but also direct their migration and differentiation [183, 187, 189]. The combined delivery of densely packed NSCs and ECs into a lesion cavity could hence provide a robust source of NSCs to repopulate the peri-infarct tissue [190]. However, implantation of densely packed NSCs and ECs produces a cell mass, rather than an integration with the peri-infarct tissue. A further downside of cells suspended in liquid vehicles is that cells will sediment and compact with time [173]. Cell-cell proximity is hence required, in addition to sufficient spacing between cells and an interstitial substrate that affords cell migration.

To achieve and maintain a close proximity of NSCs and ECs without sedimentation during the implantation and the early phase post-implantation, encapsulation of both cells types in microspheres can be envisaged to create prototypical ex vivo neural stem cell niches that define the spatial positioning of cells [1, 179]. Compared to only the encapsulation of NSCs, co-encapsulation of NSCs with ECs into polyethylene glycol (PEG) microspheres maintained NSC quiescence, improved viability and facilitated extravasation from microspheres [105]. The intra-parenchymal implantation of small volumes of encapsulated cells has been widely used to shield transplanted cells from immunological rejection [191] and has found clinical translation in patients with Parkinson's disease [192, 193]. Shielding of cells from exposure to the immunological rejection or preventing integration into the brain relies on the non-degradability and prevention of migration of encapsulated cells.

Conversely, to repopulate peri-infarct tissue with implanted cells necessitates migration of cells from the microspheres, which is contingent on the biodegradation of microspheres [194]. The implantation of microspheres into the large stroke-cavity further requires a novel delivery strategy to achieve a homogenous distribution of a large volume of microspheres throughout the tissue defect upon implantation. A homogenous distribution of microsphere provides an equal density of cells throughout the defect, as well as ensures that cells can invade the peri-infarct perimeter. Moreover, a homogenous secretion of growth factors and utilization of nutrients warrants a consistency in therapeutic effects and cell survival. PEG microsphere encapsulation acutely shields transplanted cells from shear stress caused by passage through a narrow needle bore. Encapsulation also provides a temporary protection against stroke-induced inflammation and M1-like macrophages clearing cellular debris in the lesion area. As factors secreted from transplanted cells modulate inflammation, microspheres can gradually degrade over several days following implantation to afford the migration of implanted cells into a more permissive environment. Controlling the degradation kinetics of these microspheres will hence be a key design factor to fully exploit this enabling technology.

In contrast to the intra-parenchymal implantation of microspheres, filling of a stroke cavity requires an injection-drainage approach, where biomaterials are injected through a needle and the extracellular fluid (ECF) in the tissue defect is evacuated through a second catheter [176, 179]. Firstly, the integrity and suspension of microsphere for injection through a narrow needle bore needs to ensure a minimally invasive intracerebral delivery. Secondly, a homogenous distribution and suspension of microspheres in the tissue cavity is required. The implantation is, however, dependent on the type of tissue cavity. Typically, two common tissue cavities are observed after stroke. One pathology affects purely cortical tissue that is situated at the surface of the brain and is of a smaller volume. This type of tissue defect is commonly modeled using photothrombosis. A second pathology, reflecting two thirds of all ischemic strokes, creates a

more extensive tissue cavity that extends across the striatum and cortex with a large volume. This pathology is readily modeled using a transient intraluminal middle cerebral artery occlusion (MCAo). Herein, we demonstrate that these disparate tissue defects necessitate different delivery strategies. To maintain a robust retention and distribution of microspheres in the cavities, these microspheres need to be suspended in an ECM hydrogel. Using this approach, the feasibility of delivering microsphere encapsulated NSCs and ECs to a large tissue cavity was evaluated to determine its efficiency in promoting cell survival, as well as the migration of cells throughout the damage caused by a stroke.

5.3 Methods

5.3.1 Biomaterial production and cell encapsulation

Polyethylene glycol diacrylate synthesis. Polyethylene glycol diacrylate (PEGDA) was prepared as previously described [105]. Briefly, PEG diacrylate was made by combining dry 10,000 Da PEG (Fluka, 0.1 mmol/ml) with acryloyl chloride (0.4 mmol/mL) and trimethylamine (0.2 mmol/mL) in anhydrous dichloromethane, reacting in argon overnight. The solution reacted with potassium carbonate to allow for phases to separate. Lastly, the lowest organic phase is dried with magnesium sulfate and precipitated with diethyl ether, filtered, and dried overnight. Prior to use, PEG-DA was characterized by proton nuclear magnetic resonance (NMR), observing the characteristic peak at 3.5 pm and three acrylate peaks between 5.5 and 6.5 ppm [195].

5.3.2 PEG derivative synthesis

PEG derivatives were synthesized using previously described methods [105]. Briefly, the fibronectin derived Arg-Gly-Asp-Ser (RGDS) or laminin derived peptide Tyr–Ile–Gly–Ser–Arg (YIGSR) were reacted with acryloyl-PEG-N-hydroxysuccinimide Ester (PEG-NHS, 3500 Da; JenKem Technology) at a 1:1 molar ratio in 50 mM sodium bicarbonate buffer (pH 8.5) for 2 hours at room temperature. Following reaction, the coupled peptide (acryloyl-PEG-RGDS or acryloyl-PEG-YIGSR) was dialyzed overnight and lyophilized for 2 days. In order to determine efficient

conjugation, the PEGylated peptide was characterized by NMR, observing the disappearance of the proton peak of NHS at 2.9 ppm. In order to create fluorescent polymer, Alexa Flour™ 488 was conjugated to acryloyl-PEG-RGDS [83]. PEG-RGDS was dissolved in 0.1 M sodium bicarbonate buffer (pH 8.5) and Alexa Fluor™ 488 (AF-488) NHS Ester (Succinimidyl Ester, ThermoFisher Scientific) was dissolved in dimethyl sulfoxide (DMSO, 1 mg/100 µL). AF-488 was added to PEG-RGDS at a 10:1 molar ratio of dye to conjugated polymer and reacted for 2 hours at room temperature. The fluorescent PEGylated polymer was dialyzed for 24 hours, frozen, and lyophilized. In order to render biodegradable microbeads, the degradable sequence glycine-glycine-leucine-glycine-proline-alanine-glycine-glycine-lysine (GGLGPAGGK; LGPA) was conjugated to PEG as previously described [82], reacting LGPA in sodium bicarbonate at a 1:2 (peptide:PEG) molar ratio for 24 hours at room temperature, then dialyzed for 24 hours, frozen, and lyophilized to form PEG-LGPA.

5.3.3 Photopolymerization of microspheres

Microspheres were optimized to increase packing density of microspheres into a Hamilton syringe, without damaging the integrity of the microspheres [105]. Microspheres were created using a dual-emulsion technique using previously described methods where we have optimized the size of the constructs [105]. Briefly, an aqueous hydrogel solution was prepared with additions of 0.1 g/mL 10kDA PEG-DA, 1.5% (v/v) triethanolamine in 1X Dulbecco's Phosphate Buffered Saline, 3.4 µl/mL 1-Vinyl-2-pyrrolidinone (NVP), and 10 µM Eosin Y. To create fluorescent polymer, 4 mM fluorescent PEG was added. Concentration of fluorescent PEG was determined following a titration curve (2-6 mM addition) to visualize a strong signal (data not shown). To 1 mL of a mineral oil phase, 3 µL of photoinitiator solution (300 µg 2,2Dimethoxy-2-phenyl-acetophenone in 1 mL NVP) was added. To this mineral oil and photoinitiator phase, 25 µL of the hydrogel solution was added and the phases were vortexed on full speed for 13 seconds. The oil emulsion phase was then exposed to white light from a fiber optic illuminator (Cole Parmer High Intensity Illuminator, 66.67% intensity) for 3 minutes. Microspheres were separated from the oil phase by adding 1 ml

of DPBS and centrifuging for 5 minutes at 1200 RPM, decanting mineral oil between three washes. Microspheres were transferred to a multi-well plate for imaging, then frozen in Eppendorf tubes were filled with PBS until further use.

5.3.4 Neural stem cells (NSCs) and endothelial cells (ECs)

The adult NSC cell line ANS4 (kindly provided by Dr Steven Pollard, University of Edinburgh) was derived from the subventricular zone surrounding the lateral wall of the forebrain ventricle of 2 months old mice [114, 196]. In order to differentiate endogenous and exogenous NSC in vivo, CAG synthetic promoter driven green fluorescent protein (GFP)-NSCs were utilized which have been transfected with the insertion at safe harbor loci ROSA26 [114]. Adherent GFP-NSC were cultured in serum-free basal medium supplemented with N2 and B27, as well as laminin (1 mg/mL), EGF (10 ng/mL) and FGF-2 (10 ng/mL). The immortalized mouse brain endothelial cell line (bEND.3, ATCC) was cultured in DMEM with L-glutamine (4 mM), glucose (4.5 mg/mL), sodium pyruvate (1 mM), sodium bicarbonate (1.5 mg/mL), fetal bovine serum (10%), and 1x Penicillin/Streptomycin. Culture medium was changed 3x/week at a seeding density of 2-2.5x 105 NSCs/T25 flask and 4x 106 ECs/T75 flask. Cell cultures were maintained in 5% CO2 at 37 ºC and passages 26-30 were used for all studies.

5.3.4 Cell encapsulation

Microspheres were formulated for the encapsulation of NSCs alone or NSCs co-encapsulated with ECs, as previously described [105]. For microspheres with solely encapsulated NSCs, 4 mM PEG-YIGSR was added to the concentration of photochemicals listed above, replacing PEG-DA with PEG-LGPA to allow for microsphere degradation. For co-encapsulations of NSCs and ECs, 2 mM of PEG-YIGSR and PEG-RGDS were added. Cells were lifted using Accutase or 0.25% Trypsin/EDTA to lift NSCs and ECs, respectively, which were resuspended in the pre-gel at a concentration of 75 million cells/mL (75,000 cells/μL, 34% volume fraction). Co-encapsulated microspheres had a ratio of 50:50 NSCs: ECs. Cells were suspended in the photochemical and polymer solution, which was then added to the mineral oil and photoinitiator phase. The two phases

were vortexed and crosslinked to encapsulate cells within the microspheres. Upon crosslinking, washes were performed using NSC media. Microsphere-encapsulated cells were then maintained in an incubator for assessment. An average of 110 total cells were encapsulated per microsphere. For encapsulation of both NSCs and ECs, both cell types were added in equal proportions resulting in an even mixture, i.e., 55 NSCs and 55 ECs per microsphere.

5.3.5 Protocol optimization and microsphere characterization

Pluronic F-68, a PEG based and cell-compatible surfactant, has previously shown to reduce the diameter of PEG-based microspheres, as well as achieve a more consistent bead size [75]. In order to produce microspheres that retain their integrity when taken through a Hamilton syringe, microspheres with an average of diameter range of ~150-200 μm in was targeted. A range of microsphere diameters allowed us to increase packing density of microspheres into the syringe and maximize delivery. To adjust microsphere diameter, 0.1, 0.25, and 0.5% Pluronic was added to the polymer solution. Using ImageJ, microsphere diameter and shape were quantified. A circularity of 1 defined a perfectly round shape (see below). Addition of 0.25% Pluronic to the pre-gel phase produced a mean microsphere diameter of ~150 μm. To quantify yield, 100 μL aliquots were transferred to a multi-well plate and manually counted directly following production. Packing density was quantified by transferring microspheres into an Eppendorf tube, filling the tube with PBS, and pulsing the sample in a microcentrifuge for 5 seconds. PBS was aspirated and the pelleted suspension was re-suspended into 100 μL of PBS. The sample was spun down and the volume of microspheres versus volume of PBS was calculated to determine the volume packing density.

5.3.6 Verification of Shipment and Storage Conditions

In order to evaluate the impact of dry ice shipping conditions, frozen samples of microspheres were thawed to room temperature, spun down to collect a pellet, and transferred to a multiwell plate for imaging. Frozen microspheres retained both their fluorescence and shape following freeze/thaw cycles [105]. Upon shipment to the University of Pittsburgh, microspheres were thawed and re-

assessed for quality control. Fluorescence and microsphere integrity were retained following shipment. Similar qualitative and quantitative analysis of microsphere integrity was repeated using a pipette and Hamilton syringe, to determine the impact of shear stress on microsphere integrity.

5.3.7 Cell Cytotoxicity and Cell Viability

Following the verification of shipment and storage conditions of microspheres, we further tested cell cytotoxicity and viability for cell-encapsulated microspheres. In order to assess cell cytotoxicity, an LDH assay was conducted following the manufacturer's protocol (C20300, Thermo Fisher Scientific). Culture media from plated NSCs and NSCs+ECs (10,000 cells/well in a 96 well plate) was used as a control for live and dead cells. Killing cells with lysis buffer provide a 100% dead cell control condition. The absorbance was recorded at 480 nm and 680 nm (background signal from instrument) using a spectrophotometer. To assess viability before and after cryopreservation, culture media was spun down to separate microspheres after 24 hours of culture in a 96 well plate (~200 microspheres per well). Calcein (ThermoFisher) and Hoechst 33342 (1 μg/mL, Sigma) were added to microspheres to visualize cell viability throughout the construct using a fluorescent microscope.

5.3.8 Extracellular matrix (ECM) hydrogel

The basement membrane and tunica propria of an adult porcine urinary bladder (Tissue Source, Inc., Lafayette, IN) were isolated through mechanical delamination [197]. Decellularization was performed using 0.1% peracetic acid in 4% ethanol (v/v; 120 min; 300 rpm) with agitation. Cellular debris was removed through a series of PBS and deionized water rinses. Hematoxylin & Eosin, 4',6-diamidino-2-phenylindole (DAPI) staining, agarose gel electrophoresis, and quantification of remnant DNA were used to confirm decellularization [198]. The remaining ECM was lyophilized, comminuted, and solubilized with pepsin (1 mg/mL) in 0.01 N HCL. To achieve neutral pH, 0.1 N NaOH was added. The liquid phase of the hydrogel was maintained at temperatures less than 37 degrees C. The majority of the material (~70%) is collagen [199], although other prominent ECM

proteins are also present, including fibronectin, decorin, and laminin subunit γ1 [200]. A variety of growth factors including transforming growth factor-β (TGF-β), vascular endothelial growth factor-A (VEGF-A), basic fibroblast growth factor (bFGF), and nerve growth factor (NGF), are also retained within the ECM preparation [201]. Additionally, matrix-bound nanovesicles (MBV) enriched in miRNA as well as other signaling molecules are present within the ECM preparation [202]. The ECM hydrogel was diluted to 4 mg/mL by suspension in the appropriate volume of PBS [197]. Gelation of this preparation is concentration and temperature-dependent, reaching 50% gelation in 3.2 minutes and achieving a viscosity of 0.084 Pa. The storage modulus (G') for this preparation is 76.6 Pa, which exceeded its loss modulus (G", 11.0 Pa) [179].

5.3.9 Stroke models

All animal procedures complied with the US Animal Welfare Act (2010) and were approved by the University of Pittsburgh Institutional Animal Care and Use Committee (IACUC). Male Sprague-Dawley rats (Taconic Labs, USA) with an initial body weight between 245-275 g were maintained on a 12-h light/dark schedule, with food and water available ad libitum. All surgical procedures were performed using a sterile technique under isoflurane (4% induction, 1% maintenance in 30% O2). After anesthesia induction, the hair over the surgical site was shaved using electric clippers, followed by application of betadine. A temperature-controlled heating pad was used to maintain body temperature (37 degrees C) throughout the procedures. Using a random number sequence in Excel (Microsoft, USA), animals were assigned to either undergo photothrombosis or MCAo. After recovery from surgery, animals were assessed for forelimb flexion and contralateral circling with daily post-operative care and neurological assessment until they recovered pre-operative weight [203]. Animals not exhibiting signs of stroke damage, as determined by MRI, or who failed to recover weight, were excluded [179].

5.3.10 Photothrombotic rat model of stroke

For this procedure, an incision was made over the scalp to reveal the cranial fissures and locate bregma. A sterile cotton applicator was used to remove any remaining fascia over the cranium. Under a surgical grade microscope, a speed-controlled drill was used to drill into the cranium (3 x 3 mm) over the motor cortex in a zig-zag pattern to avoid heat buildup. The cranium was thinned until the vasculature became visible through the surgical microscope. A fresh solution of Rose Bengal (330000, Sigma, USA) in sterile PBS was prepared at a concentration of 20 mg/kg before i.p. administration. After 5 minutes, the surface of the thinned skull was illuminated with white light (V-Lux 1000, Volpi, USA) using a fiber optic cable for 20 minutes. After induction, the area over the thinned skull was filled with bone wax (Fisher, USA) prior to suturing. LX4 (Ferndale, containing 4% Lidocaine) was topically applied as an analgesic and buprenorphine (0.5 mg/kg) i.p. was given for 3 days to provide a sustained pain relief.

5.3.11 Transient intraluminal right middle cerebral artery occlusion (MCAo) rat model of stroke

For this, rats were placed in the supine position and a ventral cervical midline skin incision was made under the surgical microscope. The common carotid artery was exposed and a 5-0 silicone rubber-coated monofilament (diameter 0.12 mm, length 30 mm, tip coating at 0.35 mm for 5-6 mm, 503556PK10, Doccol, USA) was advanced to the ostium of the MCA in the circle of Willis, as previously described in detail [204]. The MCA was occluded for 70 minutes, followed by reperfusion due to retraction of the filament to the common carotid bifurcation.

5.3.12 Magnetic resonance imaging (MRI) and infarct volume calculation

To determine the presence, location, and volume of tissue loss, both photothrombotic and MCAo rats were anesthetized with isoflurane (4% induction, 1% maintenance) and scanned using a T2-weigthed spin-echo MRI sequence (TR = 6000 ms, TE = 8 ms, 8 Averages, FOV 30 x 30 mm, 128 x 128 matrix, 42 slices at 0.5 thickness) on a horizontal bore 9.4 T Varian scanner 12 days post-

infarction. T2-weighted images were thresholded at 1 standard deviation above the mean of a rectangular region of interest [186] in the contralateral hemisphere, encompassing striatum, corpus callosum, and neocortex. Stroke-damage was defined on these images as tissue with a hyperintense signal [205]. For PT (n = 10) and MCAo (n = 20), rats with respective lesion volumes >20 mm3 and >40 mm3 (i.e., 20 and 40 µL) were selected for injections by random assignment to treatment or control groups.

5.3.13 Delivery parameter optimization

5.3.13.1 Needle Size

To assess the effect of needle size on microsphere delivery, a frame mounted injection pump (World Precision Instruments, USA) was used to eject 20 µL of green, fluorescent (Alex488) microspheres with no encapsulated cells (suspended in PBS) from a 250 µL Hamilton syringe with a beveled tip metal needle (inner diameters of 20G, 24G, 26G) at a constant speed of 10 µL/min. A 100 µL pipette served as a control. The shape factor's circularity, aspect ratio, and roundness were measured for each microsphere using ImageJ2 (ImageJ). These factors provide a dimensionless measure of shape, independent of size and were used to evaluate the effect of different needle sizes on microsphere shape and symmetry.

5.3.13.2 Ejection Rate

To assess the effect of ejection rate on microsphere delivery, a stereotactic frame-mounted injection pump (World Precision Instruments, USA) was used to eject 20 µL of green, fluorescent microspheres from a 250 µL Hamilton syringe with a 20G beveled tip metal needle at a constant speed (1, 5, 10 µL/min). Individual microsphere's circularity, aspect ratio, and roundness were calculated. These shape factors were used to evaluate the effect of ejection rate on microsphere shape and symmetry. Microsphere volume fraction and density were also calculated.

5.3.13.3 Diameter

Microsphere diameter (d) was measured using ImageJ2 to determine whether the size of ejected microspheres is affected by needle size. To reveal a relationship between ejection rate and microsphere diameter, a 20 µL bin size was used to compare the number and diameter of microspheres ejected.

5.3.13.4 Microsphere Volume

A perfect spherical shape was assumed for microspheres. Volume was calculated using the following formula: $V=4/3\ \pi\ (d/2)^3$.

5.3.13.5 Volume fraction

Ejected microsphere volume fraction was calculated by summing the microsphere volumes for each ejection trial and normalizing this total volume by the volume ejected (20 µL). The number of microspheres measured for each trial was used to approximate microsphere density.

5.3.13.6 Circularity

This measurement evaluates degree of deviation in symmetry from a circle, with a value of 1.0 indicating a perfect circle and a value approaching 0.0 indicating increasingly elongated shape. Circularity was calculated using the following formula: $\text{Circularity}= 4\pi*\text{Area}/〚\text{Perimeter})]^2$.

5.3.13.7 Aspect ratio

Major axis indicates the largest diameter of the microsphere, while minor axis indicates the smallest diameter. The aspect ratio of each microsphere was calculated to evaluate the effect of needle size on the ratio between microsphere height and width: Aspect Ratio= (Major Axis)/ (Minor Axis).

5.3.13.8 Roundness

A roundness value of 1.0 indicates maximum symmetry, i.e., a perfect circle. Roundness indicates how closely an object resembles a perfect circle. Microsphere roundness was measured using the following formula: $\text{Roundness}=4*\text{Area}/ (\pi*〚\text{Major Axis}]^2)$.

5.3.14 Implantation procedure

All implant procedures were performed using a 250 µL Hamilton syringe with a 20G needle and a stereotactic frame (Kopf, USA) at 14 days post-stroke for the following groups: 1) empty microspheres, 2) ECM hydrogel, 3) empty microspheres suspended in ECM, or 4) cell-encapsulated microspheres suspended in ECM. Ideally, microspheres are injected using a needle with a very small bore size to minimize injection damage to intact and damaged brain tissue [206]. However, a larger needle size (20G) is advantageous to prevent potential aggregation, gelation, and damage of microspheres, as well as obstruction of the needle lumen, to ensure efficient delivery of material. Prior to implantation, equal volumes of ECM or PBS were added to the microsphere pellet and served as the final suspension solution for implantation. A 20 µL sample of this final suspension was imaged to determine the number and size, as well as volume fraction and density, of microspheres. The suspension was gently mixed with a p1000 pipette before filling the implantation syringe.

5.3.14.1 Photothrombic implantation

For implantation into the cortical cavity, bone wax over the thinned cranium was gently removed before creating a burr hole at the center of cranial window. Next, a beveled tip needle was carefully lowered into the burr hole to make a small tear into the dura to allow a blunt tip needle to pass through without causing further damage. The blunt tip needle was then lowered to 1 mm below the cortical surface and lesion-equivalent volumes of ECM hydrogel (n=4), microspheres (n=3) or microspheres suspended in ECM (n=3) were injected. A manual injection of the required volume was performed at a speed of 10 µL/min, which was timed for the appropriate volume using a timer.

5.3.14.2 MCAo implantation

For subcortical implantation, a second burr hole was used for a drainage cannula (24G) [179]. Stereotactic coordinates for the injection needle and drainage cannula placements were defined using MR images of lesion location and volume [179, 180, 206]. Injection rate was controlled using

a frame-mounted injection pump (World Precision Instruments, USA) at a constant speed of 10 µL/min until the total volume was delivered. Lesion-equivalent volumes of ECM (n=5), microspheres (n=3) or microspheres suspended in ECM (n=3) were injected into the ventral posterior region of the cavity to displace and drain the less dense necrotic debris from the most dorsal part of the lesion [179]. Injection of PBS as vehicle served as a control condition (n=4). Previously, we demonstrated that these large volume injections require precise neurosurgical planning to avoid misplacement or leaching of material into the lateral ventricles, as well as to avoid damage to structures in the path of injection [179, 180, 207]. Implantation of microspheres with NSCs (n=2) or NSCs+ECs (n=2) embedded in ECM evaluated how co-delivery of NSCs+ECs affected the survival and distribution of NSCs in the stroke cavity.

For both stroke models, needle and cannula were left in place for 5 minutes to allow material to dissipate, before the needles were slowly withdrawn from the brain. Burr holes were filled with bone wax prior to suturing. LX4 (Ferndale, containing 4% Lidocaine) was topically applied as an analgesic and buprenorphine (0.5 mg/kg) i.p. was given to provide sustained pain relief.

5.3.15 Histological analyses

5.3.15.1 Perfusion-fixation of tissue

Animals were transcardially perfused 1-day post-implantation with 0.9% saline followed by 4% paraformaldehyde (in 0.2 M PBS) to fix brain tissue prior to its removal from the skull. Brains were post-fixed in 4% paraformaldehyde for 24 hours then cryopreserved in 30% sucrose with sodium azide (Sigma) at 4 °C. Using a cryostat (Leica), 50 µm thick histological sections were cut directly onto microscopic slides to maintain the morphology of the stroke-damaged brain and avoid washing out of implanted materials.

5.3.15.2 Immunohistochemistry

Brain sections were washed 3×5 min with 0.01 M PBS, followed by 1-hour permeabilization in PBS at room temperature (21 °C). Primary antibodies against mouse endothelial cells (anti-CD31,

1:50, SC-13537, Santa Cruz), green fluorescent protein (anti-GFP, 1:2000, Ab13970, Abcam), microglia (anti-Iba-1, 1:300, Ab5076, Abcam) Collagen I (anti-collagen I, 1:250, Ab34710, Abcam) were applied, diluted in PBS + 0.3% Triton X-100, and incubated at 4 °C overnight. After rinsing off the primary antibodies (3×5 min PBS), appropriate secondary AlexaFluor 488, 555, or 660 antibodies (1:500; Life Technologies) were applied for 1-hour at room temperature followed by 3×5 min washes with PBS. Finally, sections were cover slipped with Vectashield for fluorescence containing Hoechst 33342 (1 μg/mL, Sigma) and stored at 4 °C prior to imaging. Visualization of antibodies was performed with a fluorescence microscope (Axioimager M2, Zeiss) interfaced with a monochrome camera driven by Stereo Investigator image capture software (MBF Bioscience) using a motorized stage.

5.3.16 In situ microsphere characterization

The virtual tissue module (MBF Bioscience) tiled individual 10x magnification images to create a composite whole brain slice. Anterior-posterior whole hemisphere images (500 μm apart) were acquired to measure the total size and number of microspheres. Microsphere circularity, aspect ratio, roundness, and diameter were measured (see above). The volume of each microsphere was calculated using Formula (1). Microsphere volumes were summed and normalized by the lesion volume for each animal to determine the volume fraction and density of microspheres in the stroke cavity (i.e., delivery efficiency).

5.3.17 Quantification of engrafted cells

Engrafted cells refer to the number of cells that were derived from implanted cells. For this, the virtual tissue module (MBF Bioscience) tiled individual 20x magnification images to create a composite whole brain slice. Anterior-posterior whole hemisphere images (500 μm apart) were acquired to measure the total number of NSCs (i.e., GFP staining) and ECs (i.e., far-red staining) delivered to the cavity and the area occupied by these cells. The total number of each cell type was divided by ejection volume to approximate cell density. The area occupied by each cell type was

multiplied by the distance between images to approximate total cell distribution volume [208]. Microspheres were identified by the absence of fluorescent staining. Microsphere diameter, volume fraction, and density were measured and calculated.

5.3.18 Statistics

Graphing and statistical analyses were performed in Prism version 8 (GraphPad). The comparison of two groups was performed using an independent t-test. Multiple group comparisons with a single independent variable were evaluated using a one-way analysis of variance (ANOVA), whereas groups with 2 independent variables were assessed for statistical significance (set at $p<0.05$) using two-way ANOVAs, followed by Bonferroni post-hoc testing. Large effect sizes here afforded small sample sizes for achieving statistically significance in these proof-of-principle experiments. However, more detailed evaluations of smaller effects, especially *in vivo*, will require larger sample sizes.

5.4 Results

5.4.1 Production and quality control of microspheres

Microspheres were created through an oil emulsion technique, combining photochemicals, PEGDA and a fluorescent polymer, into a mineral oil and photoinitiator bath. These were crosslinked with white light (Figure 5.1a). It is critical that microspheres maintain their integrity as they undergo shear stresses during delivery through the Hamilton syringe. Recently, we have demonstrated the delivery of microspheres with co-encapsulated NSCs and ECs into a mouse non-injury model [194]. As we transition our delivery of cell encapsulated microspheres to injury models, we first verified that freezing and thawing of microspheres for shipment and transfer is feasible. Fluorescent, non-degradable microspheres maintained their shape and fluorescent tag following freezing and thawing (Figure 5.1b), supporting our ability to ship microspheres.

To determine the range of microsphere diameters, which can be taken-up through a pipette tip and syringe without creating a clog or becoming stuck, Pluronic was added to the pre-gel phase

in varying concentrations (0.1, 0.25, and 0.5% v/v) (Figure 5.1c). As the amount of surfactant increased, the mean microsphere diameter decreased. Addition of 0.25% Pluronic yielded microspheres with a mean diameter of 141.6 μm and a range from 76.40 to 441.1 μm (Figure 5.1d). A 1-way ANOVA followed by Bonferroni post-hoc testing revealed a significantly (p<0.001) reduced microsphere size for the 0.25% and 0.5% Pluronic conditions compared to 0%. This provided an adequate size to support successful delivery, while maintaining encapsulated cell survival through oxygen and nutrient diffusion. Microspheres yield increased as surfactant increased. More microspheres are produced from the same amount of polymer with a reduction in diameter (Figure 5.1e). A significant increase in microsphere number was hence achieve by using 0.25% and 0.5% Pluronic (1,875 ± 168.3 and 2,370 ± 231.8 microspheres, respectively, per mL). In addition to optimization of mean diameter, volume fraction was increased in order to maximize the quantity of microspheres to be injected in vivo. As Pluronic concentration increased, the percent volume fraction increased, allowing more microspheres to be packed in aqueous solution (Figure 5.1f). With no surfactant, large microspheres packed inefficiently with abundant space between individual microspheres. Addition of Pluronic at 0.25% and 0.5% concentrations resulted in a significant increase in packing density (37% ± 1.6 and 49% ± 4.6, respectively). Although a 0.25% Pluronic concentration produced some microsphere heterogeneity, this was considered advantageous, as smaller microspheres filled the spaces between larger microspheres. Pluronic had no impact on shape factor, thereby strictly impacting microsphere yield and size (Figure 5.1g).

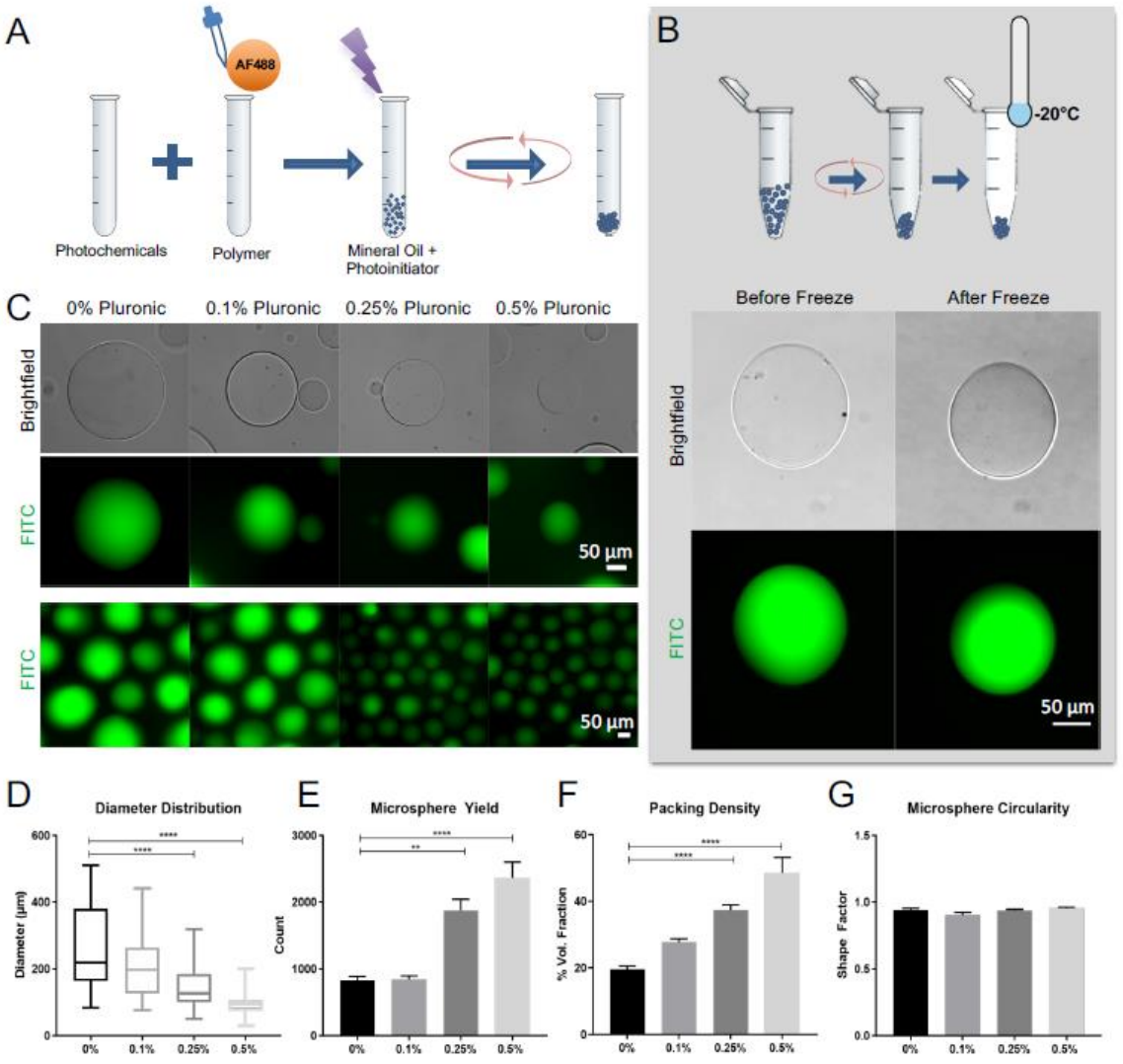

Figure 5. 1. Production of fluorescent microspheres. A. Schematic of microspheres formation protocol. Photochemicals and polymer are combined prior to being mixed with mineral oil and photoinitiator. Stirring of the solution and exposure to light produced microspheres. B. Microspheres with 0.25% Pluronic are spun down and froze to mimic storage and shipping conditions. Brightfield and fluorescent images of AF-488 tagged microspheres before and after cryopreservation demonstrate no change in integrity and shape. C. Varying Pluronic concentrations from 0 to 0.5% additions reveals its impact on the size distribution of microspheres. D. An increase in Pluronic concentration reduces microsphere size, but also produce more consistent size distribution. The box and whisker plot reflects the interquartile range with the line in the box indicating the median value. Error bars indicate the maximum and minimum value. E. As microsphere size reduces, the number of microspheres increases. Bars represent the mean value and error bars indicate the standard error of the mean. F. A reduction in size and higher number of microspheres per volume increases the packing density. G. However, the circularity of microsphere is not affected by the concentration of Pluronic. Scale bar = 50 µm, representative of all images. (** p<0.01; *** p<0.001, **** p<0.0001) determined by a one-way ANOVA.

5.4.2 Impact of injection parameters on microspheres integrity

To ensure that microspheres remained intact during the implantation procedure, injection parameters were arrayed to establish their impact on the integrity of microspheres using needles with inner diameters (ID) of 20G, 24G, and 26G. Ejection of fluorescent microspheres through a pipette onto a coverslip (Supplementary Figure A3.1a) provided a baseline for analysis of microsphere size and shape (Supplementary Figure A3.1b). The majority of microspheres were between 120-400 μm in diameter, but there were also some >500 μm (Supplementary Figure A3.1c). A wide 20G needle bore (603 μm diameter ID) for injection with a Hamilton syringe provided the best preservation of larger microspheres, but significantly reduced delivery of microspheres that were larger than 260 μm in diameter. Narrower needle bore sizes of 24G (311 μm ID) and 26G (260 μm ID) reduced the prevalence of larger particles, but also affected the presence of smaller microsphere (<100 μm). This needle bore size effect was also evident on microsphere density with a wider bore size being favorable to preserve a high microsphere density (Supplementary Figure A3.1d). A high-volume fraction of microspheres in the ejectate was also preserved with a wider bore size (Supplementary Figure A3.1d). Wider bore sizes are hence favorable to preserve the number of microspheres, as well as their size in the ejectate.

Variations in speed of ejection of microspheres through a 20G needle also impacted their prevalence in the ejectate. A slow ejection of 1 μL/min, which is suitable for cell injections into damaged tissues, only resulted in very small microspheres (<20 μm) being found in the ejectate (Supplementary Figure A3.2a). A faster ejection speed was favorable to preserve larger microspheres, with 10 μL/min being the upper limit of ejection speed available on the automated injection device. A faster ejection was advantageous to preserve microsphere density (Supplementary Figure A3.2b) and volume fraction (Supplementary Figure A3.2c). The integrity of microspheres was consistently preserved with only a few microspheres exhibiting a reduced level of circularity (Supplementary Figure A3.3a). Narrower needle bores maintained circularity better, but this is due to smaller microspheres being present in this condition compared to the wider

bore sizes. Flow rate also did not dramatically affect circularity. A high level of roundness was found for all conditions (Supplementary Figure A3.3b). There was a more gradual effect of roundness across microspheres compared to circularity, revealing some asymmetry in the microspheres. These trends were also observed in the aspect ratio (Supplementary Figure A3.3c), which measured the deformation of microspheres. These results highlight the importance of ensuring that the injection devices are matched with the dimensions of the injectable constructs.

5.4.3 Intracerebral implantation of microspheres in two rat models of stroke

Stroke causes focal ischemia and cortical tissue loss similar to a photothrombotic lesion, but more commonly produces extensive cortical and sub-cortical tissue loss due to occlusion of the MCA. Both types of tissue cavities require different implantation strategies to fill these cavities. To ensure the retention and even distribution of microspheres, ejection needs to occur in the tissue cavity without dispersion beyond the target site (Supplementary Figure A3.4a). In shallow cortical lesions, this is a challenge, as very little material is deposited and there is no overlying tissue that will hold the injectate in place. A beveled needle is advantageous to pierce through the meninges but is disadvantageous for the dispersion of microspheres within a small cortical tissue defect at a shallow depth. In cortical tissue defects caused by photothrombosis, care must be taken to ensure that the meninges are pierced to avoid delivery outside the brain (Supplementary Figure A3.4b). In these cases, microspheres will accumulate on the surface or in-between the meninges (Supplementary Figure A3.4c). Flat needles can potentially tear meninges and cause major local inflammation and allow microspheres to distribute outside the brain. A misplaced intracerebral injection will damage intact brain tissue and fail to fill the tissue defect (Supplementary Figure A3.4d). Injection of microspheres close to or into the corpus callosum will disperse along white matter tracts (Supplementary Figure A3.4e). Optimal delivery to a cortical tissue defect hence occurs by piercing the meninges with a beveled needle tip, but to deliver microspheres a flat needle inserted at an angle below the pia matter allowed a robust filling of the cavity, without dispersion of microspheres outside of the tissue defect.

The more extensive MCAo-induced tissue cavities necessitate a different delivery strategy, as the volume required for filling the defect is much larger than for cortical only cavities. MRI determines the cavity volume to guide the appropriate delivery volume with the injection of microspheres displacing the extracellular fluid (ECF) through a secondary catheter. This approach can fill the entire cavity with microspheres (Supplementary Figure A3.5a). However, delivery of insufficient microspheres will result in their sedimentation or buoyancy. In some cases, a low-density injection of microspheres resulted in a dispersed distribution that did not fill the cavity (Supplementary Figure A3.5b). Poor quality control or application of too much pressure during the ejection can lead to the deformation or destruction of microspheres. A spaghetti- or snake-like formation can occur in these circumstances (Supplementary Figure A3.5c), voiding the advantages of creating microspheres for delivery. Implantation into damage tissue can also lead to small pockets of microspheres and failure to deliver the entire volume to the cavity (Supplementary Figure A3.5d). Successful delivery of microspheres to tissue cavities caused by stroke therefore poses significant technical considerations that all need to be met to ensure a complete coverage of the tissue defect. Failure to do so will not allow these therapeutic strategies to exert their intended effects.

Delivery of microspheres to lesion cavities ideally avoids sedimentation, buoyancy, or clustering. A comparison between microspheres suspended in media (i.e., PBS) versus an ECM hydrogel allowed us to compare the retention and distribution of microspheres in both photothrombotic and MCAo tissue cavities (Figure 5.2). Injection of just media into the tissue defect produced essentially a vehicle-control condition, with just a tissue cavity surrounded by a glial scar being evident. Implantation of just ECM hydrogel filled up the tissue defects. Injection of microspheres in media were retained within the cavities, but retention was poor in the photothrombotic lesion and dispersion in the MCAo lesion was heterogenous. Implantation of microspheres in ECM hydrogel produced the most robust retention and a more homogenous dispersion through the tissue cavities. A robust dispersion along the anterior-posterior axis was

evident even in the large MCAo tissue cavities (Figure 5.3a). Individual microspheres were clearly visible on whole hemisphere images (Figure 5.3b). However, some empty spaces were also evident. In some instances, this reflected individual pockets of cavities that could not be reached with a single injection-drainage procedure, whereas in others these were caused by microspheres falling out during the sectioning or staining procedure. In between microspheres, host cells were seen invading the cavity through the surrounding ECM hydrogel (Figure 5.3c). Implantation of only ECM hydrogel also resulted in cell invasion in the cortical defect (Figure 5.4a), whereas microspheres injected with media poorly occupied the lesion and no host invasion of cells into cavities was evident (Figure 5.4b). In contrast, microspheres implanted with ECM hydrogel were dispersed throughout the cortical defect with an extensive host cell invasion through the surrounding glial scar (Figure 5.4c). In the MCAo model, microspheres delivered in ECM also revealed invasion of host cells surrounding the microspheres, but no invasion of cells into the microspheres was evident (Figure 5.4d). Most cells invading the ECM hydrogel were of a monocyte Iba1 lineage (Figure 5.4e).

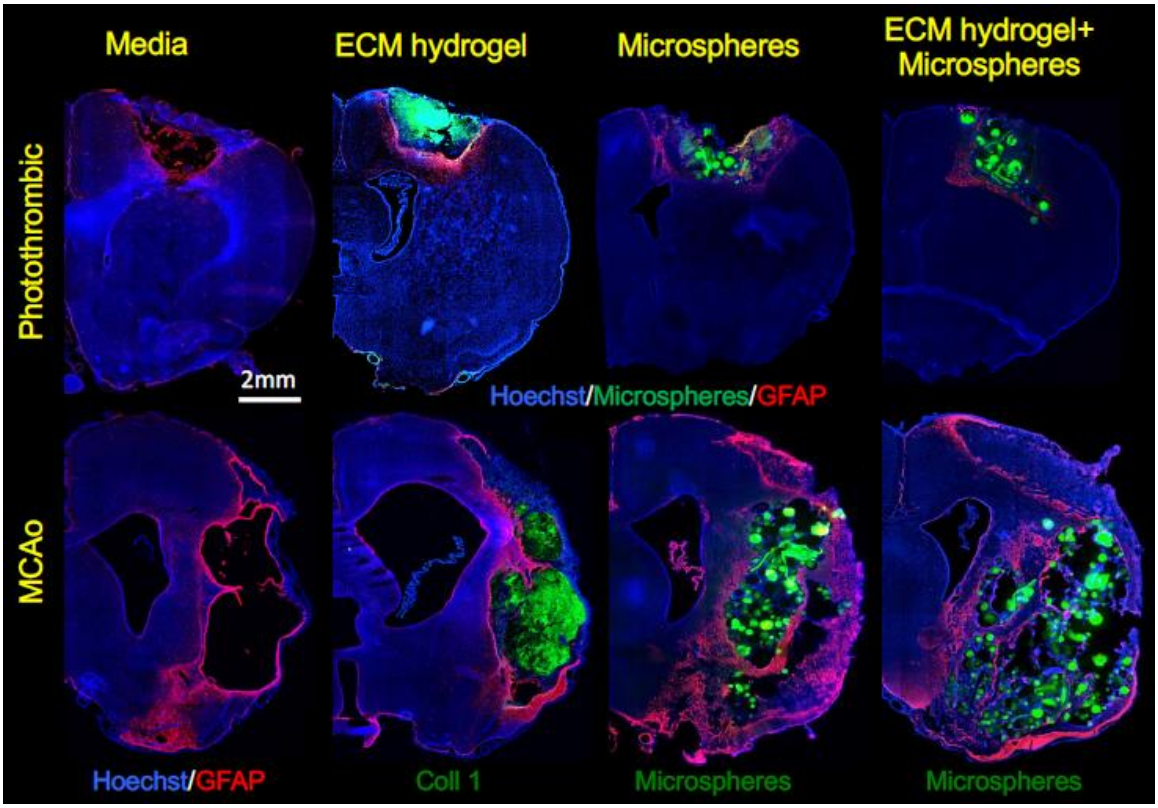

Figure 5. 2. Macroscopic comparison of microsphere delivery to tissue cavities caused by stroke. An overview of the impact of different implantation paradigm on the tissue cavities caused by cortical photothrombosis or transient intraluminal middle cerebral artery occlusion (MCAo). Injection of media did not have a major impact on the cavity, whereas injection of ECM hydrogel completely filled tissue defect. Implantation of microsphere in PBS were only partially retained with the cortical cavity, although retention within the MCAo cavity was robust. Nevertheless, there was a poor distribution of microspheres throughout the cavity. Microspheres delivered in ECM hydrogel provided a very robust retention in both tissue defects and exhibited an excellent distribution through the cavity.

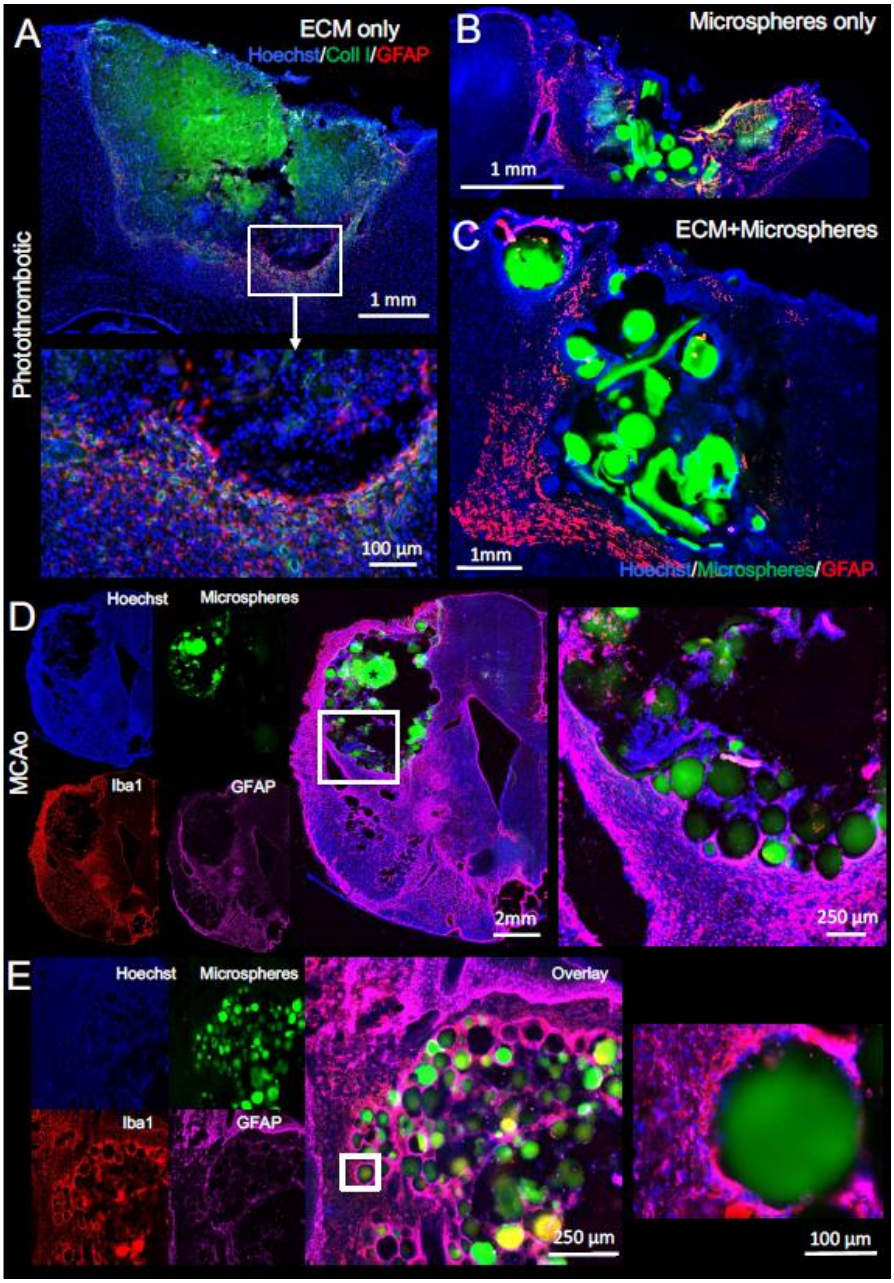

Figure 5. 3. Microspheres extensively distribute in a stroke cavity. A. Anterior-posterior view of the lesion cavity and its filling with microsphere implanted with ECM hydrogel. An extensive and homogenous distribution throughout the cavity is evident. B. A combination of immunohistochemical markers reveals the distribution of microsphere with ECM hydrogel providing essential an interstitial space to suspend these in the cavity. Reactive astrocytes delineating the cavity do not show a major invasion into the cavity. Filling of non-communicating cavities can be achieved if the injection needle punctures through these. However, histological sectioning can lead to some microspheres being washed out of the cavities (*). ECM hydrogel (collagen I+) provides a support structure to maintain microspheres in place, but also provides a conduit for implanted and host cells' migration in the cavity. Microspheres by themselves do not provide this migration support. C. However, migration of host cells (DAPI) into the ECM hydrogel, but not the microspheres, is observed.

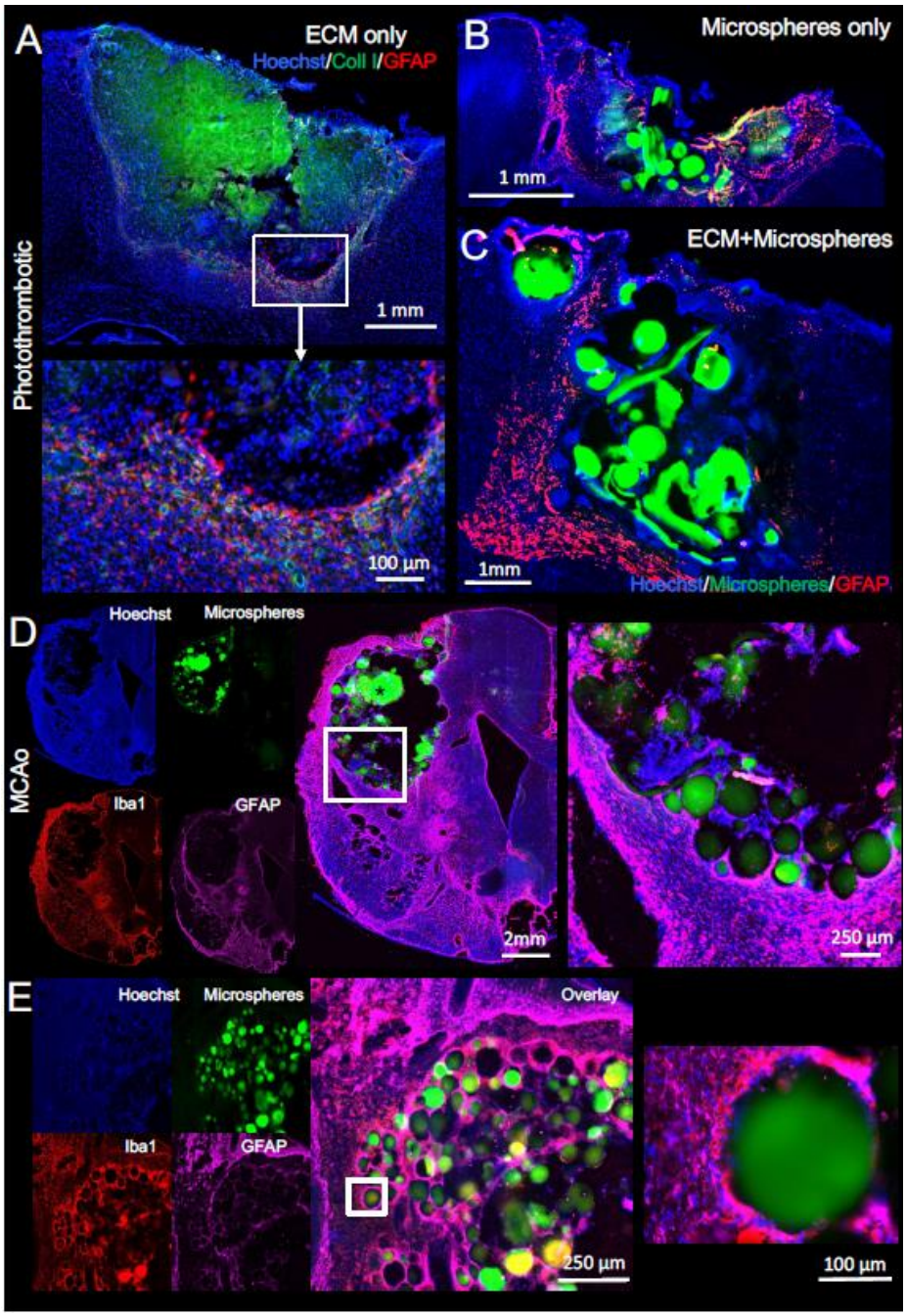

Figure 5. 4. Microsphere delivery in ECM hydrogel produces a robust retention and distribution in tissue cavities. A. ECM hydrogel filled the entire cortical tissue defect with a host cells (DAPI) migrating inwardly from the surrounding tissue, delineated by reactive astrocytes with a strong glial fibrillary acid protein (GFAP) staining. B. Implantation of only microspheres into this tissue defect partially filled up the cavity. C. Implantation of microspheres in ECM hydrogel allowed host cells to invade in between microspheres. D. Akin to the cortical defect, microspheres only partially filled the cavity caused by MCAo, with many microspheres adhering to the surrounding tissue, but it is conceivable that many microspheres were lost in sectioning or the staining procedure. E. Implantation of only microspheres also produced a local inflammatory response by microglia (Iba1), most likely a reaction to the large particles entering damaged tissue.

A quantitative comparison of the retention of microspheres further indicated that ECM hydrogel dramatically increased ($p<0.001$) the retention of microspheres of all sizes in photothrombotic cortical cavities (Figure 5.5a). Although there was an improvement ($p<0.05$) in microsphere retention with ECM hydrogel in the MCAo cavities (Figure 5.5b), this was less pronounced than in the photothrombotic model. The volume fraction of microspheres in the cavity was 1.5% for microspheres only groups in both the photothrombotic and MCAo cavities (Figure 5.5c). ECM hydrogel significantly ($p<0.05$) improved the volume fraction of microspheres in both models, but the effect size was greater for the photothrombotic model (~10% volume fraction). Microsphere density was also significantly improved with delivery in ECM hydrogel for both the photothrombotic ($p<0.01$) and MCAo model ($p<0.05$, Figure 5.5d). These results demonstrate that a robust retention and distribution of microspheres in ECM hydrogel can be achieved to completely fill stroke-induced tissue cavities.

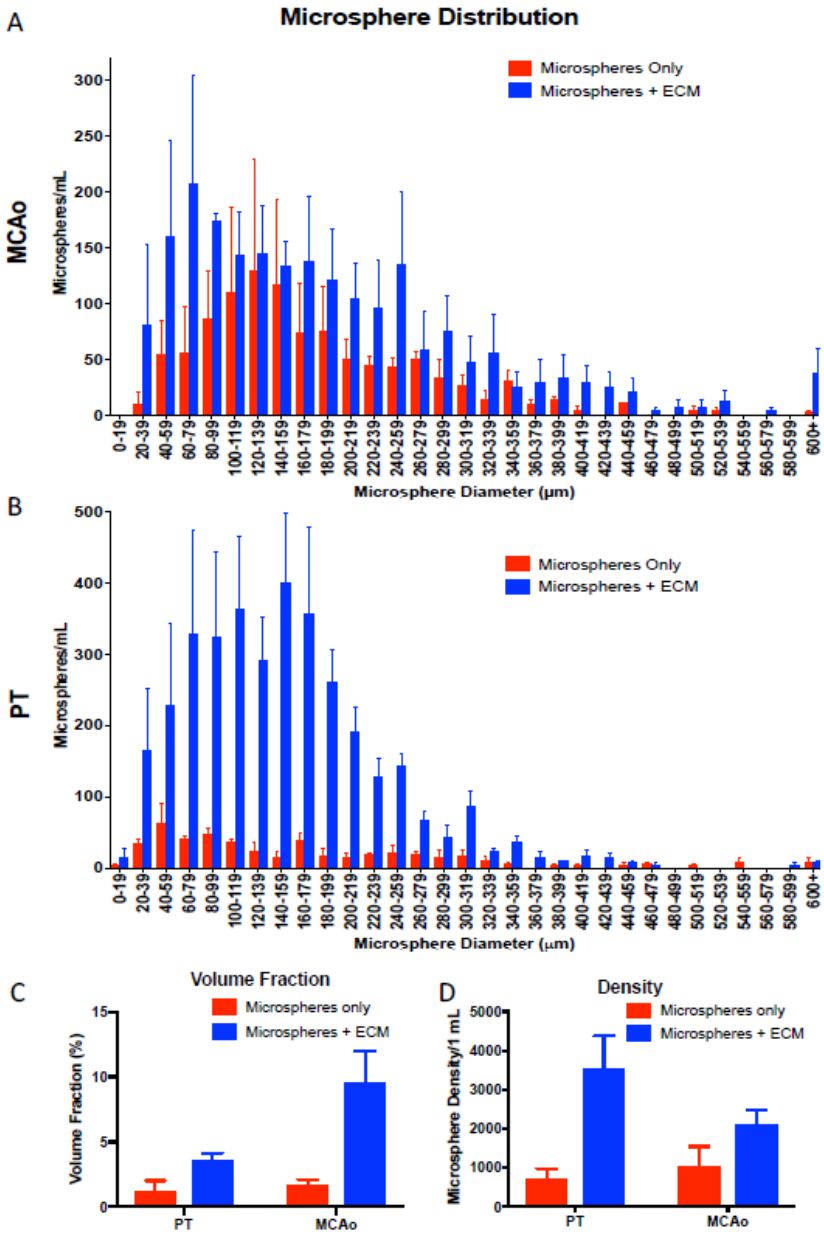

Figure 5. 5. Quantification of microsphere distribution in tissue cavities caused by stroke. A. Retention of microspheres implanted in PBS was poor, whereas implantation with ECM hydrogel dramatically improved retention for all microparticles. Microspheres implanted in PBS and ECM hydrogel into MCAO lesions revealed a similar size distribution profile, but microsphere in ECM hydrogel were more numerous for all sizes. A better retention of smaller microspheres in ECM hydrogel was also evident. B. ECM hydrogel dramatically improved the retention of microspheres in cortical strokes. C. The volume fraction of microspheres was significantly improved by implantation with ECM hydrogel. D. The density of microparticles in the lesion cavity was also significantly higher with ECM hydrogel in both types of tissue defects. On all graphs, bars represent the mean value and error bars indicate the standard deviation of the data.

5.3.4 Encapsulation of neural stem cells and endothelial cells in microsphere for intracerebral delivery

Microspheres for cell encapsulation were created using a dual emulsion technique (Figure 5.6a). NSCs and ECs were entrapped throughout the entirety of the microsphere (Figure 5.6b). To avoid rupture of microsphere during the implantation procedure, we assessed microsphere integrity by measuring circularity following uptake in a pipette tip, 20G, 24G, and 26G needle in both PBS and ECM (Figure 5.6c). There was minimal variance in microsphere circularity in either vehicle and no effect of needle size (Figure 5.6d). Microspheres maintained viability of cells after cryopreservation and passage through a 20G needle. An LDH assay revealed no cytotoxicity of encapsulated NSCs with or without ECs pre- or post-cryopreservation (Figure 5.6e). Cytotoxicity was equivalent to plated cells. Both mono- and co-encapsulated microspheres contained the vitality maker Calcein before and after cryopreservation (Figure 5.6f). Cytotoxicity for encapsulated cells before and after freezing was equivalent to live plated cells (Figure 5.6g). Encapsulated cells were therefore viable for in vivo intracerebral delivery.

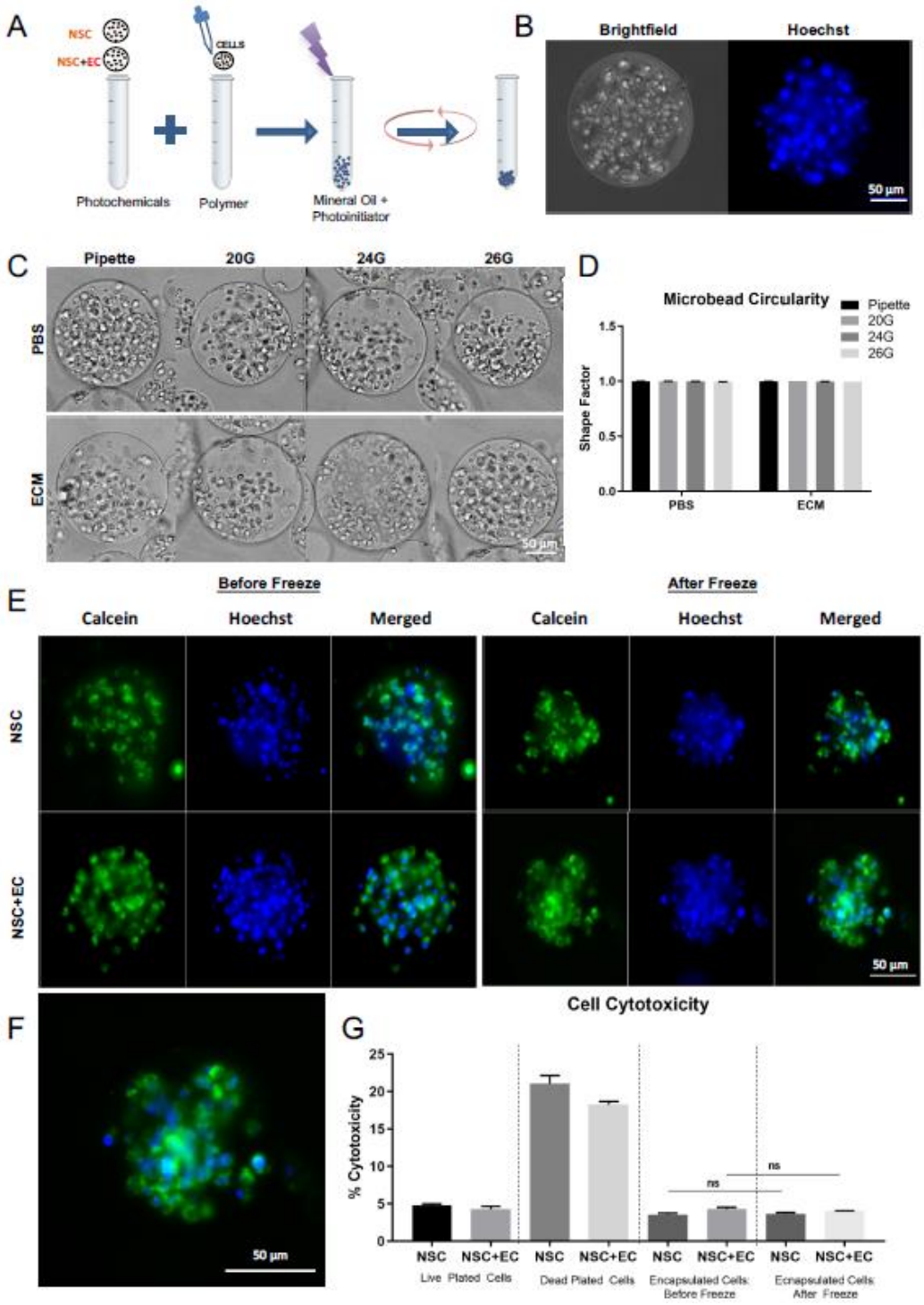

Figure 5. 6. Encapsulation of neural stem cells and endothelial cells into microspheres. A. Schematic demonstrating the cell encapsulation process. Neural stem cells (NSCs) and endothelial cells (ECs) were mixed with photochemicals and polymer prior to mixing with mineral oil and a photoinitiator. Exposure to light and stirring produced microspheres. B. A brightfield image visualize the microsphere in phase contrast and the incorporation of cells is evident using the nuclear Hoechst for fluorescence microscopy. C. To ensure a homogenous suspension of

microsphere for injection, ex vivo optimization of injection parameters was undertaken. D. To ensure the integrity of microspheres, microsphere circularity was quantified, and microspheres remain intact regardless of needle gauge size. E. To ship cell-encapsulated microsphere, viability of cells before and after freezing were evaluated. Calcein (in green) provided a vitality stain for live cells. F. Almost all cells in the microsphere were alive after freezing. G. Cytotoxicity for encapsulated cells before and after freezing was equivalent to live plated cells. There was no difference between NSCs and NSCs+ECs microspheres. Scale bar = 50 μm, representative of all images. On all graphs, bars represent the mean value and error bars indicate the standard error of the mean.

5.3.5 Intracerebral delivery of microsphere-encapsulated cells to a tissue cavity caused by stroke

Implantation of microsphere-encapsulated cells in ECM hydrogel resulted in a distribution akin to that observed with "blank" microspheres (Figure 5.7a). There was a widespread distribution of cells from the microspheres into the ECM hydrogel and into the area of damage in surrounding tissues (Figure 5.7b). Very few cells remained within the microspheres (Figure 5.7c). ECs persisted within the ECM located in the stroke cavity, rather than distributing into surrounding tissue (Figure 5.7d). In contrast, NSCs distributed more widely into the existing tissue architecture of the surrounding tissue, including multiple regions of the cortex. Migration of NSCs through cortical tissue (Figure 5.7e), as well as the corpus callosum, was evident (Figure 5.7f). A differential distribution of NSCs into damaged tissue was observed, with the degree of tissue damage influencing the degree of cells in damaged tissue. In the damaged striatum, a major influx of NSCs was apparent (Figure 5.7g). Ischemic damage in the cortex produced a non-communicating cavity that was not filled with microspheres or ECM hydrogel. Consequently, no filling of the cortical cavity occurred. However, some microspheres were lodged in the injection tract in the cortex (Figure 5.7h) and NSCs distributed into the peri-infarct tissues (Figure 5.7i). NSCs were not only observed distributing towards sites of damage, but also towards the subventricular zone (Figure 5.7j) and the stump of the occluded MCA (Figure 5.7k).

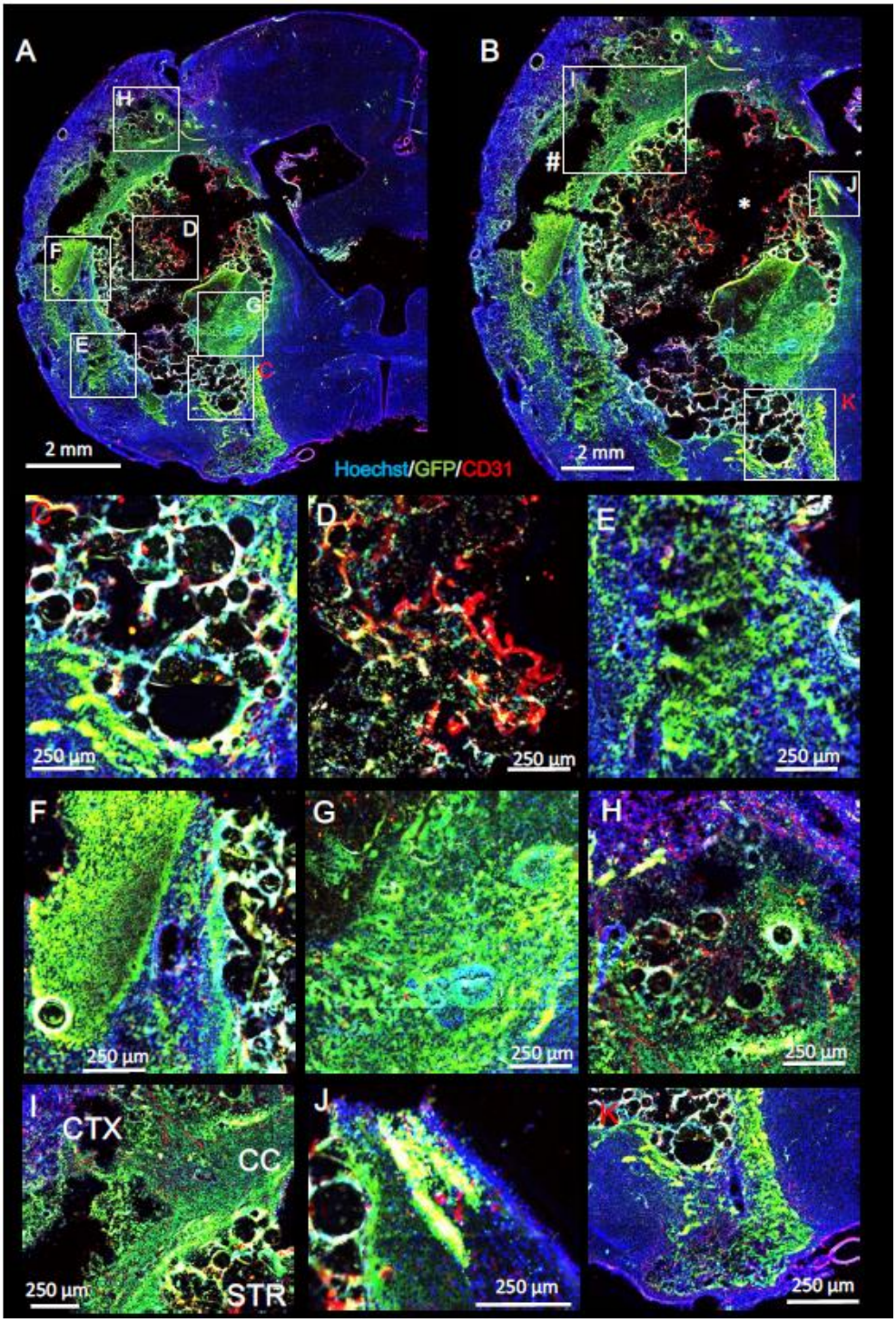

Figure 5. 7. Microsphere-based cell delivery to a tissue cavity caused by stroke. A. ECM hydrogel-based implantation of green fluorescent protein (GFP)-tagged neural stem cells (NSCs) and endothelial cells (ECs) encapsulated in microspheres. B. There is widespread distribution of microspheres throughout the cavity, but there is also evidence that a cortical tissue defects (#) was not filled due white matter separating it from the main striatal cavity. Some loss of microspheres in the main cavity are evident due to tissue processing (*). NSCs migrated to the area of cortical tissue damage and more extensively throughout the cavity as well as into surrounding damaged tissue.

ECs mainly remained within the main cavity where microspheres were implanted. C. At the base of the lesion microspheres were well compacted and presented a mixture of sizes. Some cells were evident in the microsphere, but a large number of cells populated the ECM hydrogel in between the microspheres. D. In the core of the cavity, microspheres were also well compacted and distributed, but no very large microspheres were evident. ECs were very evident in this region compared to NSCs. E. Only NSCs were invading into the surrounding tissue. F. Migration of NSCs along white matter tracts and invasion into damaged cortical tissue was also observed. G. Invasion of NSCs into the damaged striatum was widespread. H. A few microspheres were present in damaged cortical tissue, which was along the implantation pathway, but no microspheres were present in adjacent tissue. Nevertheless, extensive invasion and migration of NSCs in the damaged cortical tissue was evident. I. it is unclear in the corpus callosum if NSCs from the few microspheres in the cortex migrated along these white matter fibers or if NSCs from the main striatal tissue cavity invaded the corpus callosum to migrate to damaged cortical tissue. J. Some migration of implanted NSCs was evident towards the subventricular zone, which is the inverse migration pattern observed by endogenous NSCs. K. NSCs at the base of the tissue cavity also migrate ventrally along the trajectory of the MCA.

A comparison between microspheres containing only NSCs versus those prepared with NSCs and ECs indicated that the volume of injection was significantly higher ($p<0.05$) for NSCs+ECs (Figure 5.8a), reflecting the larger cavity size in this group. The NSCs+ECs (31%) group also contained a higher volume fraction of microspheres compared to NSCs (11%, $p<0.01$, Figure 5.8b). The microsphere size profile of both experimental groups was equivalent, but there was an overall group effect of more microspheres being contained in the NSCs+ECs experimental group (Figure 5.8c). On average 1940 microspheres/mL were delivered in the microsphere+NSCs group, whereas 5400 microspheres/mL were delivered in the microsphere+NSC+ECs group. Cell content per microsphere was equivalent (average of 110 cells), yielding a total of 213,400 encapsulated NSCs in the microsphere+NSCs group compared to a total of 594,000 NSCs and ECs (i.e., 297,000 of each cell type). Evaluation of the distribution of NSCs and ECs in relation to the tissue cavity (Figure 5.8d) indicated that NSCs occupied a territory larger than the cavity ($p<0.01$). The extent of distribution was more pronounced in the NSCs+EC group ($p<0.05$). The presence of transplanted ECs did not exceed the area occupied by the tissue cavity. Engraftment of cells (i.e., cells derived from those implanted) in the NSCs+ECs group (2,190,000 cells; 1,095,000 NSCs) was significantly higher ($p<0.01$) than in the NSCs only group (402,000 NSCs, Figure 5.8e). This

difference was further reflected in the density of cells in both groups (p<0.001), although NSC content (21,000 NSCs/microliter) was equivalent in both groups (Figure 5.8f). Co-transplanted NSCs and ECs proliferated twice as much between encapsulation (~2 days pre-transplant) and perfusion fixation of animals (+1 day) than in the NSC only group. Engraftment of cells was hence several times the average content of encapsulated NSCs (+188%) or NSCs+ECs (+368%). These results indicate that NSCs and ECs can efficiently be incorporated, expanded, stored, and transported in microspheres ex vivo prior to implantation to a stroke-induced tissue cavity to produce a very extensive cellular repopulation of the cavity and its surrounding damaged tissues.

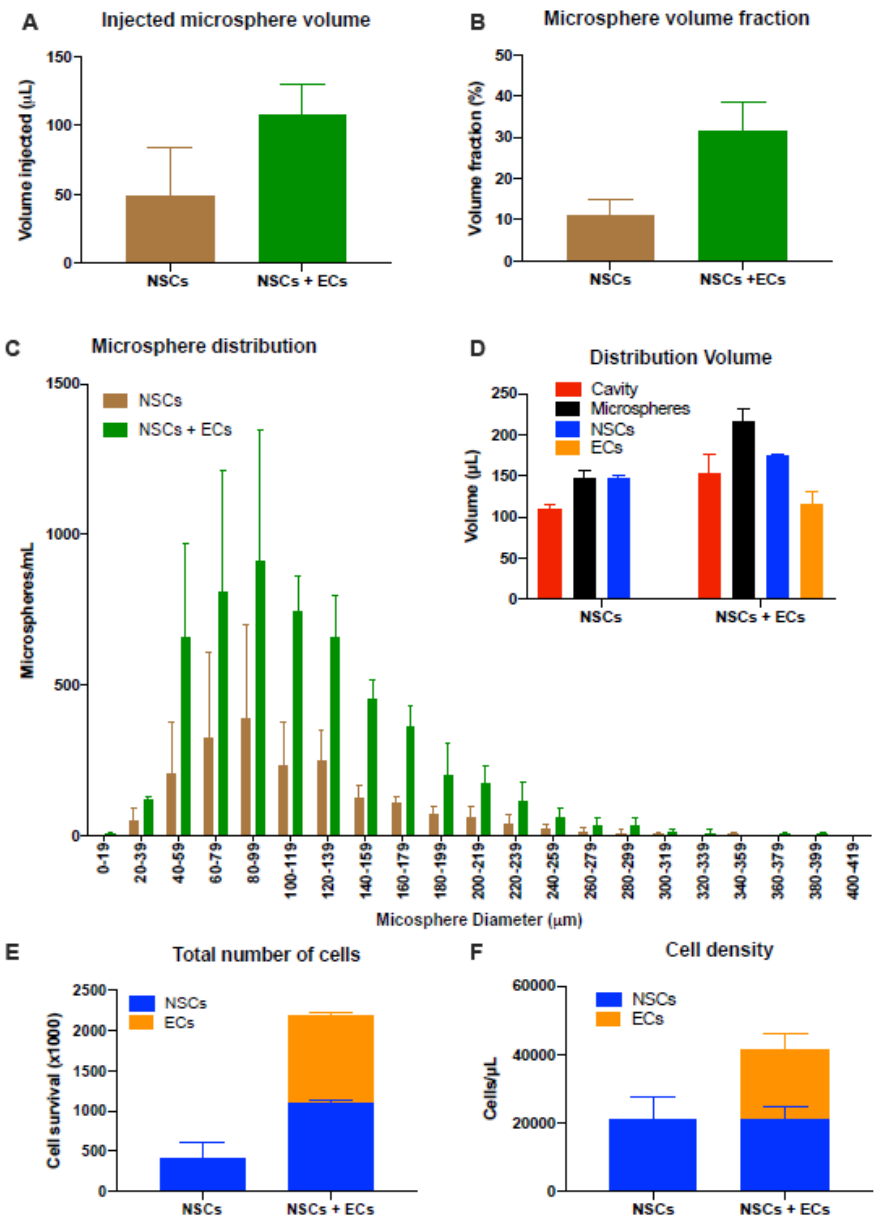

Figure 5. 8. Co-implantation of neural stem cells and endothelial cells in microspheres produces an improved survival of cells in the stroke cavity. A. The injected volume of microspheres with NSCs and ECs (n=2) was approximately twice the volume of microsphere with NSCs (n=2). B. The volume fraction within the implanted volume was approximately 3x higher for microspheres with NSCs and ECs than microspheres with only NSCs. C. The size distribution of microspheres was equivalent between both conditions, but microsphere with NSCs and ECs had a higher density after implantation for all sizes. D. A volume comparison of the cavity and microspheres, as well as the distribution volume of NSCs and ECs indicate that microspheres and NSCs covered an area larger than the cavity. ECs distributed through a volume smaller than the cavity. E. Co-implantation of ECs and NSCs resulted in a higher cell survival of NSCs. F. However, the density of grafted cells in the NSCs+ECs condition was approximately 100 cells/µL higher than in the NSC only condition. On all graphs, bars represent the mean value and error bars indicate the standard deviation of the data.

5.4 Discussion

The therapeutic success of NSC transplantation is dependent on the survival and distribution of grafted cells in the stroke-damaged brain [168]. Intra-parenchymal implantation limits the volume and number of cells that can be delivered to the brain using a single injection site [105]. We here developed a novel approach based on microsphere-encapsulation of NSCs combined with ECs to demonstrate the efficient delivery of these to a stroke cavity, resulting in a wide-spread migration of NSCs throughout the area of tissue loss, as well as peri-infarct regions. Suspension of microspheres in ECM hydrogel improved their retention, as well as distribution, but also provided an interstitial substrate for NSCs to migrate outward and colonize the areas damaged by a stroke. Encapsulation afforded growing of both cell types in the same microsphere, as well as freezing these for ease of transportation. This method will, in the future, provide a means to grow prototypical neurovascular units in a laboratory to produce an allogenic off-the-shelf product that can be stored in hospitals and be readily available for use in patients. The microsphere-encapsulation of NSCs with ECs and suspension in ECM hydrogel hence provides a new more efficient paradigm to deliver cells for tissue repair after a stroke.

5.4.1 Microsphere encapsulation of cells for implantation

Microsphere encapsulation of cells for intracerebral transplantation has mostly been applied to prevent an immunological response to implanted cells or to prevent them from integrating into brain tissue [209]. To maintain cells in an encapsulated state, these approaches have employed non-degradable biomaterials. In some cases, these consisted of capsules fabricated from polyacrylonitrile-polyvinylchloride (PAN-PVC) [210], polyethersulfone [211, 212] or polyvinyl alcohol (PVA) [213] hollow fibers with cells embedded in collagen I. Intra-putamen implantation of alginate-polyornithine capsules (600-660 micron diameter) incorporating neonatal porcine choroid plexus cells are currently undergoing a phase IIb trial for Parkinson's disease [192]. Non-degradable, but porous, microspheres loaded with cells could also be used to deliver trophic factors to peri-infarct tissues, as demonstrated here by implanting these into the lesion cavity. However,

the intra-parenchymal implantation and permanent entrapment of encapsulated cells does not afford their use to replace lost tissue or to promote a more widespread dispersion of cells in damaged tissues, a major limitation of intra-parenchymal cell implantation. To allow dispersion of cells, while reducing the impact of shear stress due to the injection procedure on cells, the suspension of cells in liquid phase hydrogels has been shown to improve the survival and differentiation of cells [208].

Little consideration has been given to microspheres or the use of cell encapsulation as a means to increase the number of cells being implanted into a tissue cavity, as occurs in up to 94% of patients with stroke [214]. A key difference for this approach is to target the lesion cavity based on non-invasive imaging [206, 215], while adopting a surgical approach that allows for displacement of the liquid that fills the cyst [179]. Using our injection-drainage approach, we can very efficiently fill the tissue cavity [179, 216]. As demonstrated in the present study, this approach needs to be adapted depending on the topography of the tissue cavity. A minimally invasive injection-drainage approach efficiently filled a large tissue cavity caused by an MCA stroke with microspheres. The retention and distribution of these microsphere was improved using ECM hydrogel for suspension. In contrast, drainage is difficult to achieve in smaller superficial cavities. Damage to the meninges during injection in these cavities can also lead to an extra-cerebral accumulation of microspheres. In some cases, photothrombosis induces necrosis of the meninges overlying the cortical defect. This facilitates access in preclinical models but is not modeling the clinical reality of cortical strokes. An angled delivery through the meninges, with passive drainage of ECF along the needle, here afforded a minimally invasive delivery and retention of microspheres and ECM within the cortical defect. Suspension of microspheres in ECM hydrogel produced a superior retention and distribution of microspheres in this type of defect. The suspension of microsphere in a secondary hydrogel therefore provided an advantageous delivery strategy. The biophysical aspects of injections are often neglected, potentially leading to sub-optimal delivery that prevents the evaluation of the true potential of these advanced therapeutic products.

Encapsulation of cells in hydrogel-based microspheres is advantageous for delivery compared to solid microparticles, where NSCs are attached to the surface [177], as the suspension of cells in hydrogels produces a higher delivery density and also protects cells from shear stress during injection. We here demonstrated a very efficient delivery of NSCs and ECs in microspheres to a stroke cavity. Average cell packing density (<1% volume fraction) in microsphere was dramatically lower compared to the 20% volume fraction (i.e. 50,000 cells/microliter) commonly used in a liquid vehicles for cell suspension [173, 174]. Additional studies are required to determine if packing density of cells will affect engraftment efficiency. Engraftment of NSCs+ECs cells in microspheres was nevertheless dramatically higher at 368% than the number of cells that were encapsulated. This contrast dramatically to the ~95% loss of cells implanted in suspension in the peri-infarct tissue [168], raising the question if a lower packing density of NSCs for cell suspension could be beneficial to intra-parenchymal implantation. The extensive "re-population" of damaged peri-infarct tissues, as well as the distribution of implanted cells throughout the tissue cavity, potentially form a combination of peri-infarct tissue repair and tissue regeneration inside the cavity. ECM hydrogel was an important conduit for migration of cells out of the biodegradable microspheres. This is consistent with other observations in which host neural progenitors and ECs migrated into ECM hydrogel implanted into a stroke cavity [180, 181, 216]. In addition to a potential cellular integration of transplanted cells as a mechanism of tissue repair, NSCs and ECs also interact with each other to increase trophic factor release to support angiogenesis as well as neuronal survival. For instance, we have previously seen a dramatic upregulating of for instance, VEGF-A and BDNF [183, 189]. Harnessing the host tissue response to an acellular ECM hydrogel for tissue restoration is also attractive, as host cells that infiltrate the cavity and populate the hydrogel avoid any adverse immunological rejection response [181]. Chimeric tissues containing host and implanted cells could hence be created to accelerate tissue replacement. The implantation of prototypical neurovascular units encapsulated in microspheres can be further envisaged to

provide the fundamental building blocks for tissue restoration, potentially reducing the protracted time frame associated with acellular bioscaffold-mediated tissue regeneration [217].

5.4.2 Intra-cerebral injection of complex cell constructs

Encapsulation of cells reduces their packing density for delivery in comparison to a simple cell suspension in a gel precursor, in which cells are more continuously dispersed. Suspension of cells in ECM hydrogel, for instance, can achieve a very high cell density for delivery and retention in a stroke cavity [208, 215]. However, a major advantage of microspheres for delivery is the potential to grow and differentiate encapsulated cells in vitro to, for instance, pre-differentiate cells for transplantation, such as striatal output neurons, which only poorly survive when implanted in suspension [218]. Results of the present study show that packaging NSCs with ECs in a microsphere enhances survival, as well as migration after implantation into a stroke cavity using microspheres embedded in ECM hydrogel. These results are consistent with observation of the same NSC:EC microsphere preparation producing an improved survival and migration of NSCs in the normal mouse brain [105]. However, longer survival times post-implantation will need to be investigated to evaluate if co-implantation and microsphere encapsulation will have beneficial effects on the prolonged survival of NSCs, on the neo-and re-vascularization of tissues, as well as the integration of NSCs into existing neural circuitries. Although these anatomical effects are commonly considered the “desired” effects of cell implantation, a wider regional distribution of paracrine effects (e.g. VEGF-A release) exerted by intra-cavity implantation of NSCs could invoke a sufficient therapeutic effect to promote some behavioral recovery, as observed after single site peri-infarct cell transplantation [168, 185].

Delivery of soluble growth factors, such as VEGF-A, through the controlled release from biomaterials has been shown to produce a re-vascularization of damaged tissues, enhanced neurogenesis and improved behavioral improvements after stroke damage [219]. Hyaluronic acid (HA) is often used as a biomaterial for these applications and has been optimized for cell delivery to selectively control NSCs survival and differentiation after stroke [208, 220]. However, other

ECM molecules, such as laminin and collagen, have also been used for cell transplantation. Herein we used PEG, as it is considered minimally immunogenic as a platform for further functionalization into complex tissue constructs [221], such as an artificial neurovascular unit. Photolithography of PEG hydrogel will further allow to imprint a microstructural organization for cells required for the formation of complex tissue structures [222, 223], including blood vessels [224, 225]. The biodegradable formulation of PEG microspheres afforded NSCs' and ECs' migration out into surrounding microenvironments. Further functionalization of the PEG backbone with ECM molecules to retain and guide their differentiation, in addition to the slow release of growth factors, can be envisaged to create complex microtissues, including prototypical vessel structures, for an accelerated tissue restoration.

We further here demonstrated that embedding of microspheres in a secondary inductive hydrogel, such as ECM, provides an interstitial conduit for cell migration and "integration" of multiple microspheres into a tissue. ECM hydrogel supported both the migration of implanted cells out of microspheres and into peri-infarct tissue, but also migration of host cells into the tissue defect. Interestingly migration of neuroblasts into the SVZ was observed, which is against the migration direction from the SVZ to the lesion, typically observed after a stroke. This cross-migration could potentially be an essential process to ensure integration of de novo and veterate brain tissue [217]. Implantation of NSCs in ECM hydrogel did not provide this cross-migration between implanted and host cells [215], potentially indicating that this acellular interstitial conduit can provide a unique environment to promote tissue formation and integration of microsphere-delivered cells. In the context of engineering large tissue volumes, it is further important to consider that in addition to microvessels and smaller vascular branches, a large vascular tree (e.g., MCA) is required to support sufficient blood volume distribution. The use of a secondary pro-angiogenic hydrogel in between preformed microspheres potentially could provide the environment for these structures to form. The studies described here provide the foundation to embark on these additional engineering challenges.

5.5 Conclusion

Although intra-parenchymal cell implantation for the treatment of stroke has progressed to clinical trials [171], the efficiency of delivery at 5% NSC survival remains poor [168]. We here demonstrated a novel approach in which NSCs and ECs are encapsulated into PEG microspheres that can be suspended in ECM hydrogel for implantation into the stroke cavity. This approach afforded the implantation of much higher cell numbers than intraparenchymal targets, as well as achieved a much higher efficiency of delivery. Intraparenchymal implants show limited distribution with the peri-infarct areas and no restoration of tissue within the stroke cavity [168]. A microsphere+ECM hydrogel delivery can achieve a much wider distribution of implanted cells and trophic factor delivery throughout the area of damage to contribute to tissue repair. Co-transplantation of ECs with NSCs improved NSCs survival and distribution, highlighting the potential to engineer complex prototypical tissue constructs. Tissue constructs can potentially accelerate tissue formation and enhance the endogenous repair response. However, further experiments are required to characterize tissue formation and integration, as well as the therapeutic potential of this approach.

Chapter 6: Endothelial Cell Secreted VEGF-C enhances NSC VEGFR3 Expression and Promotes NSC Survival

6.1 Abstract

To date, there remain insufficient therapeutic treatments to promote motor and functional recovery following intracerebral hemorrhage (ICH). Although neural stem cell (NSC) delivery demonstrates promise, NSC survival in the inflamed brain is largely limited. Here, we investigate endothelial cell (EC) and pericyte (PC) interactions with NSC in the neurogenic niche, specifically delineating the role that each cell plays in NSC survival during injury. Our results demonstrate that EC, and not PC, promote NSC cell proliferation and reduce cytotoxicity through direct cell-cell contact under glucose deprivation (GD). Additionally, NSC proliferation was increased upon treatment with EC conditioned media and this effect was inhibited with antagonism of VEGFR3. In an NSC+EC co-culture, we detected high levels of VEGF-C, not seen for NSC cultured alone. Further, exogenous VEGF-C induced NSC upregulation of VEGFR3, promoted proliferation, and reduced cytotoxicity. Finally, we delivered polymeric microbeads containing NSC+EC into a murine ICH cavity. VEGF-C was increasingly present in the injury site coincident with delivery of NSC+EC, not seen upon delivery of microbeads containing NSC alone. Together, these studies demonstrate that EC-secreted VEGF-C can promote NSC survival during injury, subsequently enhancing the potential for cell delivery therapies used to mitigate injury due to stroke.

6.2 Introduction

Intracerebral hemorrhagic stroke (ICH) is directly associated with a mortality rate of approximately 40-60% one year post event [226, 227]. Despite the high rate in death following ICH, there has been relatively little research focused on the mechanisms of injury and repair, as compared to research conducted on ischemia. ICH survivors are afflicted with broad neurological tissue impairments, making ICH the least treatable form of stroke [228]. The immediate

introduction of blood components, including leukocytes, erythrocytes, platelets, and proteins such as thrombin and fibrinogen, into the intracerebral space, and subsequent tissue injury induces a neuro-inflammatory response. Neuroinflammation is directly responsible for the subsequent increase in astrocyte abundance in the damaged area, contributing to formation of the glial scar [229]. There is potential, however, to harness the endogenous mechanisms that promote the reparative process, to facilitate effective therapeutics that limit neurological damage and facilitate regenerative repair following ICH.

Stem cell therapies have the potential to replace dead and dying cells following acute stroke and restore damaged neural circuitry and inhibit degenerative responses to tissue injury cues caused by stroke. Therapeutic intervention can use stem cell delivery as an approach to introduce healthy and viable cells to the damaged surrounding tissue in the hemorrhaged area. Neural stem cells (NSC) in particular hold promise due to their ability to differentiate into functionally specific cells following injury cues [28]. Despite the potential benefits, NSC delivery to the injured brain remains restricted in clinical translation due to low rates of cell survival post transplantation [230]. Tissue engineering strategies could lend solutions to both cell injury during delivery and cell survival following implantation.

In healthy brain tissue, NSC within the germinal regions of the adult brain interact closely with the vasculature and its cellular components, including endothelial cells (EC) and pericytes (PC). The vasculature is critical for providing intrinsic signals and extrinsic cues to the NSC within the neurogenic niches [137]. Specifically, NSC contact the vasculature directly in the germinal subventricular zone (SVZ), the largest area in the adult brain where neurogenesis occurs [9]. Beyond direct functional signaling of the NSC, vascular proliferation and neurogenesis are regulated by many of the same factors. Both neurogenesis and angiogenesis are enhanced during injury, and there is upregulation of neurotrophic factors such as brain-derived neurotrophic factor (BDNF) and angiogenic factors like vascular endothelial growth factor (VEGF) [231-233]. Interestingly, VEGF-C, the main lymphangiogenic factor, activates NSC without inducing vascular

proliferation, unlike VEGF-A, suggesting the role of VEGF-C as an activator of NSC in the SVZ and a regulator of neurogenesis in developing and adult brains [234, 235]. VEGFR3, the high affinity receptor of VEGF-C, is expressed in NSC, and conditional deletion of the receptor led to a reduction in the number of dividing neural cells [234, 236]. VEGF-C secretion and VEGFR3 expression is induced in reactive astrocytes, infiltrated macrophages, and activated microglia in a rat ischemic model [237], however the role of EC and PC secreted VEGF-C on NSC survival has yet to be elucidated.

Here, our objective is to probe the role of vascular secreted VEGF-C in promoting NSC survival during injury through NSC VEGFR3 signaling, which remains unknown. We use a glucose deprivation model (GD), as opposed to an oxygen-glucose deprivation model (OGD), since glucose has been demonstrated to be the survival limiting factor within the classic OGD [92]. Our results demonstrate that EC, though not PC, promote NSC proliferation and reduce cytotoxicity during GD. We also show that NSC proliferation is partially restored following GD when NSC are treated with EC conditioned media containing EC secreted VEGF-C. Beyond the role of EC secreted VEGF-C, we find that exogenous VEGF-C reduces NSC cytotoxicity, enhances proliferation, and increases VEGFR3 expression following GD, suggesting a pro-survival role of VEGF-C/VEGFR3. To demonstrate application of our in vitro results, we deliver degradable polyethylene glycol (PEG) microbeads containing co-encapsulated NSC and EC into the hemorrhagic stroke brain. The delivery of co-encapsulated NSC and EC within polymeric microbeads leads to increased VEGF-C secretion, not seen for NSC delivered alone. Together, the results of these studies suggest a beneficial therapeutic effect of VEGF-C/VEGFR3 signaling within the site of ICH induced injury, directly enhancing NSC survival following stroke.

6.3 Methods

6.3.1 Cell Maintenance

Adherent neural cell line (ANS4) have been characterized by S. Pollard [196] to be cultured in serum-free conditions. For tracking *in vivo* and *in vitro* co-cultures, GFP transfected ANS4s were utilized (NSC-GFP) [114]. The commercially available immortalized mouse brain endothelial cell line (bEND.3, ATCC) and mouse brain vascular pericytes cell line (MBVP, ScienCell) were cultured according to manufacturer's protocol. To deprive cells of glucose, a confluent cell layer was gently washed 3 times in 1X PBS and replaced with glucose-free NBM-27 media (Invitrogen) and were maintained at 37°C in 5% CO_2 atmosphere for 4 or 24 hours.

6.3.2. Cell Proliferation and Cell Cytotoxicity Assay

Cell proliferation and cell cytotoxicity were measured using MTT (ThermoFisher) and LDH (ThermoFisher) assays, respectively, following the manufacturer's protocols. NSC, NSC+EC, and NSC+PC were cultured in a 96 well plate at a cell-density of 10,000 cells/well. For co-cultures, a 1:1 ratio was used and maintained in NSC media. Monolayers were gently washed following 24 hours of culture, and media was replaced with GD media for 4 and 24 hours. An MTT stock was prepared at a concentration of 5 mg/ml in PBS and added to each well at a concentration of 0.005 mg/ml. Samples were incubated for 2 hours and absorbance was read at 570 nm.

The LDH assay was conducted following the culture of cells as mentioned above for baseline and glucose deprived samples, extra wells were cultured for spontaneous LDH and maximum LDH assessment. After 4 and 24 hours of glucose deprivation, the assay was conducted. Sterile ultrapure water and lysis buffers were added to designated wells for spontaneous and maximum LDH controls, respectively, and incubated for 45 minutes. Next, samples were transferred to a 96-well plate with added reaction mixture and incubated for 30 minutes. After addition of the stop solution, absorbance was measured at 490 and 680 nm.

6.3.3. Conditioned Media Treatment

NSC, EC, PC, and EC+PC were cultured in a 12 well plate at a seeding density of 100,000 cells/ml in NSC media. After 24 hours in culture, conditioned media (CM) was collected from EC, PC, and EC+PC, and the NSC monolayers were gently washed 3 times with 1X PBS. CM was gently added to the NSC monolayers which were then imaged at 4 and 24 hours.

6.3.4. VEGF-C and VEGFR3 Detection

VEGF-C secretion in culture media was detected using a VEGF-C ELISA (NovusBio) following the manufacturer's protocol. In brief, NSC, NSC+EC, and EC media were plated at a density of 100,000 cells/ml in 12 well plates in NSC media under baseline or GD. Media was collected at 4 and 24 hours for both conditions. Following protocol, absorbance was immediately measured at 450 nm.

For immunostaining of VEGF-C and VEGFR3, NSC, NSC+EC, and EC were cultured on laminin coated coverslips for 24 hours. Next, cells either remained at baseline or were glucose deprived for 4 hours. The cells were fixed with 4% PFA, blocked and permeabilized, and stained overnight with rat anti-VEGFR3 (Invitrogen, 1:100) or rabbit anti-VEGF-C (NovusBio, 1:100), and phalloidin. The following day, respective secondary antibodies were added, and cells were imaged using fluorescent microscopy (Leica). VEGFR3 expression was also quantified using flow cytometry. Following 4 and 24 hours of GD, NSC, NSC from NSC+EC, and EC were collected, where NSC in co-culture were detached using Accutase, ensuring EC remained adherent to the culture well. The cells were fixed with 4% PFA, blocked and permeabilized, and stained overnight. The following day, after secondary incubation, flow cytometry was conducted against VEGFR3 (NovusBio, 1:100 and analysis was done using FlowJo.

6.3.5. VEGFR3 Antagonism

SAR131675 (Selleckchem) is a VEGFR3 inhibitor with IC50/K_i of 23 nM/12 nM in cell-free assays, about 50- and 10-fold more selective for VEGFR3 than VEGFR1/2 and has little activity against Akt1, CDKs, PLK1, EGFR, IGF-1R, c-Met, and Flt2 [238-240]. SAR131675 was diluted to a 5 mM concentration in DMSO and following incubations at baseline or glucose deprivation, NSC VEGFR3 was blocked at a concentration of 50 nM for 24 hours.

6.3.6. Exogenous VEGF-C Treatment

Recombinant VEGF-C (Sigma) was reconstituted in 0.1% acetic acid to a concentration of 0.1 mg/ml. NSC were plated at a density of 100,000 cells/ml in 12 well plates in NSC media. Following 24 hours of culture, culture media was changed to GD media. After 4 hours of GD, VEGF-C was added at a concentration of 10 ng/ml. For comparison, NSC were also maintained at baseline or maintained under GD for an additional 24 hours. All conditions were then assessed using an MTT and LDH assay as described above. In addition, NSC were collected and VEGFR3 was quantified via flow cytometry as described above.

6.3.7. Synthesis of PEGDA and PEG Derivatives

Polyethylene glycol diacrylate (PEGDA) was prepared as previously described [82, 105, 119]. In order to create bioactive PEG derivatives, adhesive peptides and an MMP degradable sequence were conjugated to PEG using previously described methods [105, 166]. The fibronectin derived peptide arginine–glycine–aspartic acid-serine (RGDS) and laminin derived peptide tyrosine-isoleucine-glycine-serine-arginine (YIGSR) have each demonstrated the ability to support cell adhesion of EC and NSC, respectively [82, 147]. RGDS and YIGSR were reacted with acryloyl-PEG-N-hydroxysuccinimide Ester (PEG-NHS, 3500 Da) in 50 mM sodium bicarbonate (pH 8.5) at a 1:1 (peptide: PEG) molar ratio for 2 hours at room temperature, dialyzed, frozen, and lyophilized. Degradable constructs were created through the conjugation of the degradable

sequence glycine-glycine-leucine-glycine-proline-alanine-glycine-glycine-lysine (GGLGPAGGK; LGPA) to PEG as previously described [105, 163], reacting LGPA in sodium bicarbonate at a 1:2 (peptide:PEG) molar ratio for 24 hours at room temperature. The polymer was then dialyzed, frozen, and lyophilized. Lastly, for tracking of microbeads *in vivo*, a fluorescent tag was conjugated by dissolving PEG-RGDS in 0.1 M sodium bicarbonate buffer (pH 8.5) and dissolving Alexa Fluor™ 488 (AF-488) NHS Ester (Succinimidyl Ester) (ThermoFisher Scientific) in dimethylsylfoxide (DMSO, 1 mg/100 µl). AF-488 was added to PEG-RGDS at a 10:1 molar ratio of dye to conjugated polymer, reacted for 2 hours at room temperature, then dialyzed for 24 hours, frozen, and lyophilized.

6.3.8. Microbead Synthesis

Recently, we created and optimized PEG microbeads, either degradable or non-degradable, with or without encapsulated cells [105, 166]. In brief, we use an oil emulsion technique where we combine 25 µl of aqueous pre-gel solution containing 0.1 g/mL 10 kDa PEGDA, 1.5% (v/v) triethanolamine in 1X Dulbecco's Phosphate Buffered Saline (PBS), 3.4 µl/mL 1-Vinyl-2-pyrrolidinone, 10 µM Eosin Y, and 0.25% (v/v) Pluronic to an oil phase, containing 3 µl photoinitiator (300 µg 2, 2-dimethoxy-2-phenyl-acetophenone/ ml NVP) per ml mineral oil. The phases were then vortexed for 13 seconds and exposed to white light for 3 minutes. Microbeads were separated from the oil phase through a series PBS washes, centrifuging for 5 minutes at 1200 RPM, decanting mineral oil between washes. To add a fluorescent tag to microbeads, 2 mM PEG-RGDS-AF488 was added to the pre-gel solution. For cell encapsulated microbeads, 2 mM PEG-YIGSR and 2 mM PEG-RGDS were added to the aqueous pre-gel solution [105, 166]. NSC and EC pellets were resuspended in pre-gel at a final concentration of 75 x 10^6 cells/ml, using NSC:EC at a 1:1 ratio. Next, 25 µl of the pre-gel and cell suspension were mixed thoroughly and added to the mineral oil phase as previously mentioned. The polymer and cell phase were crosslinked with white light, then separated from the

oil phase through washes with NSC media and decanting the oil phase. Lastly, microbeads were transferred to a well plate and maintained in the incubator for 48 hours prior to ICH brain injections.

6.3.9. Animals

C57BL/6 mice were purchased from Jackson Laboratories. All mice were bred under specific-pathogen-free conditions with a 12-hour light/dark cycle in a temperature-controlled environment and ad libitum access to water and food pellets. All experimental protocols were conducted in accordance with the NIH guidelines and were approved by the Yale Institutional Animal Care and Use Committee.

6.3.10. Collagenase ICH mouse model and Microbeads injection

The mice were anesthetized through 2-5% isoflurane inhalation and ventilated with oxygen-enriched air (20:80%). To create an ICH lesion, mice were injected with 1 μl of 0.24 U type VII collagenase (from Clostridium histolyticum, Sigma-Aldrich) at a rate of 0.2 μl/min into the right striatum relative to the bregma: 2.1 mm lateral and 3.5 mm deep. The craniotomy was sealed with bone wax, and the scalp was closed with tissue adhesive (3M Vetbond). During the surgery, rectal temperature was maintained at 37.0 ± 0.5°C throughout the experimental and recovery periods (DC Temperature Controller 40-90-8D; FHC Inc.).

After 7, 14, or 28 days of ICH collagenase injection, mice were anesthetized by isoflurane as mentioned above. Microbeads were injected at the same injection point, depth and speed as mentioned above. Prior to sacrificing mice at 24 or 48 hours after microbead injection, Brefeldin-A was injected through a tail vein injection for each mouse using previously described methods [241]. In brief, a 0.25 mg/ml solution of Brefeldin-A was made, and 100 μl was injected to the tail vein of each mouse using an insulin syringe 6 hours prior to sacrifice.

6.3.11. Tissue Processing and Immunohistochemistry

Mice were transcardially perfused with 20 ml PBS followed by 20 ml 4% PFA. Brains were then harvested and post-fixed in 4% PFA overnight at 4°C. Next, brains were transferred to 30% sucrose

for 48 hours and embedded in OCT. Sections were cut at a thickness of 50 μm and stored in 30% glycerin prior to imaging.

Sections were rinsed 3 times in PBS and blocked and permeabilized with 5% normal donkey serum and 2% Triton X-100 in PBS for 1 hour at room temperature. Sections were then incubated with the following antibodies at 4°C overnight: chicken anti-GFP (Abcam, 1:1000), rabbit Iba-1 (NovusBio, 1:100), and rabbit anti-VEGF-C (NovusBio, 1:100). The following day, respective secondary antibodies were added for 2 hours at room temperature, sections were mounted using Dapi mounting media, and images were taken using a fluorescent microscope (Leica).

6.3.12. Statistics

All statistical analyses were performed using GraphPad Prism 7 software. Significance was determined with either a one-way ANOVA with multiple comparisons, or by an unpaired t-test as appropriate. Data were expressed as mean ± SEM and the differences were considered significant at P values of <0.05.

6.4 Results

6.4.1 EC Increase NSC Proliferation and Decrease NSC Cytotoxicity during Glucose Deprivation

EC are known to promote NSC survival, proliferation, and differentiation post transplantation into the ischemic injured brain [242]. Although this pro-survival effect of EC on NSC has been demonstrated in oxygen-glucose deprivation models, it has not been investigated solely in the absence of glucose [243]. To investigate the role of EC and PC in promoting NSC survival during GD, we cultured NSC, NSC+EC, and NSC+PC in a 1:1 ratio, and then deprived samples of glucose for 4 or 24 hours. NSC cultured alone appear unhealthy and unattached by 24 hours, mostly floating or dead (Figure 6.1a), however NSC-GFP in the presence of EC remain adherent to the culture well, in a clustered phenotype (Figure 6.1a). On the other hand, NSC-GFP in the presence of PC look unhealthy, unattached, and fragmented by 24 hours (Figure 6.1a). We

quantified cell proliferation at 4 and 24 hours using an MTT assay (Figure 6.1b), which assesses cell metabolic activity and reflects the number of viable cells present. After 4 and 24 hours, NSC had a significant reduction in proliferation (P<0.0001) compared to NSC baseline control. To our excitement, there was no significant difference between NSC+EC after 4 and 24 hours of glucose deprivation compared to NSC baseline control (P=0.8588 and P= 0.1740, respectively). In contrast, we see a significant reduction in NSC proliferation for NSC+PC at 4 and 24 hours (P<0.0001 and P=0.0001, respectively). These results were supported by the results of an LDH assay, measuring extracellular lactate dehydrogenase, to assess cytotoxicity (Figure 6.1c). NSC under 4 and 24 hours of GD had a significant increase in cytotoxicity, as compared to NSC baseline control (P <0.0001). On the other hand, we see no significant difference in cytotoxicity at 4 and 24 hours for NSC+EC compared to NSC baseline control (P=0.9067 and P= 0.0655, respectively). In contrast, NSC cultured with PC, exhibited a significant increase in cytotoxicity at both time points, as compared to NSC baseline control (P=0.0007 and P=0.0009, respectively). We also cultured EC and PC up to 48 hours under GD and evaluated their cytotoxicity to ensure effects seen were due to NSC, and not EC or PC (Supplementary Figure A4.1). In total, the results suggest that EC, and not PC, are contributors to NSC proliferation and reduced NSC cytotoxicity in response to glucose deprivation.

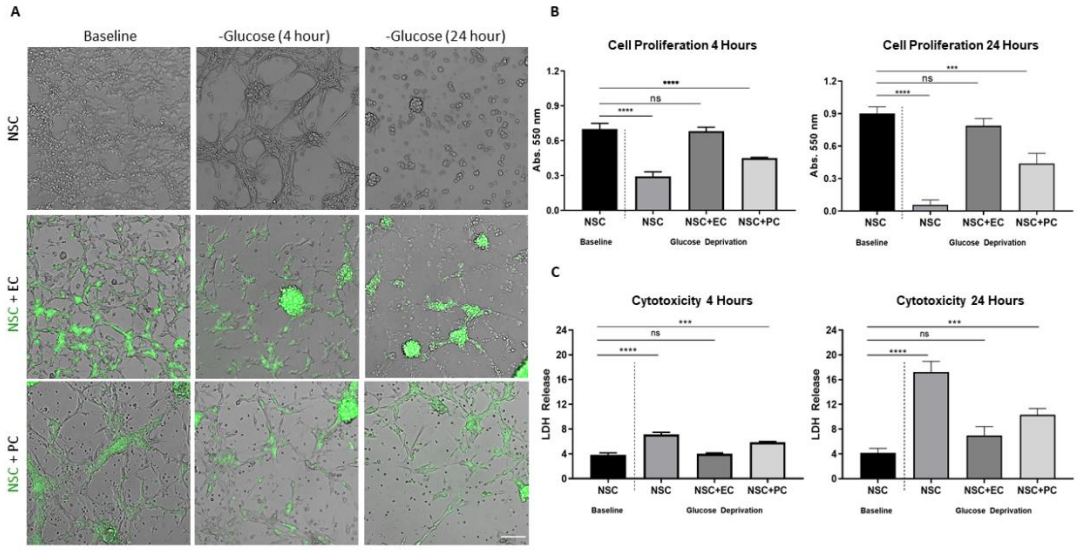

Figure 6. 1. EC increase NSC proliferation and decrease NSC cytotoxicity during glucose deprivation. A) NSC, NSC+EC, and NSC+PC at baseline (left column), 4 hours of glucose deprivation (middle column) and 24 hours of glucose deprivation (right column), using NSC with a GFP tag in co-cultures. Scale bar (100 µm representative of all images. B) Cell proliferation for NSC baseline control and NSC, NSC+EC, and NSC+PC under GD at 4 hours (left) and 24 hours (right). C) Cell cytotoxicity for NSC baseline control and NSC, NSC+EC, and NSC+PC under GD at 4 hours (left) and 24 hours (right).

6.4.2 VEGF-C Secretion is Increased in Co-Cultures of NSC+EC during Glucose Deprivation

VEGFR3 is present in SVZ resident NSC and VEGF-C is synthesized in the lateral ventricle walls, suggesting that VEGF-C may stimulate NSC expressing VEGFR3. In addition, overexpression of VEGF-C has led to stimulation of NSC VEGFR3, positively impacting neurogenesis in the SVZ [234]. To investigate the role of EC secreted VEGF-C, we quantified VEGF-C secretion through an ELISA at 4 and 24 hours for NSC, NSC+EC, and EC at baseline and GD (Figure 6.a-b). For NSC, there was a slight increase in VEGF-C secretion during GD compared to baseline at 4 hours (P= 0.0027), and there is no significant change in VEGF-C secretion at 24 hours (P= 0.1330). In contrast, NSC+EC had a significant increase in VEGF-C expression during GD compared to baseline at both 4 and 24 hours (P *<0.0001* and P= 0.0002, respectively). EC alone had similar VEGF-C secretion during baseline and GD at 4 hours (P= 0.7898) and an increase at 24 hours (P= 0.0010). Since EC VEGF-C levels are about two-fold higher compared to NSC

under GD at 4 and 24 hours, and this increase is similar for NSC+EC, these data suggest EC are the main secretors of VEGF-C during GD.

We conducted immunofluorescent staining to visualize VEGF-C nuclear and cytoplasmic localization during baseline and GD at 4 hours (Figure 6.2c-d). NSC have nuclear staining for VEGF-C during both conditions, seen through co-localization of VEGF-C and Dapi. For a co-culture of NSC+EC, we distinguish the two cell types by their nuclear size stained with Dapi and cell cytoskeleton stained with Phalloidin; NSC have small nuclei with thin, long bodies, and EC have much larger nuclei with large, extended bodies. In co-culture, EC have both nuclear and cytoplasmic presence of VEGF-C, and this is seen more intensely during GD. This agrees with our ELISA data, suggesting EC secrete higher levels of VEGF-C during GD when co-cultured with NSC. We see a similar pattern for EC nuclear and cytoplasmic staining for monocultures of EC under GD, further supporting our hypothesis that EC secreted VEGF-C both under resting conditions and further increased may act upon NSC during GD.

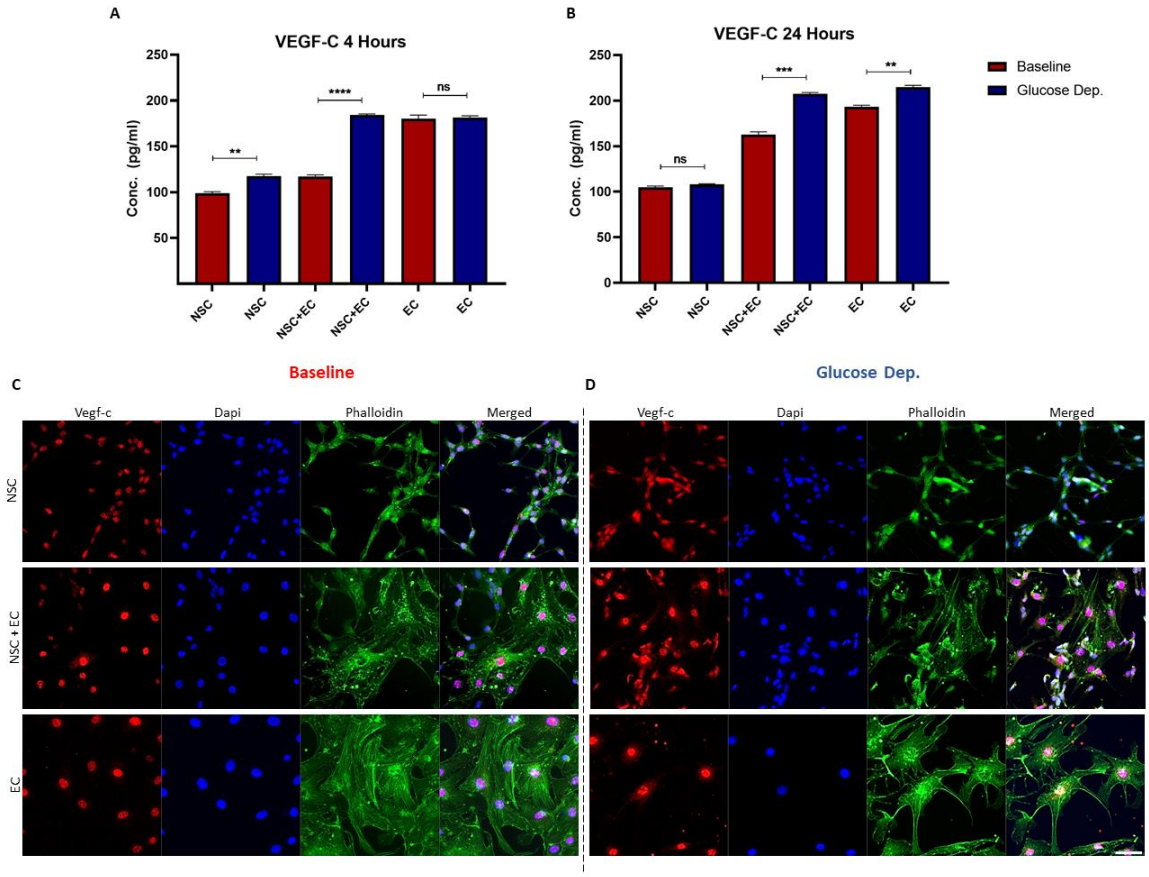

Figure 6. 2. VEGF-C secretion is increased in co-cultures of NSC+EC during glucose deprivation. A) VEGF-C secreted levels for NSC, NSC+EC, and EC at 4 hours under baseline and GD. B) VEGF-C secreted levels for NSC, NSC+EC, and EC at 24 hours under baseline and GD. C) Immunofluorescent images for NSC, NSC+EC, and EC at 4 hours under baseline (left) and GD (right), staining against VEGF-C (red), Dapi (blue), and Phalloidin (green). Scale bar (50 µm) representative of all images.

6.4.3. NSC VEGFR3 Expression is Increased in Co-Cultures of NSC+EC

VEGF-C stimulates neurogenesis by directly interacting with VEGFR3 on neural cells [236]. In addition, deletion of VEGFR3 within NSC negatively impacts neurogenesis in the mouse SVZ [234]. VEGFR3 is expressed by SVZ NSC, and VEGF-C can stimulate mitosis of VEGFR3 expressing SVZ-derived NSC. In fact, SVZ neurogenesis is VEGFR3 dependent. We quantified cell VEGFR3 expression by flow cytometry on NSC, NSC from an NSC+EC co-culture, and EC, during baseline and GD at 4 and 24 hours (Figure 6.3a-b, Supplementary Figure A6.2**)**.

Interestingly, we see a significant decrease in VEGFR3 expression for mono- cultured NSC following 4 hours of GD compared to baseline (*P<0.0001*), which was no longer significant at 24 hours (*P*=0.0537). This was not the case of NSC cultured with EC, where NSC have a significant increase in VEGFR3 expression at both 4- and 24-hours GD compared to baseline (*P*=0.0106 and *P<0.0001*, respectively), suggesting that NSC VEGFR3 expression increases with prolonged GD exposure. EC, on the other hand, expressed VEGFR3 at high levels during baseline, as expected since VEGFR3 is abundant on angiogenic blood vessels [244]. EC VEGFR3 expression remained unchanged following 4 hours of GD, and there was an increase following 24 hours of GD compared to baseline (*P*= 0.0038). In total, our results suggest that NSC VEGFR3 expression is increased in co-culture with EC, potentially by EC-derived VEGF-C, as shown in Figure 6.2.

We conducted immunofluorescent staining to visualize VEGFR3 expression at baseline and 4 hours of GD (Figure 6.3c). As above, we differentiate NSC from EC in co-cultures by the presence of thin, elongated NSC bodies with small nuclei, as compared to the large, extended EC bodies with much larger nuclei (~2 fold). We can visualize the reduction in NSC VEGFR3 expression following 4 hours of GD compared to baseline control (Figure 6.3c), which was unlike NSC VEGFR3 expression when in co-culture with EC. Our immunofluorescent staining complements our flow cytometry data, confirming the changes in NSC VEGFR3 expression during GD.

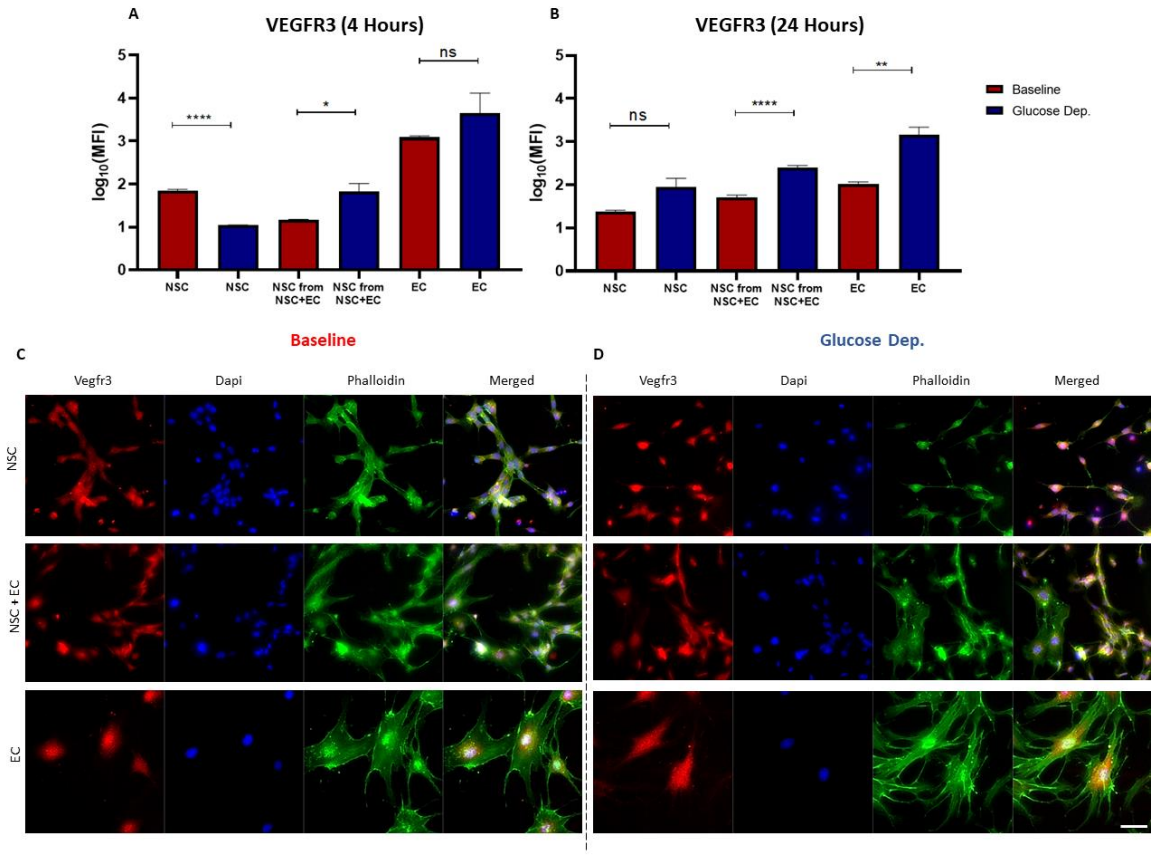

Figure 6. 3. VEGFR3 expression is increased in co-cultures of NSC+EC during glucose deprivation. A) VEGFR3 expression for NSC, NSC+EC, and EC at 4 hours under baseline and GD. B) VEGFR3 expression for NSC, NSC+EC, and EC at 24 hours under baseline and GD. C) Immunofluorescent images for NSC, NSC+EC, and EC at 4 hours under baseline (left) and GD (right), staining against VEGFR3 (red), Dapi (blue), and Phalloidin (green). Scale bar (50 µm) representative of all images.

6.4.4 EC Conditioned Media Increases NSC Proliferation Following Glucose Deprivation when VEGFR3 is not Blocked

We have demonstrated that co-culturing with EC, and not PC, has a pro-survival effect on NSC following GD, and identified VEGF-C as a potential mediator of survival and proliferation. We then investigated directly tested whether soluble factors from EC or PC could rescue NSC after GD and support NSC proliferation. We deprived NSC of glucose for 4 hours (Figure 6.4a then recovered NSC in cultured media (CM) from EC, PC, and EC+PC for 24 hours. We see that NSC recovered in EC CM are adherent, and some cells had a clustered phenotype,

which was in stark contrast to NSC recovered in PC CM, which appear to be unhealthy and unattached to the culture well (Figure 6.4b). NSC recovered in EC+PC CM appear to be partially adherent, and partially unattached (Figure 6.4b).

Next, we tested if NSC can no longer respond to pro-survival cues from supporting cells in the presence of a VEGFR3 antagonist, SAR131675, at a concentration of 50 nM for 24 hours. Interestingly, NSC were unhealthy and unattached when recovered in EC CM + VEGFR3 antagonist (Figure 6.4c). This was also apparent for NSC with VEGFR3 antagonists recovered in EC+PC CM (Figure 64c). We then quantified proliferation in this rescue paradigm for the different CM conditions by MTT assay. We found a significant increase in NSC proliferation for NSC recovered in EC CM as compared to NSC remained under GD ($P=<0.0001$), which was less significant for NSC recovered in PC CM (P=0.0220) (Figure 6.4d). When recovered in EC+PC CM, NSC had a significant increase in proliferation compared to NSC remained under GD ($P=<0.0001$) (Figure 6.4d)**,** suggesting EC are the main contributors of soluble factors that have a pro-survival impact on NSC. However, in the presence of the VEGFR3 antagonist, there was no significant difference for recovery in EC CM, PC CM, and EC+PC CM when compared to NSC remaining under GD (Figure 6.4d). This suggests that VEGFR3 is crucial for NSC to respond to pro-survival secreted factors, and without VEGFR3, NSC proliferation cannot be restored by EC-secreted factors.

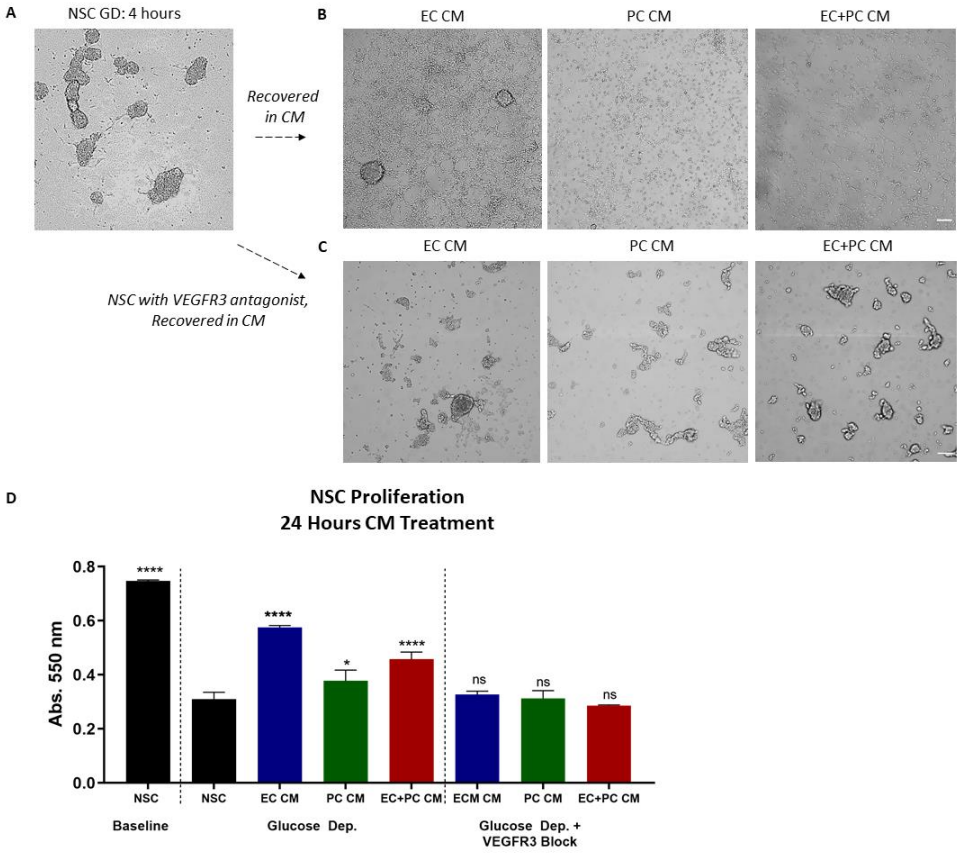

Figure 6. 4. EC conditioned media increases NSC proliferation following glucose deprivation with VEGFR3 antagonist. A) NSC under 4 hours of GD, B) recovered in EC, PC, and EC+PC conditioned media. C) NSC with VEGFR-3 antagonist recovered in EC, PC, and EC+PC conditioned media. D) NSC proliferation for baseline control and GD, NSC recovered in EC, PC, and EC+PC CM, and NSC with VEGFR3 antagonist recovered in EC, PC, and EC+PC CM. Scale bar (100 µm) representative of all images.

6.4.5 Exogenous VEGF-C Treatment Promotes NSC Proliferation, Decreases Cytotoxicity, and Increases VEGFR-3 Expression during Glucose Deprivation

Having observed that EC secrete VEGF-C, and VEGF-C was significantly higher for NSC+EC under GD compared to baseline, we sought to determine if exogenous VEGF-C promotes NSC health during GD independently of EC. We glucose-deprived a monolayer of NSC for 4 hours, then treated the NSC with exogenous VEGF-C at a concentration of 10 ng/ml, maintained for 24 hours, or kept the NSC under GD up to 24 hours. A NSC monolayer with glucose served as our

control. NSC under GD treated with VEGF-C remained mostly adherent, especially compared to NSC under GD with no treatment, which were fragmented and unattached (Figure 6.5a). Interestingly, NSC under GD with no treatment had a significant reduction in VEGFR3 expression (less than ½ -fold compared to NSC control) (Figure 6.5b). On the contrary, NSC under GD with VEGF-C treatment have a significant increase in VEGFR3 expression compared to NSC control (~1.5-fold), agreeing with our previous results that VEGFR3 expression is increased with EC co-culture and the increased EC secretion of VEGF-C after GD (Figure 6.2 and 6.3). In addition, we conducted a MTT and LDH assay for cell proliferation and cytotoxicity, respectively. We see a sharp drop in NSC proliferation for NSC remained under GD compared to NSC control (Figure 6.5c). In contrast, NSC under GD with VEGF-C treatment had a significant increase in proliferation compared to NSC remained under GD ($P<0.0001$) (Figure 6.5c). Although the addition of VEGF-C does not completely return proliferation to levels of NSC control, our results demonstrate that VEGF-C plays an important role in promoting NSC health following GD. Likewise, our cytotoxicity data demonstrates a significant increase in NSC cytotoxicity under GD compared to control ($P<0.0001$) and compared to NSC under GD treated with VEGF-C ($P<0.0001$) (Figure 6.5c). Although not completely abrogating cell death, there was a slight increase in NSC

cytotoxicity for NSC under GD treated with VEGF-C (P=0.0229) as compared to control.

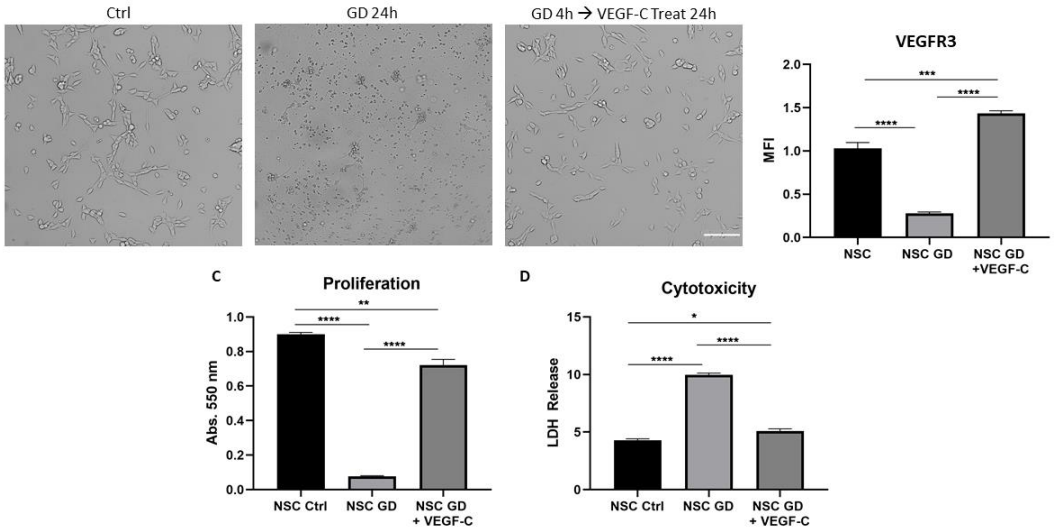

Figure 6. 5. Exogenous treatment with VEGF-C increases VEGFR-3 expression, promotes NSC proliferation, and decreases cytotoxicity. A) Brightfield images of NSC control, NSC under GD for 24 hours, and NSC under GD for 4 hours then treated with VEGF-C for 24 hours. B) VEGFR-3 quantification, C) NSC proliferation, and D) NSC cytotoxicity for NSC control, NSC under GD for 24 hours, and NSC under GD for 4 hours then treated with VEGF-C for 24 hours. Scale bar (100 µm) representative of all images.

6.4.6 NSC+EC Encapsulated Microbeads Lead to Greater VEGF-C Expression in Tissue Compared to Blank Microbeads and NSC Encapsulated Microbeads

Microbeads were created through an dual oil emulsion technique **(Figure S3)**, where microbeads have an average diameter of ~150 microns and have undergone optimization for microbead size, cells/microbead, and the cell ratio of NSC+EC co-encapsulated microbeads [105]. The microbeads are degraded by matrix metalloproteinases, allowing release of cells under inflammatory conditions. Recently, we have demonstrated that NSC co-encapsulated with EC in polymeric PEG microbeads enhanced NSC viability and maintained NSC quiescence compared to NSC encapsulated alone prior to and post injection into a non-injury mouse model. In addition, co-encapsulated NSC+EC microbeads retained NSC survival and quiescence post-delivery to a non-injury mouse model better than NSC encapsulated alone. In addition, the microbeads used to deliver

cells did not induce an immune response, compared to freely injected cells, ultimately enhancing cell viability [105].

To further assess the delivery of NSC and NSC+EC in microbeads, we began to deliver cell encapsulated microbeads *in vivo* after intracerebral hemorrhage (ICH) [245]. After ICH, the brain injury cavity where ideally NSC could help restore function no longer has a blood supply. The resulting nutrient deprivation for cells may impede NSC survival. First, we began optimizing the injection time points by delivering non-degradable, fluorescent microbeads with no encapsulated cells to ensure we were injecting into hemorrhage cavity. We found that 30 days post ICH formation, the cavity was no longer visible (Supplementary Figure A4.4), where the microbead injection causes a cavity through the pressure exerted, making this time point unsuitable injections. At 14 days, there is a cavity we can target effectively, however microbeads did not degrade, thus we moved to an earlier time point to capitalize on inflammation leading to microbead degradation. Finally, we concluded that injecting into the cavity 7 days post ICH induction and sacrificing mice 2 days following injection allowed for complete degradation of microbeads as well as cell escape from the microbeads, in addition to migration along white matter tracts where the hemorrhage commonly extends (Supplementary Figure A4.5).

Mice were injected with Brefeldin-A prior to sacrificing animals for processing to maintain cellular localization of secreted factors for immunofluorescent assessment. Brain sections were stained for VEGF-C to assess VEGF-C production by endogenous and exogenous cells in the hemorrhage cavity as well as the tissue surrounding the injury. Degradable microbead constructs with no cells result in little to no VEGF-C secretion surrounding the microbeads or hemorrhage cavity (Figure 6.6a), as expected, since PEG is known to be an inert material. When NSC were injected alone, there was slight VEGF-C secretion around the injection area (Figure 6.6b) where most NSC-GFP$^+$ cells do not express VEGF-C. In addition, there was faint secretion for VEGF-C in the injection area or in the surrounding damaged tissue. However, NSC+EC co-encapsulated microbeads produce high VEGF-C secretion in cells surrounding the microbead constructs, as well

as along the injection tract (Figure 6.6b). Here, we see many VEGF-C^{+} cells, unlike when NSC are encapsulated alone, and cells in the injection area as well as throughout the damaged tissue are VEGF-C^{+}. This suggests that both *in vitro* and *in vivo*, NSC+EC together provide a VEGF-C rich environment in response to injury.

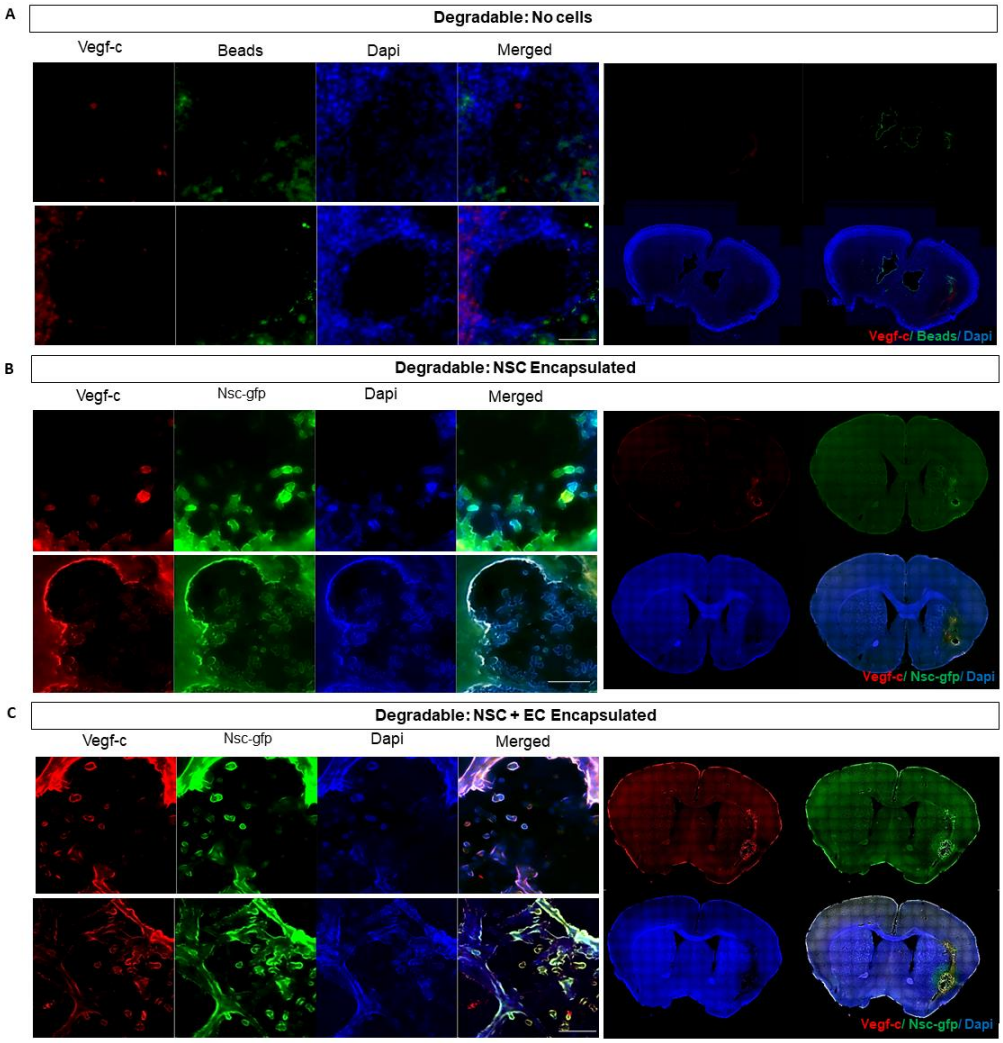

Figure 6. 6. NSC+EC encapsulated microbeads led to VEGF-C secretion in tissue A) ICH brain sections with implanted degradable green microbeads containing no cells, staining against VEGF-C (red), microbeads (green), and Dapi (blue). B) ICH brain sections with implanted degradable microbeads containing encapsulated NSC-GFP and C) co-encapsulated NSC-GFP and EC, staining against VEGF-C (red), NSC-GFP (green), and Dapi (blue). Scale bar (50 µm) representative of all images.

6.5 Discussion

Stroke is among the leading causes of death and disability worldwide, partly due to the lack of effective therapies to facilitate the recovery of damaged brain tissue [246]. In particular, ICH leads to an extremely high mortality rate and inflammatory responses may persist for weeks, leading to an inhabitable environment for NSC [247, 248]. Stem cell therapies used to treat neurological diseases are promising, owing to their innate ability to enhance endogenous repair mechanisms and promote functional recovery. Stem cell therapy has been investigated for the treatment of ICH and has shown promising results [249]. However, there are extremely low levels of transplanted cell survival within the inflamed, cytotoxic brain [250].

A successful cell delivery strategy can build upon the interactions between NSC and vascular cells to enhance NSC survival *in vivo*, recovering the abundance and differentiation of neurons in the damaged tissue. During injury, NSC from the SVZ, the largest area pool of proliferating NSC in the adult brain, become activated. NSC directly interact with EC and PC, and studies highlight the interaction between NSC and the vasculature [5, 139, 157]. The molecular mechanisms by which EC and PC impact NSC at homeostasis and during stroke are incompletely described [2, 251, 252]. Diffusible secreted signals from vasculature, specifically EC, are known to increase survival, proliferation, differentiation, and migration of NSC *in vitro* using an OGD model and *in vivo* during ischemia [88, 89]. Here, we investigate the role VEGF-C plays in NSC survival during GD, which has been speculated to be responsible for NSC transitioning into neuroblasts [236, 253].

We demonstrate that NSC cell contact with EC, but not PC, significantly enhanced NSC proliferation and reduced NSC cytotoxicity during GD. Through our CM studies, we conclude EC CM can significantly enhance NSC proliferation in response to GD as compared to NSC under GD. For NSC with a VEGFR3 antagonist, this proliferation enhancement was diminished, heightening the necessity for VEGFR3. Interestingly, we see that co-cultures of NSC+EC under GD have significantly higher levels of VEGF-C than NSC under GD, where EC alone have the highest

secreted levels, suggesting EC are the main contributors to VEGF-C secretion during GD. Along with elevated VEGF-C in co-cultures, we see NSC from NSC+EC have significantly higher levels of VEGFR3 during GD, suggesting the correlation of elevated VEGF-C with increased VEGFR3 expression because of the chemokine's availability. These data demonstrate the positive effect of VEGF-C/VEGFR3 during GD and encourage the usage of this cytokine for therapeutic exploration.

Due to NSC dependence on vascular cells for appropriate response during health and disease, a co-transplantation of NSC with a native SVZ cell type may be key to overcoming limitations of NSC survival and early differentiation seen when NSC are transplanted alone. To address the challenges of cell damage during delivery and introduction into an injured and hostile microenvironment, we recently demonstrated that the co-encapsulation of NSC+EC in PEG microbeads promoted NSC quiescence prior to and post-delivery into a non-injury model, enabling NSC protection during delivery and escape from the microbeads only upon appropriate placement of the beads into the region of interest [105]. In addition, PEG, known as an inert material, reduced inflammatory response compared to freely injected cells, suggesting these biomimetic units can be used to promote NSC survival, maintain NSC quiescence prior to injection and reduce inflammation that can inhibit NSC survival upon transplantation [105].

In the current study, we inject cell-encapsulated microbeads to an ICH cavity, rather than a non-injury model, to further validate the efficacy of our delivery system to another injury model. Here, we demonstrate that following 7 days of hemorrhage induction, the cavity was activated enough to degrade our MMP-degradable microbeads and allow for cell escape. Using a Brefeldin-A injection to allow for intracellular cytokine visualization, our results show that NSC+EC encapsulated microbeads lead to a more prominent VEGF-C secretion in the ICH cavity and tissue surrounding the cavity as compared to NSC encapsulated alone or microbeads with no cells. This provides further evidence that VEGF-C is produced by the NSC + EC cells at the site of injury and may play a significant role in promoting NSC survival.

In summary, we have demonstrated that VEGF-C/VEGFR3 could promote NSC survival in a milieu with compromised nutrient availability such as an injured brain. To our advantage, EC secrete elevated levels of VEGF-C, and NSC VEGFR3 was elevated in response to cell contact with EC and in the presence of VEGF-C. There are other pro-survival factors which can also aid this response, many of which have been attributed to enhanced NSC survival. These include insulin-growth factor-1 (IGF-1) and BDNF, which have demonstrated promising results as acute therapies. These have been administered effectively after 30 and 15 min post MCAO, respectively, and the growth factors led to a reduction in infarct volume [16]. In addition, a metabolic switch may play a role in allowing NSC to proliferate in an injury-state. It has been demonstrated that NSC survive with lactate in a glucose-free environment [254]. Interestingly, EC secrete lactate during ischemia [255], so there may be a potential link between EC promoting a metabolic switch for NSC under GD that promotes survival. Nonetheless, the effect of VEGF-C was pronounced on NSC proliferation, reduction of cytotoxicity, and enhancement of NSC VEGFR3 expression. The findings suggest that EC-derived VEGF-C aids in NSC survival and proliferation within injured tissue and should be investigated further as potential therapeutic to augment local stem cell therapies.

Chapter 7: Conclusions & Future Directions

7.1 Conclusions

In the subventricular zone (SVZ), neural stem cells (NSC) interactions with the vasculature directly impact NSC differentiation, survival, and migration. Endothelial cells (EC) and pericytes (PC) in this neurogenic niche deliver nutrients and soluble factors crucial for NSC survival [22]. These interactions are crucial for maintaining brain homeostasis and promoting the appropriate response to injury cues. Although stroke is one of the leading causes of death and disability worldwide, a treatment that promotes long term functional and motor recovery does not exist. Biologists can harness the positive impact of vascular cells on NSC functionality in order to improve the current state of stem cell therapies.

In our work, we investigate the role EC and PC have on NSC migration and survival, and created a tissue engineered construct to encapsulate and deliver cells to the stroke injured brain. In Chapter 3, we determined that EC, and not PC, promote NSC migration using a 2D scratch assay, a 3D biomimetic hydrogel, and a microfluidic system. Furthermore, we demonstrated that NSC clustering is a pre-requisite to NSC migration, and our results show that EC soluble factors are responsible for the necessary step of NSC clustering. We investigate the role of EC secreted MMP2 which enhanced NSC N-cadherin expression, diminished through the use of an MMP2 inhibitor. MMP2, known to activate the EGFR cascade that allows for NSC cell polarization and migration, is thereby necessary for NSC clustering, and we conclude that EC secreted MMP2 plays a crucial role for NSC to respond appropriately to injury.

In Chapter 4, we discuss the creation and optimization of poly- (ethylene glycol) (PEG) microbeads with NSC or NSC+EC encapsulated within. Our results show that EC promote NSC quiescence prior to and post-delivery to the mouse non-injury model. In addition, co-encapsulated microbeads have a reduction in immune cell activation and exogenous cell death as compared to

freely injected cells. In summary, our work demonstrated promise for the delivery of NSC+EC encapsulated microbeads to an injury model. This was then assessed in Chapter 5, where the delivery of microbeads was optimized for two rat stroke models – photothrombotic and middle cerebral artery occlusion (MCAo). Upon optimization of the injection parameters, we injected NSC and NSC+EC encapsulated microbeads to both models using a porcine bladder derived extracellular matrix (ECM) hydrogel as a suspension vehicle. The ECM vehicle improved retention of microbeads within the cavity and promoted cell infiltration both into the ECM as well as into the surrounding tissue, suggesting that this suspension vehicle can improve the delivery and migration of cell encapsulated constructs into the infarct area.

Lastly, in Chapter 6 we assess the role of vascular cells on NSC survival during glucose deprivation (GD). We conclude that EC, and not PC, promote NSC cell proliferation and reduce cytotoxicity through direct cell-cell contact during GD. Additionally, NSC proliferation was increased upon treatment with EC conditioned media, which was inhibited with VEGFR3 blocking. We detected that NSC+EC co-cultures have high levels of VEGF-C, not seen when NSC were cultured alone. Furthermore, exogenous VEGF-C induced NSC upregulation of VEGFR3, promoted proliferation, and reduced cytotoxicity. Finally, we delivered polymeric microbeads containing NSC+EC into the ICH cavity of a murine stroke model. VEGF-C was increasingly present in the injury site coincident with delivery of NSC+EC, while such an increase in VEGF-C was not seen upon delivery of microbeads containing NSC alone. Together, these studies demonstrate that EC-secreted VEGF-C can promote NSC survival during injury, subsequently enhancing the potential for cell delivery therapies used to mitigate injury due to stroke.

In summary, our work focusing on microvascular signaling in the neurogenic niche has provided great insight as to how neurogenesis is dependent upon vascular interactions. By building upon the pro-migratory and pro-survival effects vascular cells have on NSC, we can further enhance the state of tissue engineered delivery systems in order to create long-term, effective cell delivery therapies for neurological diseases.

7.2 Future Directions

Throughout the course of this work, many models were created and optimized in order to mimic brain train, in addition to sophisticated microfluidic chambers to aid migratory assessment. The models utilized in this work can be applied to various disease states and pathologies, such as lung fibrosis. Through the duration of this work, we utilized a 3D tissue roll with encapsulated cells to create a gradient of hypoxia and nutrient deprivation. During the optimization of this system, a large quantity of cells were required, therefore we used EC due to their rapid proliferation rate and low cost. This model can be used to mimic lung fibrosis, where EC and PC can be utilized within this 3D system, applying injury activations previously investigated by the Gonzalez lab. In addition to mimicking oxygen glucose deprivation gradients using this 3D model, NSC survival can be probed to investigate the role of metabolic switches that may play a role in cell viability. We have observed that lactate is upregulated in co-cultures of NSC and EC during glucose deprivation, therefore a metabolic switch to lactate utilization may be partially responsible for enhanced NSC survival in the presence of EC. This hypothesis requires further investigation, as detailed below.

7.2.1 3D model tissue role to mimic oxygen glucose deprivation

To better mimic the gradient achieved from ischemic core to penumbra, we have created a 3D tissue role model based on previously established methods [256-258]. This consists of a thin collagen gel (~40 μm thick), 13 mm long and 0.5 mm wide (Figure 7.1a) with encapsulated cells within. To handle the gel to create a roll, we placed a thin layer of cellulose atop the collagen gel. After 24 hours of cell remodeling in the collagen, the strip was rolled around an aluminum spool (Figure 7.1b) so that cells on the interior are limited in nutrients and oxygen compared to those on the sixth exterior layer. Thus far, we have verified high cell viability in this construct for NSC, EC, and PC, and have validated a hypoxic gradient for EC in the interior sections using EF5 stain (Figure 7.1c-d). In the future, all cell types can be assessed to probe NSC viability with and without the presence of EC and PC in this 3D setting. By digesting the collagen strip, we can conduct analysis to observe cellular response in mono-or co-cultures to probe the protective effect of EC or

PC in this setting at distinct sections of the tissue strip. In addition, this system can be easily manipulated to mimic lung fibrosis and visualize the changes in EC and PC phenotype in response to injury cues. Lastly, the system can be optimized further by using the bioprinter for the Yale Biomedical Engineering Department to print a thin collagen strip in order to simplify the process further.

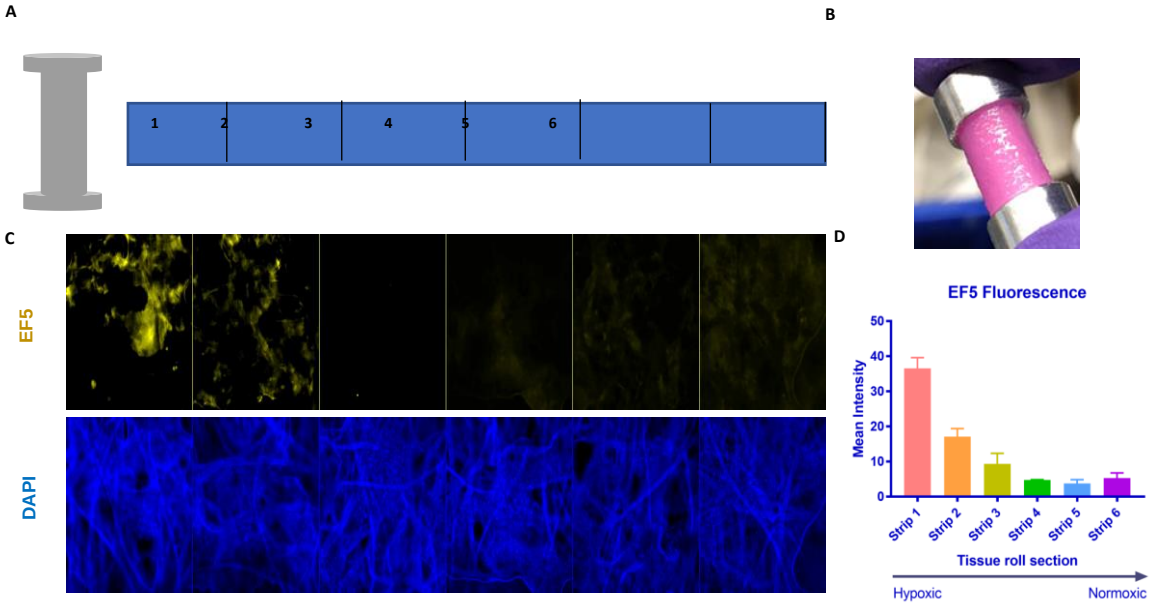

Figure 7. 1. Development of 3D hypoxic tissue roll. A) Schematic of collagen hydrogel with encapsulated cells and cellulose sheet atop which wraps around an aluminum spool (B) that can be cultured to create an oxygen and nutrient gradient between layers 1 (inner) to 6 (outer). C) EF5 immunofluorescent images and D) quantification verify creation of hypoxic core.

7.2.2 Investigation of Cell Metabolism

As discussed in Chapter 6, EC promote NSC proliferation, reduce NSC cytotoxicity, and enhance NSC VEGFR3 expression in response to glucose deprivation. Although we see a pro-survival impact on NSC by EC secreted VEGF-C, and a role for VEGF-C/VEGFR3 in NSC survival in response to injury cues, the metabolic switch of NSC in response to glucose deprivation (GD) remains undiscovered. It has been demonstrated that EC generate the majority of their energy through the glycolytic conversion of glucose to lactate [255]. In addition, neurons and neural

progenitor cells cultured in glucose-free media with lactate as the sole metabolic substrate did not have a change in relative total caspase activity, which is seen only without both glucose and lactate [254]. To assess if EC secreted lactate is increased in a co-culture of NSC+EC, we used the Lactate-Glo Assay (Promega) following manufacturer's protocol. In brief, media from NSC, NSC+EC, and EC was collected following baseline and 4 hours of GD. Following protocol, the luminescent signal was recorded which is proportional to the amount of lactate in the sample. Our results show that lactate is significantly enhanced for EC under GD, and similarly, NSC+EC have significantly higher lactate levels compared to NSC+EC under baseline conditions (Figure 7.2). This suggests that a metabolic switch may play a role in promoting NSC survival when in direct culture with EC during GD. To further probe this, research can be conducted using the Seahorse assay to observe metabolic switch in greater detail. In addition, lactate can be knocked out, and analysis conducted in Chapter 6 can be conducted once again to determine if the pro-survival impact of EC requires a switch to lactate utilization.

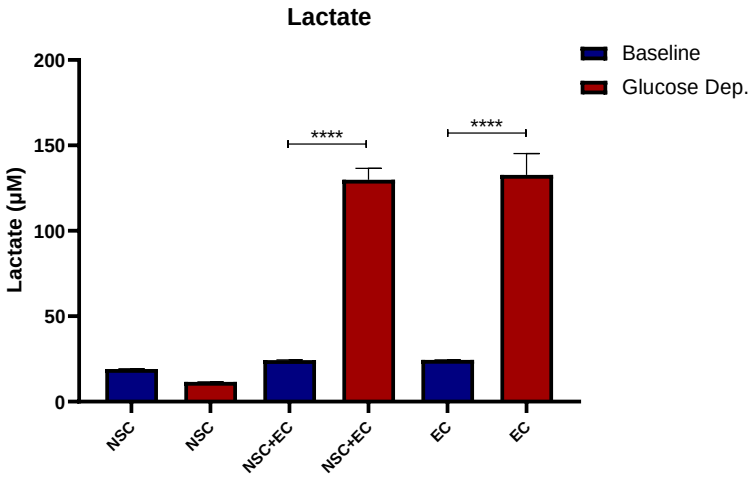

Figure 7. 2 Lactate is enhanced for NSC+EC under GD. Lactate levels were measured for NSC, NSC+EC, and EC under baseline conditions and 4 hours of glucose deprivation.

Appendix 1: Supplemental Figures from Chapter 3

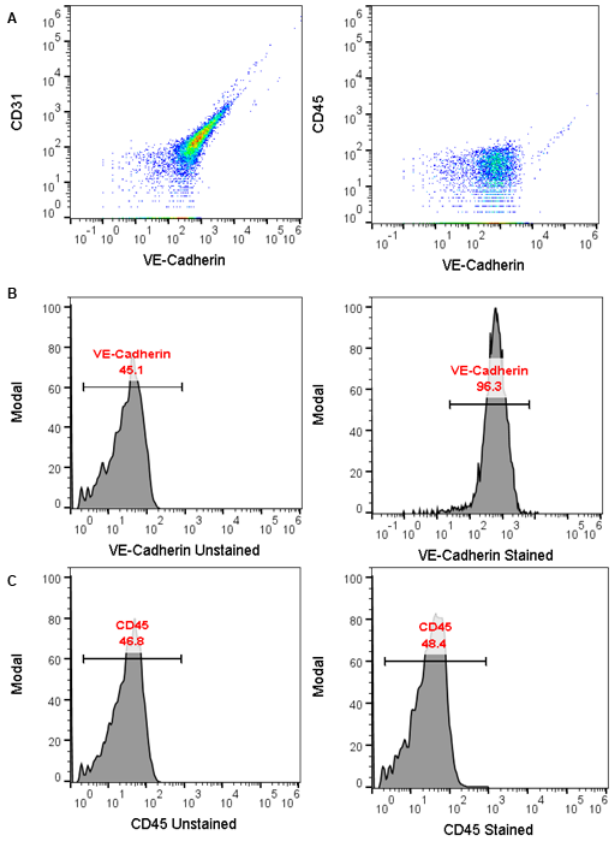

Supplementary Figure A1. 1. EC purity assessment. A) bEND.3 cells are $CD31^{+}$/VE-$Cadherin^{+}$ (left) and VE-$Cadherin^{+}$/$CD45^{-}$ (right). B) VE-Cadherin gated and positive cells for unstained control (left) and stained cells (right). C) CD45 gated and positive cells for unstained control (left) and stained cells (right). All plots were created using FlowJo.

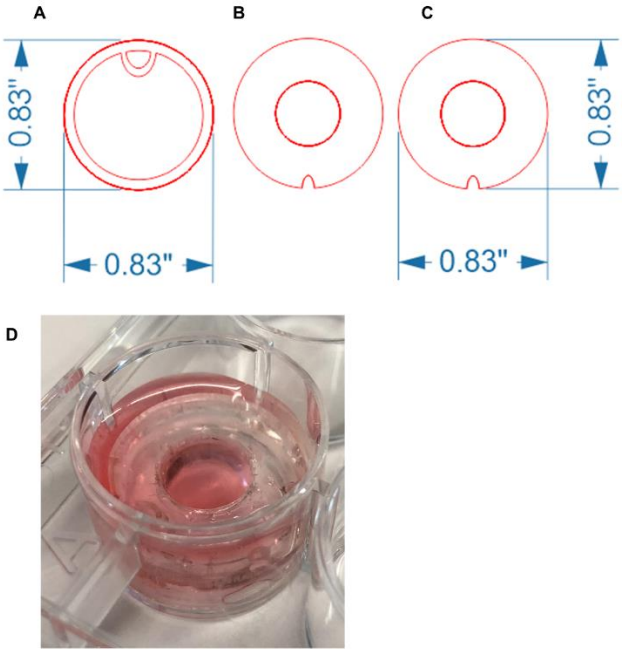

Supplementary Figure A1. 2. **3D migration experiment setup.** A) circular piece placed at the periphery of the bottom of a 12 well plate provides support for piece B) placed atop piece A, in order to elevate the hydrogel. The hydrogel is above piece B, and sandwiched by piece C, to keep the hydrogel in place. D) Assembled set up in a cell culture dish.

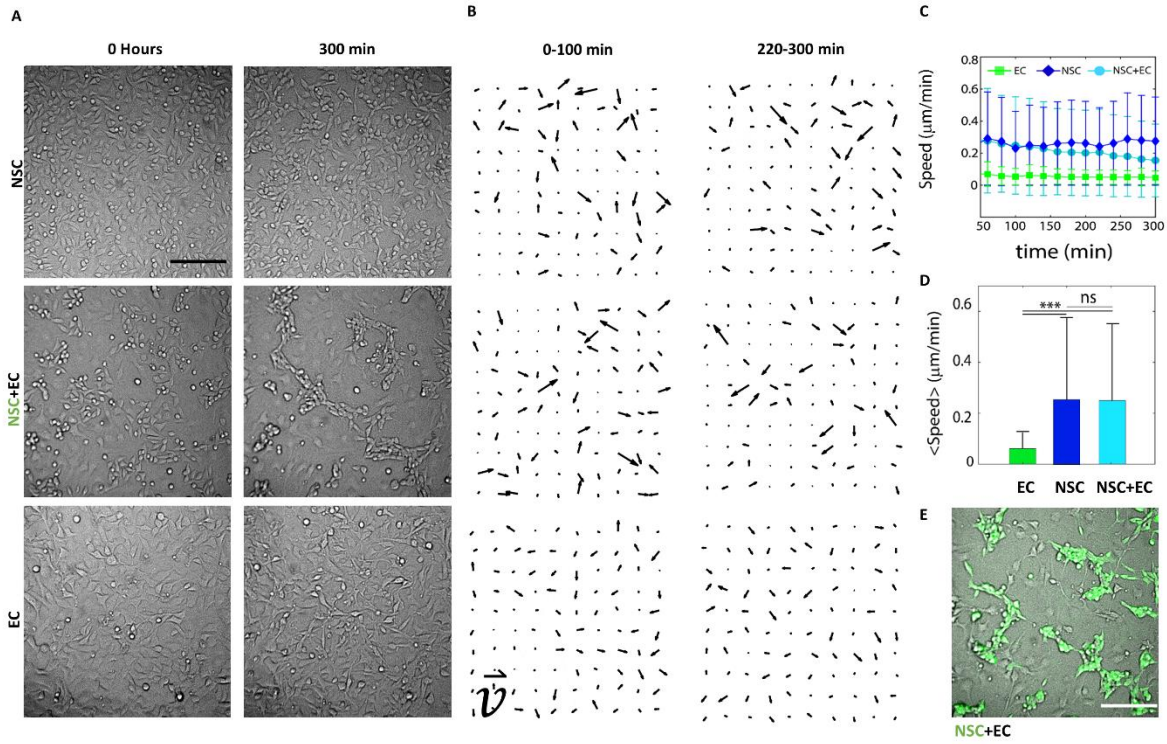

Supplementary Figure A1. 3. **EC promote NSC clustering but not speed**. A) Snapshots of time lapse images for NSC, NSC+EC, and EC cultured on glass coverslip. B) NSC cumulative displacement field. C) Instantaneous velocities variations with time. Mean is represented by dotted lines and spread is standard deviation. D) Bar plot of average speed (μm/min) for EC [16], NSC+EC (light blue) and NSC (dark blue), (error bars: +/- standard deviation). E) NSC-GFP and EC fluorescent image. Scale bar (100μm).

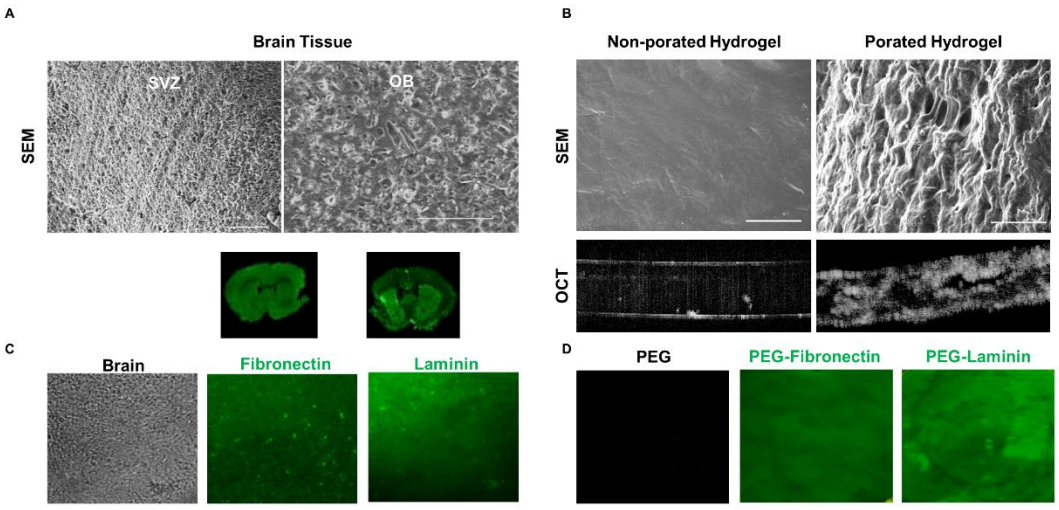

Supplementary Figure A1. 4. Templated hydrogel with bioactive protein conjugation. A) SEM images of brain tissue – subventricular zone (SVZ) and olfactory bulb (OB). B) Top: SEM images of non-porated and porated hydrogel. Bottom: Cross-section image using optical coherence tomography (OCT) of non-porated and porated hydrogel. Scale bar (50 μm) representative of all images. C) Brain slices in brightfield (left), stained against fibronectin (middle) and stained against laminin. D) PEG hydrogel with no bioactive additives stained for laminin and fibronectin (left), stained against fibronectin (middle), and stained against laminin.

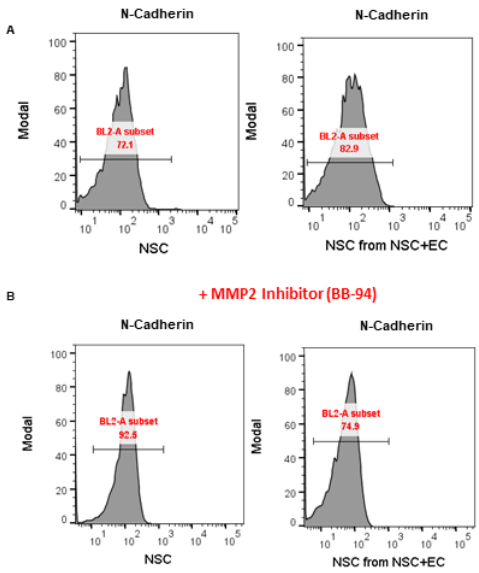

Supplementary Figure A1. 5. NSC N-cadherin expression is enhanced by EC MMP2. N-Cadherin histograms for NSC (left) and NSC from NSC+EC (right) when A) cells have access to MMP2, and B) MMP2 secretion is inhibited.

Appendix 2: Supplemental Figures from Chapter 4

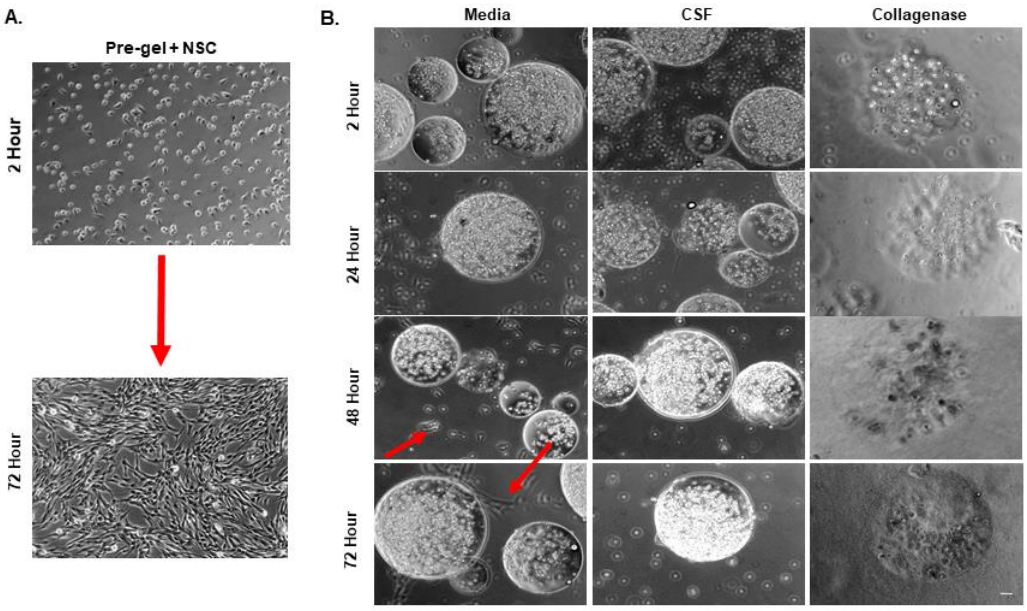

Supplementary Figure A2.1. Degradation of NSC Encapsulated Microbeads. A) As a control, NSC were plated in PEG polymer and pre-gel solution, where cells remain healthy after 72 hours. This verifies that the polymer and photocrosslinking chemicals are not toxic to the cells in culture. B) Degradable microbeads in media (first panel), CSF (second panel), and 2 mg/ml collagenase (third panel) with encapsulated NSC. Cells loosely encapsulated at the surface of microbeads adhere and elongate on the well plate as seen at 48 and 72 hours (indicated by red arrows). Microbeads swell in the nutrient rich CSF and degrade within 24 hours in the collagenase solution. Scale bar (100 µm) representative of all images.

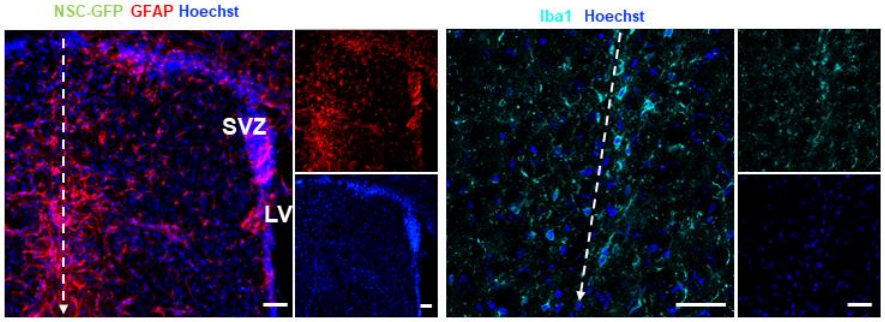

Supplementary Figure A2.2. Astrocytic and Microglial Reaction to Needle Stab. Illustrative image of astrocytic and microglial reaction to intra striatal injection. A) Astrocytes GFAP+ were visualized around the region of needle trajectory to lateral ventricle (LV) and subventricular zone (SVZ). B) A similar pattern was observed in microglial cells Iba1+ around the injection site. Scale bar (50 µm) representative of all images.

Appendix 3: Supplemental Figures from Chapter 5

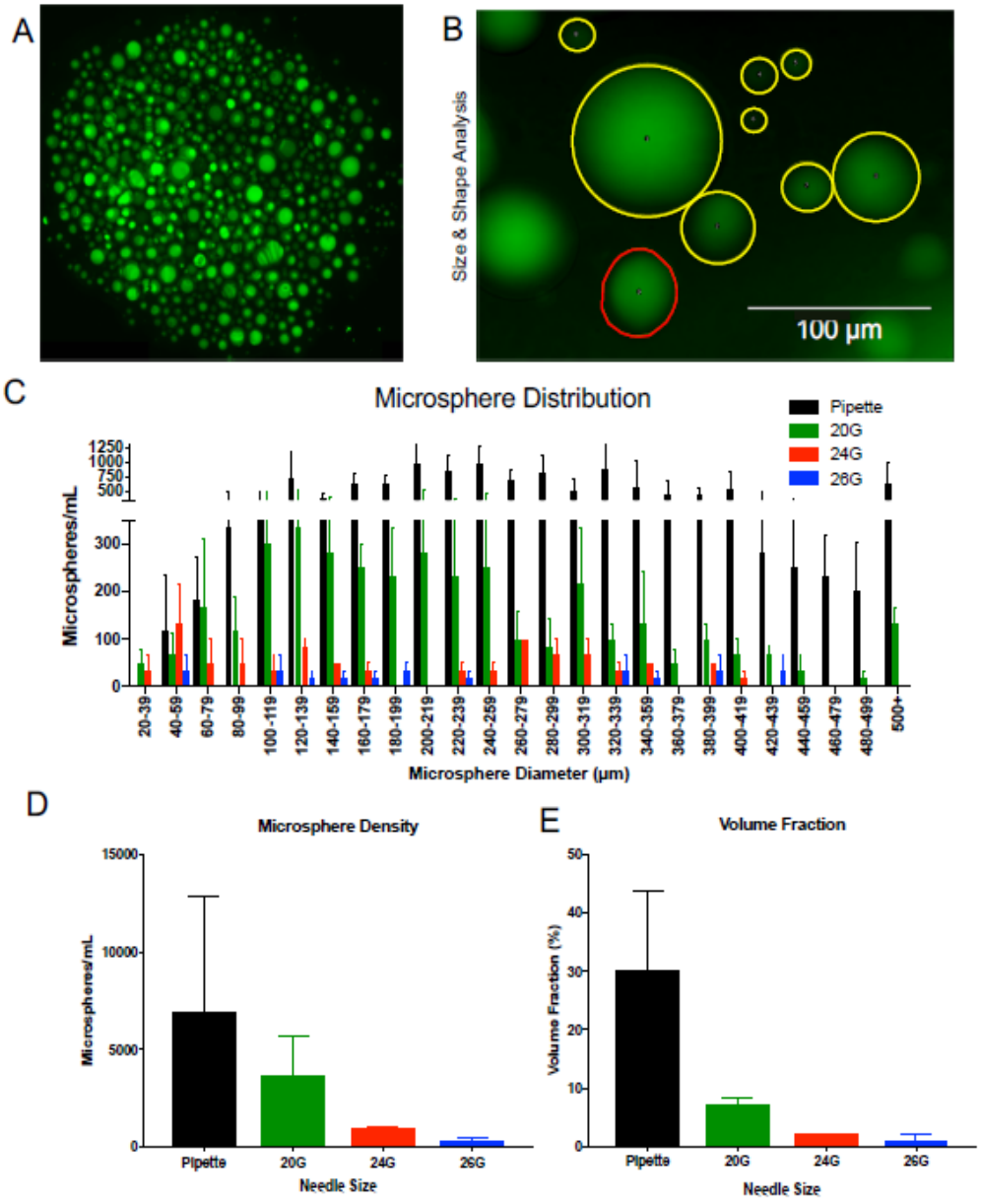

Supplementary Figure A3. 1. Impact of needle bore diameter on microsphere size distribution. A) A macroscopic view of 1 mL of microsphere on a coverslip prepared for the analysis of their size distribution. B) Quantification of microsphere size was based on delineating their circumference and measuring their diameter in the same focal plane. C) The distribution of size was highly dependent on the diameter of needle attached to a Hamilton syringe with a narrow bore size essentially eliminating large microsphere compared to a pipette with a cut off p1000 needle tip (2.5 mm diameter). D) Microsphere density (i.e., number of microspheres/ml) decreased with narrower needle bore sizes. E) This was further evident in the volume fraction (i.e., volume occupied by microspheres). On all graphs, bars represent the mean value and error bars indicate the standard deviation of the data.

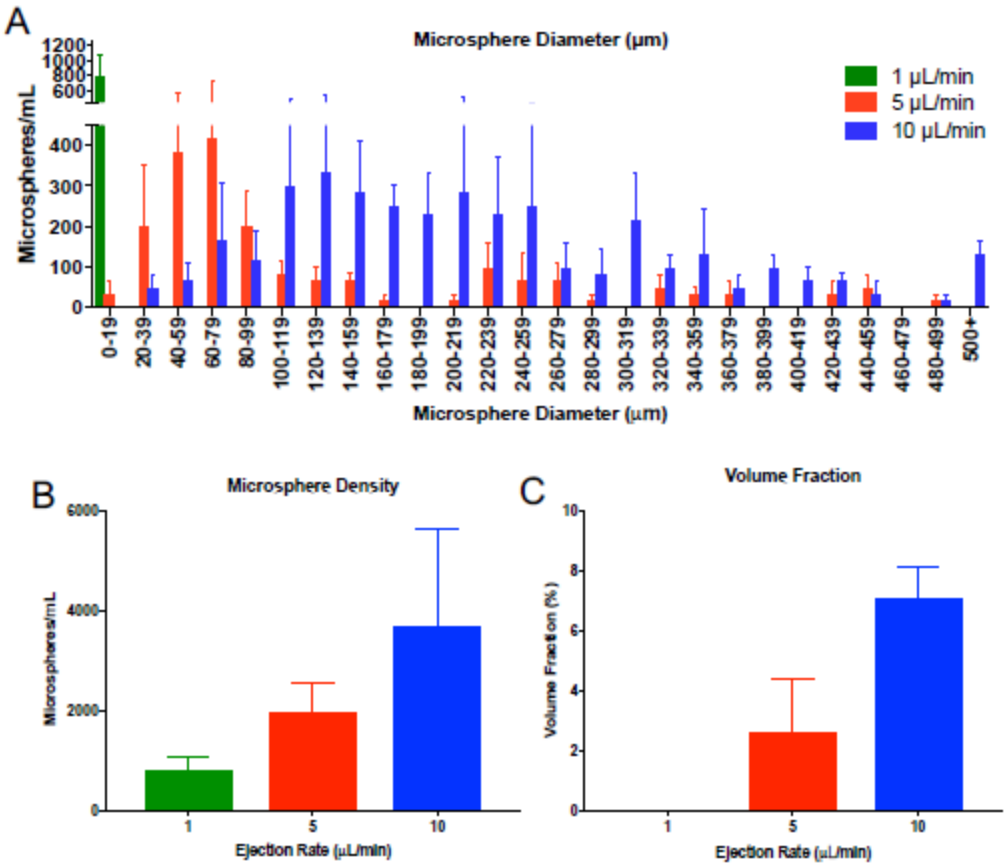

Supplementary Figure A3. 2. Impact of ejection speed on microsphere size distribution. A) Ejection speed from the Hamilton syringe influence the size distribution of microspheres, with a faster ejection resulting in larger diameters being observed with ejected microspheres. B) Microsphere density was reduced by a slower ejection rate. C) A 10 µL/min ejection rate produced the highest volume fraction of microspheres in the ejectate. On all graphs, bars represent the mean value and error bars indicate the standard deviation of the data.

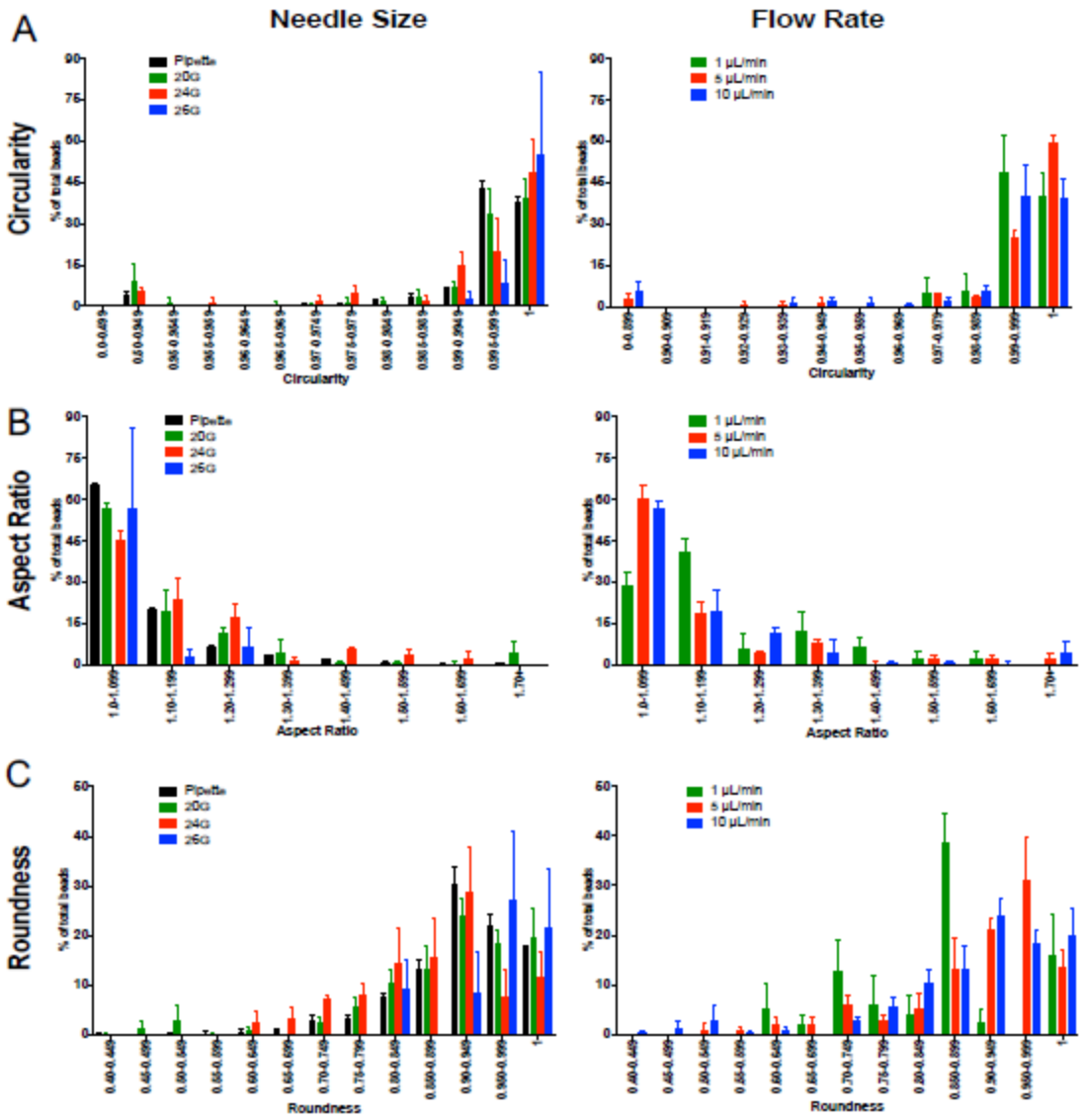

Supplementary Figure A3. 3. Impact of delivery on microsphere integrity. A) Most microspheres exhibited a high level of circularity (>0.9). B) The aspect ratio (1-1.2) was well preserved, but also revealed a gradual effect indicating that some microspheres underwent some minor deformation. C) There was a more gradual effect on roundness, which reflected the asymmetry of the microsphere (i.e., dents in the surface etc.), but still most microsphere exhibited a high level of perimeter integrity. Larger bore size and a faster ejection speed mostly affected roundedness, but this is likely also a reflection of the size distribution of microsphere that is affected by these ejection parameters. On all graphs, bars represent the mean value and error bars indicate the standard deviation of the data.

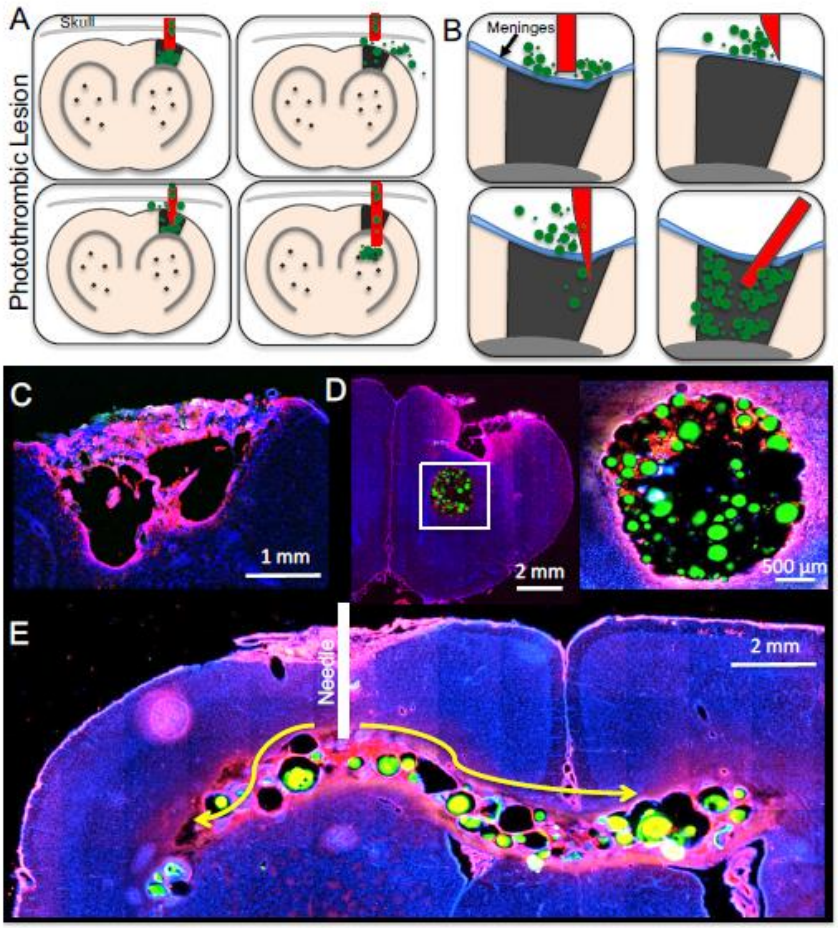

Supplementary Figure A3. 4. Microsphere delivery to a cortical tissue cavity. A) Microsphere delivery to a cortical tissue defect caused by photothrombosis. A shallow cortical lesion present considerable challenges to robustly deliver and retain microspheres. Microspheres need to sediment in the cavity and fill it up, avoiding a risk of buoyancy that could lead to microspheres displacing out of the cavity. A beveled needle carries the risk to push microsphere to one side of the cavity and hence not producing a homogenous distribution in the cavity. Placement of the needle in the cavity is also important to avoid implantation into intact tissue underneath the defect, but a too shallow position situated in the skull would also prevent filling of the cavity. B) The meninges pose a further challenge for shallow deliveries. The needle needs to pierce through, but not disrupt the meninges as otherwise immune cells can easily invade and the torn meninges will invoke a brain inflammatory response. The pia matter is needed to keep microsphere in place in the tissue cavity, rather than allow spread through the subdural space. Flat needles typically tear these layers; hence a needle prick is required to punch through without causing wide-spread tearing of these protective membranes. Beveled needles in shallow tissue defects can lead to a loss of microspheres outside the pia matter. Positioning of the needle at a shallow angle under the pia matter can produce a robust filling of the cavity without backflow into the subdural space. C) Poor delivery resulted in only a few microspheres being retained outside the tissue cavity. D) A too deep implantation delivered microsphere to intact tissue rather than the cavity, creating significant additional iatrogenic tissue damage. E) Delivery of microspheres to the corpus callosum can lead to an interhemispheric spreading along white matter.

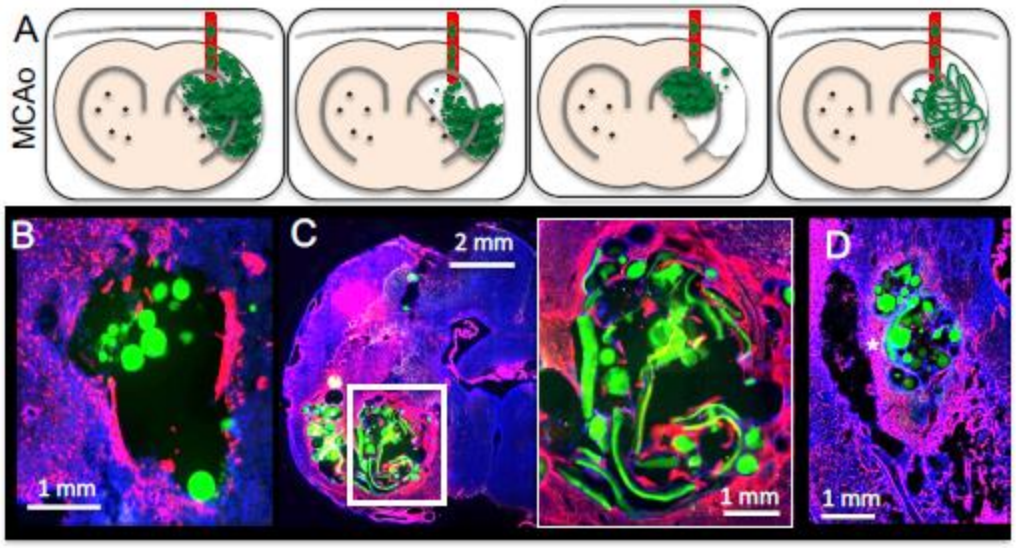

Supplementary Figure A3. 5. Microsphere delivery to a large sub-cortical and cortical tissue cavity. A) Delivery of a large volume of microsphere to a stroke cavity caused by middle cerebral artery occlusion (MCAo). Misplacement of a large volume of microsphere into intact tissue could cause major brain damage and needs to be avoided. Using an injection-drainage approach, delivery of microspheres can displace the extracellular fluid present in the tissue cavity and completely fill up this space. However, consideration needs to be given to the volume fraction that is delivered to ensure an appropriate microsphere density, avoiding buoyancy or sedimentation that could lead to sub-optimal filling of the tissue defect. A further consideration is that hydrogel-based microsphere can potentially be deformed and re-shaped during the injection process, voiding the microsphere design. B) Sub-optimal volume fraction of microsphere leaves large voids. C) Quality control of injection parameters, as well as the formation of microspheres, is essential to avoid "spaghetti-like" spindles. D) Inappropriate delivery of microspheres into intact or non-degraded damage tissue.

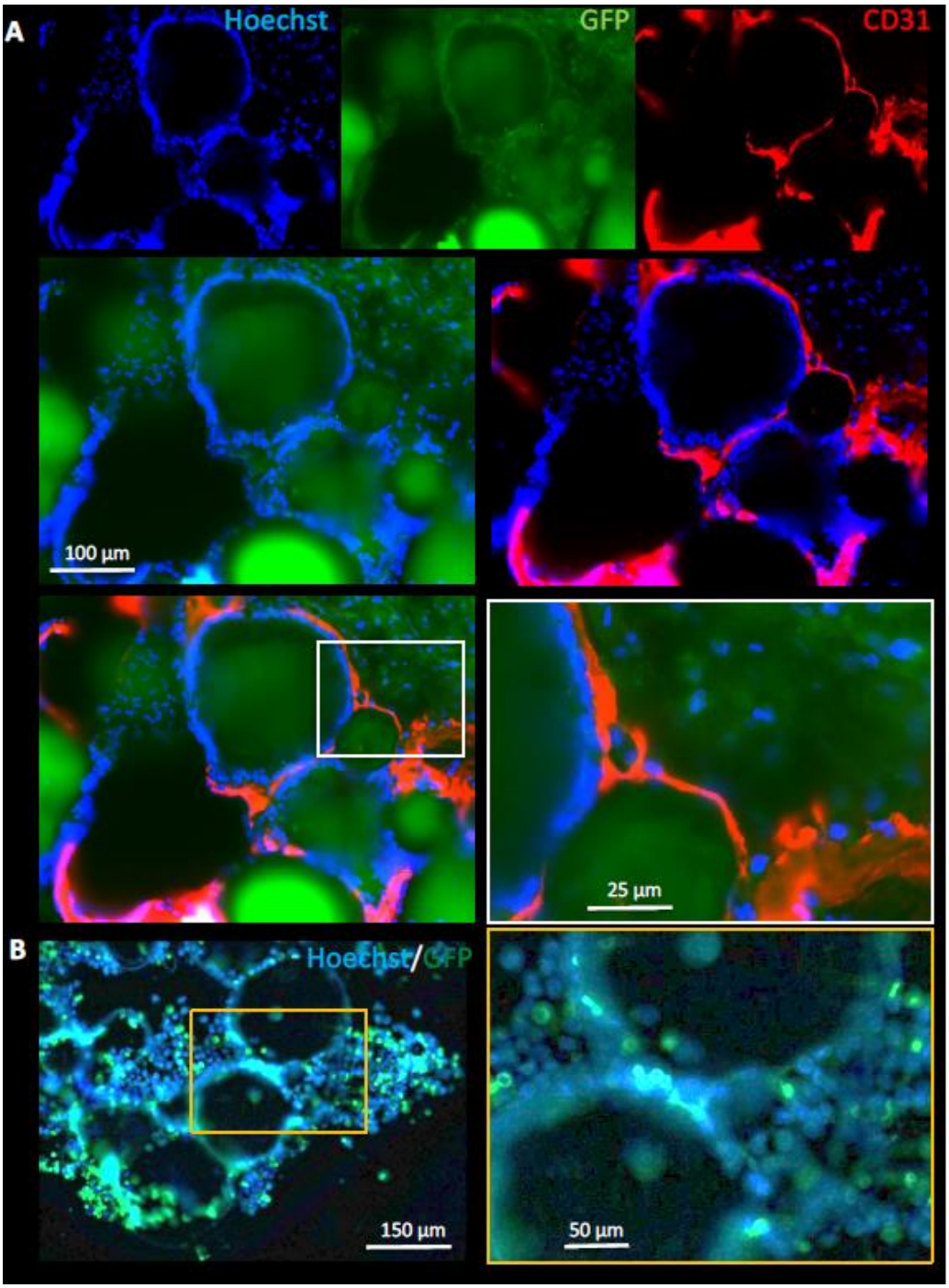

Supplementary Figure A3. 6. Cells migrate out of implanted microspheres. A) Both NSCs and ECs migrated out of the microspheres into the ECM hydrogel used for implantation. ECs showed alignment in between microspheres and highly expressed CD31. B) Cells distributed around the microspheres, with very few cells being retained inside.

Appendix 4: Supplemental Figures from Chapter 6

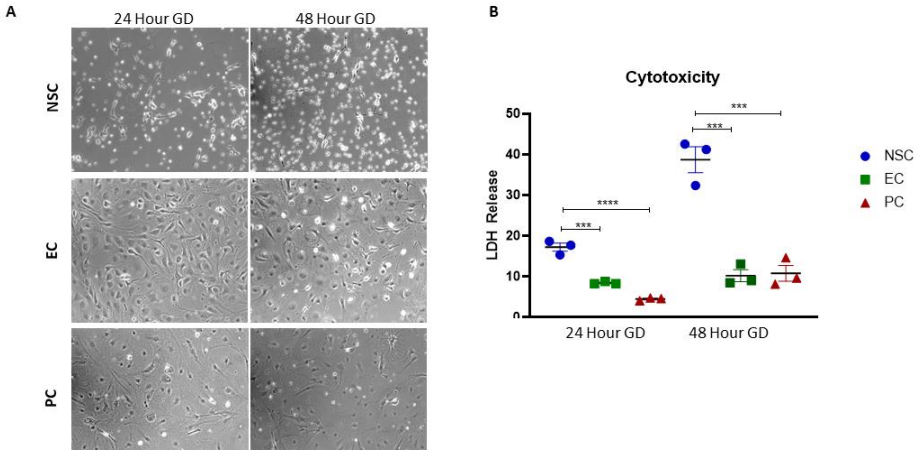

Supplementary Figure A4. 1. EC and PC remain viable during glucose deprivation. A) Brightfield images of NSC, EC and PC at 24 and 48 hours of glucose deprivation (GD). EC and PC remain adherent, unlike NSC. B) Cell cytotoxicity measured by LDH release for NSC, EC, and PC at 24 and 48 hours of GD. EC and PC have significantly less cytotoxicity compared to NSC under GD.

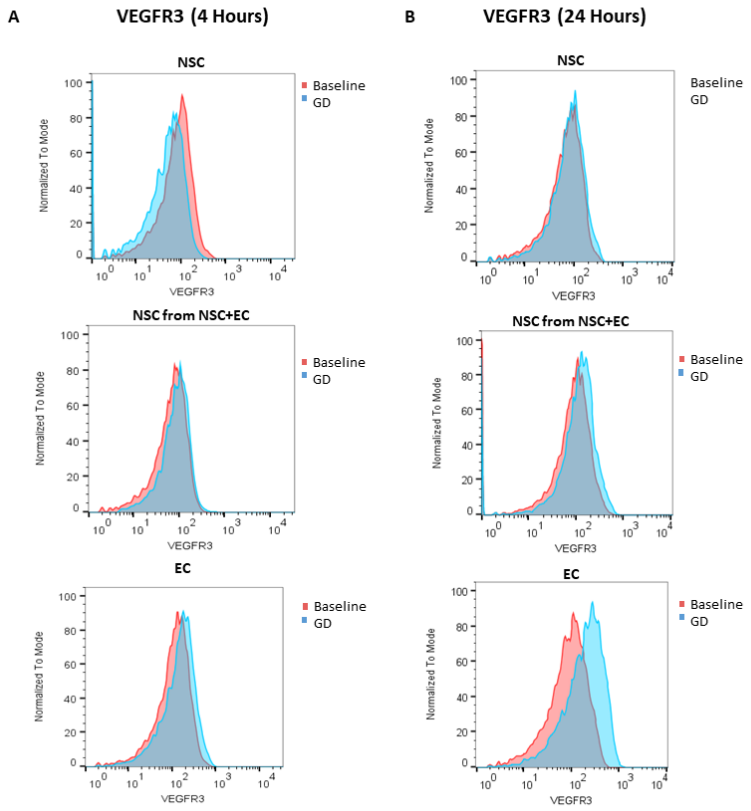

Supplementary Figure A4. 2. NSC VEGFR3 expression is increased in co-cultures of NSC+EC. A) Flow cytometry histograms for NSC, NSC from NSC+EC, and EC during baseline (red) and glucose deprivation (blue) at 4 hours and B) 24 hours.

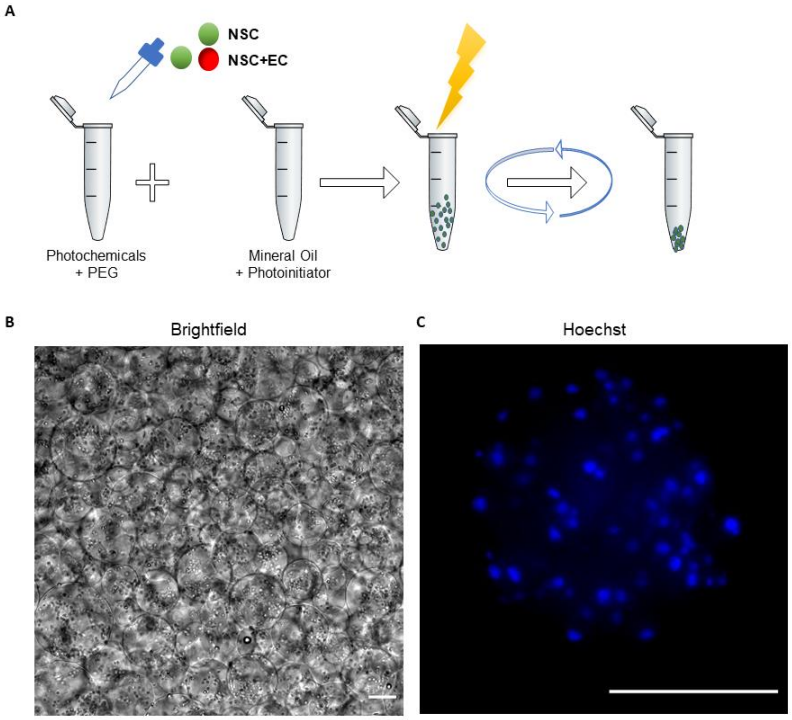

Supplementary Figure A4. 3. Creation of cell encapsulated microbeads. A) Microbeads are created by combining photochemicals and PEG, and NSC or NSC+EC. The polymer and cell phase was mixed with a mineral oil and photoinitiator phase which was vortexed and crosslinked using white light. Microbeads with encapsulated cells are then collected and removed from the mineral oil. B) Brightfield image of microbeads with encapsulated cells, C) stained with Hoechst. Scale bar (100 um) representative of all images.

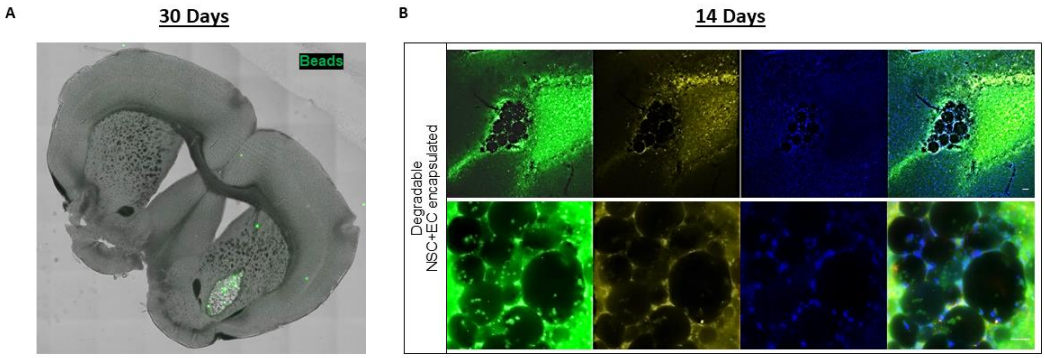

Supplementary Figure A4. 4. 30 days and 14 days post ICH are not adequate for microbead delivery. A) Whole brain section image showing GFP microbeads at 30 days post ICH. B) ICH brain sections with implanted degradable microbeads containing NSC-GFP and EC co-encapsulated, staining against NSC-GFP (green), Iba-1 (yellow) and Dapi (blue) 14 days post ICH. Scale bar (50 µm) representative of all images.

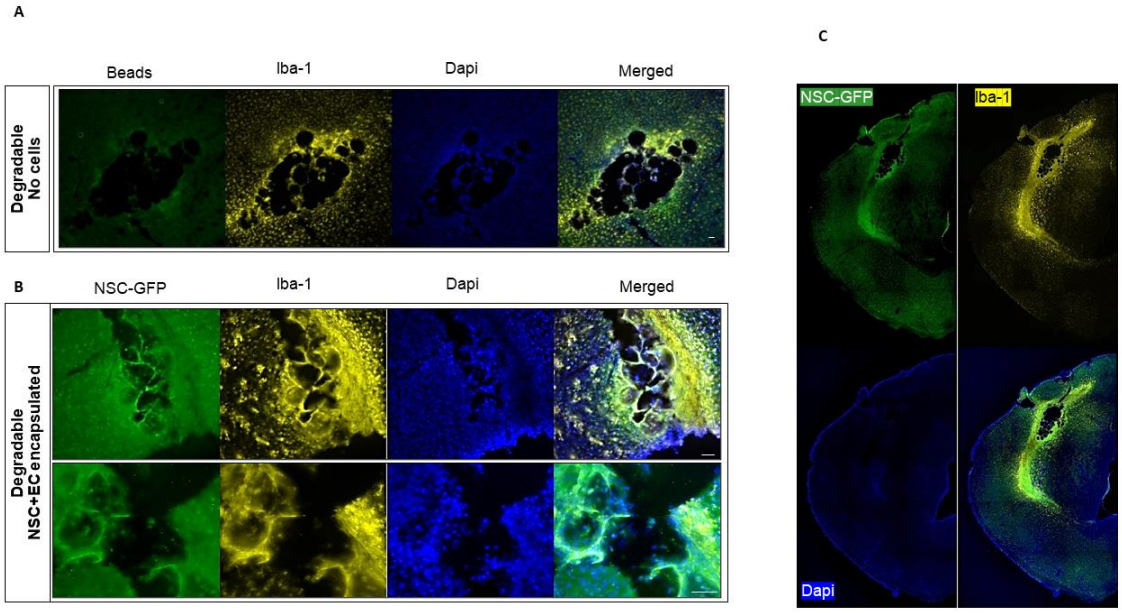

Supplementary Figure A4. 5. 7 Days post ICH is adequate for microbead delivery. A) ICH brain sections with implanted degradable GFP microbeads containing no cells, staining against beads (green), Iba-1 (yellow) and Dapi (blue) 7 days post ICH. B) ICH brain sections with implanted degradable microbeads containing NSC-GFP and EC co-encapsulated, staining against NSC-GFP (green), Iba-1 (yellow) and Dapi (blue) 7 days post ICH, with C) half-hemisphere images. Scale bar (50 µm) representative of all images.

References

1. Matta, R. and A.L. Gonzalez, *Stroke Repair via Biomimicry of the Subventricular Zone.* Frontiers in Materials, 2018. **5**(15).
2. Marlier, Q., et al., *Mechanisms and Functional Significance of Stroke-Induced Neurogenesis.* Frontiers in Neuroscience, 2015. **9**: p. 458.
3. Mozaffarian, D., et al., *Executive Summary: Heart Disease and Stroke Statistics--2016 Update: A Report From the American Heart Association.* Circulation, 2016. **133**(4): p. 447-54.
4. Boisserand, L.S.B., et al., *Biomaterial Applications in Cell-Based Therapy in Experimental Stroke.* Stem Cells International, 2016. **2016**: p. 6810562.
5. Ruan, L., et al., *Coupling of Neurogenesis and Angiogenesis After Ischemic Stroke.* Brain research, 2015. **1623**: p. 166-173.
6. Sommer, C.J., *Ischemic stroke: experimental models and reality.* Acta Neuropathologica, 2017. **133**(2): p. 245-261.
7. Nour, M., F. Scalzo, and D.S. Liebeskind, *Ischemia-Reperfusion Injury in Stroke.* Interventional Neurology, 2013. **1**(3-4): p. 185-199.
8. Alexander, L.D., et al., *Correlating lesion size and location to deficits after ischemic stroke: the influence of accounting for altered peri-necrotic tissue and incidental silent infarcts.* Behavioral and Brain Functions : BBF, 2010. **6**: p. 6-6.
9. Alvarez-Buylla, A. and J.M. García-Verdugo, *Neurogenesis in Adult Subventricular Zone.* The Journal of Neuroscience, 2002. **22**(3): p. 629-634.
10. Carmichael, S.T., *Cellular and molecular mechanisms of neural repair after stroke: making waves.* Ann Neurol, 2006. **59**(5): p. 735-42.
11. Doetsch, F., *A niche for adult neural stem cells.* Curr Opin Genet Dev, 2003. **13**(5): p. 543-50.
12. Marti, H.J.H., et al., *Hypoxia-Induced Vascular Endothelial Growth Factor Expression Precedes Neovascularization after Cerebral Ischemia.* The American Journal of Pathology. **156**(3): p. 965-976.
13. Krupinski, J., et al., *Role of angiogenesis in patients with cerebral ischemic stroke.* Stroke, 1994. **25**(9): p. 1794-8.
14. Bliss, T., et al., *Cell Transplantation Therapy for Stroke.* Stroke, 2007. **38**(2): p. 817-826.
15. Vishwakarma, S.K., et al., *Current concept in neural regeneration research: NSCs isolation, characterization and transplantation in various neurodegenerative diseases and stroke: A review.* Journal of Advanced Research, 2014. **5**(3): p. 277-294.
16. Greenberg, D.A. and K. Jin, *Growth factors and stroke.* NeuroRX, 2006. **3**(4): p. 458-465.
17. Marti, H.J.H., et al., *Hypoxia-Induced Vascular Endothelial Growth Factor Expression Precedes Neovascularization after Cerebral Ischemia.* The American Journal of Pathology, 2000. **156**(3): p. 965-976.
18. Magnon, C., D. Lucas, and P.S. Frenette, *Trafficking of Stem Cells*, in *Stem Cell Migration: Methods and Protocols*, M.-D. Filippi and H. Geiger, Editors. 2011, Humana Press: Totowa, NJ. p. 3-24.
19. Tabata, H., S. Yoshinaga, and K. Nakajima, *Cytoarchitecture of mouse and human subventricular zone in developing cerebral neocortex.* Experimental Brain Research. Experimentelle Hirnforschung. Experimentation Cerebrale, 2012. **216**(2): p. 161-168.
20. Girouard, H. and C. Iadecola, *Neurovascular coupling in the normal brain and in hypertension, stroke, and Alzheimer disease.* J Appl Physiol (1985), 2006. **100**(1): p. 328-35.

21. Goldberg, J.S. and K.K. Hirschi, *Diverse roles of the vasculature within the neural stem cell niche.* Regenerative medicine, 2009. **4**(6): p. 879-897.
22. Shen, Q., et al., *Adult SVZ Stem Cells Lie in a Vascular Niche: A Quantitative Analysis of Niche Cell-Cell Interactions.* Cell Stem Cell, 2008. **3**(3): p. 289-300.
23. Lim, D.A., et al., *Noggin antagonizes BMP signaling to create a niche for adult neurogenesis.* Neuron, 2000. **28**(3): p. 713-26.
24. Falcão, A.M., et al., *The path from the choroid plexus to the subventricular zone: go with the flow!* Frontiers in Cellular Neuroscience, 2012. **6**: p. 34.
25. Gonzalez-Cano, L., et al., *p73 is required for ependymal cell maturation and neurogenic SVZ cytoarchitecture.* Developmental Neurobiology, 2016. **76**(7): p. 730-747.
26. Stolp, H.B. and Z. Molnár, *Neurogenic niches in the brain: help and hindrance of the barrier systems.* Frontiers in Neuroscience, 2015. **9**: p. 20.
27. Lacar, B., et al., *Neural progenitor cells regulate capillary blood flow in the postnatal subventricular zone.* The Journal of neuroscience : the official journal of the Society for Neuroscience, 2012. **32**(46): p. 16435-16448.
28. Lindvall, O. and Z. Kokaia, *Stem cells in human neurodegenerative disorders — time for clinical translation?* The Journal of Clinical Investigation, 2010. **120**(1): p. 29-40.
29. Ottone, C., et al., *Direct cell-cell contact with the vascular niche maintains quiescent neural stem cells.* Nature cell biology, 2014. **16**(11): p. 1045-1056.
30. Kriegstein, A. and A. Alvarez-Buylla, *The Glial Nature of Embryonic and Adult Neural Stem Cells.* Annual review of neuroscience, 2009. **32**: p. 149-184.
31. Gage, F.H., *Mammalian Neural Stem Cells.* Science, 2000. **287**(5457): p. 1433-1438.
32. Hermann, A., M. Maisel, and A. Storch, *Epigenetic conversion of human adult bone mesodermal stromal cells into neuroectodermal cell types for replacement therapy of neurodegenerative disorders.* Expert Opinion on Biological Therapy, 2006. **6**(7): p. 653-670.
33. Imayoshi, I., et al., *Essential Roles of Notch Signaling in Maintenance of Neural Stem Cells in Developing and Adult Brains.* The Journal of Neuroscience, 2010. **30**(9): p. 3489-3498.
34. Nomura, T., et al., *EphB Signaling Controls Lineage Plasticity of Adult Neural Stem Cell Niche Cells.* Cell Stem Cell, 2010. **7**(6): p. 730-743.
35. Fanning, A.S., et al., *The Tight Junction Protein ZO-1 Establishes a Link between the Transmembrane Protein Occludin and the Actin Cytoskeleton.* Journal of Biological Chemistry, 1998. **273**(45): p. 29745-29753.
36. Brown, R.C., A.P. Morris, and R.G. O'Neil, *TIGHT JUNCTION PROTEIN EXPRESSION AND BARRIER PROPERTIES OF IMMORTALIZED MOUSE BRAIN MICROVESSEL ENDOTHELIAL CELLS.* Brain research, 2007. **1130**(1): p. 17-30.
37. Korn, J., B. Christ, and H. Kurz, *Neuroectodermal origin of brain pericytes and vascular smooth muscle cells.* J Comp Neurol, 2002. **442**(1): p. 78-88.
38. Geevarghese, A. and I.M. Herman, *Pericyte-Endothelial Cross-Talk: Implications and Opportunities for Advanced Cellular Therapies.* Translational research : the journal of laboratory and clinical medicine, 2014. **163**(4): p. 296-306.
39. Armulik, A., G. Genové, and C. Betsholtz, *Pericytes: Developmental, Physiological, and Pathological Perspectives, Problems, and Promises.* Developmental Cell, 2011. **21**(2): p. 193-215.
40. Daneman, R., et al., *Pericytes are required for blood-brain barrier integrity during embryogenesis.* Nature, 2010. **468**(7323): p. 562-6.
41. Rustenhoven, J., et al., *TGF-beta1 regulates human brain pericyte inflammatory processes involved in neurovasculature function.* Journal of Neuroinflammation, 2016. **13**(1): p. 37.

42. Dohgu, S., et al., *Brain pericytes contribute to the induction and up-regulation of blood-brain barrier functions through transforming growth factor-beta production.* Brain Res, 2005. **1038**(2): p. 208-15.
43. Weinstein, J.R., I.P. Koerner, and T. Möller, *Microglia in ischemic brain injury.* Future neurology, 2010. **5**(2): p. 227-246.
44. Ghuman, H. and M. Modo, *Biomaterial applications in neural therapy and repair.* Chinese Neurosurgical Journal, 2016. **2**(1): p. 34.
45. Patel, A.R., et al., *Microglia and ischemic stroke: a double-edged sword.* International journal of physiology, pathophysiology and pharmacology, 2013. **5**(2): p. 73-90.
46. Lalancette-Hebert, M., et al., *Selective ablation of proliferating microglial cells exacerbates ischemic injury in the brain.* J Neurosci, 2007. **27**(10): p. 2596-605.
47. Lambertsen, K.L., et al., *A quantitative study of microglial-macrophage synthesis of tumor necrosis factor during acute and late focal cerebral ischemia in mice.* J Cereb Blood Flow Metab, 2005. **25**(1): p. 119-35.
48. Barone, F.C., et al., *Tumor necrosis factor-alpha. A mediator of focal ischemic brain injury.* Stroke, 1997. **28**(6): p. 1233-44.
49. Denes, A., et al., *Proliferating resident microglia after focal cerebral ischaemia in mice.* J Cereb Blood Flow Metab, 2007. **27**(12): p. 1941-53.
50. Sobel, R.A., *The extracellular matrix in multiple sclerosis lesions.* J Neuropathol Exp Neurol, 1998. **57**(3): p. 205-17.
51. Bikbaev, A., R. Frischknecht, and M. Heine, *Brain extracellular matrix retains connectivity in neuronal networks.* 2015. **5**: p. 14527.
52. Baeten, K.M. and K. Akassoglou, *Extracellular Matrix and Matrix Receptors in Blood-Brain Barrier Formation and Stroke.* Developmental neurobiology, 2011. **71**(11): p. 1018-1039.
53. Delcroix, G.J.R., et al., *Adult cell therapy for brain neuronal damages and the role of tissue engineering.* Biomaterials, 2010. **31**(8): p. 2105-2120.
54. Bosman, F.T. and I. Stamenkovic, *Functional structure and composition of the extracellular matrix.* The Journal of Pathology, 2003. **200**(4): p. 423-428.
55. Marthiens, V., et al., *Adhesion molecules in the stem cell niche – more than just staying in shape?* Journal of Cell Science, 2010. **123**(10): p. 1613-1622.
56. Karpowicz, P., et al., *E-Cadherin Regulates Neural Stem Cell Self-Renewal.* The Journal of Neuroscience, 2009. **29**(12): p. 3885-3896.
57. Chen, S., M. Lewallen, and T. Xie, *Adhesion in the stem cell niche: biological roles and regulation.* Development (Cambridge, England), 2013. **140**(2): p. 255-265.
58. Gattazzo, F., A. Urciuolo, and P. Bonaldo, *Extracellular matrix: A dynamic microenvironment for stem cell niche().* Biochimica et Biophysica Acta, 2014. **1840**(8): p. 2506-2519.
59. Lemons, M.L. and M.L. Condic, *Integrin signaling is integral to regeneration.* Experimental Neurology, 2008. **209**(2): p. 343-352.
60. Qian, L. and W.M. Saltzman, *Improving the expansion and neuronal differentiation of mesenchymal stem cells through culture surface modification.* Biomaterials, 2004. **25**(7–8): p. 1331-1337.
61. Salinas, C.N. and K.S. Anseth, *The influence of the RGD peptide motif and its contextual presentation in PEG gels on human mesenchymal stem cell viability.* J Tissue Eng Regen Med, 2008. **2**(5): p. 296-304.
62. Karoubi, G., et al., *Single-cell hydrogel encapsulation for enhanced survival of human marrow stromal cells.* Biomaterials, 2009. **30**(29): p. 5445-55.
63. Romanic, A.M., et al., *Matrix metalloproteinase expression increases after cerebral focal ischemia in rats: inhibition of matrix metalloproteinase-9 reduces infarct size.* Stroke, 1998. **29**(5): p. 1020-30.

64. Kalladka, D. and K.W. Muir, *Brain repair: cell therapy in stroke.* Stem Cells Cloning, 2014. **7**: p. 31-44.
65. Yang, B., et al., *Intra-arterial Delivery is not Superior to Intravenous Delivery of Autologous Bone Marrow Mononuclear Cells in Acute Ischemic Stroke.* Stroke; a journal of cerebral circulation, 2013. **44**(12): p. 3463-3472.
66. Kim, S.U., *Human neural stem cells genetically modified for brain repair in neurological disorders.* Neuropathology, 2004. **24**(3): p. 159-71.
67. Duncan, K., et al., *Stem cell-paved biobridges facilitate stem transplant and host brain cell interactions for stroke therapy.* Brain Res, 2015. **1623**: p. 160-5.
68. Ishibashi, S., et al., *Human neural stem/progenitor cells, expanded in long-term neurosphere culture, promote functional recovery after focal ischemia in Mongolian gerbils.* J Neurosci Res, 2004. **78**(2): p. 215-23.
69. Lindvall, O. and Z. Kokaia, *Stem cells in human neurodegenerative disorders — time for clinical translation?* The Journal of Clinical Investigation. **120**(1): p. 29-40.
70. Zhang, M., et al., *Cardiomyocyte grafting for cardiac repair: graft cell death and anti-death strategies.* J Mol Cell Cardiol, 2001. **33**(5): p. 907-21.
71. Aguado, B.A., et al., *Improving viability of stem cells during syringe needle flow through the design of hydrogel cell carriers.* Tissue engineering. Part A, 2012. **18**(7-8): p. 806-815.
72. Potts, M.B., M.T. Silvestrini, and D.A. Lim, *Devices for cell transplantation into the central nervous system: Design considerations and emerging technologies.* Surgical Neurology International, 2013. **4**(Suppl 1): p. S22-S30.
73. Banerjee, A., et al., *The influence of hydrogel modulus on the proliferation and differentiation of encapsulated neural stem cells.* Biomaterials, 2009. **30**(27): p. 4695-4699.
74. Ghuman, H., et al., *ECM hydrogel for the treatment of stroke: Characterization of the host cell infiltrate.* Biomaterials, 2016. **91**: p. 166-181.
75. Franco, C.L., J. Price, and J.L. West, *Development and optimization of a dual-photoinitiator, emulsion-based technique for rapid generation of cell-laden hydrogel microspheres.* Acta Biomater, 2011. **7**(9): p. 3267-76.
76. Nakaguchi, K., et al., *Growth Factors Released from Gelatin Hydrogel Microspheres Increase New Neurons in the Adult Mouse Brain.* Stem Cells International, 2012. **2012**: p. 7.
77. Struzyna, L.A., K. Katiyar, and D.K. Cullen, *Living scaffolds for neuroregeneration.* Current Opinion in Solid State and Materials Science, 2014. **18**(6): p. 308-318.
78. Nur, E.K.A., et al., *Covalently attached FGF-2 to three-dimensional polyamide nanofibrillar surfaces demonstrates enhanced biological stability and activity.* Mol Cell Biochem, 2008. **309**(1-2): p. 157-66.
79. Fan, V.H., et al., *Tethered epidermal growth factor provides a survival advantage to mesenchymal stem cells.* Stem Cells, 2007. **25**(5): p. 1241-51.
80. Leipzig, N.D. and M.S. Shoichet, *The effect of substrate stiffness on adult neural stem cell behavior.* Biomaterials, 2009. **30**(36): p. 6867-78.
81. Parlato, M., et al., *Poly(ethylene glycol) Hydrogels with Adaptable Mechanical and Degradation Properties for Use in Biomedical Applications().* Macromolecular bioscience, 2014. **14**(5): p. 687-698.
82. Gonzalez, A.L., et al., *Integrin interactions with immobilized peptides in polyethylene glycol diacrylate hydrogels.* Tissue Eng, 2004. **10**(11-12): p. 1775-86.
83. Roudsari, L.C., et al., *A 3D Poly(ethylene glycol)-based Tumor Angiogenesis Model to Study the Influence of Vascular Cells on Lung Tumor Cell Behavior.* Sci Rep, 2016. **6**: p. 32726.

84. Bjugstad, K.B., et al., *Biocompatibility of poly(ethylene glycol)-based hydrogels in the brain: an analysis of the glial response across space and time.* J Biomed Mater Res A, 2010. **95**(1): p. 79-91.
85. Lampe, K.J., K.B. Bjugstad, and M.J. Mahoney, *Impact of Degradable Macromer Content in a Poly(Ethylene Glycol) Hydrogel on Neural Cell Metabolic Activity, Redox State, Proliferation, and Differentiation.* Tissue Engineering. Part A, 2010. **16**(6): p. 1857-1866.
86. Cooke, M.J., et al., *Controlled epi-cortical delivery of epidermal growth factor for the stimulation of endogenous neural stem cell proliferation in stroke-injured brain.* Biomaterials, 2011. **32**(24): p. 5688-5697.
87. Karakatsani, A., B. Shah, and C. Ruiz de Almodovar, *Blood Vessels as Regulators of Neural Stem Cell Properties.* Frontiers in Molecular Neuroscience, 2019. **12**(85).
88. Girouard, H. and C. Iadecola, *Neurovascular coupling in the normal brain and in hypertension, stroke, and Alzheimer disease.* Journal of Applied Physiology, 2006. **100**(1): p. 328-335.
89. Carmichael, S.T., *Cellular and molecular mechanisms of neural repair after stroke: Making waves.* Annals of Neurology, 2006. **59**(5): p. 735-742.
90. De Filippis, L. and D. Delia, *Hypoxia in the regulation of neural stem cells.* Cell Mol Life Sci, 2011. **68**(17): p. 2831-44.
91. Bürgers, H.F., et al., *Acute anoxia stimulates proliferation in adult neural stem cells from the rat brain.* Experimental Brain Research, 2008. **188**(1): p. 33-43.
92. Singh, G., et al., *Oxygen glucose deprivation model of cerebral stroke in PC-12 cells: glucose as a limiting factor.* Toxicol Mech Methods, 2009. **19**(2): p. 154-60.
93. Wohnsland, S., et al., *Neurons and neuronal stem cells survive in glucose-free lactate and in high glucose cell culture medium during normoxia and anoxia.* Neurochem Res, 2010. **35**(10): p. 1635-42.
94. Klingener, M., et al., *N-cadherin promotes recruitment and migration of neural progenitor cells from the SVZ neural stem cell niche into demyelinated lesions.* J Neurosci, 2014. **34**(29): p. 9590-606.
95. Matta, R., et al., *Endothelial cell secreted metalloproteinase-2 enhances neural stem cell N-cadherin expression, clustering, and migration.* The FASEB Journal, 2021. **35**(2): p. e21311.
96. Felling, R.J., et al., *Neural stem/progenitor cells participate in the regenerative response to perinatal hypoxia/ischemia.* J Neurosci, 2006. **26**(16): p. 4359-69.
97. Imitola, J., et al., *Directed migration of neural stem cells to sites of CNS injury by the stromal cell-derived factor 1alpha/CXC chemokine receptor 4 pathway.* Proc Natl Acad Sci U S A, 2004. **101**(52): p. 18117-22.
98. Miragall, F., et al., *Expression of the gap junction protein connexin43 in the subependymal layer and the rostral migratory stream of the mouse: evidence for an inverse correlation between intensity of connexin43 expression and cell proliferation activity.* Cell and Tissue Research, 1997. **287**(2): p. 243-253.
99. Marins, M., et al., *Gap junctions are involved in cell migration in the early postnatal subventricular zone.* Dev Neurobiol, 2009. **69**(11): p. 715-30.
100. Wang, C., et al., *Identification and characterization of neuroblasts in the subventricular zone and rostral migratory stream of the adult human brain.* Cell Research, 2011. **21**(11): p. 1534-1550.
101. Yang, H.K., et al., *Distribution of doublecortin expressing cells near the lateral ventricles in the adult mouse brain.* J Neurosci Res, 2004. **76**(3): p. 282-95.
102. Herman, I.M., et al., *Characterization of microvascular cell cultures from normotensive and hypertensive rat brains: Pericyte—endothelial cell interactions in vitro.* Tissue and Cell, 1987. **19**(2): p. 197-206.

103. Shen, Q., et al., *Endothelial Cells Stimulate Self-Renewal and Expand Neurogenesis of Neural Stem Cells.* Science, 2004. **304**(5675): p. 1338-1340.
104. Azevedo, P.O., et al., *Endothelial cells maintain neural stem cells quiescent in their niche.* Neuroscience, 2017. **363**: p. 62-65.
105. Matta, R., et al., *Minimally Invasive Delivery of Microbeads with Encapsulated, Viable and Quiescent Neural Stem Cells to the Adult Subventricular Zone.* Scientific Reports, 2019. **9**(1): p. 17798.
106. Wittko, I.M., et al., *VEGFR-1 regulates adult olfactory bulb neurogenesis and migration of neural progenitors in the rostral migratory stream in vivo.* J Neurosci, 2009. **29**(27): p. 8704-14.
107. Zhang , H., et al., *VEGF is a chemoattractant for FGF-2–stimulated neural progenitors.* Journal of Cell Biology, 2003. **163**(6): p. 1375-1384.
108. Zhang, P.Z., et al., *Up-regulation of stromal cell-derived factor-1 enhances migration of transplanted neural stem cells to injury region following degeneration of spiral ganglion neurons in the adult rat inner ear.* Neurosci Lett, 2013. **534**: p. 101-6.
109. Borrell, V. and O. Marín, *Meninges control tangential migration of hem-derived Cajal-Retzius cells via CXCL12/CXCR4 signaling.* Nat Neurosci, 2006. **9**(10): p. 1284-93.
110. Reiss, K., et al., *ADAM10 cleavage of N-cadherin and regulation of cell-cell adhesion and beta-catenin nuclear signalling.* The EMBO journal, 2005. **24**(4): p. 742-752.
111. Prado, A.F., et al., *Matrix metalloproteinase-2-induced epidermal growth factor receptor transactivation impairs redox balance in vascular smooth muscle cells and facilitates vascular contraction.* Redox Biol, 2018. **18**: p. 181-190.
112. Fang, T.-H. and W.-J. Chang, *Nanoindentation characteristics on polycarbonate polymer film.* Microelectronics Journal, 2004. **35**(7): p. 595-599.
113. Budday, S., et al., *Mechanical properties of gray and white matter brain tissue by indentation.* Journal of the Mechanical Behavior of Biomedical Materials, 2015. **46**: p. 318-330.
114. Bressan, R.B., et al., *Efficient CRISPR/Cas9-assisted gene targeting enables rapid and precise genetic manipulation of mammalian neural stem cells.* Development, 2017. **144**(4): p. 635-648.
115. Taraboletti, G., et al., *Shedding of the matrix metalloproteinases MMP-2, MMP-9, and MT1-MMP as membrane vesicle-associated components by endothelial cells.* The American journal of pathology, 2002. **160**(2): p. 673-680.
116. Sabass, B., et al., *High resolution traction force microscopy based on experimental and computational advances.* Biophysical Journal, 2008. **94**(1): p. 207-220.
117. McBride, R., J. Kelly, and D. McCormack, *Growth of well-defined ZnO microparticles by hydroxide ion hydrolysis of zinc saltsElectronic supplementary information (ESI) available: SEM images of initial precipitate and of particles formed by Method A. See* http://www.rsc.org/suppdata/jm/b2/b211723c. Journal of Materials Chemistry - J MATER CHEM, 2003. **13**: p. 1196-1201.
118. Pellowe, A.S., et al., *Ultrathin Porated Elastic Hydrogels As a Biomimetic Basement Membrane for Dual Cell Culture.* J Vis Exp, 2017(130).
119. Lauridsen, H.M., B.J. Walker, and A.L. Gonzalez, *Chemically- and mechanically-tunable porated polyethylene glycol gels for leukocyte integrin independent and dependent chemotaxis.* TECHNOLOGY, 2014. **02**(02): p. 133-143.
120. Lauridsen, H.M. and A.L. Gonzalez, *Biomimetic, ultrathin and elastic hydrogels regulate human neutrophil extravasation across endothelial-pericyte bilayers.* PLoS One, 2017. **12**(2): p. e0171386.
121. Prontera, C., et al., *Inhibition of gelatinase A (MMP-2) by batimastat and captopril reduces tumor growth and lung metastases in mice bearing Lewis lung carcinoma.* Int J Cancer, 1999. **81**(5): p. 761-6.

122. Corbel, M., et al., *Inhibition of bleomycin-induced pulmonary fibrosis in mice by the matrix metalloproteinase inhibitor batimastat.* J Pathol, 2001. **193**(4): p. 538-45.
123. Rammensee, S., et al., *Dynamics of Mechanosensitive Neural Stem Cell Differentiation.* Stem Cells, 2017. **35**(2): p. 497-506.
124. Auler, M., et al., *Mimicking Angiogenesis in vitro: Three-dimensional Co-culture of Vascular Endothelial Cells and Perivascular Cells in Collagen Type I Gels.* Bio-protocol, 2017. **7**(8): p. e2247.
125. Gefen, A. and S.S. Margulies, *Are in vivo and in situ brain tissues mechanically similar?* J Biomech, 2004. **37**(9): p. 1339-52.
126. Taylor, Z. and K. Miller, *Reassessment of brain elasticity for analysis of biomechanisms of hydrocephalus.* J Biomech, 2004. **37**(8): p. 1263-9.
127. *Effects of Biologic Scaffolds on Human Stem Cells and Implications for CNS Tissue Engineering.* Tissue Engineering Part A, 2014. **20**(1-2): p. 313-323.
128. Shin, Y., et al., *Reconstituting Vascular Microenvironment of Neural Stem Cell Niche in Three-Dimensional Extracellular Matrix.* Advanced Healthcare Materials, 2014. **3**(9): p. 1457-1464.
129. Ghuman, H., et al., *Long-term retention of ECM hydrogel after implantation into a sub-acute stroke cavity reduces lesion volume.* Acta Biomaterialia, 2017. **63**: p. 50-63.
130. Her, G.J., et al., *Control of three-dimensional substrate stiffness to manipulate mesenchymal stem cell fate toward neuronal or glial lineages.* Acta Biomaterialia, 2013. **9**(2): p. 5170-5180.
131. Thomas, R.C., et al., *Sacrificial Crystal Templated Hyaluronic Acid Hydrogels As Biomimetic 3D Tissue Scaffolds for Nerve Tissue Regeneration.* ACS Biomaterials Science & Engineering, 2017. **3**(7): p. 1451-1459.
132. Conant, K., et al., *Matrix metalloproteinase activity stimulates N-cadherin shedding and the soluble N-cadherin ectodomain promotes classical microglial activation.* Journal of Neuroinflammation, 2017. **14**(1): p. 56.
133. LV, D.E.O.R., et al., *Glioblastoma Factors Increase the Migration of Human Brain Endothelial Cells In Vitro by Increasing MMP-9/CXCR4 Levels.* Anticancer Res, 2020. **40**(5): p. 2725-2737.
134. Leroux, A., et al., *Sensory neurons from dorsal root ganglia regulate endothelial cell function in extracellular matrix remodelling.* Cell Communication and Signaling, 2020. **18**(1): p. 162.
135. Wang, L., et al., *Matrix metalloproteinase 2 (MMP2) and MMP9 secreted by erythropoietin-activated endothelial cells promote neural progenitor cell migration.* J Neurosci, 2006. **26**(22): p. 5996-6003.
136. Tavazoie, M., et al., *A specialized vascular niche for adult neural stem cells.* Cell Stem Cell, 2008. **3**(3): p. 279-88.
137. Ottone, C. and S. Parrinello, *Multifaceted control of adult SVZ neurogenesis by the vascular niche.* Cell Cycle, 2015. **14**(14): p. 2222-2225.
138. Genet, N., et al., *Multifaceted Roles of Connexin 43 in Stem Cell Niches.* Current Stem Cell Reports, 2018. **4**(1): p. 1-12.
139. Nakagomi, N., et al., *Endothelial cells support survival, proliferation, and neuronal differentiation of transplanted adult ischemia-induced neural stem/progenitor cells after cerebral infarction.* Stem Cells, 2009. **27**(9): p. 2185-95.
140. Matta, R. and A.L. Gonzalez, *Engineered Biomimetic Neural Stem Cell Niche.* Current Stem Cell Reports, 2019.
141. Marquardt, L.M. and S.C. Heilshorn, *Design of Injectable Materials to Improve Stem Cell Transplantation.* Current Stem Cell Reports, 2016. **2**(3): p. 207-220.

142. Zhong, J., et al., *Hydrogel Matrix to Support Stem Cell Survival After Brain Transplantation in Stroke.* Neurorehabilitation and Neural Repair, 2010. **24**(7): p. 636-644.
143. Nicodemus, G.D. and S.J. Bryant, *Cell Encapsulation in Biodegradable Hydrogels for Tissue Engineering Applications.* Tissue Engineering Part B: Reviews, 2008. **14**(2): p. 149-165.
144. V., S.B., et al., *Hydrogels in Regenerative Medicine.* Advanced Materials, 2009. **21**(32-33): p. 3307-3329.
145. Orive, G., et al., *Biomaterials for promoting brain protection, repair and regeneration.* Nature Reviews Neuroscience, 2009. **10**: p. 682.
146. Lauridsen, H.M., et al., *Tumor Necrosis Factor-α and IL-17A Activation Induces Pericyte-Mediated Basement Membrane Remodeling in Human Neutrophilic Dermatoses.* The American Journal of Pathology, 2017. **187**(8): p. 1893-1906.
147. Lampe, K.J. and S.C. Heilshorn, *Building stem cell niches from the molecule up through engineered peptide materials.* Neuroscience letters, 2012. **519**(2): p. 138-146.
148. Zhu, J. and R.E. Marchant, *Design properties of hydrogel tissue-engineering scaffolds.* Expert review of medical devices, 2011. **8**(5): p. 607-626.
149. Lee, S.H., et al., *Poly(ethylene glycol) hydrogels conjugated with a collagenase-sensitive fluorogenic substrate to visualize collagenase activity during three-dimensional cell migration.* Biomaterials, 2007. **28**(20): p. 3163-70.
150. Patel, P.N., et al., *Poly(ethylene glycol) Hydrogel System Supports Preadipocyte Viability, Adhesion, and Proliferation.* Tissue Engineering, 2005. **11**(9-10): p. 1498-1505.
151. Chhabra, A., et al., *Cell in situ zymography: an in vitro cytotechnology for localization of enzyme activity in cell culture.* In Vitro Cell Dev Biol Anim, 2012. **48**(8): p. 463-8.
152. Bjugstad, K.B., et al., *Biocompatibility of PEG-based hydrogels in primate brain.* Cell Transplant, 2008. **17**(4): p. 409-15.
153. Toda, H., et al., *Grafting neural stem cells improved the impaired spatial recognition in ischemic rats.* Neurosci Lett, 2001. **316**(1): p. 9-12.
154. Woodbury, D., et al., *Adult rat and human bone marrow stromal cells differentiate into neurons.* J Neurosci Res, 2000. **61**(4): p. 364-70.
155. Chen, J., et al., *Therapeutic benefit of intracerebral transplantation of bone marrow stromal cells after cerebral ischemia in rats.* J Neurol Sci, 2001. **189**(1-2): p. 49-57.
156. Kawai, H., et al., *Tridermal tumorigenesis of induced pluripotent stem cells transplanted in ischemic brain.* J Cereb Blood Flow Metab, 2010. **30**(8): p. 1487-93.
157. Azevedo, P.O., et al., *Endothelial cells maintain neural stem cells quiescent in their niche.* Neuroscience, 2017. **363**: p. 62-65.
158. Shen, Q., et al., *Endothelial cells stimulate self-renewal and expand neurogenesis of neural stem cells.* Science, 2004. **304**(5675): p. 1338-40.
159. Teng, H., et al., *Coupling of angiogenesis and neurogenesis in cultured endothelial cells and neural progenitor cells after stroke.* Journal of cerebral blood flow and metabolism : official journal of the International Society of Cerebral Blood Flow and Metabolism, 2008. **28**(4): p. 764-771.
160. Luo, L., et al., *Niche astrocytes promote the survival, proliferation and neuronal differentiation of co-transplanted neural stem cells following ischemic stroke in rats.* Experimental and therapeutic medicine, 2017. **13**(2): p. 645-650.
161. Ryu, S., et al., *Human neural stem cells promote proliferation of endogenous neural stem cells and enhance angiogenesis in ischemic rat brain.* Neural Regen Res, 2016. **11**(2): p. 298-304.
162. Chen, L., et al., *The role of exogenous neural stem cells transplantation in cerebral ischemic stroke.* J Biomed Nanotechnol, 2014. **10**(11): p. 3219-30.

163. Lee, S.-H., et al., *Poly(ethylene glycol) hydrogels conjugated with a collagenase-sensitive fluorogenic substrate to visualize collagenase activity during three-dimensional cell migration.* Biomaterials, 2007. **28**(20): p. 3163-3170.
164. Jennifer Mumaw, E.T.J., Corinne Sonnet, et al.,, *Rapid Heterotrophic Ossification with Cryopreserved Poly(ethylene glycol-) Microencapsulated BMP2-Expressing MSCs.* International Journal of Biomaterials, 2012. **2012**.
165. Liu, J.R. and M. Modo, *Quantification of the Extracellular Matrix Molecule Thrombospondin 1 and Its Peri-cellular Association in the Brain Using a Semi-automated Computerized Approach.* Journal of Histochemistry & Cytochemistry. **0**(0): p. 0022155418771677.
166. Ghuman, H., et al., *ECM hydrogel improves the delivery of PEG microsphere-encapsulated neural stem cells and endothelial cells into tissue cavities caused by stroke.* Brain Research Bulletin, 2020.
167. Pollock, K., et al., *A conditionally immortal clonal stem cell line from human cortical neuroepithelium for the treatment of ischemic stroke.* Exp Neurol, 2006. **199**(1): p. 143-55.
168. Smith, E.J., et al., *Implantation Site and Lesion Topology Determine Efficacy of a Human Neural Stem Cell Line in a Rat Model of Chronic Stroke.* STEM CELLS, 2012. **30**(4): p. 785-796.
169. Stroemer, P., et al., *The neural stem cell line CTX0E03 promotes behavioral recovery and endogenous neurogenesis after experimental stroke in a dose-dependent fashion.* Neurorehabil Neural Repair, 2009. **23**(9): p. 895-909.
170. Kalladka, D., et al., *Human neural stem cells in patients with chronic ischaemic stroke (PISCES): a phase 1, first-in-man study.* Lancet, 2016. **388**(10046): p. 787-96.
171. Muir, K.W., et al., *Intracerebral implantation of human neural stem cells and motor recovery after stroke: multicentre prospective single-arm study (PISCES-2).* J Neurol Neurosurg Psychiatry, 2020. **91**(4): p. 396-401.
172. Amer, M.H., et al., *Translational considerations in injectable cell-based therapeutics for neurological applications: concepts, progress and challenges.* npj Regenerative Medicine, 2017. **2**(1): p. 23.
173. Rossetti, T., F. Nicholls, and M. Modo, *Intracerebral Cell Implantation: Preparation and Characterization of Cell Suspensions.* Cell Transplant, 2016. **25**(4): p. 645-64.
174. Wahlberg, B., et al., *Ex vivo biomechanical characterization of syringe-needle ejections for intracerebral cell delivery.* Sci Rep, 2018. **8**(1): p. 9194.
175. Moriarty, N., A. Pandit, and E. Dowd, *Encapsulation of primary dopaminergic neurons in a GDNF-loaded collagen hydrogel increases their survival, re-innervation and function after intra-striatal transplantation.* Scientific Reports, 2017. **7**(1): p. 16033.
176. Modo, M., et al., *A chronic 1 year assessment of MRI contrast agent-labelled neural stem cell transplants in stroke.* Neuroimage, 2009. **47 Suppl 2**(0 2): p. T133-42.
177. Bible, E., et al., *The support of neural stem cells transplanted into stroke-induced brain cavities by PLGA particles.* Biomaterials, 2009. **30**(16): p. 2985-94.
178. Bible, E., et al., *Neo-vascularization of the stroke cavity by implantation of human neural stem cells on VEGF-releasing PLGA microparticles.* Biomaterials, 2012. **33**(30): p. 7435-7446.
179. Massensini, A.R., et al., *Concentration-dependent rheological properties of ECM hydrogel for intracerebral delivery to a stroke cavity.* Acta Biomater, 2015. **27**: p. 116-130.
180. Ghuman, H., et al., *Long-term retention of ECM hydrogel after implantation into a sub-acute stroke cavity reduces lesion volume.* Acta Biomater, 2017. **63**: p. 50-63.
181. Ghuman, H., et al., *Biodegradation of ECM hydrogel promotes endogenous brain tissue restoration in a rat model of stroke.* Acta biomaterialia, 2018. **80**: p. 66-84.

182. Cai, Q., et al. *Co-transplantation of hippocampal neural stem cells and astrocytes and microvascular endothelial cells improve the memory in ischemic stroke rat*. International journal of clinical and experimental medicine, 2015. **8**, 13109-13117.
183. Chou, C.-H. and M. Modo, *Human neural stem cell-induced endothelial morphogenesis requires autocrine/paracrine and juxtacrine signaling.* Scientific Reports, 2016. **6**(1): p. 29029.
184. Hicks, C., et al., *In vivo and in vitro characterization of the angiogenic effect of CTX0E03 human neural stem cells.* Cell Transplant, 2013. **22**(9): p. 1541-52.
185. Horie, N., et al., *Transplanted stem cell-secreted vascular endothelial growth factor effects poststroke recovery, inflammation, and vascular repair.* Stem Cells, 2011. **29**(2): p. 274-85.
186. Nih, L.R., et al., *Neuroblast survival depends on mature vascular network formation after mouse stroke: role of endothelial and smooth muscle progenitor cell co-administration.* European Journal of Neuroscience, 2012. **35**(8): p. 1208-1217.
187. Ottone, C., et al., *Direct cell-cell contact with the vascular niche maintains quiescent neural stem cells.* Nat Cell Biol, 2014. **16**(11): p. 1045-56.
188. Vissapragada, R., et al., *Bidirectional crosstalk between periventricular endothelial cells and neural progenitor cells promotes the formation of a neurovascular unit.* Brain research, 2014. **1565**: p. 8-17.
189. Chou, C.H. and M. Modo, *Characterization of gene expression changes in human neural stem cells and endothelial cells modeling a neurovascular microenvironment.* Brain Res Bull, 2020. **158**: p. 9-19.
190. Nicholls, F.J., et al., *Simultaneous MR imaging for tissue engineering in a rat model of stroke.* Scientific Reports, 2015. **5**(1): p. 14597.
191. Winn, S.R., et al., *Microencapsulated bovine chromaffin cells in vitro: effect of density and coseeding with a NGF-releasing cell line.* Journal of neural transplantation & plasticity, 1992. **3**(2-3): p. 115-124.
192. Snow, B., et al., *A phase IIb, randomised, double-blind, placebo-controlled, dose-ranging investigation of the safety and efficacy of NTCELL(®) [immunoprotected (alginate-encapsulated) porcine choroid plexus cells for xenotransplantation] in patients with Parkinson's disease.* Parkinsonism Relat Disord, 2019. **61**: p. 88-93.
193. Emerich, D.F., et al., *Encapsulated cell therapy for neurodegenerative diseases: from promise to product.* Adv Drug Deliv Rev, 2014. **67-68**: p. 131-41.
194. Leong, W. and D.-A. Wang, *Cell-laden Polymeric Microspheres for Biomedical Applications.* Trends in biotechnology, 2015. **33**(11): p. 653-666.
195. Gonzalez, A.L., et al., *Integrin interactions with immobilized peptides in polyethylene glycol diacrylate hydrogels.* Tissue engineering, 2004. **10**(11-12): p. 1775-1786.
196. Pollard, S.M., et al., *Adherent neural stem (NS) cells from fetal and adult forebrain.* Cereb Cortex, 2006. **16 Suppl 1**: p. i112-20.
197. Freytes, D.O., et al., *Preparation and rheological characterization of a gel form of the porcine urinary bladder matrix.* Biomaterials, 2008. **29**(11): p. 1630-7.
198. Crapo, P.M., T.W. Gilbert, and S.F. Badylak, *An overview of tissue and whole organ decellularization processes.* Biomaterials, 2011. **32**(12): p. 3233-43.
199. Medberry, C.J., et al., *Hydrogels derived from central nervous system extracellular matrix.* Biomaterials, 2013. **34**(4): p. 1033-1040.
200. Marçal, H., et al., *A comprehensive protein expression profile of extracellular matrix biomaterial derived from porcine urinary bladder.* Regen Med, 2012. **7**(2): p. 159-66.
201. Crapo, P.M., et al., *Biologic scaffolds composed of central nervous system extracellular matrix.* Biomaterials, 2012. **33**(13): p. 3539-47.
202. Huleihel, L., et al., *Matrix-bound nanovesicles within ECM bioscaffolds.* Sci Adv, 2016. **2**(6): p. e1600502.

203. Modo, M., *Long-term survival and serial assessment of stroke damage and recovery - practical and methodological considerations.* Journal of experimental stroke & translational medicine, 2009. **2**(2): p. 52-68.
204. Modo, M., et al., *Neurological sequelae and long-term behavioural assessment of rats with transient middle cerebral artery occlusion.* J Neurosci Methods, 2000. **104**(1): p. 99-109.
205. Ashioti, M., et al., *Multi-modal characterisation of the neocortical clip model of focal cerebral ischaemia by MRI, behaviour and immunohistochemistry.* Brain research, 2007. **1145**: p. 177-189.
206. Bible, E., et al., *Attachment of stem cells to scaffold particles for intra-cerebral transplantation.* Nat Protoc, 2009. **4**(10): p. 1440-53.
207. Jin, T., et al., *Diamagnetic chemical exchange saturation transfer (diaCEST) affords magnetic resonance imaging of extracellular matrix hydrogel implantation in a rat model of stroke.* Biomaterials, 2017. **113**: p. 176-190.
208. Moshayedi, P., et al., *Systematic optimization of an engineered hydrogel allows for selective control of human neural stem cell survival and differentiation after transplantation in the stroke brain.* Biomaterials, 2016. **105**: p. 145-155.
209. Aebischer, P., et al., *Long-term cross-species brain transplantation of a polymer-encapsulated dopamine-secreting cell line.* Exp Neurol, 1991. **111**(3): p. 269-75.
210. Tresco, P.A., et al., *Polymer-Encapsulated PC12 Cells: Long-Term Survival and Associated Reduction in Lesion-Induced Rotational Behavior.* Cell Transplantation, 1992. **1**(2-3): p. 255-264.
211. Wahlberg, L.U., et al., *Long-term, stable, targeted biodelivery and efficacy of GDNF from encapsulated cells in the rat and Goettingen miniature pig brain.* Current Research in Pharmacology and Drug Discovery, 2020. **1**: p. 19-29.
212. *Central Nervous System Delivery of Recombinant Ciliary Neurotrophic Factor by Polymer Encapsulated Differentiated C2C12 Myoblasts.* Human Gene Therapy, 1996. **7**(17): p. 2135-2146.
213. Lindvall, O. and L.U. Wahlberg, *Encapsulated cell biodelivery of GDNF: a novel clinical strategy for neuroprotection and neuroregeneration in Parkinson's disease?* Experimental neurology, 2008. **209**(1): p. 82-88.
214. Moreau, F., et al., *Cavitation after acute symptomatic lacunar stroke depends on time, location, and MRI sequence.* Stroke, 2012. **43**(7): p. 1837-42.
215. Bible, E., et al., *Non-invasive imaging of transplanted human neural stem cells and ECM scaffold remodeling in the stroke-damaged rat brain by (19)F- and diffusion-MRI.* Biomaterials, 2012. **33**(10): p. 2858-2871.
216. Ghuman, H., et al., *ECM hydrogel for the treatment of stroke: Characterization of the host cell infiltrate.* Biomaterials, 2016. **91**: p. 166-181.
217. Modo, M., *Bioscaffold-Induced Brain Tissue Regeneration.* Frontiers in Neuroscience, 2019. **13**(1156).
218. El-Akabawy, G., et al., *Implantation of undifferentiated and pre-differentiated human neural stem cells in the R6/2 transgenic mouse model of Huntington's disease.* BMC Neuroscience, 2012. **13**(1): p. 97.
219. Nih, L.R., et al., *Dual-function injectable angiogenic biomaterial for the repair of brain tissue following stroke.* Nature materials, 2018. **17**(7): p. 642-651.
220. Lam, J., et al., *Delivery of iPS-NPCs to the Stroke Cavity within a Hyaluronic Acid Matrix Promotes the Differentiation of Transplanted Cells.* Adv Funct Mater, 2014. **24**(44): p. 7053-7062.
221. Rose, J.C., et al., *Biofunctionalized aligned microgels provide 3D cell guidance to mimic complex tissue matrices.* Biomaterials, 2018. **163**: p. 128-141.

222. Culver, J.C., et al., *Three-dimensional biomimetic patterning in hydrogels to guide cellular organization.* Adv Mater, 2012. **24**(17): p. 2344-8.
223. Revzin, A., et al., *Fabrication of Poly(ethylene glycol) Hydrogel Microstructures Using Photolithography.* Langmuir, 2001. **17**(18): p. 5440-5447.
224. Lee, S.H., J.J. Moon, and J.L. West, *Three-dimensional micropatterning of bioactive hydrogels via two-photon laser scanning photolithography for guided 3D cell migration.* Biomaterials, 2008. **29**(20): p. 2962-8.
225. Peters, E.B., et al., *Poly(ethylene glycol) Hydrogel Scaffolds Containing Cell-Adhesive and Protease-Sensitive Peptides Support Microvessel Formation by Endothelial Progenitor Cells.* Cell Mol Bioeng, 2016. **9**(1): p. 38-54.
226. Sacco, S., et al., *Incidence and 10-year survival of intracerebral hemorrhage in a population-based registry.* Stroke, 2009. **40**(2): p. 394-9.
227. Flaherty, M.L., et al., *Long-term mortality after intracerebral hemorrhage.* Neurology, 2006. **66**(8): p. 1182-1186.
228. Chiu, D., et al., *Comparison of outcomes after intracerebral hemorrhage and ischemic stroke.* J Stroke Cerebrovasc Dis, 2010. **19**(3): p. 225-229.
229. Sukumari-Ramesh, S., C.H. Alleyne, and K.M. Dhandapani, *Astrogliosis: a Target for Intervention in Intracerebral Hemorrhage?* Translational Stroke Research, 2012. **3**(1): p. 80-87.
230. Hicks, A.U., et al., *Transplantation of human embryonic stem cell-derived neural precursor cells and enriched environment after cortical stroke in rats: cell survival and functional recovery.* Eur J Neurosci, 2009. **29**(3): p. 562-74.
231. Zhang, R.L., et al., *Stroke increases neural stem cells and angiogenesis in the neurogenic niche of the adult mouse.* PLoS One, 2014. **9**(12): p. e113972.
232. Zhang, R.L., et al., *Stroke increases neural stem cells and angiogenesis in the neurogenic niche of the adult mouse.* PloS one, 2014. **9**(12): p. e113972-e113972.
233. Jin, K., et al., *Vascular endothelial growth factor (VEGF) stimulates neurogenesis in vitro and in vivo.* Proceedings of the National Academy of Sciences of the United States of America, 2002. **99**(18): p. 11946-11950.
234. Calvo, C.F., et al., *Vascular endothelial growth factor receptor 3 directly regulates murine neurogenesis.* Genes Dev, 2011. **25**(8): p. 831-44.
235. Le Bras, B., et al., *VEGF-C is a trophic factor for neural progenitors in the vertebrate embryonic brain.* Nat Neurosci, 2006. **9**(3): p. 340-8.
236. Han, J., et al., *Vascular Endothelial Growth Factor Receptor 3 Controls Neural Stem Cell Activation in Mice and Humans.* Cell Reports, 2015. **10**(7): p. 1158-1172.
237. Shin, Y.-J., et al., *Expression of Vascular Endothelial Growth Factor-C (VEGF-C) and Its Receptor (VEGFR-3) in the Glial Reaction Elicited by Human Mesenchymal Stem Cell Engraftment in the Normal Rat Brain.* Journal of Histochemistry & Cytochemistry, 2014. **63**(3): p. 170-180.
238. Alam, A., et al., *SAR131675, a Potent and Selective VEGFR-3–TK Inhibitor with Antilymphangiogenic, Antitumoral, and Antimetastatic Activities.* Molecular Cancer Therapeutics, 2012. **11**(8): p. 1637-1649.
239. Espagnolle, N., et al., *Specific Inhibition of the VEGFR-3 Tyrosine Kinase by SAR131675 Reduces Peripheral and Tumor Associated Immunosuppressive Myeloid Cells.* Cancers, 2014. **6**(1): p. 472-490.
240. Blanc, I., et al., *SAR131675, a new potent selective VEGFR-3-TK inhibitor: Effect on lymphangiogenic, tumor growth, and metastasis.* Journal of Clinical Oncology, 2010. **28**(15_suppl): p. e13623-e13623.
241. Foster, B., et al., *Detection of intracellular cytokines by flow cytometry.* Curr Protoc Immunol, 2007. **Chapter 6**: p. Unit 6 24.

242. Nakagomi, N., et al., *Endothelial Cells Support Survival, Proliferation, and Neuronal Differentiation of Transplanted Adult Ischemia-Induced Neural Stem/Progenitor Cells After Cerebral Infarction.* STEM CELLS, 2009. **27**(9): p. 2185-2195.
243. Xiong, Y.-j., et al., *Proliferation and differentiation of neural stem cells co-cultured with cerebral microvascular endothelial cells after oxygen-glucose deprivation.* Journal of Huazhong University of Science and Technology [Medical Sciences], 2013. **33**(1): p. 63-68.
244. Zarkada, G., et al., *VEGFR3 does not sustain retinal angiogenesis without VEGFR2.* Proceedings of the National Academy of Sciences, 2015. **112**(3): p. 761-766.
245. Taylor, R.A., et al., *TGF-β1 modulates microglial phenotype and promotes recovery after intracerebral hemorrhage.* The Journal of Clinical Investigation, 2017. **127**(1): p. 280-292.
246. Mozaffarian, D., et al., *Executive Summary: Heart Disease and Stroke Statistics—2016 Update.* Circulation, 2016. **133**(4): p. 447-454.
247. Taylor, R.A. and L.H. Sansing, *Microglial responses after ischemic stroke and intracerebral hemorrhage.* Clin Dev Immunol, 2013. **2013**: p. 746068.
248. Askenase, M.H. and L.H. Sansing, *Stages of the Inflammatory Response in Pathology and Tissue Repair after Intracerebral Hemorrhage.* Seminars in neurology, 2016. **36**(3): p. 288-297.
249. Gao, L., et al., *Stem Cell Therapy: A Promising Therapeutic Method for Intracerebral Hemorrhage.* Cell Transplantation, 2018. **27**(12): p. 1809-1824.
250. Smith, E.J., et al., *Implantation site and lesion topology determine efficacy of a human neural stem cell line in a rat model of chronic stroke.* Stem Cells, 2012. **30**(4): p. 785-96.
251. Park, K.I., Y.D. Teng, and E.Y. Snyder, *The injured brain interacts reciprocally with neural stem cells supported by scaffolds to reconstitute lost tissue.* Nat Biotechnol, 2002. **20**.
252. Lin, R., et al., *Neurogenesis is enhanced by stroke in multiple new stem cell niches along the ventricular system at sites of high BBB permeability.* Neurobiology of Disease, 2015. **74**: p. 229-239.
253. Calvo, C.-F., et al., *Vascular endothelial growth factor receptor 3 directly regulates murine neurogenesis.* Genes & development, 2011. **25**(8): p. 831-844.
254. Wohnsland, S., et al., *Neurons and neuronal stem cells survive in glucose-free lactate and in high glucose cell culture medium during normoxia and anoxia.* Neurochem Res, 2010. **35**(10): p. 1635-42.
255. Zhang, J., et al., *Endothelial Lactate Controls Muscle Regeneration from Ischemia by Inducing M2-like Macrophage Polarization.* Cell Metabolism, 2020. **31**(6): p. 1136-1153.e7.
256. Young, M., et al., *A TRACER 3D Co-Culture tumour model for head and neck cancer.* Biomaterials, 2018. **164**: p. 54-69.
257. Rodenhizer, D., et al., *A three-dimensional engineered heterogeneous tumor model for assessing cellular environment and response.* Nat Protoc, 2018. **13**(9): p. 1917-1957.
258. Rodenhizer, D., et al., *Development of TRACER: tissue roll for analysis of cellular environment and response.* Biofabrication, 2016. **8**(4): p. 045008.